Ponašanje i površinska svojstva mikroalga kao pokazatelji stresa u vodenim ekosustavima

Novosel, Nives

Sveučilište u Zagrebu

PRIRODOSLOVNO-MATEMATIČKI FAKULTET

Nives Novosel

PONAŠANJE I POVRŠINSKA SVOJSTVA MIKROALGA KAO POKAZATELJI STRESA U VODENIM EKOSUSTAVIMA

DOKTORSKI RAD

Zagreb, 2022.

Sveučilište u Zagrebu

PRIRODOSLOVNO-MATEMATIČKI FAKULTET

Nives Novosel

PONAŠANJE I POVRŠINSKA SVOJSTVA MIKROALGA KAO POKAZATELJI STRESA U VODENIM EKOSUSTAVIMA

DOKTORSKI RAD

Mentor: Dr.sc. Nadica Ivošević DeNardis

Zagreb, 2022.

University of Zagreb

FACULTY OF SCIENCE

Nives Novosel

BEHAVIOUR AND SURFACE PROPERTIES OF MICROALGAE AS STRESS MARKERS FOR AQUATIC ECOSYSTEMS

DOCTORAL DISSERTATION

Supervisor: Nadica Ivošević DeNardis, PhD

Zagreb, 2022.

Ovaj doktorski rad izrađen je u Laboratoriju za biogeokemiju mora i atmosfere, Zavoda za istraživanje mora i okoliša Instituta Ruđer Bošković u Zagrebu, pod mentorstvom dr.sc. Nadice Ivošević DeNardis, u sklopu Interdisciplinarnog doktorskog studija Oceanologije na Prirodoslovno-matematičkom fakultetu Sveučilišta u Zagrebu. Doktorski rad izrađen je u okviru projekta Hrvatske zaklade za znanost: „Od površinskih svojstava stanica alga do pokazatelja stresa u vodenim ekosustavima“ (CELLSTRESS, IP-2018-01-5840; voditelj projekta: dr. sc. Nadica Ivošević DeNardis, viši znanstveni suradnik).

Zahvaljujem se mentorici, doktorici Nadici Ivošević DeNardis na pruženoj prilici za rad u znanosti, ukazanom povjerenju, korisnim i stručnim savjetima i prijedlozima kroz sve četiri godine moga rada, kao i prilikom pisanja ovog doktorskoga rada.

Zahvaljujem se doktorici Tei Mišić Radić i doktorici Maji Levak Zorinc na pomoći u labosu i stručnim, korisnim i prijateljskim savjetima. Također, zahvaljujem se svim članovima Laboratorija za biogeokemiju mora i atmosfere koji su uvijek bili spremni priskočiti u pomoć kad god je trebalo.

Zahvaljujem se svim članovima komisije, profesorici Ivi Juranović Cindrić, doktorici Blaženki Gašparović i profesorici Zrinki Ljubešić na korisnim komentarima, ispravcima i pomoći ne samo u doktoratu, nego i u višegodišnjoj suradnji.

Ovaj doktorski rad napravljen je kao sklop četiri znanstvena rada pa se zahvaljujem svim koautorima koji su svojim marljivim radom pridonijeli njegovom nastanku: dr. sc. Tei Mišić Radić, dr. sc. Maji Levak Zorinc, dr. sc. Joanna Zemla, dr. sc. Małgorzata Lekka, dr. sc. Ivni Vrani Špoljarić, dr. sc. Blaženki Gašarović, Luciji Horvat, Andrei Čačković, Damiru Kasumu, dr. sc. Tarzanu Legoviću, dr. sc. Petru Žutiniću i dr. sc. Mariji Gligori Udovič. I naravno dr. sc. Nadici Ivošević DeNardis koja je glavna zaslužna za nastanak svake od te četiri publikacije.

Zahvaljujem se svojim kolegicama s Oceanologije, posebice Andrei, Luciji i Sarah na svim kavama i razgovorima ohrabrenja.

Hvala mojim prijateljima i prijateljicama što ste uvijek, ali baš uvijek bili tu! Posebno mojoj Ivoni!

Posebno se zahvaljujem svojim Roditeljima! Mama i Tata hvala vam što ste mi sve omogućili, uvijek me nesebično podupirali i najglasnije navijali za mene! Presretna sam što vas imam!

Hvala mom najboljem prijatelju Borni, mom najstabilnijem osloncu, sigurnoj luci i odnedavno mužu na bezgraničnoj podršci!

TEMELJNA DOKUMENTACIJSKA KARTICA

Sveučilište u Zagrebu
Prirodoslovno-matematički fakultet
Geološki odsjek

Doktorski rad

PONAŠANJE I POVRŠINSKA SVOJSTVA MIKROALGA KAO POKAZATELJI STRESA U VODENIM EKOSUSTAVIMA

Nives Novosel

Laboratorij za biogeokemiju mora i atmosfere
Zavod za istraživanje mora i okoliša
Institut Ruđer Bošković, Zagreb

Cilj doktorskog rada bio je povezati stanični odgovor mikroalga u vidu ponašanja i površinskih svojstava u odnosu na antropogeni stresor (teški metal) i abiotičke stresore (temperatura, salinitet) kako bi se bolje razumjele strategije preživljavanja i prilagodbe stanica u vodenim ekosustavima u uvjetima klimatskih promjena. Istraživanja su provedena s tri monokulture mikroalga u laboratorijskim uvjetima primjenom elektrokemijske metode i programskoga paketa ICY uz statističku obradu. Rezultati su pokazali da adaptacijski odgovor mikroalga ovisi o istraživanoj vrsti i strukturnim značajkama njene stanične barijere, te o prirodi stresora. Izlaganjem stanica toksičnoj koncentraciji kadmija, padom temperature i saliniteta flagelatne vrste postaju slabo pokretne, stanice postaju čvršće, mijenjaju stupanj hidrofobnosti i fiziološku aktivnost, te mogu ući u stadij mirovanja. Dijatomeja *Cylindrotheca closterium* se pokazala kao najtolerantnija na variranje oba abiotička stresora u odnosu na zelene alge *Dunaliella tertiolecta* i *Tetraselmis suecica*. S obzirom na to da ponašanje i površinska svojstva mikroalga daju mjerljivu razliku u odnosu na kontrolne uvjete, mogu se smatrati pokazateljima stresa u vodenim ekosustavima.

(145 stranica, 9 slika, 112 literaturna navoda, jezik izvornika: hrvatski)

Ključne riječi: abiotički stresor, antropogeni stresor, fiziološka aktivnost, mikroalge, pokretljivost, površinska svojstva

Mentor: Dr. sc. Nadica Ivošević DeNardis, viši znanstveni suradnik

Ocjenjivači: Dr. sc. Iva Juranović Cindrić, redoviti profesor
Dr. sc. Blaženka Gašparović, znanstveni savjetnik u trajnom zvanju
Dr. sc. Zrinka Ljubešić, izvanredni profesor
Dr. sc. Petar Žutinić, docent (zamjena)

Rad prihvaćen: 9. rujna 2022.

BASIC DOCUMENTATION CARD

University of Zagreb
Faculty of Science
Department of Geology

Doctoral Thesis

BEHAVIOUR AND SURFACE PROPERTIES OF MICROALGAE AS STRESS MARKERS FOR AQUATIC ECOSYSTEMS

Nives Novosel

Laboratory for Marine and Atmospheric Biogeochemistry,
Division for Marine and Environmental Research,
Ruđer Bošković Institute, Zagreb

The objective of the PhD thesis was to relate the cellular response of microalgae in terms of behavior and surface properties in relation to anthropogenic stressors (heavy metals) and abiotic stressors (temperature, salinity) to better understand cellular survival and adaptation strategies in aquatic ecosystems under climate change. The study was conducted with three monocultures of microalgae under laboratory conditions using the electrochemical method and the software package ICY with statistical processing. The results showed that the adaptive response of microalgae depends on the studied species and its structural characteristics of the cell barrier, as well as on the type of stressor. When the cells are exposed to toxic cadmium concentration and the temperature and salinity decrease, the flagellate species become poorly motile, cells become softer, change the degree of hydrophobicity and physiological activity, and may enter the dormant stage. Diatom *Cylindrotheca closterium* has been shown to be the most tolerant to changes in both abiotic stressors compared to green algae *Dunaliella tertiolecta* and *Tetraselmis suecica*. Taking into consideration that the behavior and surface properties of microalgae show a measurable difference from control conditions, they can be considered indicators of stress in aquatic ecosystems.

(145 pages, 9 figures, 112 references, original in Croatian)

Keywords: abiotic stressor, antropogenic stressor, microalgae, motility, physiological acivity, surface properties

Supervisor: Dr. sc. Nadica Ivošević DeNardis, Senior Research Associate

Reviewers: Dr. sc. Iva Juranović Cindrić, Full Professor
Dr. sc. Blaženka Gašparović, Tenured Senior Scientist
Dr. sc. Zrinka Ljubešić, Associate Professor
Dr. sc. Petar Žutinić, Assistant Professor (substitute)

Theses accepted: 9 September 2022.

SADRŽAJ

POPIS ZNANSTVENIH RADOVA

Znanstveni radovi na kojima se temelji doktorski rad:

I. Novosel, N., Kasum, D., Žutinić, P., Legović, T., Ivošević DeNardis, N., 2020. Short-term effect of cadmium on the motility of three flagellated algal species. Journal of applied phycology 32: 4057–4067. https://doi.org/10.1007/s10811-020-02283-1

II. Novosel, N., Ivošević DeNardis, N., 2021. Structural Features of the Algal Cell Determine Adhesion Behavior at a Charged Interface. Electroanalysis 33: 1436–1443. https://doi.org/10.1002/elan.202060580

III. Novosel, N., Mišić Radić, T., Zemla, J., Lekka, M., Čačković, A., Kasum, D., Legović, T., Žutinić, P., Gligora Udovič, M., Ivošević DeNardis, N., 2022. Temperature-induced response in algal cell surface properties and behavior. Journal of applied phycology 34: 243–259.https://doi.org/10.1007/s10811-021-02591-0

IV. Novosel, N., Mišić Radić, T., Levak Zorinc, M., Zemla, J., Lekka, M., Vrana, I., Gašparović, B., Horvat, L., Kasum, D., Legović, T., Žutinić, P., Gligora Udovič, M., Ivošević DeNardis, N., 2022. Salinity induced chemical, mechanical and behavioral changes in marine microalgae. Journal of applied phycology 34: 1293–1309. https://doi.org/10.1007/s10811-022-02734-x

PROŠIRENI SAŽETAK

Globalne klimatske promjene i različiti antropogeni pritisci prijetnja su svim vodenim ekosustavima na Zemlji. Dugoročna mjerenja pokazuju globalni porast temperature zraka i mora, dok modeli predviđaju nastavak ovog trenda uz potencijalne promjene u globalnom hidrološkom ciklusu (Cavicchioli i sur., 2019). Promjene u globalnom hidrološkom ciklusu posljedično dovode do promjene saliniteta površinskoga sloja mora, ovisno o stopi evaporacije i priljeva slatke vode (Durack i Wijffels, 2010; Mihanović i sur., 2021). Mikroalge nastanjuju površinski, dobro osvijetljeni sloj vodenog stupca koji je izložen sve većim klimatskim pritiscima (porast temperature, promjena saliniteta, povećano UV zračenje, itd.) i antropogenim pritiscima (zagađenje teškim metala, naftom, plastikom, deterdžentima, itd.) (Moullec i sur., 2021). Iako biomasom male, mikroalge imaju ključnu ulogu u globalnoj primarnoj proizvodnji, glavnim biogeokemijskim ciklusima na Zemlji, te predstavljaju temelj hranidbenog lanca u vodenom okolišu (Gamal, 2010; Häder i Gao, 2015). Unatoč ekološkoj važnosti, poznato je da klimatsko i antropogeno uvjetovani pritisci u vodenom okolišu dovode do promjena u sastavu i brojnosti zajednica mikroalga što je istraženo na različitim prostorno-vremenskim skalama, u empirijskim i terenskim istraživanjima, kao i korištenjem modela (Sarmiento i sur., 2004; Boyce i sur., 2010; Huertas i sur., 2011). Adaptacijski odgovor mikroalga smatra se brzim i pouzdan pokazateljem promjena u vodenom ekosustavu, zbog njihova kratkog životnog ciklusa (Borowitzka, 2018). Međutim, adaptacijski odgovor mikroalga na nivou pojedinačnih stanica do sada nije detaljno istražen.

Cilj doktorskog rada bio je povezati stanični odgovor mikroalga u vidu ponašanja i površinskih svojstava u odnosu na antropogene i abiotičke stresore (teški metal, povišena temperatura, sniženje saliniteta) kako bi se bolje razumjele njihove strategije preživljavanja i prilagodbe u vodenim ekosustavima. Postavljene su tri hipoteze istraživanja: (1) površinska svojstva i ponašanje stanica mikroalga mogu se smatrati pokazateljima stresa; (2) stanice u stresu mijenjaju površinska svojstva i fiziološku aktivnost; (3) stanice mikroalga sa složenijom staničnom barijerom otpornije su na prisutnost stresora u vodenom okolišu.

Ovaj doktorski rad temelji se na četiri objavljena znanstvena rada. U znanstvenom radu I istražen je utjecaj antropogenog stresora u vidu kratkoročnog izlaganja toksičnoj koncentraciji teškog metala kadmija na ponašanje odabranih stanica mikroalga u smislu stanične pokretljivosti. Razvijena je metoda za analizu pokretljivosti stanica, te su određeni parametri stanične

pokretljivosti dovedeni u vezu s kompleksnošću flagelarnog sustava i strukturnim značajkama stanične barijere za tri jednostanične pokretne morske mikroalge, *Dunaliella tertiolecta* Butcher, *Tetraselmis suecica* (Kylin) Butcher i *Rhodomonas maculata* Butcher ex D.R.A.Hill & R.Wetherbee. Razvijena procedura omogućila je brzo i pouzdano praćenje, te istovremenu kvantitativnu analizu pokretljivosti nekoliko stotina stanica mikroalga.

U znanstvenom radu II istražen je utjecaj strukturnih značajki stanične barijere morskih mikroalga u kontrolnim uvjetima na adhezijsko ponašanje na nabijenoj međupovršini, što doprinosi razumijevanju ponašanja stanica na prirodnim granicama faza. Razvijen je protokol za amperometrijsku karakterizaciju stanica mikroalga, *D. tertiolecta*, *Prorocentrum micans Ehrenberg*, *T. suecica* i *Cylindrotheca closterium* (Ehrenberg) Reimann & J. Lewin, različite kompleksnosti stanične barijere, od glikokaliksa do čvrstih ljušturica. Rezultati su uspoređeni s nanomehaničkim svojstvima stanica primjenom komplementarne površinske metode mikroskopije atomskih sila (eng. Atomic Force Microscopy, AFM), što je pridonijelo boljem razumijevanju uloge strukturnih značajki stanične barijere na adheziju mikroalga na nabijenoj međupovršini. Protokoli i procedure razvijene u znanstvenim radovima I i II predstavljaju temelje za istraživanja provedena u znanstvenim radovima III i IV.

U znanstvenim radovima III i IV istraženi su utjecaji glavnih abiotičkih stresora u vodenom okolišu, temperature i saliniteta na odabrane vrste mikroalga. U znanstvenom radu III istražen je utjecaj promjene temperature (pri konstantom salinitetu) na ponašanje i površinska svojstva stanica mikroalga. Tri odabrane vrste mikroalga *D. tertiolecta, T. suecica* i *C. closterium* uzgajane su u laboratorijskim uvjetima na temperaturama koje sugeriraju godišnje varijacije u vodenom okolišu. Praćena je dinamika rasta, te je određena stanična pokretljivosti u vidu stanične brzine i puta primjenom programskog paketa otvorenog koda ICY. Primijenjenom elektrokemijske metode polarografije i kronoamperometrije na kapajućoj živinoj elektrodi okarakterizirano je adhezijsko ponašanje stanica na međupovršini, kao posljedica stanične fluidnosti i hidrofobnosti, te je određen sadržaj izlučene površinski-aktivne organske tvari. Dobiveni rezultati uspoređeni su s rezultatima komplementarne metode AFM-a u smislu određenih nanomehaničkih svojstava stanica i strukturne organizacije izlučene organske tvari, što je dalo uvid u mehanizam adaptacije stanica različitih strukturnih značajki staničnih barijera koje mogu doprinijeti temperaturnoj tolerantnosti.

U znanstvenom radu IV istražen je utjecaj smanjenja saliniteta (pri konstantnoj temperaturi) na ponašanje i površinska svojstva stanica mikroalga. U istraživanju utjecaja

saliniteta također su korištene tri morske mikroalge *D. tertiolecta, T. suecica i C. closterium,* uzgajane u laboratorijskim uvjetima koji sugeriraju raspon saliniteta u vodenom okolišu od euhalinog do mezohalinog. Na temelju dinamike rasta, analizirane stanične pokretljivosti, adhezije i fiziološke aktivnosti, te usporedbe s nanomehaničkim svojstvima stanica i lipidnim profilom, dobiven je sveobuhvatniji uvid u mehanizam adaptacije stanica na promjenu saliniteta, te ulogu strukturnih značajki stanične barijere u stresu s niskim salinitetom.

U ovom doktorskom radu pokazano je da adaptacijski odgovor stanica u smislu ponašanja i površinskih svojstava mikroalga ovisi o istraživanoj vrsti i njenim strukturnim značajkama stanične barijere, te o prirodi stresora. S obzirom da je navedeni adaptacijski odgovor mikroalga u stresu dao mjerljivu razliku u odnosu na kontrolne uvjete, može se smatrati indikatorom poremećaja u vodenom ekosustavu, što može biti od pomoći u razumijevanju prilagodbe i sudbine stanica u uvjetima klimatskih promjena, kao najvećim izazovima današnjice. Stoga su dobiveni rezultati u okviru ovog doktorskog rada potvrdili postavljene hipoteze istraživanja.

Znanstveni doprinosi doktorskog rada temelje se na (i) fundamentalnom razumijevanju adaptacijskoga odgovora stanica mikroalga, što je od ključnoga značaja za predviđanje njihovog ponašanja i sudbine u uvjetima stresa u vodenim ekosustavima, te na (ii) razvoju i primjeni učinkovitijih metoda za izravnu, brzu i ekonomičnu karakterizaciju populacija mikroalga, što može potencijalno utjecati na njihovu buduću implementaciju u ocjenjivanju stanja vodenog ekosustava.

THESIS SUMMARY

Global climate change and various anthropogenic pressures are a threat to all aquatic ecosystems on Earth. Long-term measurements show a global increase in air and sea temperatures, while models predict the continuation of this trend with potential changes in the global hydrological cycle (Cavicchioli et al., 2019). Changes in the global hydrological cycle consequently lead to changes in the salinity of the sea surface layer, depending on the rate of evaporation and freshwater inflow (Durack and Wijffels, 2010; Mihanović et al., 2021). Microalgae inhabit a surface, well-lit layer of the water column that is subject to increasing climatic pressures (increasing temperature, decreasing salinity, increasing UV radiation, etc.) and anthropogenic pressures (pollution from heavy metals, oil, plastics, detergents, etc.) (Moullec et al., 2021). Although their biomass is small, microalgae play a key role in global primary production and major biogeochemical cycles on Earth and form the basis of the food web in aquatic environments (Gamal, 2010; Häder and Gao, 2015). Despite their ecological importance, climatic and anthropogenic impacts on aquatic environments are known to cause changes in the composition and number of microalgal communities. This has been studied at different spatial and temporal scales, in empirical studies and field research, and using models (Sarmiento et al., 2004; Boyce et al., 2010; Huertas et al., 2011). The adaptive response of microalgae is a rapid, reliable, and measurable indicator of changes in the aquatic ecosystem, precisely because of their short life cycle (Borowitzka, 2018). The adaptation response of microalgae at the single cell level has not yet been studied in detail.

The aim of this dissertation was to link the cellular response of microalgae in terms of behavior and surface properties in relation to anthropogenic and abiotic stressors (heavy metal, temperature, salinity) to better understand their survival and adaptation strategies in aquatic ecosystems. Three research hypotheses were formulated: (1) the surface properties and behavior of microalgal cells can be considered indicators of stress; (2) cells under stress alter their surface properties and physiological activity; (3) microalgal cells with a more complex cell barrier are more resilient to the presence of stressors in the aquatic environment.

This dissertation is based on four published scientific papers. In a scientific paper I the influence of an anthropogenic stressor in the form of short-term exposure to toxic concentrations of the heavy metal cadmium on the behavior of selected microalgal cells in terms of cell motility was studied. A method for cell motility analysis was developed and certain parameters of cell

motility were related to the complexity of the flagellar system and structural features of the cell barrier for three unicellular motile marine microalgae, *Dunaliella tertiolecta* Butcher*, Tetraselmis suecica* (Kylin) Butcher and *Rhodomonas maculata* Butcher ex D.R.A.Hill & R.Wetherbee. The developed method allowed rapid and reliable monitoring and simultaneous quantitative analysis of the motility behaviour of several hundred microalgal cells.

Scientific paper II investigated the influence of the structural features of the cell barrier of marine microalgae, under control conditions on the adhesion behavior at the charged interface, which contributes to the understanding of cell behavior at natural interfaces. A protocol was developed for the amperometric characterization of microalgal cell species, *D. tertiolecta*, *Prorocentrum micans Ehrenberg*, *T. suecica* and *Cylindrotheca closterium* (Ehrenberg) Reimann & J. Lewin, with varying cell barrier complexity, from glycocalyx to solid cell walls. The results were compared with the nanomechanical properties of the cells using the complementary surface method of atomic force microscopy (AFM), which contributed to a better understanding of the role of the structural features of the cell barrier in the adhesion of microalgae to charged interfaces. The protocols and procedures developed in scientific papers I and II form the basis for the studies conducted in scientific papers III and IV.

In scientific papers III and IV the effects of major abiotic stressors in the aquatic environment, temperature, and salinity on selected microalgae species were studied. In scientific paper III, the effect of temperature changes (at constant salinity) on the behavior and surface properties of microalgal cells was studied. Three selected microalgal species *D. tertiolecta*, *T. suecica*, and *C. closterium* were grown under laboratory conditions at temperatures indicative of annual fluctuations in the aquatic environment. Growth dynamics were monitored and cell motility, i.e., cell speed and path, was determined using the open-source software package ICY. The electrochemical method of polarography and chronoamperometry on a dropping mercury electrode was used to characterize the adhesion behavior of the cells at the interface, as a consequence of cellular fluidity and hydrophobicity, and to determine the amount of released surface-active organic matter. The obtained results were compared with the results of the complementary AFM method to determine the nanomechanical properties of the cells and the structural organization of the released organic matter, which provided insight into the adaptation mechanism of the cells exhibiting various structural features of the cellular barriers that may contribute to temperature tolerance.

The effect of salinity reduction (at constant temperature) on the behavior and surface properties of microalgal cells was investigated in the scientific paper IV. Three marine microalgae, *D. tertiolecta, T. suecica,* and *C. closterium* were studied at salinity corresponding to a variation from euhaline to mesohaline. Based on growth dynamics, analysis of cell motility, adhesion, and physiological activity, and comparison with cell nanomechanical properties and lipid profile, a more comprehensive insight into the mechanism of cell adaptation to salinity changes and the role of the structural features of cell barrier in salinity stress was obtained.

In this dissertation, it was shown that the adaptive response of cells in terms of microalgal behavior and surface properties depended on the studied cell species and its structural features of the cell barrier, as well as on the nature of stressors. Since the adaptive response of microalgae to stress provided a measurable difference from control conditions, it can be considered as an indicator of disturbances in the aquatic ecosystem, which can help to understand the adaptation and fate of cells under climate changes as the greatest challenges of our time. Thus, the results obtained in this dissertation confirm the research hypotheses established.

The scientific contributions of the doctoral thesis are based on (i) a fundamental understanding of the adaptive response of microalgal cells, which is crucial for predicting their behavior and fate under stress conditions in aquatic ecosystems, and (ii) the development and application of more effective methods for direct, rapid, and economical characterization of microalgal populations, potentially impacting their future application in ecosystem assessment.

1. UVOD

1.1. Klimatske promjene i mikroalge

Globalne klimatske promjene utječu na brojne čimbenike okoliša, te posljedično mijenjaju primarnu produkciju, raznolikost i sastav zajednica mikroalga. Tijekom prošlog stoljeća temperature atmosfere i oceana porasle su za 0,4-0,8 °C. Do kraja 21. stoljeća klimatski modeli predviđaju zatopljenje u nekim područjima svjetskih oceana za dodatnih 3 °C (Hansen i sur., 2006), uz potencijalne promjene prosječnog površinskog saliniteta ovisno o geografskom položaju mora i oceana, odnosno o stopi evaporacije i priljeva slatke vode. Naime, kao rezultat povećane količine padalina i topljenja leda na polovima što nadmašuje isparavanje s površine oceana na višim geografskim širinama dolazi do sniženja saliniteta, dok u nižim geografskim širinama i poluzatvorenim morima, kao što je Jadransko more, dolazi do povišenja površinskog saliniteta (McNeil i Matear, 2006; Mihanović i sur. 2021). Različiti antropogeni pritisci dodatno amplificiraju učinak klimatskih promjena u ekosustavu i dovode do degradacije vodenih staništa. Promjene na dnu hranidbenog lanca u vodenim ekosustavima zbog kaskadnih učinaka utjecat će na trofičku mrežu. Ključ predviđanja utjecaja klimatskih promjena na zajednice u vodenim ekosustavima jest razumijevanje odgovora pojedinih vrsta. Odgovor mikroalga na promjene u okolišu ispituje se na različitim prostorno-vremenskim skalama, u laboratorijskim (Feng i sur., 2008) i terenskim istraživanjima (Guinder i sur., 2010; Wetz i sur., 2011) kao i modeliranjem (Sarmiento i sur., 2004; Boyce i sur., 2010).

Važnost stanica mikroalga kao pokazatelja promjena proizlazi iz činjenice da su, unatoč njihovoj mikroskopskoj veličini, odgovorne za polovicu globalne primarne proizvodnje, pokreću bitne biogeokemijske cikluse ugljika, kisika, dušika, fosfora, silicija i sumpora, te čine osnovu hranidbenog lanca u vodenim ekosustavima (Falkowski, 1980). Morski ekosustavi predstavljaju dinamična staništa sa širokim rasponom ekoloških gradijenata u vidu fizikalnih, kemijskih i hidroloških parametara (Rotter i sur., 2021). U cilju prilagodbe i rasta u morskim ekosustavima, mikroalge su evolucijski razvile različite strategije koje igraju ključne uloge za opstanak. Glavni abiotički čimbenici okoliša su temperatura, salinitet, intenzitet svjetlost i dostupnost nutrijenata (Adenan i sur., 2013). Općenito se povećanjem temperature povećava primarna produkcija, no previsoka temperatura može imati negativan utjecaj na primarnu produkciju jer utječe na održivost fotosustava II i na fluidnost tilakoidne membrane klorofila (Yong i sur., 1991). Salinitet kao važan

stresor upravlja rastom i raspodjelom, te bogatstvom vrsta i veličinom stanica (Flöder i sur., 2010; Larson i Belovsky, 2013). Morske vrste mikroalga pretežito su osmokonformeri s različitim adaptacijskim mehanizmima koji održavaju promjene staničnog ionskog sadržaja i proizvodnju odgovarajućih osmolita. Stoga se kao odgovor na promjene temperature i saliniteta sastav i sadržaj unutarstaničnih lipida, proteina i polisaharida mikroalga također može mijenjati (Converti i sur., 2009). Primjerice, povišen salinitet povećava koncentraciju zasićenih masnih kiselina te sadržaj lipida 60 do 70% kod vrste *Dunaliella tertiolecta* (Takagi i sur., 2006; Xu i Beardall, 1997). U povoljnim uvjetima rasta mikroalge prvenstveno proizvode polarne lipide (npr. glikolipide i fosfolipide) koji obogaćuju kloroplaste i stanične membrane. Međutim, u nepovoljnim uvjetima rasta mikroalge nakupljaju neutralne lipide u lipidnim kapljicama u citoplazmi, kao što je zabilježeno kod dijatomeje *Phaeodactylum tricornutum* (Minhas i sur., 2016). Mikroalge su u eufotičkoj zoni podvrgnute velikim fluktuacijama svjetlosti. Stratifikacija površine oceana zbog klimatskih promjena dodatno pojačava svjetlosni stres na mikroalge. Perturbacije u intenzitetu svjetlosti mogu biti štetne za fotosintezu i posljedično utjecati na produktivnost zajednica mikroalga. Povećanjem intenziteta svjetlosti dolazi do promjene u udjelu klorofila i fikobiliproteina u stanicama (Norici i sur., 2011). Nadalje, limitacija nutrijentima dovodi do usporavanja rasta i diobe stanica, čime stanice eliminiraju potrebu za hranjivim tvarima za sintezu novih membranskih spojeva. Stoga, kao odgovor na smanjene koncentracije nutrijenata u okolišu, stanice talože masne kiseline. Dušik je esencijalni makronutrijent za rast mikroalgi i igra važnu ulogu u sintezi proteina, lipida i ugljikohidrata (Yodsuwan i sur., 2017). Općenito, koncentracija dušika značajno utječe na rast mikroalgi i njihov biokemijski sastav, a smanjenje dušika u hranjivom mediju uzrokuje smanjenje rasta uz istodobno povećanje produkcije lipida (Van Vooren i sur., 2012). Na temelju navedenih adaptacijskih odgovora mikroalga na uvjete stresa, mikroalge se sve češće koriste u procjeni ekološkog stanja vodenih ekosustava, te su u međunarodnim smjernicama preporučene kao modelni organizmi.

1.2. Biotehnološki potencijal mikroalga

Osim ekološke važnosti, mikroalge imaju važan biotehnološki potencijal za proizvodnju biološki važnih spojeva (Moreno García i sur., 2017; Vignesh i Barik, 2019). Razvojem društva dolazi do sve veće potrebe za raznolikom prehranom, novim i funkcionalnim farmaceuticima, prirodnom kozmetikom, očuvanjem okoliša i održivim izvorima energije (Rotter i sur., 2021). Naprednim biotehnološkim postupcima i procesima omogućeno je iskorištavanje jednog od najvrjednijih i obnovljivih morskih resursa, mikroalga, u smislu ekstrakcije, izolacije i identifikacije važnih spojeva za primjenu u različitim sektorima (Rotter i sur., 2021).

Zbog svog sastava mikroalge se smatraju perspektivnom sirovinom za industriju hrane, te se istražuju kao izvor hranjivih tvari već više od šest desetljeća (Spolaore i sur., 2006; Novoveská i sur. 2019). Mikroalge se sve češće koriste kao dodaci prehrani i nutraceutici jer sadrže vitamine i esencijalne elemente kao što su kalij, cink, jod, selen, željezo, mangan, bakar, fosfor, natrij, dušik, magnezij, kobalt, molibden, sumpor i kalcij. Alge su također bogate esencijalnim aminokiselinama i omega 6 i omega 3 masnim kiselinama (Simoons, 1990; West i Zubeck, 2012). Uz sve navedeno, mikroalge iz rodova *Chlorella* i *Spirulina* se zahvaljujući velikom udjelu proteina u stanici koriste i kao hrana za astronaute na svemirskim postajama (Niederwieser i sur., 2019).

Biološki aktivne molekule izolirane iz mikroalga mogu svoju primjenu pronaći u farmaceutskoj industriji kao antioksidansi, te za sintezu antikancerogenih, antimikrobnih, antivirusnih i antibakterijskih lijekova. Osim same proizvodnje bioaktivnih molekula od interesa, mikroalge se sve više istražuju kao bioinspirirani nosači lijekova. Rekonstruirane membranske vezikule pripremljene osmotskim šokom alga, mogu se smatrati potencijalnim nosačem za ispitivanje procesa povezanih mikrotransportom materijala kroz membranu, budući da su unutarstanični biokemijski procesi eliminirani (Ivošević DeNardis i sur., 2020). Osim rekonstruiranih vezikula, biosilikatne frustule dijatomeja također se istražuju kao nosači lijekova zahvaljujući svojoj poroznoj strukturi (Bariana i sur., 2013). U posljednje vrijeme mikroalge su svoju primjenu pronašle i u kozmetičkoj industriji, posebice za njegu kože. Kozmetički proizvodi dobiveni iz mikroalga mogu ponuditi obećavajuće i inovativne alternative postojećoj kozmetici i potaknuti razvoj novih svojstava.

Sve veći interes za mikroalge kao obnovljivog izvora je za proizvodnju biogoriva. Industrijski uzgoj mikroalgi za proizvodnju biogoriva i bioproizvoda povećao se posljednjih

nekoliko desetljeća zbog njihove visoke fotosintetske učinkovitosti, velike proizvodnje biomase i brzog rasta (Miao i sur., 2004). Lipidi mikroalga mogu se koristiti u proizvodnji biodizela, ugljikohidrati za proizvodnju bioetanola i biovodika, a proteini za biognojivo (Raja i sur., 2013).

Mikroalge se mogu koristiti i u pročišćavanju otpadnih voda u različitim postupcima za uklanjanje koliformnih bakterija, smanjenje kemijske i biokemijske potrebe za kisikom, uklanjanje dušika ili fosfora, kao i za uklanjanje teških metala (Abdel-Raouf i sur., 2012). Korištenje mikroalga u pročišćavanju otpadnih voda omogućuje kruženje hranjivih tvari uz istovremeno smanjenje emisije stakleničkih plinova i uštedu energije (Olguín, 2012).

1.3. Mikroalge

Mikroalge su jednostanični eukariotski organizmi koji ne tvore tkiva i nastanjuju gotovo sve vodene sustave na Zemlji. Veličine su od nekoliko mikrometara do nekoliko stotina mikrometara i različitog tipa stanične organizacije; jednostanične, kolonijalne ili nitaste. Mikroalge se ne razlikuju samo po veličini, već i po svojoj ekološkoj rasprostranjenosti, staničnoj organizaciji, fotosintetskim pigmentima, strukturnim i rezervnim polisaharidima i evolucijskom podrijetlu. Termin alge (i mikroalge) uveden je kao neformalni naziv za veliku i raznoliku skupinu fotosintetskih eukariotskih organizama, različitog filogenetskog podrijetla, dok je formalni naziv Protista. Razlog tome je da se podrijetlo alga ne može pratiti do jednog zajedničkog pretka, već se smatra da su alge nastale endosimbiozom. Smatra se da su alge nastale ugradnjom prokariotske stanice fotosintetske cijanobakterije unutar stanice heterotrofnog eukariota, stvarajući dvomembranski primarni plastid, što je poznato kao primarna endosimbioza i kao rezultat ove endosimbioze nastale su zelene alge (i druge kopnene biljke), crvene alge i glaukofite. Sekundarna endosimbioza dogodila se kada su drugi heterotrofni eukarioti ugradili crvene i zelene alge unutar svoje stanice, zbog čega su nastale mnoge druge vrste alga, formirajući tri ili četiri membrane sekundarnog plastida.

Do sada je poznato da postoji od 200 000 do nekoliko milijuna vrsta mikroalga, u usporedbi s oko 250 000 vrsta biljaka (Norton i sur., 1996). Tri najbrojnija i najšire rasprostranjena razreda mikroalga u vodenim sustavima su dijatomeje (Bacillariophyceae), zelene alge (Chlorophyceae) i zlatnožute alge (Chrysophyceae). Iako biomasom male, nose važnu ekološku ulogu u vodenim sustavima. Glavni su primarni proizvođači na Zemlji odgovorni za produkciju otprilike 50% atmosferskog kisika u procesu fotosinteze (Rubio i sur., 2003). Fotosinteza je važan proces fiksacije ugljikova dioksida iz atmosfere, stakleničkog plina čija je koncentracija u konstantom rastu zbog sagorijevanja fosilnih goriva (Falkowski i sur., 1998). Mikroalge imaju veliku učinkovitost pretvorbe sunčeve energiju u kemijsku energiju pohranjenu u ugljikohidratima, tako tvoreći bazu hranidbenog lanca te osiguravajući energiju za više od 70% svjetske biomase (Wiessner i sur., 1995; Gamal, 2010; Melis i Happe, 2001; Harun i sur., 2010). Važno je napomenuti da osim autotrofnog načina stvaranja energije, mikroalge mogu biti i miksotrofi, odnosno fotosintetizirati ali i hraniti se organskih tvarima iz okoliša. Nadalje, mikroalge igraju

ključnu ulogu i u protoku energije u vodenim sustavima u ciklusima hranjivih tvari, ugradnjom i preraspodjelom otopljenih organskih i anorganskih tvari (Arrigo, 2005.).

Stanice mikroalga građene su od: jezgre, Golgijevog aparata, plastida, vakuola, pirenoida, endoplazmatskog retikuluma, mitohondrija, ribosoma, te stanične membrane i stanične stijenke prisutne u nekih vrsta. Stanica mikroalge može sama za sebe provoditi životne funkcije upravo zahvaljujući strukturi koja se naziva stanična barijera.

1.3.1. Morfologija i uloga stanične barijere mikroalga

Staničnu barijeru mikroalga čine stanična membrana i izvanstanične strukture; stanična stijenka ili periplast, koji nastaju kao modifikacije ekstracelularnog matriksa. Stanična membrana ili plazmalema je debljine 4-5 nm. U osnovi, stanična membrana građena je od fosfolipidnog dvosloja u kojem se amfipatski fosfolipidi spontano organiziraju tako da hidrofobni nepolarni repovi budu sakriveni od vode, dok su hidrofilne polarne glave izložene polarnom mediju tj. međusobno djeluju s unutarstaničnom (citosolnom) i izvanstaničnom stranom rezultirajućeg dvosloja. Osim lipida, membrana također sadrži proteine, uključujući integralne proteine, položene kroz membranu, koji služe kao membranski transporteri, te periferne proteine na vanjskoj strani stanične membrane. Opisani raspored proteina u membrani može se mijenjati ovisno o potrebama stanice (Zeno i sur., 2020). Šećerne komponente prisutne su samo na vanjskoj površini stanične membrane i povezane su s proteinima ili lipidima, tvoreći glikoproteine, odnosno glikolipide. Membrana je do određene mjere fluidna zbog slabih veza između molekula koje grade membranu, što proteinima u vrijeme obavljanja funkcije omogućuje „klizanje" kroz fosfolipidni dvosloj i promjenu položaja u membrani. S obzirom na sastav, veći relativni udio zasićenih masnih kiselina smanjuje fluidnost membrane čineći ju tako krućom, dok s povećanjem relativnog udjela nezasićenih masnih kiselina membrana postaje fluidnija. Molekule kolesterola također se nalaze u staničnoj membrani. Kolesterol pomaže u regulaciji krutosti membrane, dok lipidi imaju ulogu u staničnom signaliziranju i staničnom prepoznavanju.

Na staničnu membranu pričvršćuju se izvanstanične strukture (stanična stijenka ili različite modifikacije periplasta), te unutarstanične mreže proteinskih vlakana koji čine citoskelet, a zaslužni su za održavanje oblika stanice, pokretljivost cijele stanice, te stanično dijeljenje (Zeno i sur., 2020). Morfologija i oblik izvanstaničnih struktura ovise o načinu života i funkciji stanice. Neke vrste alga posjeduju staničnu stijenku koja se nalazi s vanjske strane stanične membrane, a

najčešće je građena od mikrofibrila celuloze, uklopljenih u amorfni matriks polisaharida, lipida i proteina (slika 1a). U vrsta čije stanice nemaju staničnu stijenku, na vanjskoj ili unutrašnjoj strani plazmaleme može se naći periplast, struktura slična staničnoj stijenci koju čine plazmatski ili amorfni slojevi nejednake gustoće (slika 1b). Periplast mikroalga pojavljuje se u različitim oblicima; uključujući višeslojne ljuske, visoko mineralizirane organske ljušture i glikoproteinske ovojnice (Domozych, 2012). Poznate su mnoge modifikacije periplasta specifične za određene taksonomske skupine: pelikula (euglednoidi flagelati), amfijezma (dinoflagelati), lorika, frustula (dijatomeje), kokoliti (kokolitoforidi).

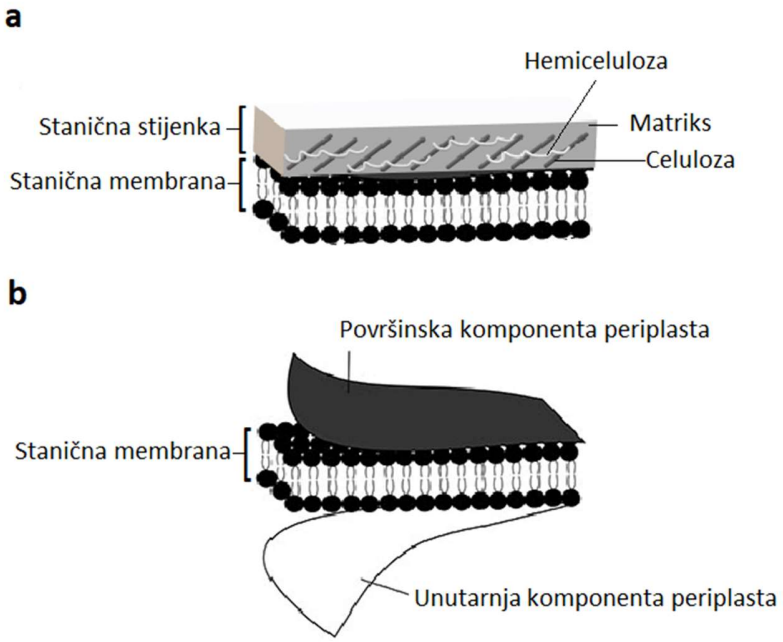

Slika 1. Pojednostavljen prikaz morfologije staničnih barijera mikroalga **a)** stanična stijenka sa staničnom membranom i **b)** periplast sa staničnom membranom (preuzeto i prilagođeno iz Gonçalves i Figueredo, 2020.).

Stanična barijera mikroalga fizički odvaja intracelularnu komponentu stanice od ekstracelularnog okruženja i tako štiti stanicu od direktnog utjecaja vanjskog okoliša (Goñi, 2014; Zeno i sur., 2020). Stanična barijera mikroalga sudjeluje u važnim staničnim procesima kao što su adhezija, fuzija, vezikularni prijenos, agregacija, komunikacija s drugim stanicama i stanični

odgovori na okolišni stres. Trenutno razumijevanje nastanka staničnih barijera mikroalga nije ni približno tako dobro istraženo kao kod kopnenih biljaka. Nedavna istraživanja, posebno ona koja koriste napredne alate molekularne biologije, biokemije, stanične biologije, imunologije i metodologije visoke propusnosti kao što je kemijska genomika (Mravec i sur., 2014.; Sørensen i sur., 2011.; Michel i sur., 2010) daju vrijedan uvid u mehanizam nastanka stanične barijere mikroalga. Za nastanak stanične barijere potrebne su vremensko-prostorno usklađene aktivnosti endomembranskog sustava i citoskeletne mreže. Razvoj površinskih metoda, kao što su skenirajuća elektronska mikroskopija (eng. *Scanning Electron Microscopy*, SEM) i mikroskopija atomskih sila (eng. *Atomic Force Microscopy*, AFM) omogućio je detaljniji uvid u strukturu staničnih barijera mikroalga. Mikroarhitektura staničnih barijera alga nije samo složena, već je i dinamična u vremenu i prostoru. Mikrofilamenti u njima se stvaraju, ugrađuju i međusobno povezuju u precizne mreže koje su regulirane genetskim i okolišnim čimbenicima.

1.3.2. Površinska svojstva mikroalga

Stanična barijera predstavlja biomeđupovršinu koja štiti stanicu te preko koje se odvijaju kompleksni procesi. Svojstva biomeđupovršine ovise o građi stanične barijere i uvjetima u okolišu (pH, temperatura, salinitet, prisutnosti biotoksičnih tvari, organskih molekula itd.) (Hadjoudja i sur., 2010). Svojstva biomeđupovršine upravljaju fundamentalnim staničnim procesima kao što su adhezija, fuzija, vezikularni prijenos, agregacija, te su odgovorna za sudbinu stanice, određivanju njene uloge i niše u morskom ekosustavu. Neka od najvažnijih površinskih svojstva stanica su površinski naboj, hidrofobnost, hidrofilnost, elastičnost, te viskoelastičnost. Hidrofobnost, kao važno površinsko svojstvo, ima glavnu ulogu u stvaranju biofilma, agregaciji i prianjanju stanica na površinu (Donlan, 2002). Upravo je zato poznavanje površinskih svojstava stanica mikroalga od biotehnološke važnosti za njihov uzgoj u fotobioreaktorima (Ozkan i Berberoglu, 2013, Gonçalves i sur., 2015; Rotter i sur., 2021.). Finim ugađanjem specifičnih uvjeta rasta mikroalga može se izbjeći njihovo obrastanje po stijenkama bioreaktora (Ozkan i Berberoglu, 2013; Gonçalves i sur., 2015). Također, za efikasnu eksploataciju biološki važnih spojeva mikroalga postupkom elektroporacije odabir parametara električnog polja ovisi upravo o površinskih svojstvima stanice (Brennan i Owende, 2010; Kotnik i sur., 2015).

Različite površinske tehnike (elektroforetska pokretljivost, uređaji za mjerenje površinskih

sila) pridonijele su važnim spoznajama o fizikalno-kemijskim svojstvima stanica (uglavnom životinjskih i bakterijskih) u smislu površinskog naboja, površinska napetosti, hidrofobnosti, hidrofilnosti, elastičnost, te viskoelastičnosti (Israelachvili, 2011). Međutim, takve su metode rijetko korištene za karakterizaciju stanica alga, te su malobrojne studije o površinskim svojstvima stanica alga prisutne u znanstvenoj literaturi. Također, još uvijek nema analitičkih metoda za izravno i jednostavno određivanje površinskih svojstava stanica bez postavljanja pretpostavki (npr. stanica sfernog oblika, primjena pojednostavljenih matematičkih modela).

Ipak, u zadnjih desetak godina prepoznata je važnost karakterizacije teško dostupnih površinskih svojstava mikroalga za različite znanstveno-istraživačke i biotehnološke svrhe, te je njihovo istraživanje u porastu. Pletikapić i suradnici su 2012. godine okarakterizirali nanomehanička svojstva (elastičnost i deformaciju) staničnog zida morske dijatomeje *C. closterium* koristeći mikroskopiju atomskih sila. Slabije silificirani dijelovi pojasa i valva stanica *C. closterium*, imali su najmanji Youngov modul elastičnosti i najvišu vrijednosti deformacije, dok su jače silificirani dijelovi pojasa imali veći Youngov modul elastičnosti i nižu vrijednost deformacije. Razlog ovakvim rezultatima je u građi morfološki različitih dijelova stanica, što je potvrđeno tretmanom sumpornom kiselinom. Na temelju rezultata, predložen je model organizacije ljušturice stanice *C. closterium* u kojem su silikatne nanočestice uklopljene u organski matriks valve. Takva organizacija valve i pojasa kućice omogućuje visoku fleksibilnost potrebnu za pokretanje stanice i njenu adaptaciju na promjene u okolišu zadržavajući integritet stanice (Pletikapić i sur., 2012). Drugim riječima, nanomehanička svojstva stanične barijere mikroalga uvjetovana su morfologijom stanica i uvjetima u okolišu, što je pokazano i u drugim istraživanjima mikroskopijom atomskih sila. Formosa-Dague i suradnici 2018. godine pokazali su da se elastičnost stanične barijere dijatomeje *Phaeodactylum tricornutum* mijenja ovisno o pH okolnog medija. Youngov modul stanica *P. tricornutum* uzgajanih pri pH 10, bio je sedam puta veći od onog izmjerenog kod stanica uzgajanih na pH 8. Ista je promjena u površinskim svojstvima uočena i u stanica vrste *Chlorella vulgaris*, slatkovodne zelene mikroalge, gdje je povećanje pH sa 6 na 8 rezultiralo trostrukim povećanjem čvrstoće stanične barijere. Nadalje, u nedavnom istraživanju su po prvi puta određena teško dostupna mehanička svojstva biflagelatne mikroalge *D. tertiolecta* u dvije faze rasta (eksponencijalnoj i stacionarnoj) (Pillet i sur., 2019). Pokazano je da stanice vrste *D. tertiolecta* starenjem gube čvrstoću i postaju hidrofilnije, što upućuje na molekularnu modifikaciju stanične ovojnice tijekom starenja, pri čemu dolazi do brže dinamike adhezije stanica

na nabijenoj međupovršini. Ozkan i Berberoglu su 2013. ispitali međudjelovanje stanica-supstrat i stanica-stanica različitih vrsta mikroalga s ciljem dobivanja boljeg uvida u mehanizme interakcije te moguće biotehnološke primjene; prevenciju bioobraštanja fotobioreaktora i drugih umjetnih površina, poticanje stvaranja biofilma u fotobioreaktorima biofilma alga i razvoj strategije bioflokulacije za energetski učinkovito prikupljanje biomase alga. Istraživane hidrofobne vrste potvrđene su kao izvrsni kandidati za formiranje biofilma zbog svojih jakih privlačne interakcije između stanica i supstrata i stanica na stanicu, dok su se istraživane hidrofilne vrste pokazale kao idealni kandidati za smanjenje biološkog obraštanja u vodenim sustavima. U istraživanju nanoadhezivnih svojstva mikroalga također se koristi mikroskopija atomskih sila, posebice za istraživanje stanica dijatomeja i njihovih izlučenih biopolimera (Gebeshuber i sur., 2002; Higgins i sur., 2002).

1.3.3. Modelne mikroalge

U ovom radu odabrane su modelne stanice mikroalga koje se razlikuju u morfologiji stanica, građi stanične barijere, pokretljivosti i toleranciji na promjene u okolišu.

Prva odabrana vrsta je zelena flagelatna alga *D. tertiolecta* Butcher (CCMP 1320, Culture Collection Bigelow Laboratory for Ocean Sciences, Bigelow, MN, USA), široko rasprostranjena u vodenim ekosustavima zbog tolerancije na širok raspon saliniteta, intenziteta svjetlosti i temperature. Stanice vrste *D. tertiolecta* su radijalno simetrične, elipsoidne ili ovalne, duljine 5-18 μm, širine 4,5-14,0 μm, kao što je prikazano na slici 2. Vrste roda *Dunaliella* pripadaju odjelu Chlorophyta, redu Volvocales, porodici Polyblepharidaceae. *D. tertiolecta* posjeduje dva izomorfna i izokontna bića na anteriornom kraju stanice (Polle i sur., 2010). Za vrste roda *Dunaliella* značajan je izostanak čvrste stanične stijenke (Borowitzka i Siva, 2007), što je karakteristika koja ih odvaja od drugih jednostaničnih zelenih algi, zbog čega ih se često naziva i „golim bičašima“. Stanica je obavijena tankom elastičnom staničnom membranom prekrivenom periplastom u obliku glikoproteinskog omotača tzv. glikokaliks debljine 9 nm (Oren, 2005). Elastičnost membrane i nedostatak čvrste stanične stijenke omogućuju brzu promjenu volumena stanica kao odgovor na promjene u osmotskom tlaku, zbog čega su vrste roda *Dunaliella* pogodne za ispitivanje osmotskih promjena u okolišu.

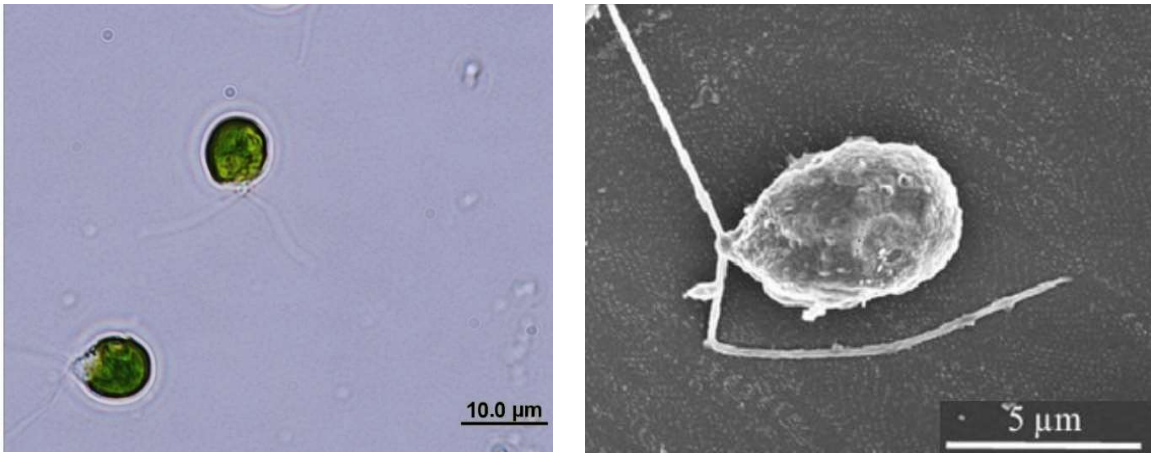

Slika 2. Stanice vrste *Dunaliella tetiolecta* u kulturi snimljene **a)** svjetlosnim mikroskopom i **b)** skenirajućim elektronskim mikroskopom (preuzeto i prilagođeno iz Malerba i sur., 2018).

Druga odabrana vrsta je morska zelena alga *T. suecica* (Kylin) Butcher (CCAP 66/22A, Collection of Algae and Protozoa, Scottish Marine Institute, Oban UK) , koja nastanjuje morske i bočate vode. Pripadnike vrste odlikuju elipsoidne ili ovalne stanice duljine 6-11 µm i širine 4-8,5 µm, kao što je prikazano na slici 3. Vrste roda *Tetraselmis* pripadaju odjelu Chlorophyta, redu Chlorodendrales, porodici Chlorodendraceae. Rod *Tetraselmis* jedinstven je među zelenim algama zbog načina stvaranja staničnog zida. Stanice su pokrivene s čvrstim staničnim pokrovom, tzv. tekom, koji nastaje ekstracelularnom fuzijom ljuskica koje se sintetiziraju unutar stanice (u Golijevom aparatu) i sekrecijskim vezikulama izlučuju van (Martignier i sur., 2018). Ispod teke vrste roda *Tetraselmis* ugrađuju mineralne inkluzije biogenog kalcita zvane mikroperle. Mikroperle nisu nasumično raspoređene unutar stanica, već čine određeni uzorak, koji se razlikuje od vrste do vrste. Stanice *T. suecica* su pokretne i posjeduju četiri biča jednake duljine, smještena na apikalnoj strani stanice, koji su također pokriveni ljuskicama.

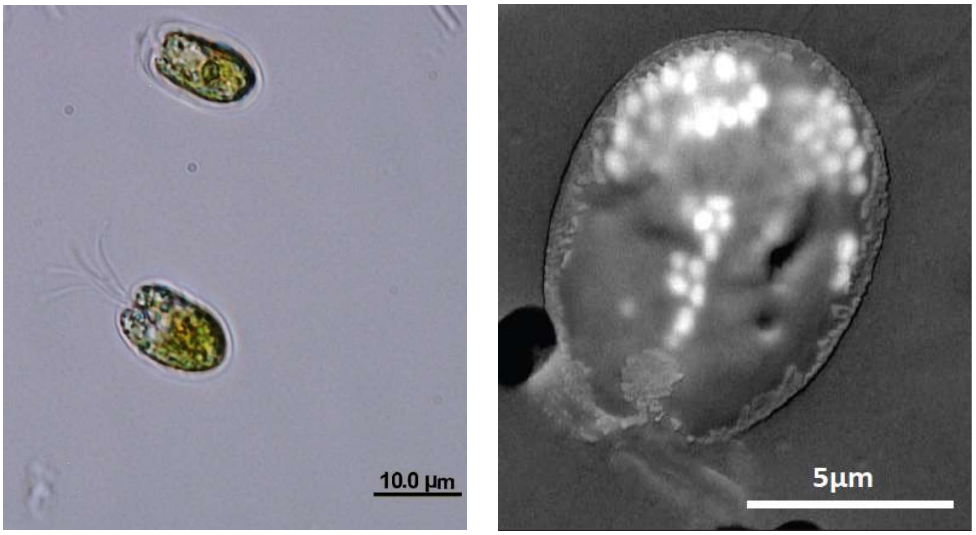

Slika 3. Stanice vrste *Tetraselmis suecica* u kulturi snimljene **a)** svjetlosnim mikroskopom i **b)** skenirajućim elektronskim mikroskopom (preuzeto i prilagođeno iz Martignier i sur., 2018).

Treća odabrana vrsta je morska bentička alga kremenjašica *C. closterium* (Ehrenberg) Reimann & J. Lewin (CCMP 1554, Culture Collection Bigelow Laboratory for Ocean Sciences, Bigelow, MN, USA). Pripadnici vrste su jednostanični organizmi, blago zakrivljenog ili sigmoidnog oblika, tankih i izduženih stanica, duljine 25-400 µm, širine 6-50 µm, kao što je prikazano na slici 4. Vrste roda *Cylindrotheca* pripadaju odjelu Bacillariophyta, redu Bacillariales, porodici Bacillariophyceae. Središte stanice je kopljastog oblika, s dva duga, tanka, savitljiva kraja. Alge kremenjašice ili dijatomeje (Bacillariophyceae) okružene su čvrstom modifikacijom periplasta nazvanim frustulom koji je izgrađen od zamršene mreže valvalnih dijelova i dijelova pojasa, a sastoji se od silicijevih struktura na organskom matriksu. Valve frustula u vrste *C. closterium* slabo su silicificirane, gotovo neperforirane, s poprečnim više ili manje transapikalnim silicificiranim dijelovima. Organski dio sastoji se od složene mreže polisaharida i različitih skupina proteina koji reguliraju sintezu frustule (Tesson i Hildebrand, 2013; Pletikapić i sur. 2012).

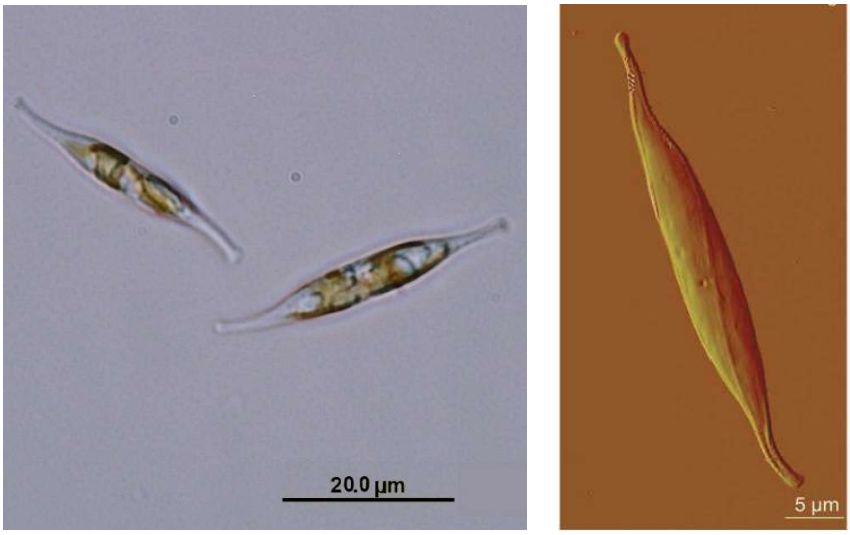

Slika 4. Stanice vrste *Cylindrotheca closterium* u kulturi snimljene **a)** svjetlosnim mikroskopom i **b)** mikroskopom atomskih sila (preuzeto i prilagođeno iz Mišić Radić i sur., 2020).

2. CILJ I HIPOTEZE ISTRAŽIVANJA

Cilj doktorskoga rada je povezati stanični odgovor mikroalga u smislu ponašanja i površinskih svojstava u odnosu na antropogeni stresor (teški metal) i abiotičke stresore (temperatura, salinitet) kako bi se bolje razumjele strategije preživljavanja i prilagodbe mikroalga u vodenim ekosustavima.

Hipoteze istraživanja:

1. ponašanje i površinska svojstva stanica mikroalga mogu se smatrati pokazateljima stresa
2. stanice u stresu mijenjaju površinska svojstva i fiziološku aktivnost
3. stanice mikroalga sa složenijom staničnom barijerom otpornije su na prisutnost stresora u vodenom okolišu

3. ZNANSTVENI RADOVI NA KOJIMA SE TEMELJI DOKTORSKI RAD

3.1. Znanstveni rad I

Novosel, N., Kasum, D., Žutinić, P., Legović, T., Ivošević DeNardis, N., 2020. Short-term effect of cadmium on the motility of three flagellated algal species. Journal of applied phycology 32: 4057–4067. https://doi.org/10.1007/s10811-020-02283-1

Journal of Applied Phycology (2020) 32:4057–4067
https://doi.org/10.1007/s10811-020-02283-1

Short-term effect of cadmium on the motility of three flagellated algal species

Nives Novosel[1] · Damir Kasum[1] · Petar Žutinić[2] · Tarzan Legović[1,3,4] · Nadica Ivošević DeNardis[1]

Received: 10 July 2020 / Revised and accepted: 23 September 2020 / Published online: 9 October 2020

Abstract

The present work aims to develop a fast and reliable procedure for motility analysis of a short-term effect of heavy metal cadmium on the algal cell response in laboratory conditions. Three unicellular motile species similar in cell length, while differing in the cell wall and the flagellar system are used as model algae. We quantitatively characterise motility in terms of swimming speed and search radius following addition of 1 mg Cd L^{-1}. Both swimming speed and search radius determined in control algal cultures reflect morphological features of the corresponding flagellated system. After 1 h of cell exposure to a toxic concentration of cadmium, a statistically significant decrease in swimming speed is determined with predominant erratic cell movement on the spot in all examined cultures. After 3 h of cell exposure to cadmium, swimming speed in most of the examined cell cultures recovered close to the control value, indicating quick cell adaptation to elevated cadmium concentration. The results support the implementation of swimming speed and search radius as motility parameters for direct screening of cell physiological state, which is applicable to ecotoxicological studies providing insight into the mechanism of cell adaptation under stress, as well as a better understanding of the spatial distribution of algal cells in aquatic systems.

Keywords Algae · Cadmium · Cell stress · Heavy metal · Motility · *Dunaliella tertiolecta* · *Rhodomonas maculata* · *Tetraselmis suecica*

Introduction

Rapid screening of algal physiological state with a reliable and easy-to-use non-taxonomic cell parameters, such as motility, is of high interest in ecology and environmental risk assessment (Lavoie et al. 2012; Pandey et al. 2014; Coquillé et al. 2015; Pandey and Bergey 2016). Motility is a fundamental property that includes many highly attuned cellular functions that enable an organism to move in a coordinated fashion. Many microorganisms use different external chemical and physical factors to direct their search toward food or a suitable niche for survival and growth (Melkonian 1992). Stressed microalgae develop different mechanisms to cope with toxicity of heavy metals like cadmium, a prominent industrial pollutant in aquatic systems. Whether a metal will act toxic is related to the cell surface interaction and intracellular accumulation (Morlon et al. 2005). The exact mechanism of how cadmium interacts with the cell still needs to be resolved. It is proposed that metals bind to cell surface ligands, enabling transport inside cells, or attach to the membrane (Scheidegger et al. 2011; Belghith et al. 2016). Debelius et al. (2009) performed a 72 h exposure toxicity tests with copper and lead on five marine microalgae: *Tetraselmis chuii*, *Rhodomonas salina*, *Chaetoceros* sp., *Isochrysis galbana* and *Nannochloropsis gaditana*. They concluded that *T. chuii* was the most tolerant to both metals, whilst *R. salina* and *I. galbana* were the most sensitive to copper exposure. They also found that the sensitivity of algal species to copper is not related to external copper binding, intracellular copper concentrations nor uptake rates. The exposure of various concentrations of Cd on two green microalgal species, *Scenedesmus obliquus* and *Desmodesmus pleiomorphus*, resulted in growth inhibition right from the lowest metal concentration tested, with strong inhibition following exposure to the highest levels (Monteiro et al. 2011). Furthermore, the long-term exposure of Cd on *Chlorella vulgaris*

✉ Tarzan Legović
legovic@irb.hr

✉ Nadica Ivošević DeNardis
ivosevic@irb.hr

[1] Ruđer Bošković Institute, Zagreb, Croatia

[2] Department of Biology, Faculty of Science, University of Zagreb, Zagreb, Croatia

[3] Libertas International University, Zagreb, Croatia

[4] OIKON - Institute for Appplied Ecology, Zagreb, Croatia

resulted in gradual decrease of cell growth and concentrations of chlorophyll *a*, chlorophyll *b* and carotenoids, as well as an increase in oxidative stress and induced antioxidant defence systems against reactive oxygen species (Cheng et al. 2016).

Various studies have examined the effect of heavy metals on algal cells using cell motility bioassays (Tanaka et al. 2005; Liu et al. 2011). Stallwitz and Häder (1994) observed that the long-term exposure to high concentrations of different heavy metals on *Euglena gracilis* affects the gravitactic orientation of cells and leads to reduction of speed. Vladimirov et al. (2004) used the laser-based tracking method for the measurement of swimming velocities of *Chlamydomonas nivalis* cells to extract quantitative motility parameters. Short- and long-term exposures of *Euglena* to copper were studied in terms of motility and photosynthetic activity (Ahmed and Häder 2010). Zheng et al. (2014) developed phytoplankton motility sensor integrated into a microfluidic chip for toxicity assessment of several heavy metals to access dose-dependent inhibition. A reduction of the swimming velocity and an increase in the variance was indicated (Mayali et al. 2008). However, a lack of sufficient data precluded the statistical significance (Danilov and Ekelund 2001; Liu et al. 2011). Recently, we reported that green alga *Dunaliella tertiolecta* survived long-term exposure to cadmium by sustaining healthy photosynthetic apparatus through an expression of membrane proteins and carotenoid production, increased physiological activity and cell stiffness, but with slower motility (Ivošević DeNardis et al. 2019). Concurrently, the accumulation of cadmium in *D. tertiolecta* cells was detected by the secondary ion mass spectroscopy demonstrating the main entry pathway of toxic metal into food chains (Pavlinska et al. 2020). Cadmium can accumulate into cells up to 2000 times by replacing zinc in the active enzyme sites, accompanied by increase of respiration and decrease of photosynthesis and transpiration (Stallwitz and Häder 1994).

In continuation to the previous study, the aim is to develop a fast and reliable procedure for motility analysis of a short-term effect of cadmium on the algal cell response in laboratory conditions. We selected three algal species similar in size, while differing in the complexity of their flagellar system. The obtained results could provide insight into the mechanism of cell adaptation under stress referring to the algal physiological response to polluted aquatic environments.

Material and methods

Cell suspensions

The unicellular marine algae *Dunaliella tertiolecta* Butcher (CCMP 1320, Chlorophyceae), (Culture Collection, Bigelow Laboratory for Ocean Sciences), *Rhodomonas maculata* Butcher ex D.R.A.Hill & R.Wetherbee (CCAP 979/14, Cryptophyceae) (Culture Collection of Algae and Protozoa, Scottish Marine Institute) and *Tetraselmis suecica* (Kylin) Butcher 1959 (CCAP 66/22A, Chlorophyceae), (Culture Collection of Algae and Protozoa, Scottish Marine Institute) were cultured in seawater (38‰) enriched with F/2 medium (Guillard 1975) and kept in a water bath at 18 °C with constant shaking (15 rpm), 12:12 light: dark cycle with irradiance 31 μmol photons m^{-2} s^{-1}. The cell density of 2×10^6 cells mL^{-1} was determined on 19 days of growth. Three sample replicates were used to determine cell density in Fuchs-Rosenthal haemocytometer. The sample was fixed before counting due to pronounced cell motility. Stock solutions of $Cd(NO_3)_2$ were added to cultures on 19 days after the inoculum to reach concentrations of 1 mg L^{-1}. The selected concentration of cadmium was chosen based on the calculation of the free Cd(II) using the generalised mathematical model for the complex formation of a single ligand with several trace metals (Ivošević DeNardis et al. 2019). The cadmium concentration of 1 mg L^{-1} corresponds to the 600 μg L^{-1} of free Cd(II) which acts toxic to cells and causes the reduction in growth (Ivošević DeNardis et al. 2019). Exposure time was set to 1 and 3 h which is shorter than cells generation time. Three parallels were set to ensure the repeatability of each sample.

Motility and statistical analysis

Aliquots of cell culture placed on a glass slide and covered with coverslip were observed under Olympus BX51 microscope using a magnification of × 10. Video files of 5 s were recorded consecutively 10 times in the same sample (50–60 frames per second, image size: 340 × 250, 4 × 4 binning). Video files stored in .avi format were used as the input to Open Source Image Processing Software ICY (http://icy.bioimageanalysis.org) to analyse cells motility and their trajectories. Inside the ICY software, we used three plugins: spot tracking, track manager and motion profiler. All data were imported to Microsoft Excel (Microsoft, USA) for analysis of about 1500 cells. The ICY output is an ASCII file of row data (sample size, the spatio-temporal position of cells, number of motile and non-motile cells with the corresponding minimum and maximum, speeds, search radius and their average value). Search radius is the maximum distance from the initial point. The R software package (R Core Team 2020) was utilised to perform additional statistical analyses on data from the motion profiler, which included box plots, plots of probability distribution of speed and search radius, Shapiro and Wilcoxon-Mann-Whitney tests.

Results

Dunaliella tertiolecta

Figure 1 provides a qualitative insight of *D. tertiolecta* cells movement before and after exposure to cadmium.

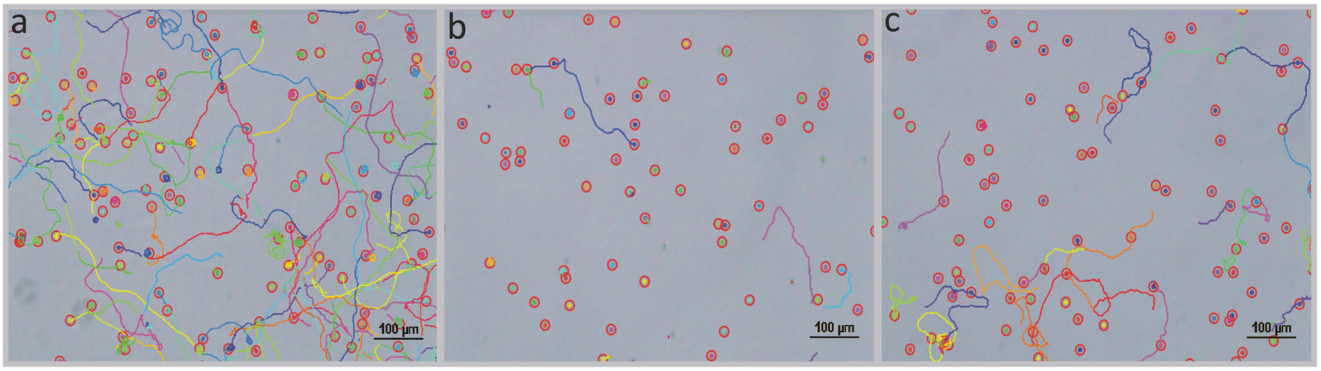

Fig. 1 Reconstructed ICY images of *D. tertiolecta* cells before (**a**), and after exposure time of 1 h (**b**) and 3 h to cadmium (**c**). Distance bar denotes 100 µm. Cell and its trajectory are denoted with a coloured circle and curved coloured line, respectively

A total of 264 cells were counted in the control sample of *D. tertiolecta*, of which 72% demonstrated random movement depicted with line type of trajectories (Fig. 1a). After a 1 h exposure time to Cd, 83% of cells still retained flagella but exhibited erratic on-the-spot movement (Fig. 1b), whilst only a few trajectories were noted. After 3 h of exposure, 38% of cells showed a restored movement, although with shorter trajectories (Fig. 1c). Box plots of swimming speed and search radius with corresponding probability density distributions over tested exposure time to Cd for *D. tertiolecta* are shown in Fig. 2.

In the control sample *D. tertiolecta* cells were moving with an average speed of 71.83 ± 1.84 µm s^{-1} which is close to 8 body lengths per second. The maximum speed, as shown in the probability density distribution (Fig. 2), was slightly exceeding 100 µm s^{-1}. The Shapiro test confirmed that the data are not normally distributed. After the exposure time of 1 h, the average cell speed dropped to 36.45 ± 1.77 µm s^{-1} (the distributions differ significantly, $W = 28{,}829$, $p < 2.2\text{e-}16$). Although most of the observed cells displayed the slower speed pattern, about 17% of cells retained the speed between 50 and 108 µm s^{-1}. After the exposure time of 3 h, the average speed increased to

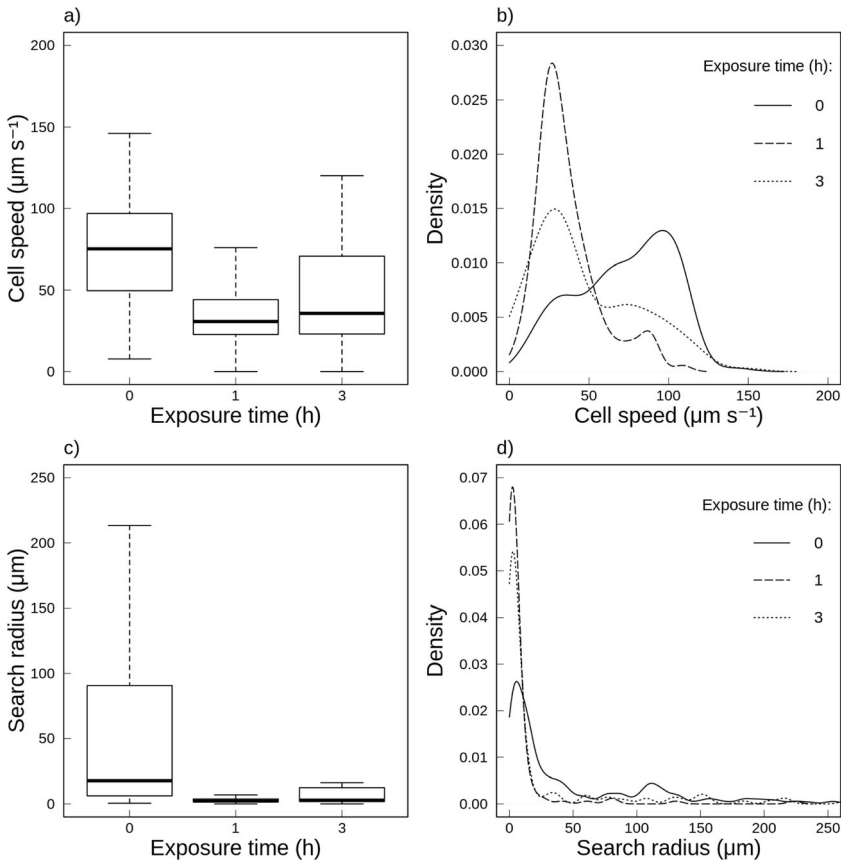

Fig. 2 Box plot of swimming speed of *D. tertiolecta* cells before and after exposure to cadmium (**a**); probability density distribution of swimming speed (**b**); box plot of the search radius (**c**) and probability density distribution of the search radius (**d**). The box plots show the median (thick horizontal line); the first and the third quartile (edges of the box) and the interquartile range of the data (whiskers). Distributions of swimming speed after 1 h and 3 h exposure differ significantly from the control

47.24 ± 2.95 μm s^{-1} (there is a significant difference with regard to the control: $W = 23{,}755$, $p = 7.8$ e-12).

As seen from the probability density distribution of speeds, there was a significant proportion of cells (ca. 40%) which have restored their speed between 50 and 147 μm s^{-1}.

In the control sample, the average search radius of *D. tertiolecta* cells was 57.43 ± 4.76 μm, while the median was 17.83 μm. The probability density distribution graph (Fig. 2) also revealed a higher number of cells with a small search radius of about 30 μm and a few cells with a very large search radius. The observed pattern of cell movement did not conform to a straight line, but made up to 12 turns moving either back and forth, in circles or narrow spirals. However, there was about 14% of cells with the search radius of nearly 120 μm. Given their average speed during 5 s, these cells made about two turns.

After the exposure time of 1 h, the average search radius of cells dropped to 8.04 ± 2.14 μm, which was close to average cell length. As shown in the probability density distribution (Fig. 2), there was virtually no cell which kept the search radius near the one recorded in the control sample. Instead, most of the cells showed very little movement, mostly spiralling around the initial point. After the exposure time of 3 h, the average search radius increased to 26.68 ± 4.80 μm. However, the greatest number of cells did not recover their initial search radius.

Rhodomonas maculata

We have done extensive search for studies dealing with the impact of cadmium on the cell motility of genus *Rhodomonas*, and such results, to the best of our knowledge, are not reported in the literature. Herein, we provide qualitative and quantitative insight in *R. maculata* cells movement before and after exposure to cadmium (Fig. 3).

In the control sample, the cells showed vigorous movement with the zig-zag pattern trajectories. However, after a 1 h exposure time, nearly all cells either did not move or exhibited oscillatory movement about a fixed point. After a 3 h exposure, a large proportion of cells were active again, although with a smaller search radius. Box plots of swimming speed and search radius with the corresponding probability density distributions over tested exposure time to Cd for *R.* maculata are shown in Fig. 4.

From a total of 208 cells of *R. maculata* detected in the control sample, 86% were motile with an average speed of 55.03 ± 1.53 μm s^{-1}, or about 7 body lengths per second. As shown in the probability density distribution (Fig. 4), the maximum number of cells moved in a speed range between 40 and 80 μm s^{-1}. After the exposure time of 1 h, average cell speed dropped to 29.97 ± 1.37 μm s^{-1} (the distributions differ significantly, $W = 20{,}026$, $p < 2.2$e-16).

The highest number of cells maintained speed in the range from 20 to 50 μm s^{-1}. After the exposure time of 3 h most of the cells maintained the average speed, which increased to 54.36 ± 1.36 μm s^{-1} (there is no significant difference with regard to the control: $W = 18{,}950$, $p = 0.7964$).

The average search radius of *R. maculata* cells in the control sample was 65.54 ± 4.33 μm, with the median search radius of 49.20 μm. As shown in the probability density distribution (Fig. 4), the search radius of most cells ranged between 50 and 130 μm. These cells did not display a linear movement, but rather a random back and forth motion, crossing about 2 to 4 turns in circles or spirals. However, the search radius of about 20% cells exceeded 150 μm. Given their average speed during 5 s, these cells made about one to two turns. After the exposure time of 1 h, the average search radius of cells dropped to 3.42 ± 0.44 μm. As shown in the probability density distribution (Fig. 4), most of the cells did not move, whilst the search radius of the few cells that moved was below 33 μm. After the exposure time of 3 h, the average search radius increased to 52.22 ± 4.24 μm. The probability density distribution is close to the one in the control, except for a somewhat higher number of cells which demonstrated slow movement and the smaller search radius obtained by the fastest thriving cells.

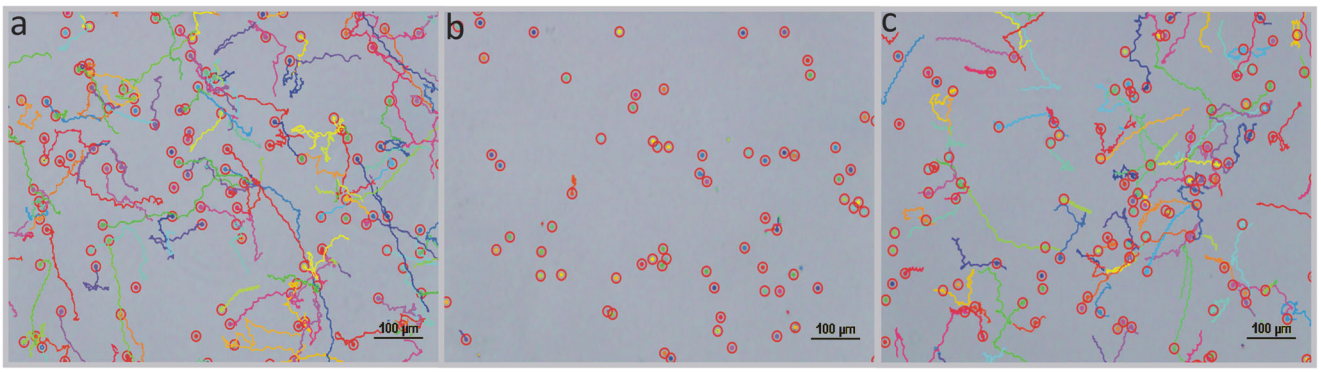

Fig. 3 Reconstructed ICY images of *R. maculata* before (**a**), after exposure time of 1 h (**b**) and 3 h to cadmium (**c**). Distance bar denotes 100 μm. Cell and its trajectory are denoted with coloured circle and curved coloured line, respectively

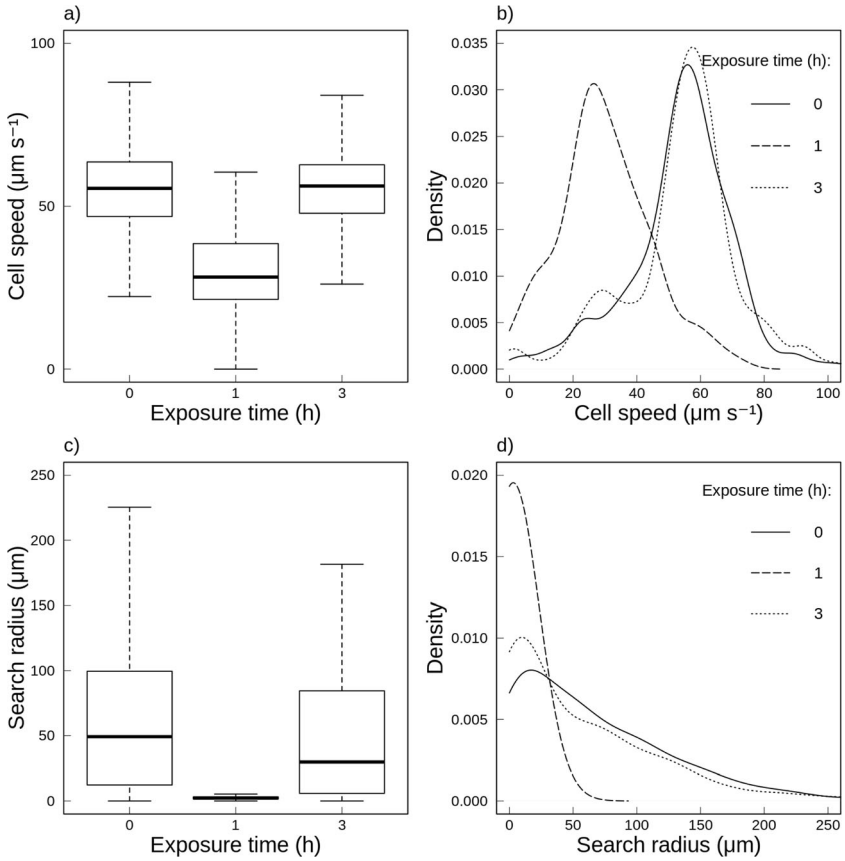

Fig. 4 Box plot of swimming speed of *R. maculata* cells before and after exposure to cadmium (**a**); probability density distribution of swimming speed (**b**); box plot of the search radius (**c**) and probability density distribution of the search radius (**d**). The box plots show the median (thick horizontal line); the first and the third quartile (edges of the box) and the interquartile range of the data (whiskers). The distribution of swimming speed after 1 h differs significantly from the control while the distribution after 3 h exposure does not

Tetraselmis suecica

Qualitative indication of *T. suecica* cells movement in the control sample after a 1 h and 3 h exposure to Cd is shown in Fig. 5.

Compared to *D. tertiolecta* and *R. maculata,* the cells of *T. suecica* in the control sample showed more vigorous movement and the cell trajectories did not deviate much from the straight line. However, after a 1 h exposure time, most of the cells did not move or showed very little movement. In addition, their trajectory lengths were much shorter, showing similar behaviour as *D. tertiolecta* and *R. maculata*. After a 3 h exposure, a large proportion of cells were again moving, with the observed increase in their trajectories by more than half of the control sample. Box plots of swimming speed and search radius with corresponding probability density distributions are shown in Fig. 6.

Based on analysis of 257 cells in the control sample of *T. suecica* cells, 94% of cells in the population displayed pronounced motility, moving with an average speed of 190.10 ± 5.26 μm s^{-1}, which correspond to about 22 body lengths per second. As shown in the probability density distribution, high number of cells moved with a speed between 150 and 350 μm s^{-1}. The velocity of remaining cells ranged from 30 to 150 μm

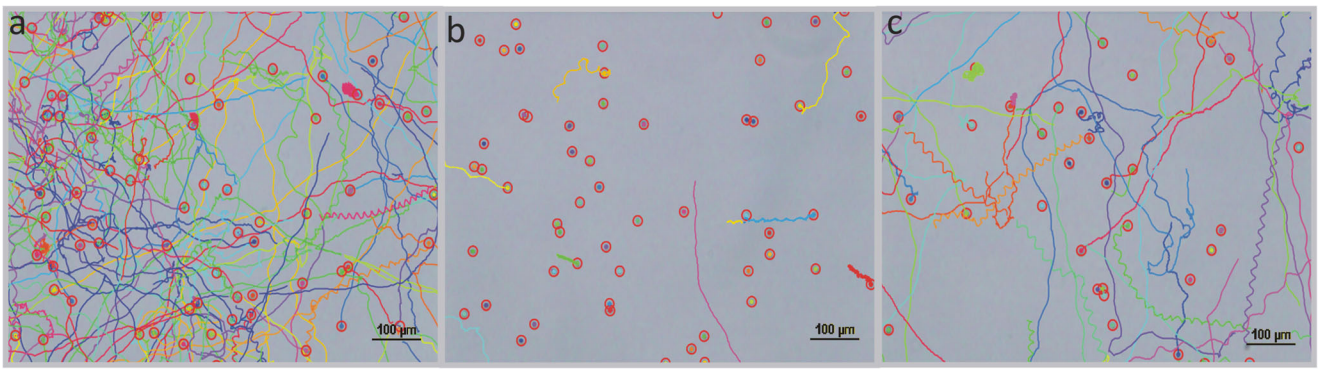

Fig. 5 Reconstructed ICY images of *T. suecica* before (**a**), and after exposure to cadmium for 1 h (**b**) and 3 h (**c**). Distance bar denotes 100 μm. Cell and its trajectory are denoted with coloured circle and curved coloured line, respectively

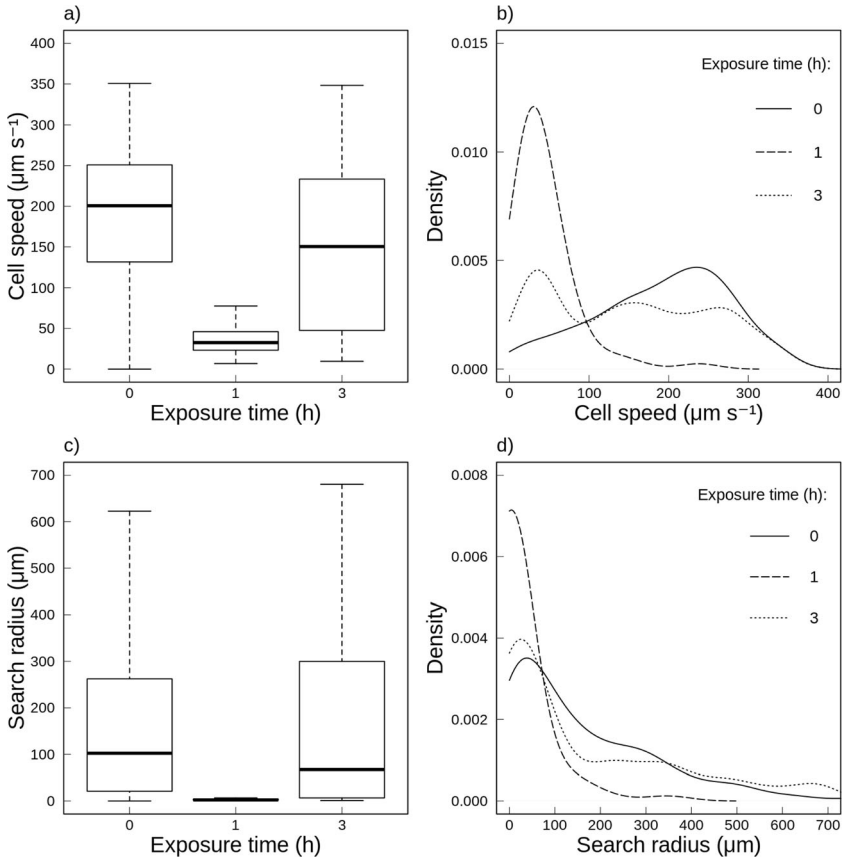

Fig. 6 Box plot of swimming speed of *T. suecica* cells before and after exposure to cadmium (**a**); probability density distribution of swimming speed (**b**); box plot of the search radius (**c**) and probability density distribution of the search radius (**d**). The box plots show the median (thick horizontal line); the first and the third quartile (edges of the box) and the interquartile range of the data (whiskers). Distributions of swimming speed after 1h and 3 h exposure differ significantly from the control

s^{-1}. After the exposure time of 1 h, the average cell speed dropped nearly four times, i.e. to 42.54 ± 4.63 μm s^{-1} (the distributions differ significantly, W = 15,463, p < 2.2e-16). The highest number of cells maintained the speed below 80 μm s^{-1}. After the exposure time of 3 h, the average cell speed increased to 151.42 ± 11.10 μm s^{-1} (there is a significant difference with regard to the control: W = 13,072, p = 0.01995). As shown in the probability density distribution, speed of cells is almost equally distributed between 100 and 300 μm s^{-1}.

The average search radius of *T. suecica* cells in the control sample was 163.16 ± 10.77 μm. Since the search radius median was 102.25 μm, most cells move slower than the average. The highest single density found was around 50 μm. Given their average speed during 5 s, these cells made at least 20 turns. A high number of cells had the search radius between 200 and 800 μm, showing almost linear movement. The remaining cells displayed nearly spiral moving patterns of up to four turns. After the exposure time of 1 h, average cell search radius dropped to 20.95 ± 7.13 μm. As shown in the probability density distribution (Fig. 6), most of the cells did not move, and the search radius of the few moving cells was below 350 μm. After the exposure time of 3 h, the average search radius increased to 169.26 ± 21.99 μm, completely recovering to the value of the search radius measured in the control sample. For most of the cells, the search radius was below 200 μm, with the cells crossing a path equal to more than four turns. The proportion of cells with the search radius between 350 and 680 μm was low, but higher than in the control sample.

A comparison of Cd effects on motility parameters of three flagellated algal species

The comparison of swimming speeds of algal cells in the control sample, after a 1 h and after a 3 h exposure to Cd is presented in Table 1.

In the control sample, cells of *T. suecica* moved 2.6 times faster than *D. tertiolecta* and 3.5 faster than *R. maculata.* After 1 h of Cd exposure, the speeds of all species corresponded; hence, the strongest effect of the exposure was recorded on *T. suecica.* After 3 h of exposure to Cd, *R. maculata* cells demonstrated an almost complete speed recovery, followed by an 80% speed recovery in *T. suecica* and finally *D. tertiolecta*, whose cell speed recovered to 66% of the control sample. The search radius of algal cells in the control sample, after a 1 h and after a 3 h exposure to Cd is shown in Table 2.

The search radius of *T. suecica* cells in the control sample was 2.8 times larger than of *D. tertiolecta*, and 2.5 times the search radius of *R. maculata*. After a 1 h exposure search radius of *R. maculata* decreased 19.3 times followed by a

Table 1 The swimming speed of algal cells before and after exposure to cadmium (Q1, the first quartile; Q3, the third quartile; STD, standard deviation; SEM, standard error of the mean)

Sample and exposure time	Min (μm s^{-1})	Q1 (μm s^{-1})	Median (μm s^{-1})	Mean (μm s^{-1})	Q3 (μm s^{-1})	Max (μm s^{-1})	Sample size	STD	SEM
D. tertiolecta									
0 h	7.77	49.71	75.19	71.83	96.89	146.10	264	29.93	1.84
1 h	0.00	22.78	30.73	36.45	44.18	108.84	133	20.38	1.77
3 h	0.00	23.25	35.71	47.24	70.47	147.98	126	33.08	2.95
R. maculata									
0 h	0.00	46.84	55.48	55.03	63.62	221.09	208	22.13	1.53
1 h	0.00	21.46	28.32	29.97	38.37	71.64	112	14.55	1.37
3 h	0.00	47.84	56.20	54.36	62.75	116.00	185	18.55	1.36
T. suecica									
0 h	0.00	131.50	200.60	190.10	250.80	350.70	257	84.27	5.26
1 h	6.85	23.24	32.55	42.54	45.98	238.12	65	37.32	4.63
3 h	9.62	47.61	150.37	151.42	233.38	348.32	83	101.14	11.10

decrese of 7.8 times in *T. suecica* and 7.2 times in *D. tertiolecta*. After a 3 h exposure, the search radius of *T. suecica* recovered completely, followed by 80% in *R. maculata* and only 46% in *D. tertiolecta*.

Discussion

In contrast to essential trace metals that play an important role in cell growth, heavy metals like cadmium can have a potentially harmful impact on the algal cells (Ben-Amotz et al. 2009). Toxicity of the heavy metal does not depend on the total metal concentration but on the bioavailable fraction, i.e. free metal, which is generally not considered (Millán de Kuhn et al. 2006). The growth medium contains strong chelating agent EDTA, essential trace metals, salts, and vitamins in seawater. The preferences metals for complexing with single ligand EDTA in the growth medium depend on concentrations of metals and constants of metal-ligand formation. The mathematical model enables the calculation of metal speciation, i.e. complex vs. free metal (Ružić 1982; Van Den Berg 1982; Ivošević DeNardis et al. 2019). Without the model, which is usually neglected, a solely heavy metal impact on the cells could neither be resolved nor differentiated.

Three model species were selected based on distinct structural differences in the flagellar system, which are further

Table 2 The search radius of algal cells before and after exposure to cadmium (Q1, the first quartile; Q3, the third quartile; STD, standard deviation; SEM, standard error of the mean)

Sample and exposure time	Min (μm)	Q1 (μm)	Median (μm)	Mean (μm)	Q3 (μm)	Max (μm)	Sample size	STD	SEM
D. tertiolecta									
0 h	0.59	6.23	17.83	57.43	90.34	358.97	264	77.36	4.76
1 h	0.00	1.66	2.23	8.04	3.83	223.35	133	24.69	2.14
3 h	0.00	1.86	2.94	26.68	12.36	263.99	126	53.84	4.80
R. maculata									
0 h	0.00	12.35	49.20	65.54	99.47	315.66	208	62.49	4.33
1 h	0.00	1.63	2.24	3.42	3.11	33.33	112	4.66	0.44
3 h	0.00	5.88	29.78	52.22	84.46	266.03	185	57.65	4.24
T. suecica									
0 h	0.00	21.04	102.25	163.16	262.22	878.22	257	172.61	10.77
1 h	0.59	1.74	2.29	20.95	3.95	347.59	65	57.52	7.13
3 h	1.02	6.58	67.21	169.26	299.93	680.54	83	200.31	21.99

reflected in a specific motility pattern. *D. tertiolecta* and *T. suecica* cells show a linear type of pathway, whilst *R. maculata* exhibits a zig-zag pattern. *D. tertiolecta* has two isokont flagella emerging from the anterior pole of the cell. The flagella are usually twice as long as the cell body, directed forward, with distal ends slightly curved backward or sideways. During forward motion, the flagella perform typical ciliary beats consisting of the effective stroke where flagella move backward alongside the cell body, and the recovery stroke in which the initial position is restored by the propagation of the bends along the flagella. However, they show dissimilarity in the frequency of beating, as well as in the angle of the beating plane, thus resulting in the change in the movement direction and rotation of the cell (Schoevaert et al. 1988; Ben-Amotz and Avron 1992; Barsanti and Gualtieri 2014). *Rhodomonas maculata* has two dorsoventrally aligned flagella which emerge from the right side of a subapical depression called the vestibulum. They are usually long as the cell body, with one flagellum being somewhat longer than the other. The flagella have mastigonemes and fine hairs and are covered with tiny organic scales (Melkonian 1992; Brodie and Lewis 2007). At rest, anterior end of the cell is enveloped by both flagella as they curve backwards. When moving frontally, the flagella are directed forward along spiral shaped paths, while the cell also revolves about its longitudinal axis (John et al. 2011). *Tetraselmis suecica* has four scale-covered flagella of equal length, symmetry, and structure, positioned at the anterior side of the cell in two opposite, nearly collinear pairs (Wan and Goldstein 2016; Borowitzka 2018). The flagella show a ciliary beat, where an oar-like movement is followed by a return stroke. During forward swimming, the outer flagella of each pair show coordinated beat in a nearly planar fashion (Salisbury et al. 1981; Melkonian 1992) and cells display the transverse gallop movement analogous to horses (Wan and Goldstein 2016). Our findings support the notion that swimming velocity decreases with reduced flagellar system complexity in the following order: *T. suecica* > *D. tertiolecta* > *R. maculata*. Besides locomotory function, eukaryotic flagella also play a vital role in signalling, controlling cell motility, sensing environmental cues (mechano-, chemo-, and photo-sensing), and mediating signal transduction (Marshall 2013; Long et al. 2015). Compared to non-flagellated species like diatoms, whose gliding velocity corresponds to about 10 μm s^{-1} (Cohn and Disparti 1994) and some dinoflagellates, whose velocity can be impaired by the bacterial putative secreted proteases (Mayali et al. 2008), the studied algal cells showed rapid swimming.

On a short-time scale, algae take up metal more readily from contaminated water than from sediment (Calmano et al. 1988). Since the selected algal species lack a rigid cell wall (Becker et al. 1990; Hill 1991; Ben-Amotz et al. 2009), they are more exposed to the external stressors and, in order to survive, are forced to an immediate response by changing their life strategy. The toxicity impact of cadmium greatly depends on the age of algal cells (Gaur and Rai 2001). During the exponential growth phase, the cells of *D. tertiolecta* are stiffer and more hydrophobic than the ones in the stationary growth phase (Pillet et al. 2019). Nevertheless, the long-term exposure (19 days) of cadmium on *D. tertiolecta* cells yields adverse effects on the cell growth dynamics. Increased expression of membrane proteins, such as a chlorophyll a–b–binding protein and carbonic anhydrase, was identified in the cells of *D. tertiolecta* cells during stress with cadmium (Ivošević DeNardis et al. 2019). Those proteins play an important role in maintaining photosynthesis, thus facilitating cell biomass increase and concurrent decrease in metal toxicity (Moreno-Garrido et al. 2000). Furthermore, the adaptation response of *D. tertiolecta* is manifested through cell shape deterioration, slower motility, increase of physiological activity, and increased stiffness due to the molecular modification of plasma membrane (Ivošević DeNardis et al. 2019). There is a very limited number of reported studies on temporal recovery of algal cell motility stressed with cadmium on a short-time scale spanning a couple of hours. Liu et al. (2011) conducted an in vitro study of dose-dependent motility inhibition of *I. galbana* and *T. chuii* after a 1 h exposure to Cd concentration ranging from 3 to 975 mg L^{-1} by using computer-assisted movement tracking (ImageJ software). Motility of *I. galbana* and *T. chuii* was significantly reduced at 11.2 mg L^{-1} and 3.48 mg L^{-1}, respectively. In our study during a short-time exposure of 1 h to cadmium, severe impairment in motility behaviour of all flagellated species was detected, manifested in movement around the spot, and an abrupt decrease of swimming speed as a response to stress. The swimming speed recovery after 3 h could indicate cell adaptation response accompanied with the biosynthesis of proteins, as detected during a 3 h exposure of *Prorocentrum micans* to copper (Lage et al. 1996) and a long-term exposure of *D. tertiolecta* and *Chorella* sp. to cadmium (Carfagna et al. 2013; Ivošević DeNardis et al. 2019). When comparing the data of Liu et al. (2011) with this study, cells of *I. galbana* follow the same velocity trend as *D. tertiolecta*, while *T. chuii* and *T. suecica* cell speeds show the same trend, thus correlating with the number of flagella that cells possess. *T. chuii* was more sensitive to all tested metals than *I. galbana*, which is in accordance with results on *T. suecica* and Cd impact on its motility provided in this study. The motility of *I. galbana* was significantly reduced at 100 μmol L^{-1}, whilst the motility reduction of *T. chuii* at 10 μmol L^{-1} could be directly related to cellular respiration processes that provide energy for motility (Liu et al. 2011). In our in vitro study, *D. tertiolecta, R. maculata,* and *T. suecica* showed different sensitivities to cadmium, as well as differences in the cell speed recovery. These differences can be attributed to distinctions in ecological preferences or contrasting strategies of metal bioaccumulation and removal. On the other hand, based on the fieldwork data, the

elevated concentration of cadmium in the hot spots of the Mediterranean basin and Northern Europe were up to 6.41 μg L^{-1} (UNEP/MAP 2012). Thus, the in vitro conducted motility study on two-order higher concentrations of cadmium than those reported from the impacted environment, could contribute to a better understanding of the use of algae in the bioremediation of toxic metals for biotechnological application. *D. tertiolecta* is one of the most tolerant microalgal species to cadmium, and its growth persisted in the cultures exposed to 150 mg L^{-1} Cd (Folgar et al. 2009), while the dose that killed 50% of the microalgal population of species *T. chuii* was 5.2 mg L^{-1} Cd (Cordero et al. 2005). On the other hand, after mechanical damage induced to the flagella, the cells of *Dunaliella salina* can fully repair flagella within 180 min (Liu and Bourne 1999).

The differences in recovery of cell speed and search radius in all three species (Tables 1 and 2) presumably derives from an interplay between the outer layer morphological distinctions and several intracellular adaptations. Stark structural differences in the surface morphology of selected species are present, where *D. tertiolecta* cell is enclosed within a thin elastic plasma membrane with a mucous surface coat, *R. maculata* is covered with a multilayered scaly periplast, whilst *T. suecica* encased with a thin scale–covered theca. The surface of microalgal cells is negatively charged, thus providing binding sites for Cd to non-metallic sites such as theca plates, scales or membrane proteins (Monteiro et al. 2011). Furthermore, the suggested Cd cell uptake appears via Ca and Fe transporters (Volland et al. 2014). The intracellular sequestration of heavy metals can occur in pyrenoids, vacuoles, and lipid droplets as a highly efficient protective mechanism (Lage et al. 1996; Monteiro et al. 2011). Proteins, as the principal components of pyrenoids, could provide a binding spot for Cd on their thiol groups, as well as the starch grains around the pyrenoid which can bind Cd on the carboxyl groups (Bräutigam et al. 2011; Penen et al. 2020). Metal stress exerted on cells can stimulate a multifold increase in starch storage, thus imitating nutrient starvation conditions (Nishikawa et al. 2003). The results indicated *T. suecica* as the most sensitive species to Cd-induced short-term disruption of motility, whilst the fastest recovery was noted by *R. maculata*. Both species exhibited significant recovery with over 80% of restoration in speed and search radius recorded in the control samples. Here within, we propose possible explanations for such fast recovery of *R. maculata*. Firstly, as a mixotrophic microorganism it is able to utilise organic as well as inorganic carbon sources for self-sustainment. Since the exposure to Cd disrupts photosynthetic pathways (Faller et al. 2005) and impairs inorganic carbon intake, i.e. CO_2 fixation, both pyrenoidal Cd sequestration and accumulation of carbon from acetate in the pyrenoid are initiated (Penen et al. 2020). This accumulation of organic carbon, as an evolutionary mixotrophic trait, can thus grant advantage in surviving toxic metal pollution events (Penen et al. 2020). Secondly, the proteinaceous periplast, a sandwich-layered structure consisting of inner and surface periplast components that embrace the plasma membrane (Brett et al. 1994), represents a strong adsorbent of heavy metals with numerous functional groups which include carboxyl, hydroxyl, amino, mercapto, and phosphate groups (Das et al. 2008; Gupta and Rastogi 2009; Zhang et al. 2020). Furthermore, polyphosphate granules (Rai et al. 1981; Jensen et al. 1982) and vacuole (Silverberg 1975) also play an important role in heavy metal sequestration. Under Cd-induced stress, vacuolar compartmentalization provided biosorption in *Dunaliella bioculata*, *Skeletonema costatum*, and *Cladophora rupestris* (Heuillet et al. 1986; Nassiri et al. 1997; Zhang et al. 2019).

Conclusion

For the first time we applied a new computer-assisted open access cell tracking tool for simultaneous quantitative analysis of algal cell motility. We developed fast, reliable, and cost-effective procedure for high-throughput analysis of captured video data of several hundreds of cells, thus providing an ample material for comprehensive statistical analysis. We related the flagellar system morphology and structural features of the cell barrier with the velocity, metal tolerance, and motility of algal cells, respectively, thus providing a deeper understanding of cell adaptation mechanism. The increase in flagellar system complexity increases the swimming speed of cells and consequentially affects the trajectory shape. The experimental study revealed that cells of *D. tertiolecta, R. maculata*, and *T. suecica* show time-dependent alteration of motility behaviour under the exposure to cadmium. All selected species tolerated short-term exposure to toxic cadmium concentration, and their adaptation response was demonstrated through the quick recovery of their motility to near control values. The cells of *T. suecica*, which are encased within a thin scale–covered theca, experienced a pronounced negative effect on swimming speed and the search radius after a 1 h exposure to Cd, which could be due to the heavy metal binding to non-metallic sites such as theca plates, starch grains, and lipid droplets. Hence, this species was shown to be the most susceptible to Cd. However, after a 3 h exposure *R. maculata* cells, which are covered with a multilayered scaly periplast, demonstrated an almost complete speed recovery, while the search radius recovered to 80% of the control. *T. suecica* recovered their speed to 80% and their search radius completely. Hence, both species exhibited significant recovery. In contrast, *D. tertiolecta* cells enclosed within a thin elastic plasma membrane with a mucous surface coat recovered their speed to 65% and their search radius recovered to 46% indicating that, although this species is not the most susceptible, its recovery is the slowest of the three species.

A detailed analysis described herein facilitates the implementation of motility as the parameter for rapid and direct screening of cells physiological state applicable to fundamental cell biology, ecology, environmental risk assessment, and monitoring programmes.

Acknowledgments We thank two anonymous reviewers and the editor for a number of useful suggestions.

Funding This work is supported by the Croatian Science Foundation Project "From algal cell surface properties to stress markers for aquatic ecosystems" (IP-2018-01-5840) and the International Visegrad Grant "Algal cell biophysical properties as markers for environmental stress in aquatic systems" (No. 21720055).

References

Ahmed H, Häder D-P (2010) A fast algal bioassay for assessment of copper toxicity in water using *Euglena gracilis*. J Appl Phycol 22: 785–792

Barsanti L, Gualtieri P (2014) Algae: anatomy, biochemistry, and biotechnology, 2nd edn. CRC Press, Boca Raton

Becker D, Becker B, Satir P, Melkonian M (1990) Isolation, purification, and characterization of flagellar scales from the green flagellate *Tetraselmis striata* (Prasinophyceae). Protoplasma 156:103–112

Belghith T, Athmouni K, Bellassoued K, El Feki A, Ayadi H (2016) Physiological and biochemical response of *Dunaliella salina* to cadmium pollution. J Appl Phycol 28:991–999

Ben-Amotz A, Avron M (eds) (1992) *Dunaliella*: physiology, biochemistry, and biotechnology. CRC Press, Boca Raton

Ben-Amotz A, Polle JEW, Subba Rao DV (eds) (2009) The alga *Dunaliella*: biodiversity, physiology, genomics and biotechnology. Science Publishers, Enfield, New Hampshire

Borowitzka MA (2018) Biology of microalgae. In: Levine IA, Fleurence J (eds) Microalgae in health and disease prevention. Academic Press, Amsterdam, pp 23–72

Bräutigam A, Schaumlöffel D, Preud'homme H, Thondorf I, Wesenberg D (2011) Physiological characterization of cadmium-exposed *Chlamydomonas reinhardtii*. Plant Cell Environ 34:2071–2082

Brett SJ, Perasso L, Wetherbee R (1994) Structure and development of the cryptomonad periplast: a review. Protoplasma 181:106–122

Brodie J, Lewis J (eds) (2007) Unravelling the algae: the past, present, and future of algal systematics. CRC Press, Boca Raton

Butcher RW (1959) An introductory account of the smaller algae of British coastal waters. Part I: Introduction and Chlorophyceae. Fisheries Investigations, London, series IV 1: 1–74, 15 pls.

Calmano W, Ahlf W, Baade H, Förstner U (1988) Transfer of heavy metals from polluted sediments under changing environmental conditions. In: Astruc M, Lester JN (eds) Heavy metals in the hydrological cycle. Proceedings of the International Conference on Chemicals (Heavy Metals) in the Environment. Selper, London, pp 501–506

Carfagna S, Lanza N, Salbitani G, Basile A, Sorbo S, Vona V (2013) Physiological and morphological responses of lead or cadmium exposed *Chlorella sorokiniana* 211-8 K (Chlorophyceae). Springerplus 2:147

Cheng J, Qiu H, Chang Z, Jiang Z, Yin W (2016) The effect of cadmium on the growth and antioxidant response for freshwater algae *Chlorella vulgaris*. Springerplus 5:1290

Cohn SA, Disparti NC (1994) Environmental factors influencing diatom cell motility. J Phycol 30:818–828

Coquillé N, Jan G, Moreira A, Morin S (2015) Use of diatom motility features as endpoints of metolachlor toxicity. Aquat Toxicol 158: 202–210

Cordero J, Guevara M, Morales E, Lodeiros C (2005) Efecto de metales pesados en el crecimiento de la microalga tropical *Tetraselmis chuii* (Prasinophyceae). Rev Biol Trop 53:3–4

Danilov RA, Ekelund NGA (2001) Effects of pH on the growth rate, motility and photosynthesis in *Euglena gracilis*. Folia Microbiol 46:549–554

Das N, Vimala R, Karthika P (2008) Biosorption of heavy metals – an overview. Indian J Biotechnol 7:159–169

Debelius B, Forja JM, DelValls Á, Lubián LM (2009) Toxicity and bioaccumulation of copper and lead in five marine microalgae. Ecotoxicol Environ Saf 72:1503–1513

Faller P, Kienzler K, Krieger-Liszkay A (2005) Mechanism of Cd^{2+} toxicity: Cd^{2+} inhibits photoactivation of Photosystem II by competitive binding to the essential Ca^{2+} site. Biochim Biophys Acta Bioenerg 1706:158–164

Folgar S, Torres E, Pérez-Rama M, Cid A, Herrero C, Abalde J (2009) *Dunaliella salina* as marine microalga highly tolerant to but a poor remover of cadmium. J Hazard Mater 165:486–493

Gaur JP, Rai LC (2001) Heavy metal tolerance in algae. In: Rai LC, Gaur JP (eds) Algal adaptation to environmental stresses: physiological, biochemical and molecular mechanisms. Springer, Berlin, pp 363–388

Guillard RRL (1975) Culture of phytoplankton for feeding marine invertebrates. In: Smith WL, Chanley MH (eds) Culture of marine invertebrate animals: proceedings—1st Conference on Culture of Marine Invertebrate Animals Greenport. Springer US, Boston, pp 29–60

Gupta VK, Rastogi A (2009) Biosorption of hexavalent chromium by raw and acid-treated green alga *Oedogonium hatei* from aqueous solutions. J Hazard Mater 163:396–402

Heuillet E, Moreau A, Halpern S, Jeanne N (1986) Cadmium binding to a thiol-molecule in vacuoles of *Dunaliella bioculata* contaminated with $CdCl_2$: electron probe microanalysis. Biol Cell 58:79–86

Hill DRA (1991) A revised circumscription of *Cryptomonas* (Cryptophyceae) based on examination of Australian strains. Phycologia 30:170–188

Ivošević DeNardis N, Pečar Ilić J, Ružić I, Novosel N, Mišić Radić T, Weber A, Kasum D, Pavlinska Z, Katalin Balogh R, Hajdu B, Marček Chorvátová A, Gyurcsik B (2019) Algal cell response to laboratory-induced cadmium stress: a multimethod approach. Eur Biophys J 48:231–248

Jensen TE, Rachlin JW, Jani V, Warkentine B (1982) An x-ray energy dispersive study of cellular compartmentalization of lead and zinc in *Chlorella saccharophila* (Chlorophyta), *Navicula incerta* and *Nitzschia closterium* (Bacillariophyta). Environ Exp Bot 22:319–328

John DM, Whitton BA, Brook AJ (2011) The freshwater algal flora of the British Isles: an identification guide to freshwater and terrestrial algae, 2nd edn. Cambridge University Press, Cambridge

Lage OM, Parente AM, Vasconcelos MTSD (1996) Potential tolerance mechanisms of *Prorocentrum micans* (Dinophyceae) to sublethal levels of copper. J Phycol 32:416–423

Lavoie I, Lavoie M, Fortin C (2012) A mine of information: Benthic algal communities as biomonitors of metal contamination from abandoned tailings. Sci Total Environ 25:231–241

Liu J-g, Bourne WF (1999) Dynamic studies on flagellar regeneration in *Dunaliella salina*. Chin J Oceanol Limnol 17:200–206

Liu G, Chai X, Shao Y, Hu L, Xie Q, Wu H (2011) Toxicity of copper, lead, and cadmium on the motility of two marine microalgae *Isochrysis galbana* and *Tetraselmis chui*. J Environ Sci 2:330–335

Long H, Wang Q, Huang K (2015) Ciliary/flagellar protein ubiquitination. Cells 4:474–482

Marshall WF (2013) Cilia, Part A. Academic Press Elsevier, NY

Mayali X, Franks PJS, Tanaka Y, Azam F (2008) Bacteria-induced motility reduction in *Lingulodinium polyedrum* (Dinophyceae). J Phycol 44:923–928

Melkonian M (ed) (1992) Algal cell motility. Springer, Berlin

Millán de Kuhn R, Streb C, Breiter R, Richter P, Neesse T, Häder D-P (2006) Screening for unicellular algae as possible bioassay organisms for monitoring marine water samples. Water Res 40:2695–2703

Monteiro CM, Fonseca SC, Castro PML, Malcata FX (2011) Toxicity of cadmium and zinc on two microalgae, *Scenedesmus obliquus* and *Desmodesmus pleiomorphus*, from Northern Portugal. J Appl Phycol 23:97–103

Moreno-Garrido I, Lubián LM, Soares AMVM (2000) Influence of cellular density on determination of EC50 in microalgal growth inhibition tests. Ecotoxicol Environ Saf 47:112–116

Morlon H, Fortin C, Adam C, Garnier-Laplace J (2005) Cellular quotas and induced toxicity of selenite in the unicellular green alga *Chlamydomonas reinhardtii*. Radioprotection 40:S101–S106

Nassiri Y, Mansot JL, Wéry J, Ginsburger-Vogel T, Amiard JC (1997) Ultrastructural and electron energy loss spectroscopy studies of sequestration mechanisms of Cd and Cu in the marine diatom *Skeletonema costatum*. Arch Environ Contam Toxicol 33:147–155

Nishikawa K, Yamakoshi Y, Uemura I, Tominaga N (2003) Ultrastructural changes in *Chlamydomonas acidophila* (Chlorophyta) induced by heavy metals and polyphosphate metabolism. FEMS Microbiol Ecol 44:253–259

Pandey LK, Bergey EA (2016) Exploring the status of motility, lipid bodies, deformities and size reduction in periphytic diatom community from chronically metal (Cu, Zn) polluted waterbodies as a biomonitoring tool. Sci Total Environ 550:372–381

Pandey LK, Kumar D, Yadav A, Rai J, Gaur JP (2014) Morphological abnormalities in periphytic diatoms as a tool for biomonitoring of heavy metal pollution in a river. Ecol Indic 36:272–279

Pavlinska Z, Chorvat D, Mateasik A, Jerigova M, Velic D, Ivošević DeNardis N, Marcek Chorvatova A (2020) Fluorescence responsiveness of unicellular marine algae *Dunaliella* to stressors under laboratory conditions. J Biotechnol 6:100018

Penen F, Isaure M-P, Dobritzsch D, Castillo-Michel H, Gontier E, Le Coustumer P, Malherbe J, Schaumlöffel D (2020) Pyrenoidal sequestration of cadmium impairs carbon dioxide fixation in a microalga. Plant Cell Environ 43:479–495

Pillet F, Dague E, Pečar Ilić J, Ružić I, Rols M-P, Ivošević DeNardis N (2019) Changes in nanomechanical properties and adhesion dynamics of algal cells during their growth. Bioelectrochemistry 128:154–162

R Core Team (2020) R: A language and environment for statistical computing. R Foundation for Statistical Computing, Vienna, Austria. https://www.R-project.org/

Rai LC, Gaur JP, Kumar HD (1981) Protective effects of certain environmental factors on the toxicity of zinc, mercury, and methylmercury to *Chlorella vulgaris*. Environ Res 25:250–259

Ružić I (1982) Theoretical aspects of the direct titration of natural waters and its information yield for trace metal speciation. Anal Chim Acta 140:99–113

Salisbury JL, Swanson JA, Floyd GL, Hall R, Maihle NJ (1981) Ultrastructure of the flagellar apparatus of the green alga *Tetraselmis subcordiformis*. Protoplasma 107:1–11

Scheidegger C, Behra R, Sigg L (2011) Phytochelatin formation kinetics and toxic effects in the freshwater alga *Chlamydomonas reinhardtii* upon short- and long-term exposure to lead (II). Aquat Toxicol 101:423–429

Schoevaert D, Krishnaswamy S, Couturier M, Marano F (1988) Ciliary beat and cell motility of *Dunaliella*: computer analysis of high speed microcinematography. Biol Cell 62:229–240

Silverberg BA (1975) Ultrastructural localization of lead in *Stigeoclonium tenue* (Chlorophyceae, Ulotrichales) as demonstrated by cytochemical and X-ray microanalysis. Phycologia 14:265–274

Stallwitz E, Häder D-P (1994) Effects of heavy metals on motility and gravitactic orientation of the flagellate, *Euglena gracilis*. Eur J Protistol 30:18–24

Tanaka H, Nishimura O, Nakamura S, Sudo R (2005) Effect of alkylphenols on motility of *Chlamydomonas reinhardtii* and crustacea *Daphnia magna*. J Jpn Soc Water Environ 28:333–338

UNEP/MAP (2012) State of the Mediterranean Marine and Coastal Environment, UNEP/MAP – Barcelona Convention. United Nations Environment Programme/Mediterranean Action Plan (UNEP/MAP), Technical Report, Athens

Van Den Berg CMG (1982) Determination of copper complexation with natural organic ligands in seawater by equilibration with MnO_2 I. Mar Chem 11:307–322

Vladimirov VA, Wu MS, Pedley TJ, Denissenko PV, Zakhidova SG (2004) Measurement of cell velocity distributions in populations of motile algae. J Exp Biol 207:1203–1216

Volland S, Bayer E, Baumgartner V, Andosch A, Lütz C, Sima E, Lütz-Meindl U (2014) Rescue of heavy metal effects on cell physiology of the algal model system *Micrasterias* by divalent ions. J Plant Physiol 171:154–163

Wan KY, Goldstein RE (2016) Coordinated beating of algal flagella is mediated by basal coupling. Proc Natl Acad Sci U S A 113:E2784–E2793

Zhang HM, Geng G, Wang JJ, Xin Y, Zhang Q, Cao DJ, Ma YH (2019) The remediation potential and kinetics of cadmium in the green alga *Cladophora rupestris*. Environ Sci Pollut Res 26:775–783

Zhang J, Zhou F, Liu Y, Huang F, Zhang C (2020) Effect of extracellular polymeric substances on arsenic accumulation in *Chlorella pyrenoidosa*. Sci Total Environ 704:135368

Zheng GX, Li Y-J, Qi L-L, Liu X-M, Wang H, Yu S-P, Wang Y-H (2014) Marine phytoplankton motility sensor integrated into a microfluidic chip for high-throughput pollutant toxicity assessment. Mar Pollut Bull 84:147–154

3.2. Znanstveni rad II

Novosel, N., Ivošević DeNardis, N., 2021. Structural Features of the Algal Cell Determine Adhesion Behavior at a Charged Interface. Electroanalysis 33: 1436–1443. https://doi.org/10.1002/elan.202060580

Full Paper

Wiley Online Library

ELECTROANALYSIS

DOI: 10.1002/elan.202060580

Structural Features of the Algal Cell Determine Adhesion Behavior at a Charged Interface

Nives Novosel*[a] and Nadica Ivošević DeNardis*[a]

Abstract: We aimed to examine the effects of algal structural features on adhesion at a charged interface. Results showed that algae with a glycocalyx, and with a cellulose amphiesma adhered at a charged interface at species-specific potential ranges. Algae, encased with a calcite-encrusted theca, and with an organosilicate cell wall, did not adhere to the interface. These differences in the amperometrically determined adhesion behavior of algal cells are in agreement with reported cell mechanical properties. Critical interfacial tensions of adhesion show differences between the studied soft algal cells as a consequence of their distinct cell barrier structure, composition, and properties.

Keywords: Cell adhesion · Electrochemistry · Interfaces · Mercury · Sensors

1 Introduction

A major and prominent part of the aquatic biota that forms the base of the marine food web is the unicellular phytoplankton organisms, microalgae. The structural features of unicellular microalgae determine their life, such as which niches in the ecosystem the cell will occupy. They play an important role in the regulation of the material transported between the intracellular cytosol and the external environment. Numerous and expanding applications of microalgae in the biotechnology field rely on understanding cell-cell and cell-substrate interactions. Bioanalytical methods nowadays are seeking convenient, rapid, and effective approaches for cell characterization, but pronounced algal motility can be an experimental challenge. Standard microscopical methods are outstanding in terms of algae species identification, although it is time demanding, and sample preparation can introduce artifacts. As a result, different approaches have been developed for algal cell characterization and separation based on size, electric properties, optical properties, use of magnetic beads, fluorescence, labeled surface biomolecules, adhesion to hydrophobic and hydrophilic materials, and PCR electrochemical detection [1–15].

Extensive research has been done on the development of an electrochemical method of polarography and chronoamperometry on a charged dropping mercury electrode for characterization of adhered organic particles such as organic droplets, living cells, lipid vesicles, bacterial aggregates, natural fluid, and flexible particles [16–25]. Electrochemical adhesion detection is based on interfacial properties (hydrophobicity and fluidity) and particle supramolecular organization [23]. The electrochemical adhesion-based characterization of algal cells has not been extensively studied; thus, here, we aim to examine the effect of structural features of the algal cell on adhesion and spreading at the model charged interface. We selected four algal cell species differing in the structure of the cell barrier: *Dunaliella tertiolecta* cells, with a thin elastic plasma membrane and glycocalyx surface coat, *Prorocentrum micans*, with cellulose amphiesma, *Tetraselmis suecica*, with thin calcite-encrusted theca, and *Cylindrotheca closterium*, with an organosilicate cell wall.

2 Experimental

2.1 Cell Suspensions

We used the laboratory monocultures of four marine algal species, *Dunaliella tertiolecta* (Chlorophyceae, CCMP 1320, Culture Collection Bigelow Laboratory for Ocean Sciences), *Tetraselmis suecica* (Chlorophyceae, CCAP 66/22 A, Collection of Algae and Protozoa, Scottish Marine Institute), *Cylindrotheca closterium* (Bacillariophyceae, CCMP 1554, Culture Collection Bigelow Laboratory for Ocean Sciences), and *Prorocentrum micans* (Dinophyceae, CCAP 1136/15, Collection of Algae and Protozoa, Scottish Marine Institute). Algal cells of *D. tertiolecta*, *T. suecica*, and *C. closterium* were cultured in seawater (38‰) filtered through a 0.22 μm pore filter and enriched with F/2 growth medium [26]. Algal cells of *P. micans* were cultured in L1 growth medium [27]. Algal cell batch cultures were kept in a water bath at 18 °C, with constant shaking (20 rpm), 12 : 12 light:dark cycle with irradiance 31 μmol photons $m^{-2}s^{-1}$. Cell densities were determined at stationary phase, on the 19th day of growth under a light microscope (Olympus BX51, Olympus Corporation, Japan) using a haemacytometer. The stock cell suspension is prepared by centrifuging the cells from

[a] N. Novosel, N. Ivošević DeNardis
Ruđer Bošković Institute, POB 180, 10 000 Zagreb, Croatia
E-mail: nives.novosel@irb.hr
ivosevic@irb.hr

the growth medium (1,500 g, 3 min), rinsing the pellet twice with filtered seawater, and resuspending it in the final volume of 2 mL of filtered seawater for further measurements.

2.2 Plasma Membrane Vesicles Derived From Algae

The isolated *D. tertiolecta* cell pellet was used as a stock suspension to prepare plasma membrane vesicles. The algal pellet was diluted 40 times with ultrapure water, vortexed, and kept at room temperature for half an hour. Due to hypoosmotic shock, *D. tertiolecta* cells broke and released partially or completely intracellular content. The suspension was centrifuged (1,500 g, for 5 min.). The pellet contained debris, half-emptied and empty plasma membrane vesicles, while the supernatant contained mainly emptied plasma membrane vesicles and some debris. The supernatant was further centrifuged at 15,000 g for 15 min. The new supernatant was further centrifuged at 45,000 g for 15 min. The empty plasma membrane vesicle observed microscopically in the pellet was resuspended in 3 mL of ultrapure water ($\sim 10^4$ vesicles mL^{-1}) [28,29].

2.3 Electrochemical Method

In this study polarography and chronoamperometry of oxygen reduction at the dropping mercury electrode (DME) were used. The electrochemical method allows to directly distinguish between dissolved and dispersed organic constituents in the sample based on the specific electrochemical response [23–25,30]. Dissolved organic matter is detected through adsorption at the interface in a well defined potential range. Adsorption of dissolved organic matter corresponds to collective response which is registered as a gradual decrease of oxygen reduction current on the polarogram or chronoamperometric curves. Dispersed organic particles are detected by adhesion which is registered as well-defined amperometric signals [19–21]. The appearance of amperometric signals of organic particles is a stochastic process that depends on the heterogeneous distribution of the particles at the mercury/aqueous electrolyte interface. The amplitude and number of amperometric signals reflect the size and concentration of particles in the sample, respectively [16,19,31]. The interaction of organic droplet at the mercury/aqueous electrolyte interface is given with the modified Young-Dupré equation where the total Gibbs energy equals:

$$-\Delta G = A(\gamma_{12} - \gamma_{23} - \gamma_{13}) \quad (1)$$

γ_{12}, γ_{13}, and γ_{23} correspond to interfacial energies at mercury/water, mercury/organic liquid, and water/organic liquid interfaces, respectively.

The spreading coefficient (S_{132}) at the three interfaces in contact [32] equals to

$$S_{132} = \gamma_{12} - \gamma_{23} - \gamma_{13} \quad (2)$$

For positive values of S_{132}, the adhesion and spreading of the organic droplet at the interface will occur spontaneously because of the droplet's stronger affinity for water than cohesion between droplets. When $S_{132}=0$, the critical interfacial tension of adhesion $(\gamma_{12})_c$ will be $(\gamma_{12})_c=\gamma_{13}+\gamma_{23}$.

2.4 Electrochemical Measurements

Electrochemical measurements were performed in a 50 mL Methrom glass cell open to air and thermostated at 25 °C. The three-electrode system consists of: the working electrode DME (drop life of 2.0 s, a flow rate of 6.0 mg s^{-1}, and a maximum surface area of 4.57 mm^2), reference Ag/AgCl (0.1 M NaCl), and Pt as the counter electrode. Aliquots of the stock cell and vesicle suspensions were added to the 25 mL of 0.1 M NaCl (pH 8.2). Taking into account cell physiological activity freshly prepared cell samples were characterized during 50 consecutive current-time curves at each constant potential. Under controlled experimental conditions (flow rate of mercury, the concentration of redox species, concentration of aqueous electrolyte solution, cell abundance, and no presence of surface-active matter) measurements are reproducible. Electrochemical measurements were performed on Princeton Applied Research Polarographic Analyzer model 174 A connected to a computer. Data acquisition was performed using a DAQ card-AI-16-XE-50 (National Instruments, Austin, TX, USA) input device, and the data were analyzed using the application developed in LabView 6.1 software (National Instruments). The polarogram of oxygen reduction (I-E curve) was recorded at a slow linear potential scan rate (10 mV s^{-1}). The chronoamperometric curves (I-t curves) were recorded at a constant potential over 50 mercury drop lifetimes and a resolution of 50 µs. The signal frequency corresponds to the number of adhesion events over 100 s due to the stochastic nature of the adhesion process.

3 Results and Discussion

Four selected microalgal species, *D. tertiolecta*, *P. micans*, *T. suecica*, and *C. closterium* which greatly diverse in all brackish and marine systems were used as model organisms. Selected organisms with distinct size and structural features of the cell barrier were characterized by polarography and amperometry at the DME. Mercury electrode is widely used for membrane studies where fluidity and easy potentiostatic control of interfacial properties are of great importance to mimics interactions with other interfaces in contact. By variation of the applied potential (E) at the mercury/0.1 M NaCl interface (from 0 to −1.8 V), the surface charge density, (σ_{Hg}, from +22 to −24 µC cm^{-2}) and the interfacial tension (γ_{12}, from 240 to

426 mJ m^{-2}) change accordingly. Measurements were performed in an aqueous electrolyte solution of 0.1 M NaCl due to the large set of electrocapillary data and the more pronounced amperometric signals of cells than in seawater.

3.1 Adhesion Behavior of Soft Algal Cells and Plasma Membrane Vesicles at the DME

Figure 1a shows a polarogram of oxygen reduction recorded in the presence of *D. tertiolecta* cell suspension and an overlaid curve in the organic free electrolyte.

The polarogram shows irregular perturbations in the defined potential range, while outside of this potential range (more positively and negatively), there are no recorded perturbations. Irregular perturbations on the polarogram are the result of the adhesion and spreading of cells at the charged mercury electrode. Cell adhesion at the wide potential range was analyzed from the recorded chronoamperometric curves at constant potentials. The dependence of the signal frequency on applied potentials is shown in Figure 1b. The potential range of adhesion was denoted with the most positive critical potential (Ec^{+}), and the most negative critical potential (Ec^{-}) where at least one amperometric signal of particle has appeared per ten consecutive chronoamperometric curves [16,17]. Critical potentials of *D. tertiolecta* cells adhesion correspond to −110 mV and −1100 mV. The signal frequency of soft particles varies with applied potential since interfacial tension changes accordingly. The maximum number of amperometric signals occurred at the potential of −400 mV. At this potential, the mercury surface bears a positive charge ($E > E_{pzc}$, $\sigma_{Hg} = +3.8\ \mu C\,cm^{-2}$), and the interfacial tension is close to the maximum value (electrocapillary maximum), and transport of cells is enhanced by convective streaming nearby the mercury interface. By shifting the potential more positively or negatively than −400 mV, interfacial energy and the number of amperometric signals of the cells decreases, accordingly.

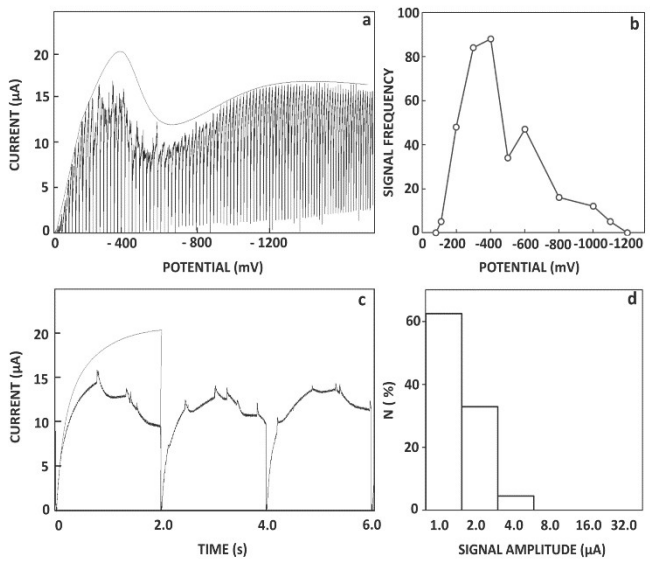

Fig. 1. **a)** Polarogram of oxygen reduction recorded in the suspension of *D. tertiolecta* cells (6.34×10^6 cell mL^{-1}) in 0.1 M NaCl. The thin line is the envelope of polarogram recorded in an organic-free electrolyte solution; **b)** values of signal frequency of *D. tertiolecta* cells as a function of the applied potentials; **c)** chronoamperometric curves for oxygen reduction at −400 mV for three consecutive mercury drops for *D. tertiolecta* cell suspension in 0.1 M NaCl; The thin line corresponds to chronoamperometric curves recorded in an organic-free electrolyte solution; **d)** the distribution of adhesion signal amplitudes of *D. tertiolecta* cells in suspension at −400 mV.

The number of adhesion signals was about five times higher at −400 mV ($E > E_{pzc}$, $\sigma_{Hg} = +3.8\ \mu C\,cm^{-2}$) than at −800 mV, ($E < E_{pzc}$, $\sigma_{Hg} = -6.5\ \mu C\,cm^{-2}$) indicating the influence of electrostatic attractions between the positively charged electrode and the negatively charged cell, which is in agreement with a reported surface charge density of *D. tertiolecta* cells in 0.1 M NaCl of $-0.63\ \mu C\,cm^{-2}$ [6]. At the potential of −500 mV ($E \sim Epzc$, $\sigma_{Hg} \sim 0\ \mu C\,cm^{-2}$), the signal frequency drops since there is almost no double-layer charge to be displaced but adhesion exists as measured with amperometric signals of the reduction of molecular oxygen from the electrode-solution interface. This so-called butterfly dependence of the signal frequency of algal cells on applied potential is a reproducible feature. Representative consecutive chronoamperometric curves of oxygen reduction recorded at −400 mV in *D. tertiolecta* cell suspension containing 6.34×10^6 cell mL^{-1} is shown in Figure 1c.

Amperometric signals were similar in shape while they differed in signal amplitude, which is in line with their cell size. Amplitudes of individual amperometric signals of cells recorded at −400 mV were analyzed, and the distribution of amperometric signal amplitudes is shown in Figure 1d. Most of the amperometric signals (95 %) appear in the amplitude size ranges between 1.0 μA and 2.0 μA, which is in line with *D. tertiolecta* cell size from 6 to 12 μm. The remaining fractions of larger particles could be attributed to adhered coagulated products of cellular metabolism or secretion and mother cell preceding cell division, respectively. Taking into account that each amperometric signal corresponds to the adhesion of individual cells, signal frequency linearly increases with cell density in the range of 10^5 to 10^7 cells L^{-1}, enabling translation of frequency into particle concentration [31]. This approach was applied for the monitoring of spatial and temporal distributions of reactive fluid and flexible particles in the Northern Adriatic sea to potentially predict the massive mucilage formation [24,25,33,34].

Plasma membrane vesicles are formed by membrane fusion after the osmotic shock of *Dunaliella* cells. Plasma membrane vesicles are known as ghost vesicles since they are not easily visualized under a microscope. Ghost vesicles have a thick envelope labeled by pigmented photosynthetic apparatus and a nearly empty vesicle interior [28,29]. Ghost vesicles vary in size between 1 and

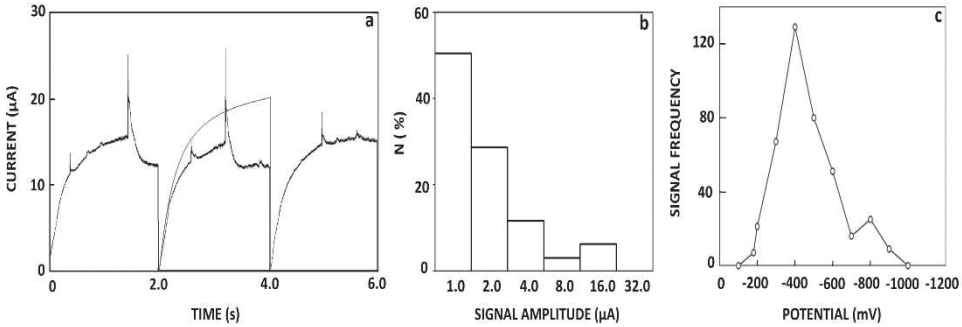

Fig. 2. **a)** Chronoamperometric curves for oxygen reduction at −400 mV for three consecutive mercury drops recorded in plasma membrane vesicle suspension (1×10^4 cell mL^{-1}) in 0.1 M NaCl. The thin line corresponds to chronoamperometric curves recorded in an organic-free electrolyte solution; **b)** The distribution of the signal amplitudes of plasma membrane vesicles in suspension at −400 mV; **c)** the dependence of the signal frequency of plasma membrane vesicle suspension on applied potentials.

50 μm. The adhesion behavior of plasma membrane vesicles was examined. Representative consecutive chronoamperometric curves of oxygen reduction recorded at −400 mV in the ghost vesicle suspension are shown in Figure 2a.

Amperometric signals of ghost vesicles show the difference in signal shape and amplitude compared to amperometric signals of intact algal cells. The amplitudes of individual amperometric signals of vesicles recorded at a constant potential of −400 mV were analyzed, and the distribution of signal amplitudes is shown in Figure 2b. Amperometric signals in the amplitude size ranged up to 1.0 μA, probably corresponding to released debris after cell rupture, and vesicle size up to 5 μm, respectively. Highly pronounced amperometric signals corresponded to the adhesion of giant ghost vesicles at the charged DME. The dependence of the signal frequency of ghost vesicles on applied potentials is shown in Figure 2c. The maximum number of amperometric signals occurred at a potential of −400 mV. By shifting the potential more positively or negatively than −400 mV, the number of amperometric signals of ghost vesicles decreased.

The number of adhesion signals was about five times higher at −400 mV ($E > E_{pzc}$, $\sigma_{Hg} > 0$) than at −800 mV. ($E < E_{pzc}$, $\sigma_{Hg} < 0$). The critical potentials of adhesion of the plasma membrane vesicles were determined to be −180 mV and −900 mV, which was a narrower potential range than that for *D. tertiolecta* cell adhesion. The adhesion of *D. tertiolecta* cells at the interface is a more complex process than the adhesion of ghost vesicles. A previous study compared adhesion kinetics of *Dunaliella* cells at the charged interface with nearly empty ghost vesicles. The results showed that the adhesion kinetics of *Dunaliella* cells at the charged interface were determined to be ten times slower due to the spreading of released intracellular content over the interface [28]. The visualized pore-like structure on the ghost membrane formed during osmotic shock supports the fast adhesion kinetics and the highly permeable nature of the ghost membrane for calcein [29].

A polarogram of oxygen reduction in the presence of *P. micans* cell suspension of 4.64×10^5 cell mL^{-1} is shown in Figure 3a. The adhesion of *P. micans* cells also induced the appearance of irregular perturbations at the polarogram in the species-specific potential range at the DME. To get a better insight into this behavior, the chronoamperometric curves recorded at different constant potentials were analyzed. The dependence of amperometric signal frequency on applied potentials is shown in Figure 3b. Characteristic amperometric signals occurred only in the range of critical potentials from −150 mV to −900 mV, and beyond that range, there was no adhesion

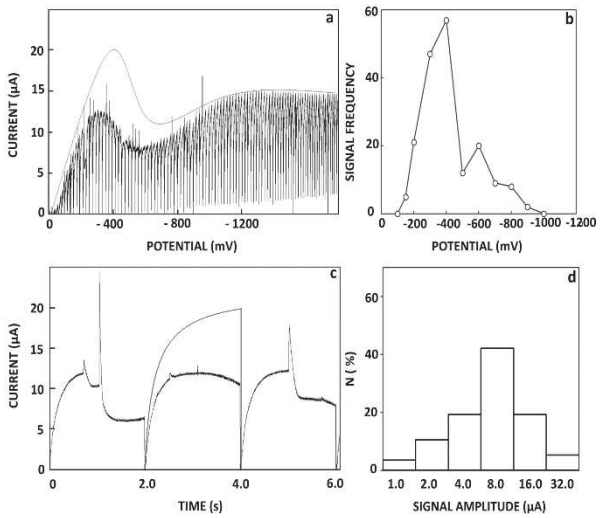

Fig. 3. **a)** Polarogram of oxygen reduction recorded in the suspension of *P. micans* cells (4.64×10^5 cell mL^{-1}) in 0.1 M NaCl. The thin line is the envelope of polarogram recorded in an organic-free electrolyte solution; **b)** the dependence of the signal frequency of *P. micans* cells on applied potentials; **c)** Chronoamperometric curves for oxygen reduction at −400 mV for three consecutive mercury drops recorded in *P. micans* cell suspension in 0.1 M NaCl. The thin line corresponds to chronoamperometric curves recorded in an organic-free electrolyte solution; **d)** the distribution of adhesion signal amplitudes of *P. micans* cells at −400 mV.

of *P. micans* cells at the charged DME. At −400 mV, the maximum number of adhesion signals of *P. micans* occurred. The number of adhesion signals of *P. micans* cells is about seven times higher at −400 mV ($E > E_{pzc}$, $\sigma_{Hg} > 0$) than at −800 mV ($E < E_{pzc}$, $\sigma_{Hg} < 0$), which could point out the effect of electrostatic attractions between the positively charged electrode and the negatively charged cell.

The representative consecutive chronoamperometric curves for oxygen reduction in the *P. micans* cell suspension of 4.64×10^5 cell mL^{-1} recorded at −400 mV are shown in Figure 3c. By analyzing 50 consecutive chronoamperometric curves, the dependence of the frequency on signal amplitude is shown in Figure 3d. *P. micans* cell size varies from 50 to 70 μm. About 61 % of the amperometric signals of *P. micans* were in the amplitude size range from 8.0 to 32.0 μA. Signal amplitudes of *P. micans* were about ten times higher than *D. tertiolecta* signal amplitudes, which is in correspondence with the ratio of cell sizes of the investigated species.

3.2 The Behavior of Rigid Algal Cells at the DME

The electrochemical characterization of *T. suecica* and *C. closterium* cell suspensions are shown in Figure 4. The polarograms were perfectly regular, and the maximum was slightly suppressed due to the adsorption of released biopolymers at the charged DME. Chronoamperometric curves of the oxygen reduction were recorded at −400 mV in cell monosuspensions of *T. suecica* and *C. closterium.*

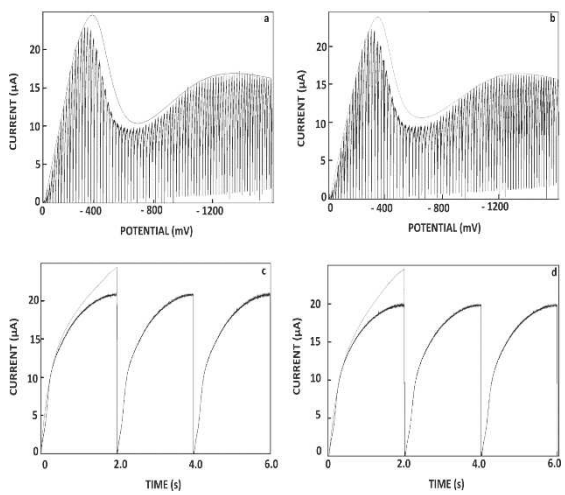

Fig. 4. **a)** Polarogram of oxygen reduction recorded in *T. suecica* cell suspension (5.33×10^6 cell mL^{-1}). The thin line is the envelope of polarogram recorded in an organic-free electrolyte solution; **b)** Polarogram of oxygen reduction recorded in *C. closterium* cell suspension (6.78×10^6 cell mL^{-1}); **c)** Chronoamperometric curves for oxygen reduction at −400 mV for three consecutive mercury drops recorded in *T. suecica* and **d)** *C. closterium* cell suspensions. The thin line corresponds to chronoamperometric curves recorded in an organic-free electrolyte solution

The cronoamperometric curves were also regular, and the oxygen reduction current was also slightly suppressed (Figure 4c,d). The decreased oxygen reduction current was probably related to the physiological activity of algal cells through the release of an extracellular polymeric substance. The extracellular polymeric substance is mainly polysaccharide fibrils that form a fine network attached to the cell wall of *C. closterium* or released in the surrounding medium [34,35].

3.3 Comparison of Adhesion Behavior of Soft Particles and Ghost Vesicles at the DME

The structural features, composition, and collective properties of soft particles play an important role in the dynamics of adhesion and the rate of spreading at the interface. Most of the published work on the adhesion of algal cells on substrate focuses on the properties of the substrate, while structural features and surface properties of algae have been neglected. Table 1 summarises the structural features of algal species and ghost vesicles, including measured critical potentials (E_c^+, E_c^-), with the corresponding interfacial tensions of adhesion at the positively $(\gamma_{12})_c^+$ and negatively $(\gamma_{12})_c^-$ charged mercury/aqueous electrolyte interface, respectively.

The algal cell *D. tertiolecta* possesses a 9 nm thick plasma membrane modified on the surface with glycoproteins forming glycocalyx [19,36]. The nanomechanical characterization of *D. tertiolecta* in the exponential and stationary growth phases was studied [36]. The results showed that cells were significantly more hydrophobic and stiffer in the exponential than in the stationary growth phase, probably due to the molecular modification of the cell envelope (31 kPa, 19 kPa, respectively). The higher stiffness of *D. tertiolecta* cells in the exponential growth phase reflected on the slower cell adhesion kinetics at the interface. On the other hand, *Dunaliella* cells′ adaptation response when exposed to heavy metal stresses manifested with a significant increase in stiffness due to the expression of surface proteins associated with the photosynthetic activity, which was reflected on slower initial attachment and deformation [37].

P. micans cells possess a barrier called amphiesma, made of cellulose. Amphiesma consists of the continuous

Table 1. Critical potentials and corresponding interfacial tensions of adhesion at the positively and the negatively charged DME/0.1 M NaCl interfaces determined for selected algal cell suspensions and ghost vesicle.

System	Type of barrier	E_c^+ (mV)	E_c^- (mV)	$(\gamma_{12})_c^+$ (mJ m^{-2})	$(\gamma_{12})_c^-$ (mJ m^{-2})
D. tertiolecta	Glycocalyx	-110	-1100	396	390
Ghost vesicle	Plasma membrane	-180	-900	408	408
P. micans	Cellulose amphiesma	-150	-900	403	408
T. suecica	Calcite incrustrated theca	n.d.	n.d.	n.d.	n.d.
C. closterium	Organosilicate cell wall	n.d.	n.d.	n.d.	n.d.

plasma membrane underlined by membrane vesicles called amphiesmal vesicles, filled with cellulose thecal plates [38]. Amphiesma is assumed as a dynamic structure that changes the life cycle of dinoflagellates [39]. Aguilera and Gonzalez-Gil [13] examined the surface glycocalyx of the dinoflagellate species using fluorescent lectins. They found that the composition of the cell surface sugars varied with the physiological state of the dinoflagellate cells during the cell cycle. Sugar moieties of α-mannosyl and α-glucosyl were detected in *P. micans* when using ConA. *T. suecica* cells are covered with theca made of small non-mineralized scales consisting mainly of acidic polysaccharides [40]. Furthermore, *T. suecica* cells possess calcite bio pearls inclusions that are located preferentially under the plasma membrane and seem to form a definite pattern that gives the cell structural strength [41].

The cell wall of *C. closterium* is a weakly silicified frustulum [42], covered by an organic envelope essentially composed of polysaccharides and proteins. A previous study reported the nanostructural and nanomechanical characterization of *C. closterium* [34,35] and showed the variation of elasticity from 29.8 MPa in the valve region to 200 MPa in the fibulae region, thus, the elasticity *Cylindrotheca* was about 3–4 orders of magnitude higher than the elasticity of *D. tertiolecta* cells.

The algal cells of *D. tertiolecta* and *P. micans* adhered to the species-specific potential range at the DME interface. The potential ranges for algal cell adhesion become broader by increasing the complexity of plasma membrane structure in the following sequence: plasma membrane < cellulose amphiesma < glycocalyx. The potential range of adhesion was defined with critical potentials of adhesion at the positively and the negatively charged interfaces. Experimentally measured critical potentials allow the determination of critical interfacial tensions using the electrocapillary curve [43]. The determined values of $(\Upsilon_{12})_c^+$, $(\Upsilon_{12})_c^-$ for soft cells were not equal because of the specific adsorption of chloride anions at the positively charged interface, and electrostatic repulsion between a negatively charged cell and the negatively charged interface, respectively. The determined values of $(\Upsilon_{12})_c^+$, $(\Upsilon_{12})_c^-$ for ghost vesicles were equal, as for the adhesion of hydrophobic organic liquids. Values of $(\Upsilon_{12})_c$ for adhesion of *Dunaliella* cells are lower than for naked and nearly empty plasma membrane vesicles, which could be a contribution of the glycocalyx surface coat. The lower value of $(\Upsilon_{12})_c$ for *D. tertiolecta* adhesion corresponds to the lower interfacial tension between mercury and the cell.

To put this in a broader context, it is known that the general adhesion behavior of algal cells at the charged interface shows an analogy with the proposed adhesion mechanism of droplets of organic liquids in terms of attachment, deformation, spreading over the interface, taking into account that particle surface properties determine the dynamics of adhesion and the rate of spreading over the interface. Experimentally determined values of critical interfacial tensions $(\Upsilon_{12})_c^+$, $(\Upsilon_{12})_c^-$ for adhesion of different hydrocarbon droplets were equal at the positively and negatively charged interfaces, which showed the importance of London dispersion forces in hydrocarbon interactions with the mercury and water interface and the agreement with the modified Young-Dupré equation for the three-phase systems [17,18,44]. On the other side, the Young-Dupré equation shows limitations for adhesion of algal cells at the mercury interface due to the system complexity (cell surface charge, cell mechanics, physiological activity, age of the cell in culture, concomitant biochemical processes within the cell, etc). The effect of electrostatic interactions is manifested in the adhesion behavior between the negatively charged algal cells and the negatively charged electrode by lower critical interfacial tension for adhesion, signal frequency, and contact interface area [19]. Further evidence of electrostatic interactions was demonstrated in the related simplified system of lipid vesicle adhesion by the specific interaction of positively charge choline groups with mercury in the range around the point of zero charges [44,45].

T. suecica and *C. closterium* cells did not adhere to the DME and acted as inert and non-deformable particles, which is probably due to their calcite-encrusted theca and weakly silicified cell wall. In contrast, adsorption of extracellular polymeric substance released by cells prevails and can affect adhesion, playing an important role in cell surface interactions [40].

Figure 5 shows surface charge densities at the mercury electrode/0.1 M NaCl interface (σ_{Hg}) for the adhesion of selected algal cells and ghost vesicles in comparison with the adhesion range of the reported organic droplets and lipid vesicles.

Droplets of non-polar hydrocarbons such as hexadecane had a narrow surface charge density range for

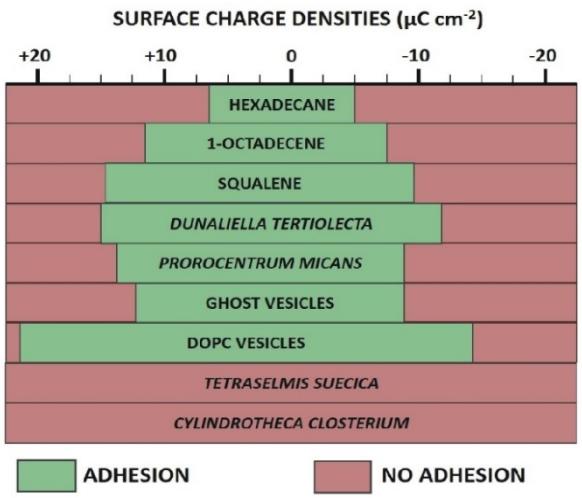

Fig. 5. The surface charge density range at the DME/0.1 M NaCl interface where the adhesion of the model particles and living cells take place, marked as a green region. The red region denotes the surface charge density range without adhesion.

adhesion ($+6.5\ \mu C\,cm^{-2}$ to $-5.0\ \mu C\,cm^{-2}$). As the polarity of the hydrocarbons increased, with branching, or the presence of double bonds, the interfacial tension with water increased, and the surface charge density range of adhesion became wider. Thus, the surface charge density range for adhesion of slightly polar 1-octadecene corresponds to $+11.5\ \mu C\,cm^{-2}$ to $-7.4\ \mu C\,cm^{-2}$. The ranges of surface charge density for adhesion of *D. tertiolecta* and *P. micans* are species-specific, reflecting their unique structural features and surface properties. *D. tertiolecta* cells as less stiff adhered in a broader range of surface charge density ($+15.0\ \mu C\,cm^{-2}$ to $-11.6\ \mu C\,cm^{-2}$) than *P. micans* ($+13.5\ \mu C\,cm^{-2}$ to $-8.3\ \mu C\,cm^{-2}$). *T. suecica* and *C. closterium* do not adhere at the mercury interface regardless of the generated surface charge densities. In contrast to non-polar organic liquids, living cells possess a negative fix charge and they adhere to the positive but also negatively charged interfaces, which demonstrate the predominance of hydrophobic over electrostatic interaction in the adhesion process [19]. The highest adhesion affinity at the charged interface was detected in the related model system of lipid vesicles (DOPC) where the surface charge density range spanned from $+21.09$ to $-13.6\ \mu C\,cm^{-2}$ [20,21,45]. Effect of different surface charge densities on hydrocarbon and lipid molecule orientation and action of forces were revealed in detail by molecular dynamics simulation [44].

We demonstrated how electrochemical characterization can be applied for the study of non-specific adhesion of single, motile algae to the charged, fluid mercury/aqueous electrolyte interface. The mercury interface has a high interfacial energy and the degree of hydrophobicity is varied with the applied potential. The non-specific adhesion of a single motile algal cell to interfaces has not been extensively explored. The reason for this could be the pronounced motility of *D. tertiolecta* and *T. suecicca* cells which correspond to 8 and 22 body lengths per second depending on the number of flagella that cell possess (e.g. 71 $\mu m\,s^{-1}$ and 190 $\mu m\,s^{-1}$), respectively [46].

In a related study, the non-specific adhesion of non-motile algae in the exponentially (log) growth phase on uncharged, solid substrates with low surface energy was investigated using contact angle measurements of water [7]. They investigated the adhesion behavior of cells on the solid substrates with respect to the algal surface properties. *Chlorela vulgaris* (*C. vulgaris*) is a unicellular green alga with a rigid cell wall while *Botryococcus sudeticus* (*B. sudeticus*) forms cell colonies associated with the released extracellular matrix. Both species belong to the phylum Chlorophyta (green algae) as motile cells of *D. tertiolecta* and *T. suecicca.* Results showed that glass surface and *C. vulgaris* were hydrophilic, while ITO surface and *B. sudeticus* were hydrophobic [7a]. These differences in cell surface properties were considered to originate from cell wall structure and surface groups. The hydrophilic property of the *C. vulgaris* arises from the cellulose-based cell wall. *C. vulgaris* attached to ITO, and not firmly attached to the glass while the surface tension of the cell was higher from the surface tension of ITO and lower than for glass. This unexpected behavior could derive from the surface properties of *C. vulgaris* in the log phase of growth. Change of surface properties during the exponential and stationary growth phases of *D. tertiolecta* was studied [36]. The results showed that *D. tertiolecta* was hydrophobic during the exponential growth phase as for the *C. vulgaris.* Further, the hydrophobic nature of *B. sudeticus* cell originated from long-chain hydrocarbons, and hydrophobic surface groups on the cell wall (methyl and methylidene). *B. sudeticus* greatly and strongly attached to both surfaces, and the surface tension of the cell was lower than the surface tensions of both substrates. The cells of *B. sudeticus* and *D. tertiolecta* showed similarities in adhesion to substrates with different degree of hydrophobicity and both species are rich with fatty acids and lipids.

The authors showed that XDLVO model successfully predicted the strength of adhesion of algal cells to the surface. In our separate study, the highest strength of adhesion forces was visualized at the point of zero charge, where macroscopic organic droplet deposited onto the charged mercury pool electrode formed a stable lense. When the adhesion forces became weak by shifting of applied potential, the contact area decreased, the droplet became spherical and the contact angle increased accordingly [47].

Finally, the electrochemical approach at the mercury electrode enables fast and simultaneous detection of adhered individual, soft algal cell, and adsorbed surface-active matter in a time of a couple of minutes without sample pretreatment. This fundamental study can contribute to the understanding of algae-surface interactions which is necessary for the development of biotechnological applications.

4 Conclusions

We have demonstrated that structural features of the algal cell determine their adhesion behavior at the charged interface. Algal cell species possessing organosilicate cell walls and calcite-encrusted theca behave as rigid, non-deformable, and inert at the charged, fluid interface, without the generation of amperometric signals of cells. Algal cell species possessing a glycocalyx surface coat and cellulose amphiesma behave as soft and deformable, which is registered as an amperometric signal of the cells at the species-specific potential range. These differences in the amperometrically determined adhesion behavior of algal cells are in agreement with reported cell nano-mechanical properties. Surface charge density ranges for algal adhesion at mercury interface become broader by increasing the complexity of plasma membrane structure in the following sequence: plasma membrane < cellulose amphiesma < glycocalyx. The critical interfacial tension can thus be considered as a parameter for adhesion differentiation of soft algal cells. The electrochemical method at DME offers direct and fast, high-throughput

differentiation of cells, thus, this approach can help to better understand the behavior of algal cells at the complex interfaces in aquatic systems and serve for biotechnology needs.

Acknowledgements

This work is supported by the Croatian Science Foundation Projects "From algal cell surface properties to stress markers for aquatic ecosystems" (IP-2018-01-5840). We thank anonymous Reviewers for their valuable comments.

Data Availability Statement

Data available on request from authors.

References

[1] C. Butterwick, S. I. Heaney, J. F. Talling, *Br. Phycol. J.* **1982**, *17*, 69–79.
[2] C. Sinigalliano, J. Winshell, M. Guerrero, G. Scorzetti, J. Fell, R. Eaton, L. Brand, K. Rein, *Phycologia* **2009**, *48*, 249–257.
[3] D. R. Bayne, J. M. Lawrence, *Limnol. Oceanogr.* **1972**, *17*, 481–489.
[4] S. A. Pomponi, T. L. Cucci, *Cytometry* **1989**, *10*, 580–586.
[5] M. Beutler, K. Wiltshire, B. Meyer, C. Moldaenke, C. Lüring, M. Meyerhöfer, U.-P. Hansen, D. Huong, *Photosynth. Res.* **2002**, *72*, 39–53.
[6] V. Svetličić, A. Hozić, *Electrophoresis* **2002**, *23*, 2080–2086.
[7] a) A. Ozkan, H. Berberoglu, *Colloids Surf. B* **2013**, *112*, 287–293; b) A. Ozkan, H. Berberoglu, *Biofouling* **2013**, *4*, 469–482; c) A. Ozkan, H. Berberoglu, *Colloids Surf. B* **2013**, *112*, 302–309.
[8] Y. Cui, W. Yuan, J. Cheng, *Appl. Biochem. Biotechnol.* **2014**, *173*, 1692–1702.
[9] X. Zhang, Z. Jiang, M. Li, X. Zhang, G. Wang, A. Chou, L. Chen, H. Yan, Y. Y. Zuo, *Anal. Chem.* **2014**, *86*, 8751–8756.
[10] M. J. LaGier, J. W. Fell, K. D. Goodwin, *Mar. Pollut. Bull.* **2007**, *54*, 757–770.
[11] G. Prochazkova, N. Podolova, I. Safarik, V. Zachleder, T. Branyik, *Colloids. Surf. B. Biointerfaces.* **2013**, *112*, 213–218.
[12] L. Xu, C. Guo, F. Wang, S. Zheng, C. Z. Liu, *Bioresour. Technol.* **2011**, *102*, 10047–51.
[13] A. Aguilera, S. Gonzalez-Gil, *J. Exp. Mar. Biol. Ecol.* **2001**, *256*, 149–166.
[14] E. P. Espinosa, M. Perrigault, J. E. Ward, S. E. Shumway, B. Allam, *Biol. Bull.* **2010**, *218*, 75–86.
[15] S. Bauer, J. A. Finlay, I. Thomé, K. Nolte, S. C. Franco, E. Ralston, G. E. Swain, A. S. Clare, A. Rosenhahn, *Langmuir* **2016**, *32*, 5663–71.
[16] V. Žutić, S. Kovač, V. Svetličić, *J. Electroanal. Chem.* **1993**, *349*, 173–186.
[17] N. Ivošević, J. Tomaić, V. Žutić, *Langmuir* **1994**, *7*, 2415–2418.
[18] N. Ivošević, V. Žutić, J. Tomaić, *Langmuir* **1999**, *15*, 7063–7068.
[19] V. Svetličić, N. Ivošević, S. Kovač, V. Žutić, *Bioelectrochemistry* **2001**, *53*, 79–86.
[20] N. Ivošević DeNardis, V. Žutić, V. Svetličić, R. Frkanec, J. Tomašić, *Electroanalysis* **2007**, *19*, 2444–2450.
[21] N. Ivošević DeNardis, V. Žutić, V. Svetličić, R. Frkanec, *Chem. Biochem. Eng. Q.* **2009**, *23*, 87–92.
[22] V. Žutić, N. Ivošević, V. Svetličić, R. A. Long, F. Azam, *Aquat. Microb. Ecol.* **1999**, *17*, 231–238. ž.
[23] V. Žutić, V. Svetličić, N. Ivošević, A. Hozić, O. Pečar, *Period. Biol.* **2004**, *106*, 67–74.
[24] V. Svetličić, E. Balnois, V. Žutić, J. Chevalet, A. Hozić Zimmermann, S. Kovač, N. Vdović, *Croat. Chem. Acta.* **2006**, *79*, 107–113.
[25] G. Pletikapić, N. Ivošević DeNardis, *Nat. Hazards. Earth. Syst. Sci.* **2017**, *17*, 31–44.
[26] R. R. L. Guillard, *Culture of Phytoplankton for Feeding Marine Invertebrates. In: Smith W. L., Chanley M. H. (eds) Culture of Marine Invertebrate Animals*, Springer, Boston, MA, **1975**.
[27] R. R. L. Guillard, P. E. Hargraves, *Phycologia* **1993**, *32*, 234–236.
[28] N. Ivošević DeNardis, J. Pečar Ilić, I. Ružić, G. Pletikapić, *Electrochim. Acta.* **2015**, *176*, 743–754.
[29] N. Ivošević DeNardis, G. Pletikapić, R. Frkanec, L. Horvat, P. T. Vernier, *Bioelectrochemistry* **2020**, *134*, 107524.
[30] N. Ivošević, V. Žutić, *Croat. Chem. Acta.* **1997**, *70*, 167–178.
[31] S. Kovač, R. Kraus, S. Geček, V. Žutić, *Croat. Chem. Acta.* **2000**, *73*, 279–291.
[32] J. N. Israelachvili, *Intermolecular forces & Surface forces*, Academic Press Limited, New York **1992**.
[33] T. Mišić Radić, V. Svetličić, V. Žutić, B. Boulgaropoulos, *J. Mol. Recognit.* **2011**, *24*, 397–405.
[34] G. Pletikapić, T. Mišić Radić, A. Zimmermann Hozić, V. Svetličić, M. Pfannkuchen, D. Marić, J. Godrijan, V. Žutić, *J. Mol. Recognit.* **2011**, *24*, 436–445.
[35] G. Pletikapić, A. Berquand, T. Mišić Radić, V. Svetličić, *J. Phycol.* **2012**, *48*, 174–185.
[36] F. Pillet, E. Dague, J. Pečar Ilić, I. Ružić, M.-P. Rols, N. Ivošević DeNardis, *Bioelectrochemistry* **2019**, *128*, 154–162.
[37] N. Ivošević DeNardis, J. Pečar Ilić, I. Ružić, N. Novosel, T. Mišić Radić, A. Weber, D. Kasum, Z. Pavlinska, R. Katalin Balogh, B. Hajdu, A. Marček Chorvátová, B. Gyurcsik, *Eur. Biophys. J.* **2019**, *48*, 231–248.
[38] K. Hausmann, N. Hülsmann, *Protistology* **2010**, *6*, 139–146.
[39] I. Pozdnyakov, S. Skarlato, *Protistology* **2012**, *7*, 108–115.
[40] B. Becker, M. Melkonian, J. P. Kamerling, *J. Phycol.* **1998**, *34*, 779–787.
[41] A. Martignier, M. Filella, K. Pollok, M. Melkonian, M. Bensimon, F. Barja, F. Langenhorst, J.-M. Jaquet, D. Ariztegui, *Biogeosciences* **2018**, *15*, 6591–6605.
[42] B. E. F. Reimann, J. C. Lewin, *J. Microsc.* **1964**, *83*, 283–296.
[43] J. Lyklema, R. Parsons, *Electrical Properties of Interfaces. Compilation of Data on the Electrical Double Layer on Mercury Electrodes*, Office of Standard Reference Data, National Bureau of Standards, Department of Commerce, Washington, DC, **1983**.
[44] Z. Levine, N. Ivošević DeNardis, P. T. Vernier, *Langmuir* **2016**, *32*, 2808–2819.
[45] N. Ivošević DeNardis, V. Žutić, V. Svetličić, R. Frkanec, *J. Membr. Biol.* **2012**, *245*, 573–582.
[46] N. Novosel, D. Kasum, P. Žutinić, T. Legović, N. Ivošević DeNardis, *J. Appl. Phycol.* **2020**, *32*, 4057–4067.
[47] N. Ivošević, V. Žutić, *Langmuir* **1998**, *14*, 231–234.

Received: November 27, 2020
Accepted: February 9, 2021
Published online on February 18, 2021

3.3. Znanstveni rad III

Novosel, N., Mišić Radić, T., Zemla, J., Lekka, M., Čačković, A., Kasum, D., Legović, T., Žutinić, P., Gligora Udovič, M., Ivošević DeNardis, N., 2022. Temperature-induced response in algal cell surface properties and behavior. Journal of applied phycology 34: 243–259. https://doi.org/10.1007/s10811-021-02591-0

Journal of Applied Phycology (2022) 34:243–259
https://doi.org/10.1007/s10811-021-02591-0

Temperature-induced response in algal cell surface properties and behaviour: an experimental approach

N. Novosel[1] · T. Mišić Radić[1] · J. Zemla[2] · M. Lekka[2] · A. Čačković[1] · D. Kasum[1] · T. Legović[1,3,4] · P. Žutinić[5] · M. Gligora Udovič[5] · N. Ivošević DeNardis[1]

Received: 18 February 2021 / Revised and accepted: 12 August 2021 / Published online: 22 October 2021

Abstract

Microalgae are considered an accurate indicator of ecosystem perturbations induced by global climate change. The present work aims to investigate the alteration of temperature on surface properties and behaviour of three algal species using the complementary surface methods (electrochemical and atomic force microscopy). The results showed that the temperature-induced response of algae is species-specific due to the structural features of the cell envelope. Wall-less algae experience the largest nanomechanical and chemical change, while algae with silicified walls show the pronounced chemical change in the degree of hydrophobicity. Alterations of surface properties suggest a molecular modification of the algal barrier and cytoskeletal rearrangements due to a change in cell size, while algal morphology reveals no change. The physiological activity of cells showed a different organisation of released extracellular substances in the form of fine fibrillar structures, aggregated particles, and dense networks. Both types of algal responses, physiological activity, and molecular modification of the cell barrier determine the cell adhesion and motility. This study highlights the role of surface properties in cell-substrate and cell–cell interactions, which is important for the understanding of algal behaviour at natural interfaces and the mechanism of algal biofilm and aggregate formation in aquatic systems under the stress.

Keywords Algae · Adhesion · Hydrophobicity · Morphology · Motility · Stiffness

Introduction

Marine microalgae support about half of the global primary production, drive essential biogeochemical cycles, and form the basis of the aquatic food web. Their short life cycle enables them to respond rapidly to climate change or the presence of pollutants (Beaugrand 2005; Hays et al. 2005). The slight change in environmental factors such as light, nutrients, pH, and temperature influences the growth rate and productivity of microalgae (Falkowski and Raven 2007).

✉ N. Ivošević DeNardis
ivosevic@irb.hr

1 Ruđer Bošković Institute, Zagreb, Croatia

2 Institute of Nuclear Physics Polish Academy of Sciences, Kraków, Poland

3 Libertas International University, Zagreb, Croatia

4 OIKON-Institute for Applied Ecology, Zagreb, Croatia

5 Department of Biology, Faculty of Science, University of Zagreb, Zagreb, Croatia

Temperature is one of the key factors that directly affects various cell physiological processes, e.g. biomass production, metabolic reactions, respiration, photosynthesis, and ecological interactions (Lewandowska and Sommer 2010; Guinder and Molinero 2013). An increase in temperature in the water column caused by higher solar radiation leads to oxidative stress of algal cells (Roncarati et al. 2008; Huertas et al. 2011; Häder and Gao 2015). As an adaptive response to environmental conditions, algae can adjust membrane fluidity by altering fatty acid saturation levels, reduce protein synthesis to avoid an increase in misfolded proteins, accumulate compatible solutes to maintain cell osmolarity, regulate photosynthesis to balance energy production and consumption (Barati et al. 2019, Pavlinska et al. 2020), and release extracellular polymeric substances (EPS; Decho and Gutierrez 2017; Kumar et al. 2017).

We focused on the biointerface (i.e. algal cell envelope) that separates cells from the external medium and where complex processes occur simultaneously. The surface properties of the biointerface are responsible for the behaviour, fate, and role of cells in aquatic systems (Klenerman

et al. 2011). Our previous studies showed that the surface properties of algal cells are subject to change during the growth phase (Pillet et al. 2019). In the exponential phase, *Dunaliella tertiolecta* cells were stiffer and hydrophobic, while algae became softer and hydrophilic in the stationary phase. Such alterations of algal surface properties were considered to reflect molecular modification of the cell envelope. Changes in the surface properties of algae consequently reflect on the adhesion kinetics of algae at the model charged interface. The alteration of surface properties, morphology, and physiological activity were determined when algae were exposed to heavy metal cadmium (Ivošević DeNardis et al. 2019). *Dunaliella tertiolecta* cells became stiffer due to the expression of surface proteins, such as chlorophyll *a-b* binding protein and carbonic anhydrase, which are responsible for maintaining the photosystem (Lane et al. 2005). The frustule of *Cylindrotheca closterium* showed nanomorphological changes accompanied by enhancing organic matter production as a feedback response to the heavy metal of cadmium (Mišić Radić et al. 2020).

Microalgal responses to temperature variations have been examined at different spatiotemporal scales, both in empirical and field investigations, as well as using modelling approaches (Sarmiento et al. 2004; Boyce et al. 2010; Huertas et al. 2011). A number of recent studies have investigated the effect of temperature on algal growth and surface properties for applicative usage (Ozkan and Berberoglu 2013; Ras et al. 2013; Gross et al. 2016; Xia et al. 2017; Ahmad et al. 2020). However, the comprehensive biophysical examination of algae on the single-cell level focusing on biointerface and the ecological implications of the aforementioned interaction have been poorly explored.

This study aims to investigate the temperature-induced response in the surface properties and behaviour of three widely distributed marine algal species, taking into account their structural features that can contribute to temperature tolerance. We selected the biflagellate green alga *D. tertiolecta* with a mucous plasma membrane called a glycocalyx, the tetraflagellate green alga *Tetraselmis suecica* enveloped within a calcite-encrusted theca, and the gliding diatom *C. closterium* with a rigid organosilicate cell wall to be examined at selected temperatures simulating the annual variations in aquatic systems. We will combine complementary surface method approach such as electrochemical methods and atomic force microscopy. High-resolution imaging will enable the visualisation of structural details of the cell surface and the organisation of the released biopolymers at the molecular level. Nanomechanical measurements will determine the physicochemical properties of the cells (e.g. elasticity and adhesion). The electrochemical measurements will determine the adhesion behaviour of the cell at the interface as a consequence of material fluidity and hydrophobicity and the content of released surface-active matter. Cell motility will be analysed in terms of cell speed and search radius, both of which reflect the physiological state of the cell. This study, conducted in batch cultures under controlled laboratory conditions, will enable a better understanding of algal responses to the temperature shifts induced by climate change.

Materials and methods

Cell suspensions

Three marine algal species used were *Dunaliella tertiolecta* (DT, Chlorophyceae, CCMP 1320, Culture Collection Bigelow Laboratory for Ocean Sciences, Bigelow, MN, USA), *Tetraselmis suecica* (TS, Chlorophyceae, CCAP 66/22A, Collection of Algae and Protozoa, Scottish Marine Institute, Oban UK), and *Cylindrotheca closterium* (CC, Bacillariophyceae, CCMP 1554, Culture Collection Bigelow Laboratory for Ocean Sciences, Bigelow, MN, USA). Cells were cultured in natural seawater (salinity of 38 ‰) filtered through a pore size of 0.22 µm and enriched with F/2 growth medium (Guillard 1975). Cultures were maintained in a water bath with constant shaking (20 rpm) under a 12:12 light:dark cycle with an irradiance of 31 µmol photons m^{-2} s^{-1}. Algal species were cultured at three selected temperatures of 12 °C, 18 °C, and 30 °C. Between each temperature change, cells were acclimated at 18 °C for 14 days before exposure at 12 °C and 30 °C. The average cell abundance was determined in three sample replicates using Fuchs-Rosenthal haemocytometer (Fein-Optik Jena, Germany, depth 0.2 mm) and light microscope (Olympus BX51, Olympus Corporation, Japan). The determination of growth rate and duplication time in the exponential growth phase of algal cells were provided by Kim (2015). Cells were harvested at the stationary phase (19 days) by centrifugation (1,500 x*g*, 3 min) followed by rinsing and resuspending pellet twice with filtered seawater. The final pellet was resuspended in 2 mL of filtered seawater and served as the stock suspension.

Motility analysis

Aliquots of cell culture were observed under an Olympus BX51 microscope (10x). Video files of 5 s were recorded 10 times consecutively in the sample (50–60 frames per second, image size: 340 × 250, 4 × 4 binning). The video files saved in.avi format were used as input to the open-source image processing software ICY (http:icy.bioimageanalysis.org) to analyse cell motility and trajectories (Novosel et al. 2020). Three plugins were used: Spot Tracking, Track Manager, and Motion Profiler. Data from the analyses of 1000 cells were imported into Microsoft Excel (Microsoft Corporation, Redmond, WA, USA). The output of ICY is an ASCII

file with row data (sample size, the spatiotemporal position of cells, the number of motile and non-motile cells with the corresponding minimum, median, arithmetic mean, and maximum speeds and search radius). The search radius is the maximum distance from the initial point. Linearity is the ratio between the search distance and total path length. The R software package (R Development Core Team 2020) was used to perform additional statistical analyses that included box plots, plots of probability density distributions of speed and search radius, and the Shapiro and Wilcoxon-Mann–Whitney tests.

Electrochemical method

We used the electrochemical method of polarography and chronoamperometry of oxygen reduction at the dropping mercury electrode (DME). The organic constituents such as biopolymers and fluid microparticles in aqueous electrolyte solution can be classified by their electrochemical responses (Figure S1) based on the phenomena of molecular adsorption or particle adhesion at the DME (Žutić et al. 2004; Svetličić et al. 2006; Pletikapić and Ivošević DeNardis 2017). The adsorption of organic molecules at the DME results in a decrease of the surface tension gradient at the mercury electrode/solution interface, which causes the suppression of convective streaming. A gradual decrease in the oxygen reduction current on the chronoamperometric curve corresponds to biopolymer adsorption, which is proportional to the surfactant concentration in the sample and is called surfactant activity. Surfactant activity can be measured by recording the polarographic maximum of Hg(II) ions and offers an alternative approach to measuring dissolved organic carbon in seawater (Hunter and Liss 1981). The surfactant activity is expressed as the equivalent amount of the nonionic synthetic surfactant Triton-X-100 (polyethylene glycol tert-octylphenyl ether, $MW = 600$) in milligram per litre. In contrast, the adhesion of fluid organic particles causes a transient increase in interfacial turbulence, resulting in the spike-shaped amperometric signals (Kovač et al. 2000; Svetličić et al. 2000, 2001; Ivošević DeNardis et al. 2007). The adhesion of a single organic particle from the suspension to the charged interface is recorded as an amperometric signal. The occurrence of amperometric signals of particles is random due to the spatial heterogeneity inherent to a dispersed system and the stochastic nature of the particles' encounter with the electrode. At constant electrode potential, the current amplitude reflects the size of the adhered particle, while the signal frequency reflects the particle concentration in the suspension (Kovač et al. 2000). Whether the adhesion is spontaneous and how fast it progresses depends on the interfacial properties of the three interfaces in contact (particle-medium-electrode). According to the modified Young–Dupré equation (Israelachvili1992), the total Gibbs energy of the interaction between an organic droplet and the aqueous mercury interface is:

$$-\Delta G = A\left(\gamma_{12} - \gamma_{23} - \gamma_{13}\right) \tag{1}$$

$$-\Delta G = A\, S_{132} \tag{2}$$

where γ_{12}, γ_{13}, and γ_{23} are the interfacial energies at the mercury/water, mercury/organic liquid, and water/organic liquid interfaces. The expression in parentheses is equal to the spreading coefficient at the three-phase boundary S_{132}. When $S_{132} > 0$, the attachment and spreading of organic droplets are spontaneous processes, while when $S_{132} < 0$, spreading is not spontaneous. The critical interfacial tension of adhesion $\left(\gamma_{12}\right)_c$ at the $S_{132} = 0$ is equal to $\gamma_{13} + \gamma_{23}$.

Electrochemical measurements of algal cells

Electrochemical measurements were performed in an air-permeable Metrohm vessel with a three-electrode system. The dropping mercury electrode served as the working electrode (dropping time, 2.0 s; flow rate, 6.0 mg s^{-1}; maximum surface area, 4.57 mm^2). All potentials were referenced to a potential measured at an Ag/AgCl (0.1 M NaCl) reference electrode separated from the measured dispersion by a ceramic frit. Platinum served as the counter electrode. An aliquot of the stock cell suspensions was added to 25 mL of filtered seawater (pH 8.0) and then poured into a thermostatted Metrohm vessel at 20 °C. Electrochemical measurements were conducted using a 174A Polarographic Analyser (Princeton Applied Research, Oak Ridge, TN) connected to a computer. Analogue data acquisition was performed using a DAQ card-AI-16-XE-50 (National Instruments, Austin, TX), and data were analysed using the application developed in LabView 6.1 software (National Instruments). The interaction of cells with the electrode is measured by recording polarograms of oxygen reduction (current–potential curve with a scan rate of 10 mV s^{-1}) and current–time curves over 50 mercury drop lives at constant potentials (time resolution: 50 s). Signal frequency is expressed as the number of amperometric signals over 100 s. The surfactant activity is measured by adding 0.5 mL of 0.1 M $HgCl_2$ to the sample before measurement is taken.

Atomic force microscopy imaging

Atomic force microscopy (AFM) measurements were performed using a multimode scanning probe microscope with a Nanoscope IIIa controller (Bruker, Billerica, MA) with a vertical engagement (JV) 125 µm scanner. For imaging in the air, contact mode using silicon nitride contact mode cantilevers (DNP, Bruker, nominal frequency of 18 kHz, nominal spring constant of 0.06 N m^{-1}) were used throughout the

experiments. The linear scan rate was optimised between 1.5 and 2 Hz with a scan resolution of 512 samples per line. The set point was kept at the lowest possible value to minimise the interaction forces between the tip and the surface. Image processing and analysis were performed using the NanoscopeTM software (Bruker, Billerica, MA, USA).

Sample preparation for AFM imaging of cells and released extracellular polymers

The protocol for cell isolation from the growth medium is described in "Cell suspensions" section. The slightly modified protocol for cell isolation was only used for *T. suecica* grown at 12 °C for AFM measurements. The volume of 40 mL *T. suecica* culture was centrifuged at 4,000 ×*g* for 5 min. The loose pellet was washed twice with filtered seawater and diluted with filtered seawater to a final volume of 5 mL, which served for AFM imaging of the cells and released extracellular polymers. The sample preparation protocol for AFM imaging required the fixation of only *D. tertiolecta* stock suspension. *D. tertiolecta* and *C. closterium* were deposited on a bare mica surface, while for *T. suecica*, mica surface was modified with polyethyleneimine (PEI; Sigma-Aldrich Corporation, St. Louis, MS) because of the pronounced cell movement. A 5-µL aliquot of cell suspension was pipetted onto freshly cleaved mica and placed in a closed Petri dish for 1 h to allow the cells to settle and attach to the surface. The mica was then rinsed by immersing three times in a glass with ultrapure water for 30 s and allowed to dry. Afterwards, it was glued to a metal sample pack with double-sided tape and imaged with AFM. In the case of *T. suecica*, the mica was coated with PEI before the immobilisation of the algal cells as follows. A 50 µL aliquot of 0.2% PEI was placed on a freshly cleaved mica surface and incubated for 30 min. The mica was then washed with ultrapure water and dried with nitrogen followed by the cell deposition procedure described above.

Atomic force microscopy working in force spectroscopy mode

AFM measurements of physicochemical properties (i.e. cell elasticity and adhesion) were performed using the Nanowizard IV AFM system (Bruker-JPK, Germany) equipped with a liquid cell setup. Algal cells were indented with MLCT-D silicon nitride cantilevers, characterised by a nominal spring constant of 0.03 N m^{-1} and half open-angle of 21°. Spring constants of the cantilevers were calibrated using the thermal noise method (Sader et al. 1995). Force curves were recorded in the central area of the cell body within a scan area of 3 µm × 3 µm, within which a grid of 6 × 6 points was set. The force curves were recorded at an approach and retract velocity of 8 μms^{-1}, a maximum force of 4 nN, and curve lengths of 4 µm (*C. closterium* and *T. suecica*) and 6 µm (*D. tertiolecta*). The measurements were performed in seawater at room temperature. Recorded data, i.e. force curves, were analysed using JPK Data Processing Software (Bruker-JPK, Germany).

Young's modulus determination

The apparent Young's modulus value was obtained by applying the Hertz-Sneddon contact model (Sneddon 1965). In our study, we used cantilevers with a tip being a four-sided pyramid. Thus, the following equation was applied to describe the relationship between the load force F and the indentation depth δ:

$$F = \frac{E'}{1-\mu^2}\frac{tana}{\sqrt{2}}\delta^2 \tag{3}$$

where μ is the Poisson's ratio, and α is the open-angle of the cantilever's tip. E' is the reduced Young's modulus given by:

$$\frac{1}{E'} = \frac{1-\mu_{tip}^2}{E_{tip}} + \frac{1-\mu_{cell}^2}{E_{cell}}. \tag{4}$$

When $E_{cell} << E_{tip}$, the following relation is obtained:

$$E' = \frac{E_{cell}}{1-\mu_{cell}^2}, \tag{5}$$

where μ_{cell} and μ_{tip} are Poisson's ratios related to the compressibility of the algal cell and indenting cantilever. In our analysis, Poisson's ratio was set to 0.5, assuming that the algal cells are incompressible. AFM data were fitted to the model over a whole indentation range. However, the maximum indentation depth did not exceed 1 µm. The apparent Young's moduli distributions were presented as box plots, where the median and the first (Q_1) and third (Q_3) quartile values are marked.

To quantify the adhesive and hydrophobic properties of algal cells, the retract part of the force curve was analysed. As a result, a maximum work of adhesion (W_{adh}) was determined, which was defined as the area encompassing the negative force values. The value obtained for bare (unmodified) cantilevers quantifies the adhesive surface properties. To obtain the information on the surface hydrophobicity of cells, cantilevers were modified with a hydrophobic trichlorooctadecylsilane (OTS; Sigma-Aldrich) by chemical vapour deposition. Silanisation of the cantilevers was performed in a desiccator for 2 h. Each set of AFM experiments was performed with newly prepared cantilevers that were used immediately after OTS deposition. Thirty-six force curves over 3 µm × 3 µm of the cell body were collected at a

velocity of 8 µm s^{-1} and the maximum load force of 4 nN. The number of cells examined varied from 20 to 30 per case.

The difference between the maximum work of adhesion, extracted from force curves collected with bare and CH_3-functionalised AFM cantilevers, determined the algal cell hydrophobicity level:

$$\Delta W_{adh} = W_{adh(noOTS)} - W_{adh(OTS)} \quad (6)$$

Sample preparation for force spectroscopy measurements

To prepare samples for AFM force spectroscopy measurements, the following protocol was applied. First, 1.5 mL of suspensions of *D. tertiolecta* and *T. suecica* were centrifuged for 3 min at 265 x*g* and for 5 min at 940 x*g*, respectively. Then, 1 mL of the medium was removed, and a pellet of the algal cells was vortexed. After that, 1 mL of filtered seawater was added, and the cells were centrifuged again at the same speed and time. The supernatant was removed, and the cells were suspended in 400 µL of the filtered seawater. A glass coverslip with a PEI coated surface was used as a substrate. PEI was deposited on a glass slide using the drop-casting technique for 1 h and then subsequently dried with a stream of nitrogen. Afterwards, 100 µL of cell suspension was placed for 30 min. Later, the samples were rinsed 3 times, with 100 µL of the filtered seawater. Finally, the samples were covered with seawater, and AFM experiments were performed. *C. closterium* cells (100 µL) were immobilised on a microscopic glass slide cleaned with an oxygen plasma system (Zepto, Diener Electronics GmbH, Germany) in conditions of 0.5 mbar for 1 min at the room temperature. Then, glass slides were left overnight. The samples were rinsed and covered with filtered seawater. Regardless of the algal cell types, the force spectroscopy was performed immediately after sample preparation.

Results

Cell growth dynamics

The growth curves of three selected algal monocultures (*D. tertiolecta*, *T. suecica*, *C. closterium*) at three growth temperatures (12 °C, 18 °C, and 30 °C) are shown in Figure S2. The data showed that growth depends on temperature conditions. The initial number of cultured cells in the growth medium was similar for all species studied, approximately 2.0×10^4 cells mL^{-1}. Table S1 summarises calculated growth rate and doubling time of three selected algae in the exponential growth phase at 12 °C, 18 °C, and 30 °C. For *D. tertiolecta* and *T. suecica*, the fastest growth and the shortest doubling time were obtained at 18 °C, which was considered a favourable temperature. For *C. closterium*, the fastest growth and the shortest doubling time were determined at 30 °C.

Motility characterisation

Qualitative insight of *D. tertiolecta* cells movement at selected temperatures is presented in Fig. 1.

At the temperature of 12 °C, about 40% of cells (69 cells) were stationary or exhibited erratic on-the-spot movement (Table S2), while the quantified trajectories of the majority of cells (101 cells) had a linearity ratio of 0.12 with an average movement time of 3.6 s. At the temperature of 18 °C, a total of 264 cells were counted in the sample, of which 21% were stationary, while 79% demonstrated random movement depicted with the broken-line type of trajectories and the linearity ratio of 0.36 during an average movement time of 2.5 s. At the temperature of 30 °C, about 22% of cells were stationary, while 78% showed similar qualitative movement to the control at 18 °C, but with a higher linearity ratio of 0.45 during an average movement time of 3.2 s.

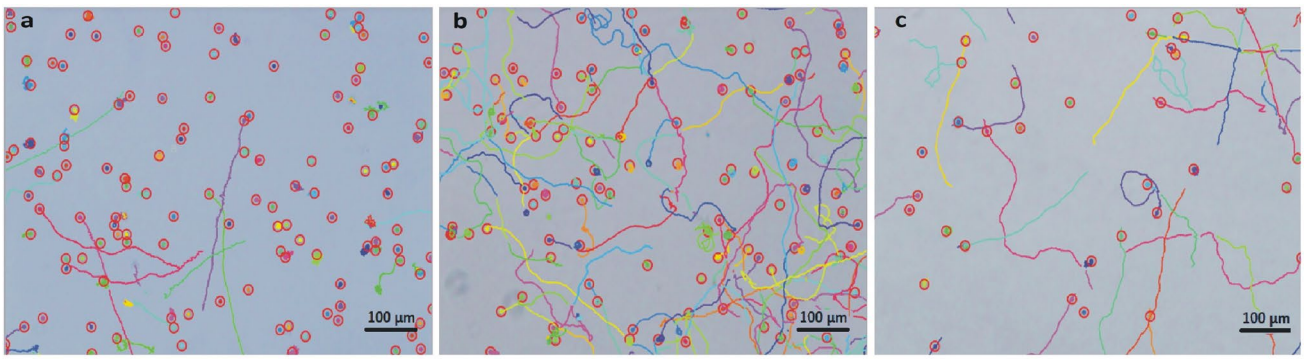

Fig. 1 Reconstructed ICY images of *D. tertiolecta* grown at temperatures of (**a**) 12 °C ($2.3x10^6$ cells mL^{-1}), (**b**) 18 °C ($5.3x10^6$ cells mL^{-1}), and (**c**) 30 °C ($1.7x10^6$ cells mL-1). Distance bar denotes 100 µm. Cells and their trajectory are denoted with coloured circles and curved coloured lines, respectively

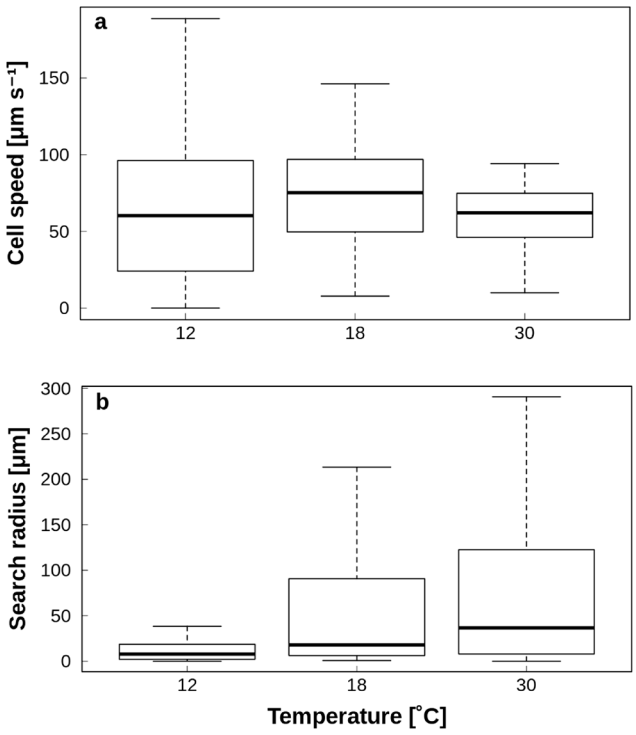

Fig. 2 Box plots of cell speed (**a**) and search radius (**b**) of *D. tertiolecta* grown at temperatures of 12 °C ($2.3x10^6$ cells mL^{-1}), 18 °C ($5.3x10^6$ cells mL^{-1}) and 30 °C ($1.7x10^6$ cells mL^{-1})

Box plots of cell speeds are presented in Fig. 2a.

The medians at 12 °C and 30 °C were almost identical. At the temperature of 12 °C, the average cell speed corresponded to 63 ± 3 µm s^{-1}, while at the 30 °C, the average speed is 62 ± 4 µm s^{-1} (Table S3). At 18 °C, cells were moving with an average speed of 72 ± 2 µm s^{-1}, which amounts to 6 body lengths per second.

From the whiskers above and below the median at 12 °C and 30 °C, it follows that the corresponding distributions of speeds deviated from the normal distribution. Indeed, the probability density distributions of cells speed (Figure S3a) revealed that all three distributions deviated from the normal distribution (for 12 °C, $\alpha_3 = 0.6$; for 18 °C, $\alpha_3 = -0.3$; for 30 °C, $\alpha_4 = 12$). The Shapiro–Wilk test confirmed that all three distributions differed significantly from the normal (for 12 °C, $W = 0.94$, $p = 9.3e\text{-}07$; for 18 °C, $W = 0.96$, $p = 1.8e\text{-}06$; and for 30 °C, $W = 0.84$, $p = 4.4e\text{-}07$). The Wilcoxon rank sum test showed that the median speed at 12 °C differed significantly from the median at 18 °C ($W = 18{,}487$, $p = 0.002$) and that the median at 30 °C differed significantly from the median at 18 °C ($W = 11{,}322$, $p = 0.0009$). However, the median at 12 °C did not differ significantly from the median at 30 °C ($W = 5707$, $p = 0.9$) as it is observable from the box plot (Fig. 2a), although the corresponding distributions are very different (Figure S3a): (a) the peak of the probability density distribution for 12 °C was close to 20 µm s^{-1}, while for 30 °C, it was close to 60 µm s^{-1}; and (b) the distribution at 12 °C resembled chi-square distribution with $k = 3$, i.e. positively skewed with a long tail, while the distribution at 30 °C was much closer to the Maxwell–Boltzmann distribution of velocities with the scaling factor of $a = 2$.

At the temperature of 12 °C, the average search radius of cells in the sample was 24 ± 4 µm. At the temperature of 18 °C, the average search radius of cells was almost doubled and was 57 ± 5 µm, while the median was only 18 µm. At the temperature of 30 °C, the average search radius increased further to 80 ± 12 µm. The box plots in Fig. 2b showed a progressive increase in the median of the search radius going from 12 °C until 30 °C. However, they also showed that with the increase in the search, radius comes a greater variation toward higher values.

The probability density distributions plot (Figure S3b) of the three samples showed that the distributions of search radius are far from normal. Indeed, Shapiro–Wilk test confirmed that the distributions are significantly different from the normal distribution (for 12 °C, $W = 0.4$, $p < 2.2e\text{-}16$; for 18 °C, $W = 0.7$, $p < 2.2e\text{-}16$; and for 30 °C, $W = 0.8$, $p = 1.503e\text{-}08$). The Wilcoxon rank sum test showed that the medians at 12 °C and 18 °C were significantly different ($W = 14{,}201$, $p = 1.051e\text{-}10$) and also that the medians at 12 °C and 30 °C were significantly different ($W = 3345.5$, p value $= 3.902e\text{-}07$). However, the test revealed that the medians at 18 °C and 30 °C were not significantly different ($W = 8054.5$, $p = 0.192$). This result arose from predominantly similar tails of the distributions but certainly not from the difference in their peaks. The peak of the probability density distribution at 18 °C was only 60% of the higher peak of the probability density distribution at 30 °C. Also, the average search radius of moving cells at 12 °C was about 40% of the value at 30 °C (Table S2).

It should be noted that the percentage of vibrating cells, i.e. cells with almost no net movement at 12 °C, was double the percentage at 30 °C (Table S2). The average speed of vibrating cells was about 40% of the speed of the moving cells. Their search radius was about 3% of the search radius of the moving cells. Examination of speed and search radius of moving cells only (Table S2) revealed that cells at 12 °C have the highest speed (87 ± 3 µm s^{-1}) versus 81 ± 2 µm s^{-1} at 18 °C and 71 ± 4 µm s^{-1} at 30 °C. Moreover, they have the smallest search radius: 40 ± 4 µm at 12 °C versus 72 ± 5 µm at 18 °C and 102 ± 12 µm at 30 °C. With a raise in temperature from 12 °C to 30 °C, the search radius increased 2.6 times.

Figure 3 provides a qualitative insight into *T. suecica* cell movement at the three selected temperatures.

In contrast to *D. tertiolecta, T. suecica* cells showed more pronounced movement. Box plots of median speed, average speed, and search radius with corresponding probability density distributions are presented in Fig. 4a and b and Figures S4a and b, respectively.

The medians of speed at 18 °C (201 µm s^{-1}) and 30 °C (194 µm s^{-1}) were similar, while the median at 12 °C was considerably smaller (113 µm s^{-1}). At the temperature of 12 °C, the average cell speed in the sample corresponded to 128 ± 14 µm s^{-1}, while the average speed at the 30 °C was 179 ± 7 µm s^{-1}. At the 18 °C, cells moved with the highest average speed of 190 ± 5 µm s^{-1} which is nearly 13 body lengths per second (Table S4a).

From the whiskers above and below the median at 12 °C and 30 °C, it can be observed that the speed distributions were not normal. The probability density distributions (Figure S3) revealed that none of the three distributions are likely to be normal (for 12 °C, $\alpha_3 = 0.4$; for 18 °C, $\alpha_3 = -0.4$; for 30 °C, $\alpha_3 = -0.1$). Indeed, the Shapiro–Wilk test confirmed that all the three distributions differed significantly from the normal (for 12 °C, $W = 0.91$, p value = 0.002; for 18 °C, $W = 0.97$, $p = 8.8e\text{-}05$; and for 30 °C, $W = 0.97$, $p = 0.004$. The Wilcoxon rank sum test showed that the median speed at 12 °C differed significantly from the median at 18 °C ($W = 3853$, $p = 3.7e\text{-}05$), but the median at the 18 °C did not differ significantly from the median at 30 °C ($W = 20{,}366$, $p = 0.19$). Finally, the median at 12 °C differed significantly from the median at 30 °C ($W = 2411$, $p = 0.001$), as shown on the box plot.

The negatively skewed probability density distributions at 18 °C and 30 °C did not differ significantly and their peak was at about 240 µm s^{-1} (Figure S4a), as was confirmed by the Wilcoxon's test. The positively skewed probability density distribution of speeds at 12 °C had two peaks, the dominant one at about 50 µm s^{-1} and the inferior one at approximately 230 µm s^{-1}.

Box plots of cells' search radii in the sample at the three temperatures are presented in Fig. 4b. The medians of the search radius at 12 °C (16 µm) and 30 °C (31 µm) are closer to each other than the median at 18 °C, which is from 3 to 6 times larger (102 µm). At the temperature of 12 °C, the average cell search radius of the sample

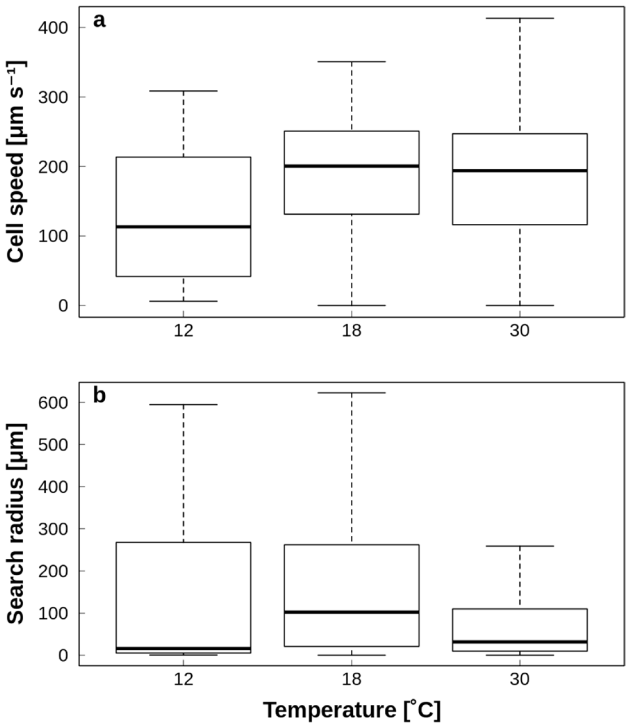

Fig. 4 Box plots of cell speed (**a**) and search radius (**b**) of *T. suecica* grown at temperatures of 12 °C (2.3x10^5 cells mL^{-1}), 18 °C (1.9x10^6 cells mL^{-1}) and 30 °C (9.4x10^5 cells mL^{-1})

corresponded to 127 ± 26 µm, while at the 30 °C the average speed was 80 ± 9 µm (Table S4a, b). At the 18 °C, the average search radius of *T. suecica* was 163 ± 11 µm which amounted to about 12 body lengths.

As noted from the whiskers above and below the median at all tested temperatures and from Figure S4b, all three distributions were positively skewed and far from a normal distribution. Indeed, the Shapiro–Wilk test confirmed that all three distributions differ significantly from the normal (for 12 °C, $W = 0.73$, p value = 5.5e-08; for 18 °C, $W = 0.84$,

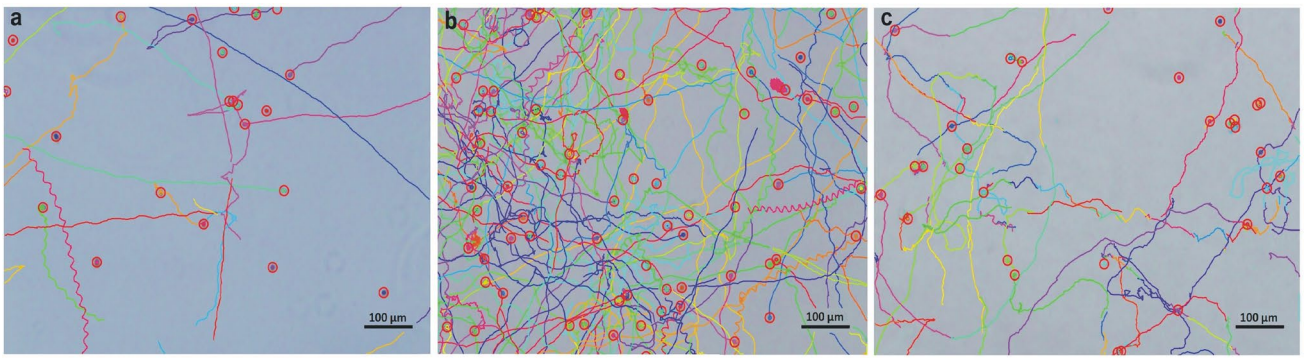

Fig. 3 Reconstructed ICY images of *T. suecica* grown at temperatures of (**a**) 12 °C (2.3x10^5 cells mL^{-1}), (**b**) 18 °C (1.9x10^6 cells mL^{-1}), and (c) 30 °C (9.4x10^5 cells mL^{-1}). Distance bar denotes 100 µm. Cells and their trajectory are denoted with coloured circles and curved coloured lines, respectively

$p = 1.4e\text{-}15$; and for 30 °C, $W = 0.73$, $p = 3.4e\text{-}15$). The Wilcoxon rank sum verified that the median of search radius at 12 °C differed significantly from the median at 18 °C ($W = 4561$, $p = 0.004$). In addition, the median at the 30 °C differed significantly from the median at 18 °C ($W = 24{,}953$, $p = 7.9e\text{-}08$), but the median at 12 °C did not differ significantly from the median at 30 °C ($W = 3377.5$, $p = 0.66$), as it was shown on the box plot.

The positively skewed probability density distributions showed that the search radius and the speed of cells were increasing from 12 to 18 °C. On the other hand, the average search radius at 30 °C was the smallest, although the average speed of cells was the highest. This showed that the linearity of movement was much lower, i.e. the cells wiggled much more than at progressively smaller temperatures.

Electrochemical characterisation of algal cells and released surface-active matter

Electrochemical adhesion-based characterisation of isolated algal cells resuspended in seawater was performed by recording polarograms of oxygen reductions. The polarogram recorded in the *D. tertiolecta* cell suspension showed the appearance of irregular perturbations in the defined potential, resulting from the cell adhesion at the charged interface (Fig. 5a).

No perturbations were recorded outside of this potential range (more positive and negative), indicating that cell adhesion is not present. The polarograms recorded in the cell suspensions of *T. suecica* and *C. closterium* were perfectly regular, without the occurrence of perturbations, i.e. these cells behaved as inert and no adhesion takes place. Therefore, only the cells of *D. tertiolecta* were used to test the effect of temperature on cell adhesion behaviour at the wide potential range. The dependence of the amperometric signal frequency on applied potentials at three temperatures in *D. tertiolecta* suspensions with similar cell densities is shown in Fig. 5b. The narrowest potential range of adhesion was recorded in the *D. tertiolecta* cell culture grown at 12 °C, denoted by critical potentials of –192 mV and –1200 mV in seawater. The most negative and the most positive potential in which at least one amperometric signal per 10 consecutive I–t curves appears corresponded to critical potentials (Ec^+, Ec^-, Žutić et al. 1993; Ivošević et al. 1994). For the cell suspension grown at the 30 °C, the measured critical potentials of adhesion corresponded to −184 and −1170 mV, while the broadest potential range of cell adhesion was recorded in the cell suspension grown at the temperature of 18 °C, from −110 to −1240 mV, which offers a favourable growth condition for the corresponding cell. The lowest number of amperometric signals of cells was recorded in cell suspension grown at 12 °C. The number of recorded amperometric signals increased with the increase in temperature used in cell culture. The maximum number of amperometric signals occurred at the potential of –400 mV at all three examined temperatures, since interfacial tension is close to the maximum value (electrocapillary maximum). At this potential, the mercury electrode is positively charged and electrostatic attraction prevails in between the positively charged interface and the negatively charged *D. tertiolecta* cells. By shifting the potential either positively or negatively from –400 mV, interfacial energy decreases, and the number of amperometric signals of the cells decreases accordingly. On the other hand, at the potential of −800 mV, the mercury electrode is negatively charged, and signal frequency is lower due to the electrostatic repulsion with the negatively charged *D. tertiolecta* cells.

Quantitative characterisation of the released surface-active matter in the growth medium was determined by recording polarograms of Hg(II). The polarographic maximum of Hg(II) is sensitive for the adsorption of dissolved organic matter and submicron particles, which is manifested cumulatively as a gradual decrease in the reduction current proportional to surfactant concentration in the sample. Surfactant activity at different growth temperatures was determined and expressed per cell (Fig. 5c). The data showed that surfactant activity is the highest in *C. closterium* at 12 °C, then in *D. tertiolecta* at 30 °C, while the lowest surfactant activity is determined in *T. suecica* cells.

Nanoscale imaging of algal cell and released extracellular biopolymers

Morphological characterisation of *D. tertiolecta, T. suecica*, and *C. closterium* cells at 12 °C, 18 °C, and 30 °C was performed by AFM. The representative images of individual algal cells for each species are shown in Fig. 6.

All three species maintained the same overall cell shape regardless of the temperature, with no nanostructural changes observed on the cell surface. The cells of *D. tertiolecta* had an ovoid shape with two flexible flagella that were distinguishable from the cell body (Fig. 6a). The cell body length was in the range of 7.5–12.1 µm, and the cell width was 4.5–6.8 µm. Flagella had a length of 17–20 µm and a height of 90 nm. The cells of *T. suecica* had an ellipsoid shape with four flexible flagella that were distinguishable from the cell body (Fig. 6b). The cell body length was in the range 14.0–20.1 µm and cell width 8.5–14.7 µm. The flagella had a length of 8.7–10.2 µm and a height of about 200 nm. Granular structures observed on the surface of *T. suecica* probably correspond to micropearls previously identified by SEM (Martignier et al. 2018), thus

being the first AFM-based observation of micropearls in the genus *Tetraselmis*.

Cylindrotheca closterium cells possessed an elongated shape with flexible rostrae that could be clearly distinguished from the central part of the cell (Fig. 6c). The cell body length was in the range 30.5–60.2 µm, and cell width was 2.8–8 µm. Three morphologically different parts of the frustule could be distinguished: the girdle band, the valve, and the raphe. The longitudinal slit raphe extends along with the valve and is bridged by the fibulae. The spacing between fibulae was 250–350 nm, and fibulae arches underneath the cell wall were noticeable. High-resolution images of the central part of the cell revealed a non-structured and smooth surface of the valve, whereas the girdle band showed a structured surface consisting of a set of parallel bands. Morphological parameters including cell length, cell width, cell height, and cell surface roughness of the cells grown at different temperatures based on AFM image analysis are summarised in Table S5. The length, width, and height of *D. tertiolecta* grown at 12 °C and 18 °C were similar. However, the cells grown at 30 °C were smaller in both length and width, but with a maintained cell height. The roughness of *D. tertiolecta* cell surface was in a similar range for all temperatures. The length, width, and height of *T. suecica* grown at 12 °C and 18 °C were similar, while cells grown at 30 °C were smaller in both length and width and with no change in cell height. The roughness of *T. suecica* cell surface grown at different temperatures was in a similar range. The size (length, width, and height) of *C. closterium* had the highest values at 12 °C. The length, width, and height of *C. closterium* grown at 18 °C and 30 °C were similar. The roughness of *C. closterium* valve and girdle increased accordingly with the increase in temperature.

Supramolecular organisation of released materials of *C. closterium, D. tertiolecta*, and *T. suecica* at temperatures of 12 °C, 18 °C, and 30 °C were imaged (Fig. 7).

The extracellular polymer substance (EPS) of *C. closterium* formed a network of fibrils at all examined temperatures. The EPS of *C. closterium* grown at 12 °C was located all around the cell and the network appeared denser (Fig. 7a). The height range of fibrils was in the range of 1.5–4 nm. At temperatures of 18 °C and 30 °C, the released EPS fibrils were mostly located around the apices of rostra with a height range of 1–4 nm (Fig. 7b, c). The released material was visible around *D. tertiolecta* cells (Fig. 7d) grown at 12 °C and consisted of the fibrillar network (height 0.7–1.5 nm) with incorporated globules (height 2.5–10 nm). At the temperatures of 18 °C and 30 °C, only aggregated particles (height 2–5 nm) were observed around *D. tertiolecta* cells (Fig. 7e). Although fixation could introduce artefacts, the relative change in the organisation of released polymers from *D. tertiolecta* cells was distinguished. At selected temperatures, only aggregated particles with a height range of 5–25 nm were observed around the cells of *T. suecica* (Fig. 7f).

Nanomechanical characterisation of algal cells by AFM

An individual algal cell was localised on the substrate using an inverted optical microscope (Fig. 8a). Force curves were recorded at the central area of the cell body within a scan area of 3×3 µm. Representative maps of local elastic (Young's modulus, *E*) and adhesive properties (maximum work of adhesion, W_{adh}) of the *D. tertiolecta* cell are shown in Fig. 8c and d, respectively.

The overlay of the box-plots and Young's modulus distributions obtained for *D. tertiolecta*, *T. suecica*, and *C. closterium* cells cultured at 12 °C, 18 °C, and 30 °C are presented in Fig. 9.

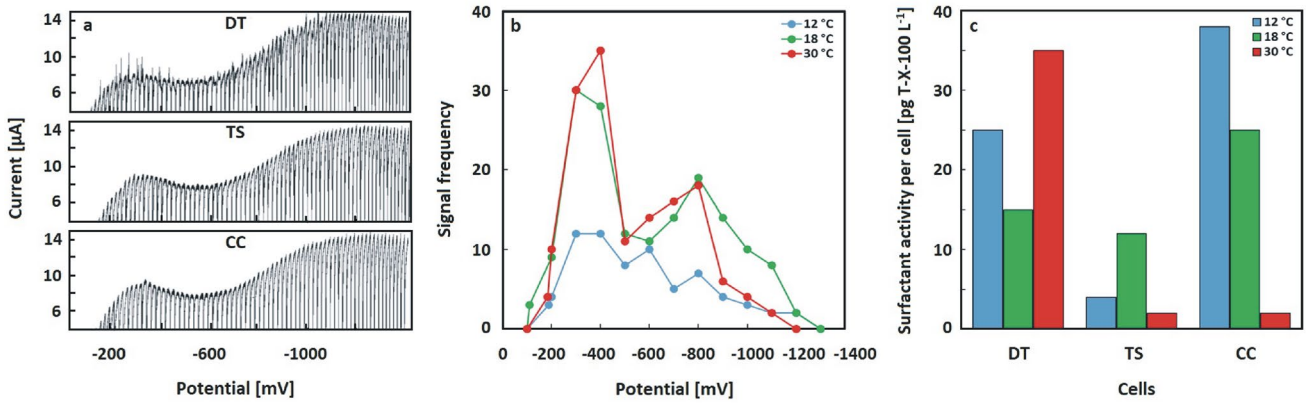

Fig. 5 Polarograms of oxygen reduction recorded in *D. tertiolecta, T. suecica* and *C. closterium* cell suspensions in seawater (**a**); potential dependence of the signal frequency of *D. tertiolecta* cells grown at temperatures of 12 °C, 18 °C, and 30 °C (**b**) and surfactant activity for examined cell species at selected temperatures (**c**)

Regardless of the temperature conditions, *D. tertiolecta* cells are characterised by the lowest Young's modulus ranging from a few to 40 kPa. *T. suecica* cells are stiffer with the *E* varying from 1 to 300 kPa. For *C. closterium*, the *E* values varied even within one single cell from kPa to MPa. Considering that Young's moduli distributions are broad and non-symmetric, we have compared median values among the studied cell populations. The median was accompanied by an interquartile range (*Q3-Q1*), which describes where the central 50% of data lie.

The mechanical properties of algal cells were dependent on the temperature (Fig. 9). We found that *D. tertiolecta* cells stiffen at low temperature (a median of the Young's modulus is equaled to 6.4 kPa (*Q3-Q1* = 9.1 kPa)) at 12 °C and become more compliant at higher temperatures, i.e. 3.5 kPa (*Q3-Q1* = 3.2 kPa) at 18 °C and 1.5 kPa (*Q3-Q1* = 4.6 kPa) at 30 °C. The statistical significance for all groups was below 0.0001 for the 0.05 significance level (Kruskal–Wallis ANOVA test). Median (*Q3-Q1*) values determined for *T. suecica* at 12 °C, 18 °C, and 30 °C were 42.8 kPa (75 kPa), 45.9 kPa (80.2 kPa), and 44.7 kPa (65.7 kPa), respectively. Data sets for algal cells cultured at 12 °C and 18 °C and algal cells cultured at 18 °C and 30 °C showed a statistical significance ($p < 0.05$ for all data groups). No statistical difference was observed for 12 °C and 30 °C. *C. closterium* cells are characterised by the largest modulus distributions. Despite that, analogously to *T. suecica*, a statistical significance ($p < 0.05$) was noted among the groups of algal cells cultured at various temperatures. The corresponding medians (*Q3-Q1*) were 292 kPa (332 kPa), 214 kPa (436 kPa), and 152 kPa (577 kPa).

Adhesive and hydrophobic properties of algal cells

The change in the hydrophobic properties (ΔW_{adh}) of the algal cell surface is quantified from the subtraction of the work of adhesion determined for bare and OTS-coated cantilevers (Fig. 10a, b; expression 6).

The positive value of ΔW_{adh} denotes the domination of hydrophilic interactions, while its negative values indicate that the hydrophilicity is smothered by the hydrophobicity. Table S6 presents the mean value of the maximum work of adhesion (± standard error of the mean, *SEM*) obtained from measurements with bare and OTS-coated cantilevers. The relative probability of adhesion (*P*) between each studied cell line with the bare and CH_3-functionalised silicon nitride AFM probe is presented in Figure S5. The results obtained from the maximum work of adhesion, as well as adhesion probability, showed species-specific and temperature-dependent changes. In the case of *D. tertiolecta* cells, the probe modification resulted in a slight decrease in adhesion probability regardless of temperature conditions. A contrasting trend was observed for *T. suecica* cells cultured at 18 °C and 30 °C, where probe modification significantly diminished adhesion probability. Interestingly, this was not the case for cells cultured at 12 °C, for which the probability of adhesion increased from 31 to 47%. A similar observation referred to *C. closterium* cells cultured at 12 and 30 °C. When probed with an OTS-modified tip, *P* value increased from 2 to 13% and from 42 to 55%, respectively. At 18 °C, the probability of adhesion between a bare probe and *C. closterium* cell was higher than between an OTS-modified tip and the cell.

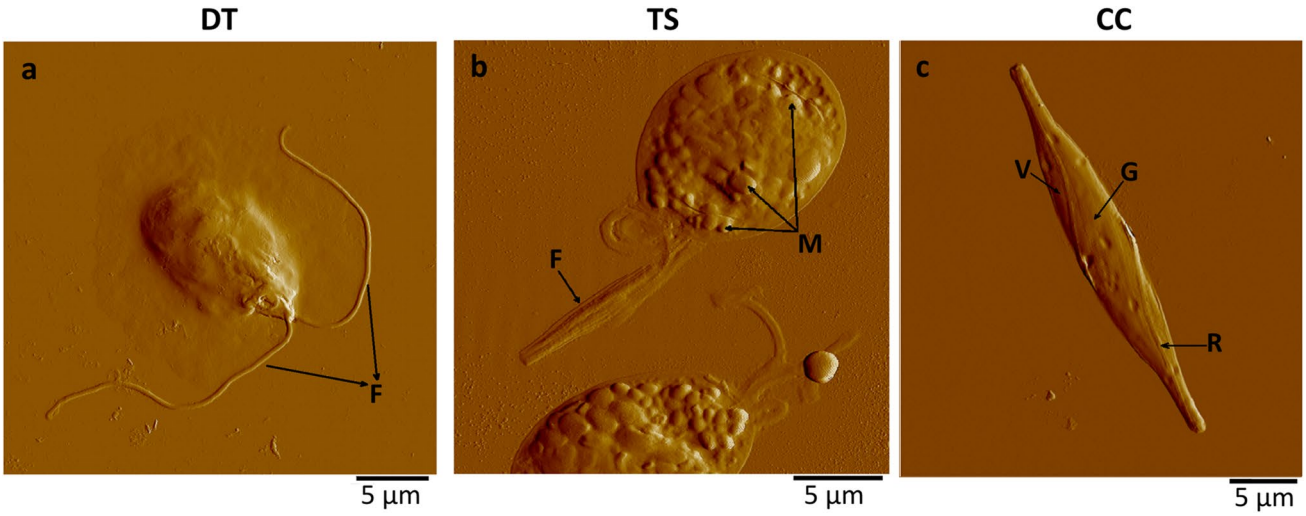

Fig. 6 AFM deflection images of *D. tertiolecta* (**a**), *T. suecica* (**b**) and *C. closterium* (**c**) cells. Images are acquired using contact mode in the air with scan sizes: 30x30 µm (**a**) 25x25 µm (**b**) and 40x40 µm (**c**). Letters F, M, V, G and R indicate the following features: flagellae, micropearls, valve, girdle band, and raphe opening, respectively

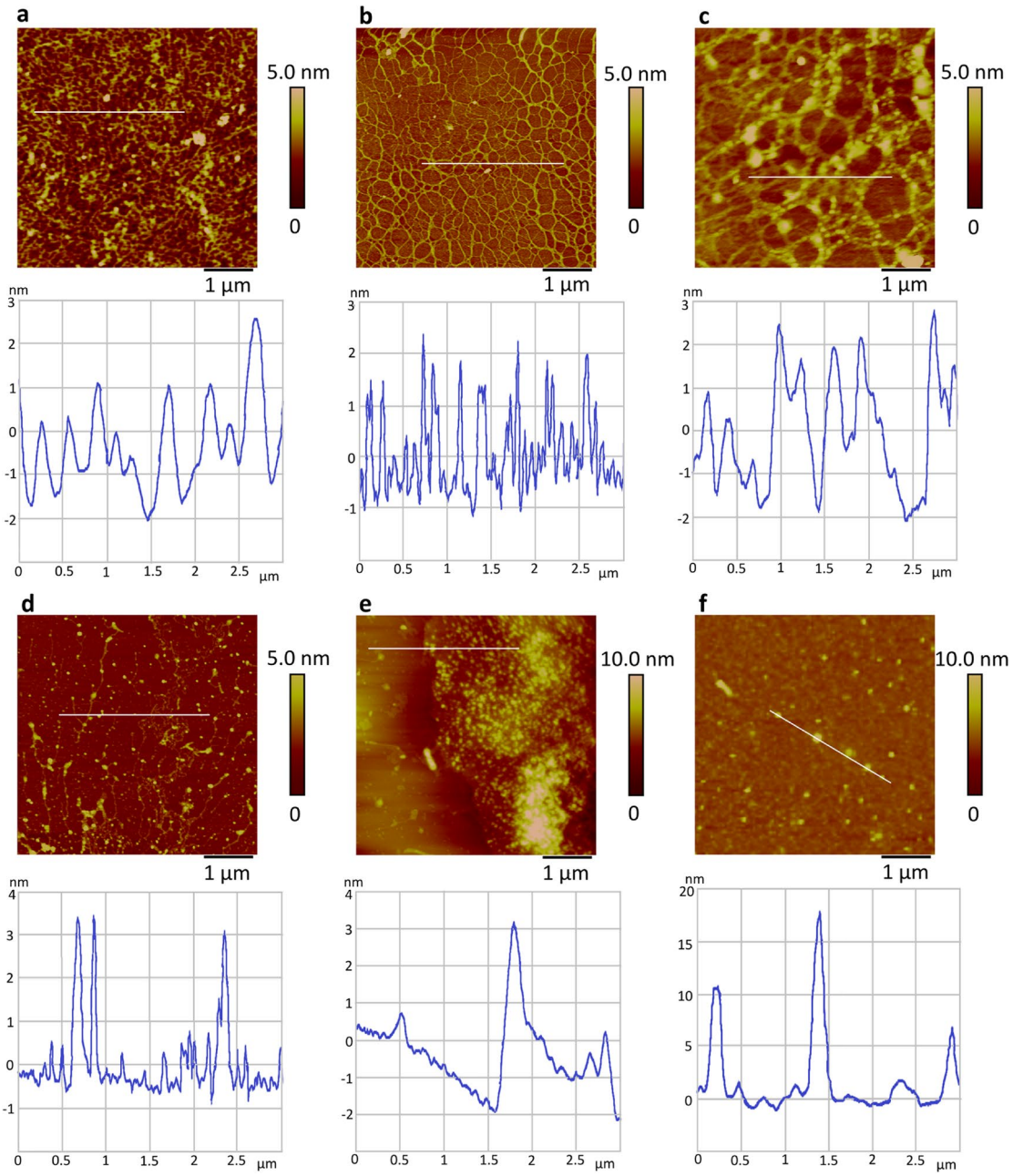

Fig. 7 AFM topographical images of extracellular polymers of *C. closterium* grown at 12 °C (**a**), 18 °C (**b**) and 30 °C (**c**). *D. tertiolecta* grown at 12 °C (d) and 18 °C (e); *T. suecica* grown at 18 °C (f); Images are acquired using contact mode in air and presented as height data with vertical profiles along indicated lines. Scan sizes: 5x5 µm

The balance between the hydrophobic and hydrophilic properties of algal cells is depicted in Fig. 10c. The first observable showed variability among the studied algal cells and temperature. Starting from 12 °C, the surface of *D. tertiolecta* and *T. suecica* cells demonstrated hydrophilic character, while the surface of *C. closterium* seems to be more hydrophobic. The relation between surface properties of algal cells extending from hydrophilic to hydrophobic can be expressed as *D. tertiolecta* > *T. suecica* > *C. closterium*, respectively. The increase to 18 °C caused an abrupt change in the surface properties, with the cells of *C. closterium* possessing the most hydrophilic surface. A similar degree of surface hydrophilicity present on the cells of *D. tertiolecta* and *T. suecica* was outlined by extremely low values of ΔW_{adh}, i.e. 0.0094 ± 0.0018 fJ and 0.0063 ± 0.0028 fJ, respectively. However, the overall net surface properties

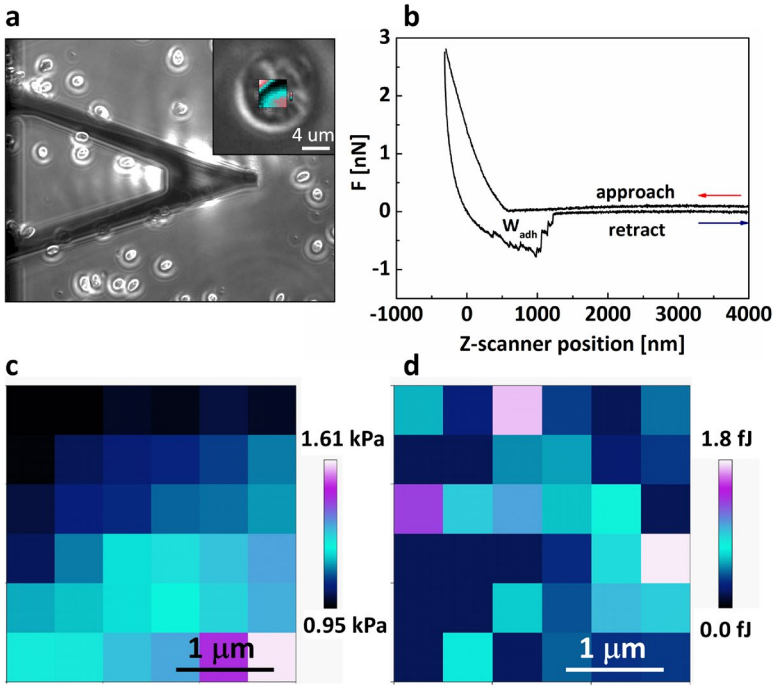

Fig. 8 Phase-contrast microscopic image of the bare MLCT-D cantilever and *D. tertiolecta* cells cultured at 30 °C (**a**). An example of the corresponding force curve recorded on a single *D. tertiolecta* cell (**b**). Representative maps of local elastic (Young's modulus, (**c**)) and adhesive properties (maximum work of adhesion (**d**))

were still hydrophilic. Further increase to 30 °C changed the relationship between the surface properties of algal cells once more.

The surface of *D. tertiolecta* and *T. suecica* cells was characterised by high $W_{adh\ (no\ OTS)}$ and low $W_{adh\ (OTS)}$ values ending in a similar level of hydrophilicity. For *D. tertiolecta* cells, this value reached the level observed for 12 °C, while a much higher hydrophilicity level was observed for *T. suecica* cells. The high negative value of ΔW_{adh} obtained for *C. closterium* cells (-0.77 ± 0.08 fJ) indicates that algal cells become strongly hydrophobic at 30 °C.

Discussion

The possible ecological implications of temperature as a physical stressor on the fate of microalgae in aquatic systems are still inadequately understood. To the best of our knowledge, the effect of temperature on the surface properties and behaviour of selected microalgae has not been reported. In this study, we related temperature changes to algal response, taking into account their structural characteristics that may contribute to temperature tolerance. A summary of relationships between cell morphological characteristics and the studied parameters determined at 12 °C, 18 °C, and 30 °C, respectively, are given in Table 1.

The results showed that algal species successfully adapt to all tested temperatures. The favourable growth temperature (T_f) for *D. tertiolecta* and *T. suecica* was 18 °C, whilst it was 30 °C for *C. closterium*, which is congruent to the natural habitat conditions that the species occupy. Slow growth rates were determined when algal species were cultured at $T \neq T_f$.

Behavioural responses of algal species were analysed in terms of motility, adhesion at the charged electrode, and physiological activity. Motility analysis of flagellated species provides an insight into the physiological state of algal cells in culture. Both *D. tertiolecta* and *T. suecica* showed pronounced motility ranging from 6 to 13 body lengths per second (cell lengths approximately 6–12 µm, respectively). Algal cell speed depends on the number of flagella that a cell possesses; thus, *T. suecica* is about 3 times faster than *D. tertiolecta* at T_f. At lower temperature ($T<T_f$), *D. tertiolecta* and *T. suecica* responded with significantly slower cell speeds and erratic movements around the spot. At higher temperature ($T>T_f$), *D. tertiolecta* and *T. suecica* responded without a significant change in cell speeds, while the search path increased with a greater variation for *D. tertiolecta*. Change in the motility behaviour of *D. tertiolecta* is probably related to change in cell stiffness and physiological activity. Mayali et al. (2008) reported that marine bacteria caused a decrease in the speed of motile phytoplankton through the release of enzymes, which could provide plausible justification of our results.

Electrochemical adhesion-based detection of algae depends on the collective surface properties (fluidity, hydrophobicity, cell surface charge) of the cell exterior. Only soft and deformable species like *D. tertiolecta* adhere to charged fluid interface in the well-defined potential range. At $T<T_f$,

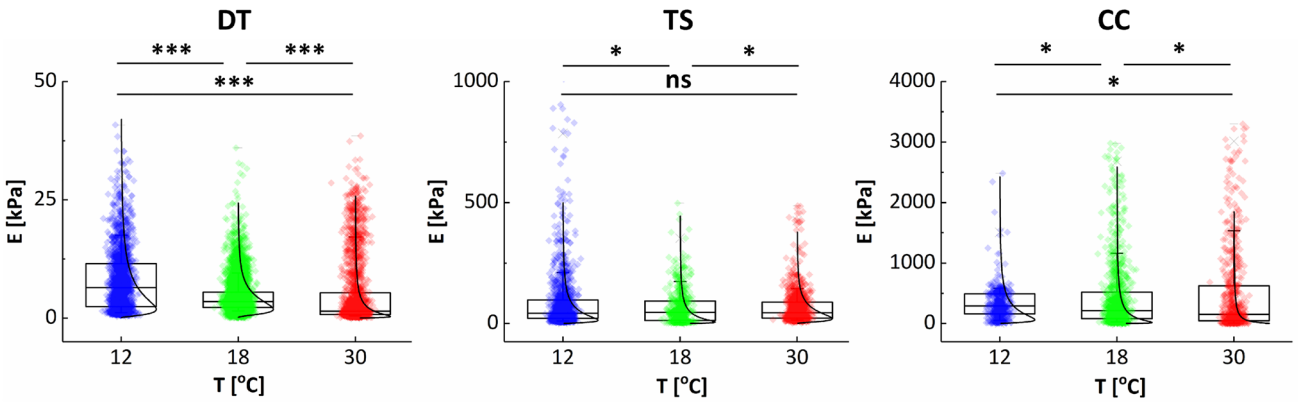

Fig. 9 Overlay of the box plots with Young's modulus distributions, obtained for *D. tertiolecta* (**a**), *T. suecica* (**b**), and *C. closterium* (**c**) cells cultured at 12 °C, 18 °C and 30 °C, were fitted with the log normal function (black line). A box with whiskers represents a median ± interquartile range (Q3-Q1). Statistical significance was obtained from Kruskal-Wallis ANOVA test at the level of 0.05 (*** $p < 0.0001$, ns – not statistically significant)

the potential range of adhesion is the narrowest, due to determined stiffness and a distinct physiological activity of *D. tertiolecta*. The adhesion efficiency of *D. tertiolecta* is the lowest at $T<T_f$ due to the competitive adsorption of released organic material which masks single cell adhesion (Ivošević and Žutić 1997; Kovač et al. 1999). At T_f, the cells of *D. tertiolecta* adhered in the broadest range designated with the critical potentials from −110 to −1240 mV. The adhesion of *D. tertiolecta* cells exists within a wide range of surface charge density, where the electrode carries positive and negative polarities, thus showing the predominance of hydrophobic over electrostatic interactions in the adhesion process (Svetličić et al. 2001). The high probability (over 75%) of adhesion between an AFM probe and *D. tertiolecta* cells also supports this conclusion (Figure S5). The manifestation of electrostatic interactions between the negatively charged cell and the negatively charged electrode is detected through lower signal frequency and critical interfacial tension of adhesion. The critical interfacial tensions can be determined from the critical potentials and electrocapillary data for an aqueous electrolyte solution. Since electrocapillary data for natural seawater is not available, the reported critical interfacial tensions for adhesion of *D. tertiolecta* at mercury/0.1 M NaCl showed to be different at the positively and negatively charged interface probably due to the electrostatic repulsion (Svetličić et al. 2001; Novosel and Ivošević

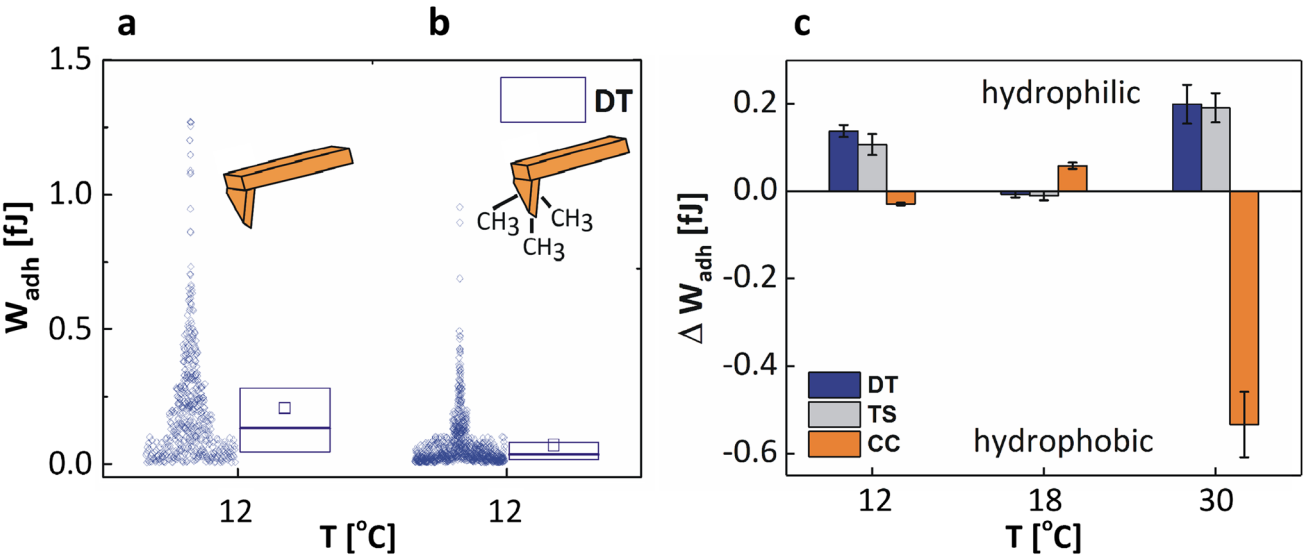

Fig. 10 Exemplary distribution of maximum work of adhesion obtained for *D. tertiolecta* cells cultured at 12 °C and probed with a bare silicon nitride ($W_{adh\ (no\ OTS)}$, **a**) and CH_3–modified (hydrophobic) AFM cantilevers ($W_{adh\ (OTS)}$, **b**). The balance between hydrophilic and hydrophobic properties of algal cell surface plotted for 12 °C, 18 °C, and 30 °C (data are presented as $\Delta W_{adh} \pm$ maximum error, **c**)

DeNardis 2021). In contrast, the adhesion and spreading of *T. suecica* and *C. closterium*, which are stiffer by 2–3 orders of magnitude, are hindered by the mechanical strength of the cells; therefore, these species were not detected at the fluid interface. The mechanical properties of cells are related to fatty acid composition and content. Low content of polyunsaturated fatty acids (PUFAs) was present in diatoms (Barreira et al. 2015), as opposed to the very high content of PUFAs (higher than 50% of total fatty acids, FAs), which are commonly found in green algae (most notably in *D. tertiolecta* and to some less extent in *T. suecica*).

Physiological activity of the cells, expressed as electrochemically measured surfactant activity, refers to released organic material, which appears to be species-specific and temperature-dependent. The most pronounced surfactant activities were determined at 12 °C for *C. closterium* and at 12 °C and 30 °C for *D. tertiolecta*, which were shown to be unfavourable to cell growth. The lowest amount of released organic material is determined for *T. suecica* regardless of the temperature (Fig. 5c).

Our results show differences in the supramolecular organisation of extracellular polymeric substances in the selected species as a function of temperature change. The structural organisation of the released organic material probed by AFM revealed the form of a polysaccharide-rich EPS network around the entire cells of *C. closterium.* Since the corresponding cells cannot easily escape, they must cope with environmental changes by altering their cellular metabolism through considerable physiological activity (Hader et al. 2015). Physiologically, cells secrete an excessive amount of structurally and compositionally diverse biopolymers, mainly consisting of polysaccharides, proteins, nucleic acids, and lipids. The microalgal EPS is acidic, negatively charged and somewhat hydrophobic due to the anionic components of the polysaccharide chains, such as acetyl groups, uronic acids and sulphates, which are important for its adhesive properties (Bertocchi et al. 1990; Dade et al. 1990; Mata et al. 2006; Urbani et al. 2005; Mishra et al. 2011). The EPS of *C. closterium* and *D. tertiolecta* was organised in the form of dense fibrils or globular structures. *T. suecica* was characterised by the lowest release of extracellular material, regardless of temperature, with no effect on the material organisation. Both surface methods concurred that a pronounced extracellular release was observed in *C. closterium*. Wolfstein et al. (2002) reported that the highest amounts of EPS were produced at 15 °C and 25 °C during the early stationary growth phase of diatoms. When EPS concentrations were normalised to chlorophyll *a*, maximum values were measured at 4 °C and 10 °C, which is consistent with our results.

The detailed AFM characterisation of algal surface morphology showed no specific change under temperature variation, but the change was detected in the size of algal species. The cells of *T. suecica* and *D. tertiolecta* were smallest at 30 °C. However, the cells of *C. closterium* grown at 18 °C and 30 °C were similar in size, but smaller compared to cells grown at 12 °C. Temperature-induced change in cell size probably indicates cytoskeletal rearrangements. An inverse relationship between cell size and temperature, known as the temperature-size rule, is commonly observed in eukaryotes (Atkinson et al. 2003). At higher temperatures, the reduced organism size corresponds to an adaptive plastic response

Table 1 Relationship between morphology and studied parameters examined at 12 °C and 30 °C versus 18 °C

Temperature & Parameters	Morphology		
	Biflagellated naked cell	Tetraflagellated cell with calcite incrusted theca	Gliding cell with organosilicate cell wall
12 °C			
Growth rate	Lowest	Lowest	Lowest
Cell size	No change	No change	Increase
Cell speed	Low	Lowest	n.a
Adhesion efficiency	Lowest	n.a	n.a
Physiological activity	High	Low	Highest
Stiffness	Highest	No change	Highest
Hydrophobicity	Hydrophilic	Hydrophilic	Hydrophobic
30 °C			
Growth rate	High	High	Highest
Cell size	Increase	Increase	No change
Cell speed	Lowest	Low	No change
Adhesion efficiency	Highest	n.d	n.d
Physiological activity	Highest	Lowest	Lowest
Stiffness	Lowest	No change	Lowest
Hydrophobicity	Highest hydrophilicity	Highest hydrophilicity	Highest hydrophobicity

resulting from earlier reproduction as the population growth rate increases, as well as accelerated completion of the life cycle at the expense of maturation size.

Furthermore, AFM measurements revealed that the surface properties of algal cells were both species-specific and temperature-dependent and can be linked to the structural features of the algal cell lines. *D. tertiolecta* does not possess a cell wall, while *T. suecica* is embedded in a thin calcite-encrusted theca. Temperature had the strongest impact on *D. tertiolecta*, exerting both mechanical and chemical changes. Increasing temperature caused a decrease in the stiffness of *D. tertiolecta*, in addition to changes in the degree of hydrophilicity. Correspondingly, the cells of *C. closterium* became softer at $T>T_f$ and temperature triggered a chemical change, so cells become hydrophobic, suggesting a molecular modification of the cell wall. Besides the change in the cells, their main secretion products were mainly characterised as hydrophilic in the early growing phase, whilst the later phase was characterised by predominantly hydrophobic compounds (Ciglenečki et al. 2018). Our previous study revealed heterogeneity within the elasticity maps of *C. closterium*, with the valve appearing softer (29.8 MPa) than the girdle region (43.7 MPa on silica strips and 21.3 MPa between the strips, respectively). The obtained results suggest that the valve has a lower silica content and is enriched with organic material (Pletikapić et al. 2012). In the case of *T. suecica* cells, the temperature-dependent direction of these changes cannot be defined. A very low level of hydrophilicity observed at 18 °C, increases with the temperature change. Also, *T. suecica* cells are softer at 12 °C and 30 °C ($T \neq T_f$), as opposed to the stiffer cells at 18 °C. The probability of adhesion is determined to be similar whether *D. tertiolecta* adheres to a bare or OTS-modified cantilever, which is in line with electrochemical-adhesion based study of *D. tertiolecta* in the wide potential range (Fig. 5b). In addition, more pronounced differences are found in the adhesion probability obtained for the other two algae adhering to a hydrophilic and hydrophobic AFM probe (Figure S5).

We demonstrated that the physicochemical properties of the biointerface provide a detectable species-specific and temperature-dependent change in the adaptive response of algal cells. Differences in the adaptive response of cells on temperature alterations can be understood through the difference in the underlying mechanisms. The algal response includes changes in the fatty acids composition through changes in hydrocarbon length, degree of saturation, charge, and headgroup of phospholipids (de Carvalho & Caramujo 2018). The ratio of PUFAs to saturated fatty acids (SFAs) determines the response of the cell membrane to exerted stress, as short-chain SFAs form less-viscous membranes, whereas PUFAs form more fluid membranes. During temperature variation, most algal cells employ several primary mechanisms for membrane stabilisation (Barati et al. 2019), which include the enhanced production of membrane unsaturated FA to decrease the membrane lipid solidification at low temperatures (Lyon and Mock 2014) or intensified synthesis and binding of saturated FA into membrane lipids and the activation of membrane-stabilising proteins (Los et al. 2013). Moreover, high temperature triggers the expression of membrane-bound heat-shock proteins that regulate protein homeostasis (Katz et al. 2007; Fulda et al. 2010) and contribute to the molecular protection and repair of membrane proteins (Ritossa 1996; Kobiyama et al. 2010; Guo et al. 2015). The fact that *T. suecica* cells do not respond similarly to temperature changes as *D. tertiolecta* and *C. closterium* could arise from differences in the ratio of membrane FAs that could be responsible for maintaining higher membrane stability and greater thermal protection (de Carvalho and Caramujo 2018).

On a fundamental level, our findings can contribute to a better understanding of the mechanism of diatom aggregation in the marine environment. *Cylindrotheca closterium* is a diatom species capable of forming benthic biofilms, as well as resuspending from the benthos and forming aggregates during bloom in aquatic systems (Wolfstein et al. 2002). Diatom aggregates are a primary source of marine snow (Thornton 2002), a ubiquitous feature of the ocean and an important means of transporting energy and nutrients in marine ecosystems. The initially hydrophilic cells of *C. closterium* only become hydrophobic when a significant increase in abundance is achieved, for which the trigger is a temperature increase. The rise in temperature promotes faster reproduction with a consequent reduction in cell size, with a concomitant decrease in EPS production and an increase in EPS hydrophobicity. At higher temperatures, the hydrophobic properties of the EPS of *C. closterium* suggest metabolic changes that enable cells to cope with challenging conditions of climate change-induced warming. The feedback generated stimulates a further diatom bloom and increases the aggregation potential of cells, thus promoting the development of marine snow and the consequent flow of nutrients through the water column (Riebesell 1991; Thornton 2002).

Conclusion

Our study showed that the surface properties and behaviour of algal cells exhibit detectable, species-specific, and temperature-dependent changes that can be related to the structural properties of the cell envelope. The most sensitive to temperature changes is the wall-less alga *D. tertiolecta*, as it exhibits the greatest mechanical and chemical changes. All cells stiffen at lower temperatures and become more compliant at higher temperatures, indicating a molecular change in the cell envelope. The increase in temperature causes an imbalance in cell hydrophobicity. *D. tertiolecta*

and *T. suecica* showed a highly hydrophilic character, while *C. closterium* became the most hydrophobic, which is of ecological importance for understanding the mechanism of algal biofilm formation. Furthermore, temperature induces a change in physiological activity in terms of concentration and structural organisation of released extracellular polymers, ranging from fibrils to dense networks. The change in cell surface properties and physiological activity is reflected in motility and adhesion behaviour at the interface. All selected algal cells maintained their overall shape without nanostructural changes at the surface. This study demonstrated that temperature-dependent surface properties and behaviour provide important evidence for understanding the adaptive mechanism of algae at the single cell level, which can be used to indicate ecosystem disturbance, algal bloom, as well as finding adequate commercial application.

Supplementary Information The online version contains supplementary material available at https://doi.org/10.1007/s10811-021-02591-0.

Funding This work is supported by the Croatian Science Foundation Project "From algal cell surface properties to stress markers for aquatic ecosystems" (IP-2018–01-5840).

Data availability The datasets generated during the current study are available from the corresponding author on reasonable request.

References

Ahmad S, Kothari R, Shankarayan R, Tyagi VV (2020) Temperature dependent morphological changes on algal growth and cell surface with dairy industry wastewater: an experimental investigation. 3 Biotech 10:24

Atkinson D, Ciotti BJ, Montagnes DJS (2003) Protists decrease in size linearly with temperature: ca. 2.5% degrees C-1. Proc Roy Soc B 270:2605–2611

Barati B, Gan SY, Lim PE, Beardall J, Phang S-M (2019) Green algal molecular responses to temperature stress. Acta Physiol Plant 41:26

Barreira L, Pereira H, Gangadhar KN, Custódio L, Varela J (2015) Medicinal effects of microalgae-derived fatty acids. In: Kim S-K (ed) Handbook of Marine Microalgae. Academic Press, Boston, pp 209–231

Beaugrand G (2005) Monitoring pelagic ecosystems using plankton indicators. ICES J Mar Sci 62:333–338

Bertocchi C, Navarini L, Cesàro A, Anastasio M (1990) Polysaccharides from cyanobacteria. Carbohydr Polym 12:127–153

Boyce DG, Lewis MR, Worm B (2010) Global phytoplankton decline over the past century. Nature 466:591–599

Ciglenečki I, Dautović J, Cvitešić A, Pletikapić G (2018) Production of surface active organic material and reduced sulfur species during the growth of marine diatom *Cylindrotheca closterium*. Croat Chem Acta 4:455–461

Dade WB, Davis JD, Nichols PD, Nowell ARM, Thistle D, Trexler MB, White DC (1990) Effects of bacterial exopolymer adhesion on the entrainment of sand. Geomicrobiol J 8:1–16

De Carvalho CCCR, Caramujo MJ (2018) The various roles of fatty acids. Molecules 23:2583–2619

Decho AW, Gutierrez T (2017) Microbial extracellular polymeric substances (EPSs) in ocean systems. Front Microbiol 8:922

Falkowski PG, Raven JA (2007) Aquatic photosynthesis. Princeton University Press, New Jersey

Fulda S, Gorman AM, Hori O, Samali A (2010) Cellular stress responses: cell survival and cell death. Int J Cell Biol 2010:214074

Gross M, Zhao X, Mascarenhas V, Wen Z (2016) Effects of the surface physico-chemical properties and the surface textures on the initial colonization and the attached growth in algal biofilm. Biotechnol Biofuels 9:38

Guillard RRL (1975) Culture of phytoplankton for feeding marine invertebrates. In: Smith WL, Chanley MH (eds) Culture of marine invertebrate animals: Proceedings—1st conference on culture of marine invertebrate animals greenport. Springer, Boston, pp 29–60

Guinder VA, Molinero JC (2013) Climate change effects on marine phytoplankton. In: Arias AH, Menéndez MC (eds) Marine ecology in a changing world. CRC Press-Taylor & Francis, Boca Raton, pp 68–90

Guo R, Youn SH, Ki J-S (2015) Heat Shock Protein 70 and 90 genes in the harmful dinoflagellate *Cochlodinium polykrikoides*: genomic structures and transcriptional responses to environmental stresses. Int J Genomics 2015:e484626

Häder D-P, Gao K (2015) Interactions of anthropogenic stress factors on marine phytoplankton. Front Environ Sci 3:14

Hays GC, Richardson AJ, Robinson C (2005) Climate change and marine plankton. Trends Ecol Evol 20:337–344

Huertas IE, Rouco M, López-Rodas V, Costas E (2011) Warming will affect phytoplankton differently: evidence through a mechanistic approach. Proc Roy Soc B 278:3534–3543

Hunter KA, Liss PS (1981) Polarographic measurement of surface-active material in natural waters. Water Res 15:203–215

Israelachvili JN (1992) Intermolecular forces & surface forces. Academic Press, New York

Ivošević N, Tomaić J, Žutić V (1994) Organic droplets at an electrified interface: critical potentials of wetting measured by polarography. Langmuir 7:2415–2418

Ivošević N, Žutić V (1997) Polarography of marine particles: a model study. Croat Chem Acta 70:167–178

Ivošević DeNardis N, Žutić V, Svetličić V, Frkanec R, Tomašić J (2007) In situ amperometric characterization of liposome suspensions with concomitant oxygen reduction. Electroanalysis 19:2444–2450

Ivošević DeNardis N, Pečar Ilić J, Ružić I, Novosel N, Mišić Radić T, Weber A, Kasum D, Pavlinska P, Katalin Balogh R, Hajdu B, Marček Chorvátová A, Gyurcsik B (2019) Algal cell response to laboratory-induced cadmium stress: a multimethod approach. Eur Biophys J 48:231–248

Katz A, Waridel P, Shevchenko A, Pick U (2007) Salt-induced changes in the plasma membrane proteome of the halotolerant alga *Dunaliella salina* as revealed by blue native gel electrophoresis and nano-LC-MS/MS analysis. Mol Cell Proteomics 6:1459

Kim S-K (ed)(2015) Handbook of marine microalgae. Academic Press, London

Klenerman D, Korchev YE, Davis SJ (2011) Imaging and characterisation of the surface of live cells. Curr Opin Chem Biol 15:696–703

Kobiyama A, Tanaka S, Kaneko Y, Lim P-M, Ogata T (2010) Temperature tolerance and expression of heat shock protein 70 in the toxic dinoflagellate *Alexandrium tamarense* (Dinophyceae). Harmful Algae 9:180–185

Kovač S, Svetličić V, Žutić V (1999) Molecular adsorption vs. cell adhesion at an electrified aqueous interface. Colloids Surf A 149:481–489

Kovač S, Kraus R, Geček S, Žutić V (2000) Cell suspension as a model system for electrochemical analysis. Croat Chem Acta 73:279–291

Kumar D, Kvíderová J, Kaštánek P, Lukavský J (2017) The green alga *Dictyosphaerium chlorelloides* biomass and polysaccharides production determined using cultivation in crossed gradients of temperature and light. Eng Life Sci 17:1030–1038

Lane TW, Saito MA, George GN, Pickering IJ, Prince RC, Morel FM (2005) A cadmium enzyme from a marine diatom. Nature 435:42

Lewandowska A, Sommer U (2010) Climate change and the spring bloom: a mesocosm study on the influence of light and temperature on phytoplankton and mesozooplankton. Mar Ecol Prog Ser 405:101–111

Los DA, Mironov KS, Allakhverdiev SI (2013) Regulatory role of membrane fluidity in gene expression and physiological functions. Photosynth Res 116:489–509

Lyon BR, Mock T (2014) Polar microalgae: New approaches towards understanding adaptations to an extreme and changing environment. Biology 3:56–80

Martignier A, Filella M, Pollok K, Melkonian M, Bensimon M, Barja F, Langenhorst F, Jaquet J-M, Ariztegui D (2018) Marine and freshwater micropearls: biomineralization producing strontium-rich amorphous calcium carbonate inclusions is widespread in the genus *Tetraselmis* (Chlorophyta). Biogeosciences 15:6591–6605

Mata JA, Béjar V, Llamas I, Arias S, Bressollier P, Tallon R, Urdaci MC, Quesada E (2006) Exopolysaccharides produced by the recently described halophilic bacteria *Halomonas ventosae* and *Halomonas anticariensis*. Res Microbiol 157:827–835

Mayali X, Franks PJS, Tanaka Y, Azam F (2008) Bacteria-induced motility reduction in *Lingulodinium polyedrum* (Dinophyceae). J Phycol 44:923–928

Mishra A, Kavita K, Jha B (2011) Characterization of extracellular polymeric substances produced by micro-algae *Dunaliella salina*. Carbohydr Polym 83:852–857

Mišić Radić T, Čačković A, Penezić A, Dautović J, Lončar J, Omanović D, Juraić K, Ljubešić Z (2020) Physiological and morphological response of marine diatom *Cylindrotheca closterium* (Bacillariophyceae) exposed to cadmium. Eur J Phycol 24:36

Novosel N, Kasum D, Žutinić P, Legović T, Ivošević DeNardis N (2020) Short-term effect of cadmium on the motility of three flagellated algal species. J Appl Phycol 32:4057–4067

Novosel N, Ivošević DeNardis N (2021) Structural features of the algal cell determine adhesion behavior at a charged interface. Electroanalysis 33:1436–1443

Ozkan A, Berberoglu H (2013) Physico-chemical surface properties of microalgae. Colloids Surf B 112:287–293

Pavlinska Z, Chorvat D, Mateasik A, Jerigova M, Velic D, Ivošević DeNardis N, Marcek Chorvatova A (2020) Fluorescence responsiveness of unicellular marine algae *Dunaliella* to stressors under laboratory conditions. J Biotechnol 6:100018–100028

Pillet F, Dague E, Pečar Ilić J, Ružić I, Rols M-P, Ivošević DeNardis N (2019) Changes in nanomechanical properties and adhesion dynamics of algal cells during their growth. Bioelectrochemistry 128:154–162.

Pletikapić G, Berquand A, Mišić Radić T, Svetličić V (2012) Quantitative nanomechanical mapping of marine diatom in seawater using peak force tapping atomic force microscopy. J Phycol 48:174–185

Pletikapić G, Ivošević DeNardis N (2017) Application of surface analytical methods for hazardous situation in the Adriatic sea: monitoring of organic matter dynamics and oil pollution. Nat Hazards Earth Syst Sci 17:31–44

Ras M, Steyer J-P, Bernard O (2013) Temperature effect on microalgae: a crucial factor for outdoor production. Rev Environ Sci Biotechnol 12:153–164

Riebesell U (1991) Particle aggregation during a diatom bloom II. Biological Aspects Mar Ecol Prog Ser 69:281–291

Ritossa F (1996) Discovery of the heat shock response. Cell Stress Chaperon 2:97–98

Roncarati F, Rijstenbil JW, Pistocchi R (2008) Photosynthetic performance, oxidative damage and antioxidants in *Cylindrotheca closterium* in response to high irradiance, UVB radiation and salinity. Mar Biol 153:965–973

Sader JE, Larson I, Mulvaney P, White LR (1995) Method for the calibration of atomic force microscope cantilevers. Rev Sci Instrum 66:3789–3798

Sarmiento JL, Slater R, Barber R, Bopp L, Doney SC, Hirst AC, Kleypas J, Matear R, Mikolajewicz U, Monfray P, Soldatov V, Spall SA, Stouffer R (2004) Response of ocean ecosystems to climate warming. Global Biogeochem Cycl 18:1–23

Sneddon IN (1965) The relation between load and penetration in the axisymmetric boussinesq problem for a punch of arbitrary profile. Int J Eng Sci 3:47–57

Svetličić V, Ivošević N, Kovač S, Žutić V (2000) Charge displacement by adhesion and spreading of a cell: amperometric signals of living cells. Langmuir 16:8217–8220

Svetličić V, Ivošević N, Kovač S, Žutić V (2001) Charge displacement by adhesion and spreading of a cell. Bioelectrochemistry 53:79–86

Svetličić V, Balnois E, Žutić V, Chevalet J, Hozić Zimmermann A, Kovač S, Vdović N (2006) Electrochemical detection of gel microparticles in seawater. Croat Chem Acta 79:107–113

Thornton D (2002) Diatom aggregation in the sea: mechanisms and ecological implications. Eur J Phycol 37:149–161

Urbani R, Magaletti E, Sist P, Cicero AM (2005) Extracellular carbohydrates released by the marine diatoms *Cylindrotheca closterium*, *Thalassiosira pseudonana* and *Skeletonema costatum*: Effect of P-depletion and growth status. Sci Total Environ 353:300–306

Wolfstein K, de Brouwer JFC, Stal LJ (2002) Biochemical partitioning of photosynthetically fixed carbon by benthic diatoms during short-term incubations at different irradiances. Mar Ecol Prog Ser 245:21–31

Xia L, Huang R, Li Y, Song S (2017) The effect of growth phase on the surface properties of three oleaginous microalgae (*Botryococcus* sp. FACGB-762, *Chlorella* sp. XJ-445 and *Desmodesmus bijugatus* XJ-231). PloS One 12:e0186434

Žutić V, Kovač S, Svetličić V (1993) Heterocoalescence between organic microdroplets and charged conductive interface. J Electroanal Chem 349:173–186

Žutić V, Svetličić V, Ivošević N, Hozić A, Pečar O (2004) Northern Adriatic mesocosm experiment Rovinj 2003: dynamics of organic microparticles studied by the electrochemical technique. Period Biol 106:67–74

3.4. Znanstveni rad IV

Novosel, N., Mišić Radić, T., Levak Zorinc, M., Zemla, J., Lekka, M., Vrana, I., Gašparović, B., Horvat, L., Kasum, D., Legović, T., Žutinić, P., Gligora Udovič, M., Ivošević DeNardis, N., 2022. Salinity induced chemical, mechanical and behavioral changes in marine microalgae. Journal of applied phycology 34: 1293–1309. https://doi.org/10.1007/s10811-022-02734-x

Journal of Applied Phycology (2022) 34:1293–1309
https://doi.org/10.1007/s10811-022-02734-x

Salinity-induced chemical, mechanical, and behavioral changes in marine microalgae

N. Novosel[1] · T. Mišić Radić[1] · M. Levak Zorinc[1] · J. Zemla[2] · M. Lekka[2] · I. Vrana[1] · B. Gašparović[1] · L. Horvat[1] · D. Kasum[1] · T. Legović[1,3,4] · P. Žutinić[5] · M. Gligora Udovič[5] · N. Ivošević DeNardis[1]

Received: 21 December 2021 / Revised and accepted: 17 March 2022 / Published online: 7 April 2022

Abstract

This study examines how salinity reduction triggers the response of three marine microalgae at the molecular and unicellular levels in terms of chemical, mechanical, and behavioral changes. At the lowest salinity, all microalgal species exhibited an increase in membrane sterols and behaved stiffer. The glycocalyx-coated species *Dunaliella tertiolecta* was surrounded by a thick actin layer and showed the highest physiological activity, negatively affecting cell motility and indicating the formation of the palmella stage. The lipid content of membrane and the hydrophobicity of cell were largely preserved over a wide range of salinity, confirming the euryhaline nature of *Dunaliella*. The species with calcite-encrusted theca *Tetraselmis suecica* exhibited the highest hydrophobicity at the lowest salinity of all cells examined. At salinity of 19, the cells of *T. suecica* showed the lowest growth, flagellar detachment and the lowest cell speed, the highest physiological activity associated with a dense network of extracellular polymeric substances, and a decrease in membrane lipids, which could indicate development of cyst stage. The organosilicate encrusted species *Cylindrotheca closterium* appeared to be salinity tolerant. It behaved hydrophobically at lower salinity, whereas becoming hydrophilic at higher salinity, which might be related to a molecular change in the released biopolymers. This study highlighted the interplay between chemistry and mechanics that determines functional cell behavior and shows that cell surface properties and behavior could serve as stress markers for marine biota under climate change.

Keywords Extracellular polymeric substances · Hyposalinity · Lipids · Microalgae · Motility · Nanomechanics

Introduction

Microalgae differ in their ability to survive and thrive in saline environments under the influence of osmotic stress (Helm et al. 2004). Because salinity can affect metabolic processes and water balance above or below the cell's isosmotic point (Kefford et al. 2002), microalgae have evolved various intracellular and extracellular osmoregulatory mechanisms to control osmotic stress in the face of salinity changes in the external environment (Gustavs et al. 2010; Shetty et al. 2019). At the cellular level, a change in salinity causes a variety of non-specific biochemical changes in the synthesis of active compounds, such as lipids, carbohydrates, carotenoids, steroids, sterols, and other secondary metabolites, changes in membrane permeability with a disruption of ion homeostasis (Benavente-Valdés et al. 2016; El-Kassas and El-Sheekh 2016; Minhas et al. 2016).

How microalgae adapt to environmental changes in salinity has been extensively studied (Borowitzka 2018a, b; Foflonker et al. 2018). The adaptive response of microalgae could be manifested by altering membrane fluidity, reducing protein synthesis, accumulating compatible solutes to maintain cell osmolarity, regulating photosynthesis to balance energy production and consumption (Barati et al. 2019; Pavlinska et al. 2020), and releasing extracellular polymeric substances (Decho and Gutierrez 2017; Ivošević DeNardis et al. 2019; Mišić Radić et al. 2021).

✉ N. Ivošević DeNardis
ivosevic@irb.hr

1 Ruđer Bošković Institute, Zagreb, Croatia

2 Institute of Nuclear Physics Polish Academy of Sciences, Kraków, Poland

3 Libertas International University, Zagreb, Croatia

4 OIKON-Institute for Applied Ecology, Zagreb, Croatia

5 Department of Biology, Faculty of Science, University of Zagreb, Zagreb, Croatia

The present study investigates the response of marine microalgae to salinity fluctuation in terms of chemical, mechanical, and behavioral changes to improve our understanding of the mechanisms and pathways through which a salinity stressor modulates the adaptive responses of microalgae at the individual cell level. Three widely distributed marine algal species, a biflagellate green alga with glycocalyx surface coating *Dunaliella tertiolecta*, a tetraflagellate green alga with calcite-encrusted theca *Tetraselmis suecica*, and a gliding diatom with organosilicate cell wall *Cylindrotheca closterium*, were studied at selected salinity levels that simulated changes from the euhaline to the mesohaline range of the salinity spectrum in marine systems.

Materials and methods

Cell suspensions

Three species of marine algae were selected as model organisms: *Dunaliella tertiolecta* (Chlorophyceae, CCMP 1320, Culture Collection Bigelow Laboratory for Ocean Sciences, Bigelow, MN, USA), *Tetraselmis suecica* (Chlorophyceae, CCAP 66 / 22A, Collection and Protozoa, Scottish Marine Institute, Oban, UK), and *Cylindrotheca closterium* (Bacillariophyceae, CCMP 1554, Culture Collection Bigelow Laboratory for Ocean Sciences). Cells were grown in 0.22-µm filtered natural seawater (salinity of 38), diluted to a specific salinity with MilliQ water, and then enriched with f/2 growth medium (Guillard 1975). Cultures were maintained in a water bath under controlled conditions (constant shaking (20 rpm), 12 h:12 h light to dark cycle with an irradiance of 31 µmol photons m^{-2} s^{-1}). Algal species were grown at four selected salinities of 9, 19, 27, and 38 (control). The average cell abundance in triplicate samples was determined using a Fuchs-Rosenthal hemocytometer. Growth rate and doubling time were determined in the exponential growth phase of algal cells (Kim 2015). Cells were harvested at stationary phase (15 days) by centrifugation (2000 × *g*, 3 min), and the washed pellets were resuspended twice with seawater of the corresponding salinity. The last pellet was resuspended in 2 mL of filtered seawater and served as the stock cell suspension.

Confocal microscopy

Confocal measurements were performed with a Leica TCS SP8 Laser Scanning Confocal Microscope (Leica Microsystems GmbH, Germany) equipped with a white-light laser and using a 63 × (N.A. = 1.4) oil immersion objective. The excitation wavelengths and emission ranges were optimized using the spectral scan option. A commercial dye SiR-Actin (excitation maximum 650 nm, detection range 670–700 nm) was used to visualize actin filament structures of *D. tertiolecta* and *T. suecica*. Visualization of the actin filament structures of *C. closterium* was not possible, probably because of its organosilicate cell wall. Autofluorescence of the algal cells was detected at an excitation maximum of 650 nm and a detection range of 720–750 nm.

Sample preparation for confocal imaging

The slides for confocal microscopy were washed in glass beakers with ethanol followed by ultrapure water. A stream of nitrogen was used to dry the slides. To prepare the slides for cell immobilization, 50 µL of 0.2% (w/v) polyethyleneimine (PEI, Sigma-Aldrich, USA) was added to the center of the clean slide and allowed to stand for 30 min. The PEI droplet was then removed and the center of the slide was rinsed three times with ultrapure water. The isolated algal cells (as described in the "Cell suspensions" section) were fluorescently labeled using the Sir-Actin kit (50 nmol Sir-Actin, 1 µmol Verapamil) from Tebu-bio (Ile-de-France, France). A stock solution of 500 µM Sir-Actin was prepared in anhydrous dimethyl sulfoxide (99.8% DMSO). To an aliquot of 50 µL of the washed cells, 0.5 µL of the Sir-Actin fluorescent dye was added. Finally, 20 µL of the stained cultures was added to the center of the glass slide and allowed to settle for 30 min. To prevent evaporation of the droplet, the slides were kept in a Petri dish with moist absorbent paper until imaging.

Motility analysis

Cell movements were recorded as 10 consecutive video files (.avi format, duration 5 s, 50–60 frames per second, image size: 340 × 250, 4 × 4 binning) under an Olympus BX51 microscope (10 × magnification). The video files were used as input to the open-source image processing software ICY (http:icy.bioimageanalysis.org) to analyze motility and trajectories of 1118 cells. Details of motility analysis are given in Novosel et al. (2020, 2021). The software package R (R Core Team, 2020) was used for additional statistical analyses. Box plots and plots of probability density distributions of speed and search radius were obtained. The distributions for different salinities were tested using the Shapiro normality test and the Wilcoxon-Mann–Whitney test.

Electrochemical method

The electrochemical method of polarography and chronoamperometry of oxygen reduction at the dropping mercury electrode (DME) was utilized to characterize the organic constituents, such as biopolymers and fluid microparticles in the aqueous electrolyte solution based on molecular adsorption or particle adhesion to the DME (Žutić et al.

1999, 2004; Svetličić et al. 2006; Pletikapić and Ivošević DeNardis 2017). Briefly, adsorption of organic molecules at the DME interface can be characterized by recording the polarographic maximum of Hg(II) ions, which is an alternative approach to measuring dissolved organic carbon in seawater (Hunter and Liss 1981). The surfactant activity of seawater is expressed as the equivalent amount of the nonionic synthetic surfactant Triton-X-100 (polyethylene glycol tert-octylphenyl ether) in milligram per liter. In contrast, the adhesion of fluid organic particles to the DME interface can be characterized by recording spike-shaped amperometric signals (Kovač et al. 2000; Svetličić et al. 2000; Ivošević DeNardis et al. 2007, 2012, 2015; Novosel et al. 2021). Whether the adhesion is spontaneous depends on the properties of the three interfaces in contact, based on the modified Young-Dupré equation (Israelachvili 1992).

Electrochemical measurements of algal cells

Electrochemical measurements of algal cell samples were performed in an air-permeable and thermostatic Metrohm vessel with a three-electrode system. The working electrode, the dropping mercury electrode, had the following characteristics: dropping time: 2.0 s, flow rate: 6.0 mg s^{-1}, maximum surface area: 4.57 mm^2. All potentials were referenced to a potential measured at a reference electrode, i.e., Ag/AgCl (0.1 M NaCl) separated from the measured dispersion by a ceramic frit. A platinum wire was used as the counter electrode. An aliquot of the cell suspensions was added to 25 mL of filtered seawater (pH 8.0) of the corresponding salinity and then poured into a Methrom vessel at 20 °C. Electrochemical measurements were performed using a 174A Polarographic Analyser (Princeton Applied Research, USA) connected to a computer. Analog data acquisition was performed using a DAQ card-AI-16-XE-50 (National Instruments, USA). Data analysis was performed using the application developed in LabView 6.1 software (National Instruments). Electrochemical characterization of the algal cell samples was performed by recording polarograms of oxygen reduction (current–potential curves) and current–time curves over 50 mercury drops at constant potentials (time resolution: 50 s). Signal frequency was expressed as the number of amperometric signals from the cells over a 100-s period. Surfactant activity was measured by adding 0.5 mL of 0.1 M $HgCl_2$ to the sample before measurement.

Atomic force microscopy imaging

Atomic force microscopy (AFM) imaging was performed using a Multimode Scanning Probe Microscope with Nanoscope IIIa controller (Bruker, USA) equipped with a 125 µm vertical engagement (JV) scanner. Contact mode imaging in air was performed with silicon nitride cantilevers (DNP, Bruker, nominal frequency of 18 kHz, nominal spring constant of 0.06 N m^{-1}). The linear scanning rate was between 1.5 and 2 Hz and the scan resolution was 512 samples per line. To minimize the interaction forces between the tip and the surface, the set point was kept at the lowest possible value. NanoscopeTM software (Bruker) was used to process and analyze the images.

Sample preparation for AFM imaging of cells and released extracellular polymers

Cells of *D. tertiolecta*, *T. suecica*, and *C. closterium* grown at salinities of 9, 19, 27, and 38, respectively, were separated from the growth medium by centrifugation as described in the "Cell suspensions" section. Unmodified mica was used as substrate for AFM imaging of *D. tertiolecta* and *C. closterium*, whereas polyethyleneimine (PEI; Sigma-Aldrich) modified mica was used for imaging of *T. suecica* (Novosel et al. 2021). The sample preparation protocol for AFM imaging required fixation of the *D. tertiolecta* suspension. A 5 µL aliquot of the cell suspension was pipetted onto freshly cleaved or PEI-modified mica and placed in a closed Petri dish for 1 h to allow the cells to settle and adhere to the surface. For rinsing, the mica was immersed in a glass of ultrapure water for 30 s three times and then dried. The mica discs were then taped to a metal sample pack with double-sided tape and imaged with the AFM.

Atomic force microscopy working in force spectroscopy mode

Measurements of the physical properties of the algal cells were performed using the Nanowizard IV AFM system (Bruker-JPK, Germany) in force spectroscopy mode in combination with an Olympus IX72 inverted optical microscope (Olympus Corporation, Japan). MLCT-D silicon nitride cantilevers were used to indent the algal cells. They were characterized by a nominal spring constant of 0.03 N m^{-1} and a half-opening angle of 21°. The spring constants of the cantilevers were calibrated using the thermal noise method (Sader et al. 1995). Measurements were made in the central region of the cell body regardless of the type of algal cells. However, in the case of *D. tertiolecta* and *T. suecica* cells, a scan area of 3 µm × 3 µm was chosen, over which a grid of 6 × 6 points was placed. For the cells of *C. closterium*, the size of the scan area was 1 µm × 1 µm, over which a grid of 2 × 2 points was defined. Force curves were recorded at an approach and retract velocity of 8 µm s^{-1} with a maximum force of 4 nN and curve lengths of 4 µm (*C. closterium* and *T. suecica*) and 6 µm (*D. tertiolecta*). Measurements were made at 18 °C in seawater at salinities of 9, 19, 27, and 38.

The recorded data, i.e., the force curves, were analyzed using JPK Data Processing Software (Bruker-JPK, Germany).

Young's modulus determination

The apparent Young's modulus (E) was determined by applying the Hertz-Sneddon contact model (Sneddon 1965). Here, the four-sided pyramid probe was used. Therefore, the relationship between the loading force F and the indentation depth δ is:

$$F = \frac{E'}{1-\mu^2}\frac{tan\alpha}{\sqrt{2}}\delta^2 \quad (1)$$

where E' is the reduced Young's modulus considering the elastic modulus of algal cells (E_{cell}) and cantilever (E_{tip}) is given by:

$$\frac{1}{E'} = \frac{1-\mu_{tip}^2}{E_{tip}} + \frac{1-\mu_{cell}^2}{E_{cell}}. \quad (2)$$

α is the open-angle of the tip, μ is the Poisson's ratio (μ_{cell} and μ_{tip} are Poisson's ratios related to the compressibility of the algal cells and indenting cantilever). Since $E_{\text{cell}} << E_{\text{tip}}$, the following approximation is obtained:

$$E' = \frac{E_{cell}}{1-\mu_{cell}^2}, \quad (3)$$

In our analysis, μ_{cell} equals 0.5 because we assume that the algal cells are incompressible. The maximum indentation depth did not exceed 1 µm, and the AFM data fit the model over a whole indentation range. The calculated E values were presented as box plots, distinguishing the median and the first (Q1) and third (Q3) quartiles.

The adhesive and hydrophobic properties of the algae were extracted from the retracting part of the force curve. They were quantified using the maximum work of adhesion (W_{adh}), defined as the area enclosing the negative force values. Hydrophilic (bare, silicon) and hydrophobic (trichlorooctadecylsilane (OTS, Sigma-Aldrich)) cantilevers were used to characterize the adhesive and hydrophobic properties of cell probes with different chemical properties. The functionalization of the OTS tips was performed by chemical vapor deposition. Silanization of the cantilevers was performed in a desiccator for 2 h, and the probes were used immediately. Scanning area, grid density, velocity, and the number of examined cells are specified in the "Atomic force microscopy working in force spectroscopy mode" section. The degree of hydrophobicity of the algal cell was defined as the difference between maximum adhesion values obtained for the interaction of the algal cell with untreated and CH_3-functionalized AFM cantilevers. It was quantified with $\Delta W_{\text{adh}} = W_{\text{adh (no OTS)}} - W_{\text{adh (OTS)}}$ (Novosel et al. 2021).

Sample preparation for force spectroscopy measurements

The protocol for sample preparation was recently published in Novosel et al. (2021). Briefly, algal cells were immobilized on a glass coverslip coated with PEI. The PEI was deposited by drop-casting technique (1 h), rinsed with seawater and dried with a stream of nitrogen. In the case of *C. closterium*, a 200-µL cell suspension was placed on a substrate for 1 h. The sample was then rinsed 3 times with 200 µL of filtered seawater. For *D. tertiolecta* and *T. suecica* cells, the following procedure was used. A volume of 1.5 mL of *D. tertiolecta* and *T. suecica* suspensions was centrifuged at 265 × *g* for 3 min and at 940 × *g* for 5 min, respectively. After removing 1 mL of the medium, the obtained pellet of algal cells was vortexed. Then, 1 mL of seawater was added and the cells were centrifuged at the same speed and duration. The supernatant was removed and the cells were suspended in 400 µL of the filtered seawater. Then, 100 µL of the cell suspension was placed on a PEI-coated glass slide for 30 min. Finally, the samples were rinsed 3 times with 100 µL of the filtered seawater.

Lipid extraction

Lipid extraction was performed from 50 mL of algal cell monoculture at the stationary growth phase. The sample was filtered through a pre-fired (450 °C/5 h) 0.7 µm Whatman GF/F filter. Extraction was performed using a modified one-phase solvent mixture of dichloromethane-methanol–water (Bligh and Dyer 1959): 10 mL of one-phase solvent mixture dichloromethane/methanol/deionized water (1:2:0.8 v/v/v) and 5–8 µg of standard methyl stearate (to estimate recoveries in subsequent steps of sample analysis) were added to the cut filters. They were then ultrasonicated for 3 min, stored overnight in the refrigerator, filtered through a sinter funnel into a separatory funnel, washed again with 10 mL of the one-phase solvent mixture and then once with 10 mL of dichloromethane/0.73% NaCl solution (1:1 v/v) and finally with 10 mL of dichloromethane. Lipid extracts collected in dichloromethane were evaporated to dryness under nitrogen flow and dissolved in 34 to 54 µL dichloromethane before analysis. All solvents were purchased from Merck Corporation (USA).

Lipid analysis

Lipid classes were determined by thin-layer chromatography with flame ionization detection (TLC–FID; Iatroscan MK-VI, Iatron, Japan). Lipids were separated on Chromarods S5. Quantification was determined by external calibration of lipid classes. Analysis was performed using a hydrogen flow of 160 mL min^{-1} and an airflow of

2000 mL min^{-1}. We determined representative membrane lipid classes: three glycolipids (GL) (monogalactosyldiacylglycerols (MGDG), digalactosyldiacylglycerols (DGDG), and sulfoquinovosyldiacylglycerols (SQDG)), three phospholipids (PL) (phosphatidylglycerols (PG), phosphatidylethanolamines (PE), and phosphatidylcholines (PC)), and sterols (ST). The total membrane lipid concentration was the sum of individual membrane lipids. The standard deviation determined from duplicate runs was 0–15%. The detailed procedure is described in Gašparović et al. (2015, 2017).

Results

Cell growth dynamics

Figure S1 shows the growth curves of three selected algal monocultures (*D. tertiolecta*, *T. suecica*, *C. closterium*) studied at four selected salinities (9, 19, 27, and 38). The initial number of inoculated cells in the growth media was similar for all species studied, approximately 4.0×10^4 cells mL^{-1}. All selected microalgae persisted in the salinity range from 9 to 38. The calculated growth rates and doubling times of three algae in the exponential growth phase at the salinity studied are summarized in Table S1. All microalgae had the shortest doubling time and fastest growth at salinity of 9.

Confocal images of algal cells grown at the corresponding salinities are shown in Figures S2–S4. Microscopic observations of *D. tertiolecta* at salinity of 27 showed no changes in autofluorescence or actin composition compared to cells grown at salinity of 38 (Figure S2a and b). At salinity of 19, *D. tertiolecta* cells build up actin layer (Figure S2c), which is particularly pronounced at salinity of 9 (Figure S2d). In addition, as observed in the transmitted light channel, at salinity of 9, some cells lost their flagella and became rounder, and the actin layer appeared thicker than in the control. No changes in autofluorescence or actin composition were observed in *T. suecica* over the entire range of salinity examined (Figure S3a-d). However, as observed in the transmitted light images, *T. suecica* cells tend to lose their flagella as salinity decreases. This effect was most evident at salinities of 19 and 9, where almost all cells have lost their flagella and the detached flagella accumulate around the cells. The cells of *C. closterium* maintained both shape and autofluorescent properties throughout the salinity drop (Figure S4a-d). As observed in the transmitted light channel, droplets accumulated inside the cells with decreasing salinity, although no trend was noted.

Motility characterization

Qualitative insights into the movement of *D. tertiolecta* cells at selected salinities are shown in Figure S5. At salinity of 9, approximately 66% of the cells (109 cells) were stationary or oscillating around a center (Tables S2.1), while the remainder (55 cells) exhibited considerable trajectories. At salinity of 19, a total of 68 cells were counted in the sample, of which about 57% (39 cells) were stationary. At salinity of 27, approximately 63% (41 cells) were stationary, while 37% (24 cells) exhibited considerable movement and were quantified. In contrast, at salinity of 38, most cells (79%) were in motion, while the minority (21%) were stationary.

Box plots of cell speeds of *D. tertiolecta* are shown in Fig. 1a.

The median of the speed at salinity of 9 was 29 μm s^{-1}, while the medians at salinities of 19 and 27 were identical: 50 μm s^{-1}. At salinity of 38, the median speed was significantly higher: 75 μm s^{-1}. The Shapiro test for normality yielded $p = 2.7 \times 10^{-10}$, 1.5×10^{-9}, 3.4×10^{-5}, and 1.8×10^{-6}, confirming that the density distributions of speeds were very far from normal. The Wilcoxon rank sum test showed that the density distributions of speeds were significantly different for cells grown at salinities of 9 and 19, 27 and 38, but not for cells grown at 19 and 27.

Because the group of cells that were stationary or vibrating around the center exhibited significantly different motion than the group of cells that were moving, it was important to note the speeds of the moving cells. The average speeds at salinities of 9, 19, 27, and 38 were 74 μm s^{-1}, 103 μm s^{-1}, 77 μm s^{-1}, and 81 μm s^{-1}, respectively (Table S2.2a).

Boxplots of the search radius of *D. tertiolecta* cells are shown in Fig. 1b. The median search radius at salinity of 9

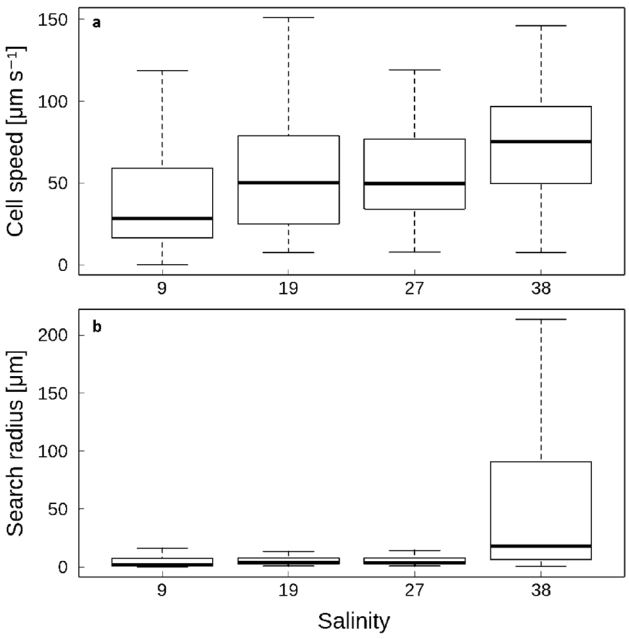

Fig. 1 Box plots of cell speed (**a**) and search radius (**b**) of *D. tertiolecta* grown at salinities of 9, 19, 27, and 38 (control)

was 2 µm, whereas the medians at salinities of 19 and 27 were 4 and 3 µm, respectively. At salinity of 38, the median search radius was significantly larger: 18 µm (Table S2.2.b). The Shapiro test for normality yielded $p = 2.2 \times 10^{-16}$, 7.3×10^{-16}, 2.1×10^{-13}, and 2.2×10^{-16}, respectively, confirming that all density distributions of the search radius were very far from normal. The Wilcoxon rank sum test showed that the density distributions of the search radius were significantly different for cells grown at salinities of 9 and 19, 27 and 38, but again not for cells grown at 19 and 27 ($p = 0.88$). The group of cells that moved consistently had an average search radius of 12 µm, 27 µm, 79 µm, and 72 µm at salinities of 9, 19, 27, and 38, respectively. In the same order of salinity, the linearity of motion was 0.1, 0.09, 0.32, and 0.45, respectively. Thus, the linearity was the same at salinities of 9 and 19 and 3 to 4.5 times smaller than at 27 and 38.

Qualitative insights into the movement of *T. suecica* cells grown at selected salinities are shown in Figure S6. At salinity of 9, approximately 43% of cells (35 cells) were stationary or showed oscillatory movement in place (Tables S3.1), whereas the majority of cells (46 cells) were clearly moving. At salinity of 19, a total of 124 cells were counted, with approximately 59% being stationary (73 cells). At salinity of 27, approximately 27% (26 cells) were stationary, while 73% (69 cells) showed significant movement and were quantified. In contrast, at salinity of 38, only 6% of cells were stationary, while 94% of cells moved vigorously.

Box plots of cell speeds of *T. suecica* are shown in Fig. 2a.

The median of the speed was 78 µm s^{-1} at salinity of 9, while the medians were 50 µm s^{-1} at salinity of 19 and 112 µm s^{-1} at salinities of 27. At salinity of 38, the median speed was significantly higher: 201 µm s^{-1} (Table S3.2a). The Shapiro test for normality yielded $p = 4 \times 10^{-4}$, 1.8×10^{-10}, 0.07, 8.8×10^{-5}, respectively. Only the density distribution at salinity of 27 did not deviate significantly from normality. The Wilcoxon rank sum test showed that the density distributions of speed were significantly different from each other, except for the distributions at salinities of 9 and 27, for which $p = 0.05$ was determined. The group of uniformly moving cells grown at salinities of 9, 19, 27, and 38 had an average speed of 124 µm s^{-1}, 155 µm s^{-1}, 137 µm s^{-1}, and 201 µm s^{-1}, respectively (Table S3.2).

Boxplots of the search radius of *T. suecica* cells are shown in Fig. 2b. The median search radius at salinity of 9 was 6 µm, while the medians at salinities of 19 and 27 were 4 and 12 µm, respectively. At salinity of 38, the median search radius was an order of magnitude larger: 102 µm (Table S3.2b). The Shapiro test for normality yielded $p = 4.6 \times 10^{-16}$, 2.2×10^{-16}, 6×10^{-16}, and 1.4×10^{-15}, respectively, confirming that all density distributions of the search radius are very far from normal. The Wilcoxon rank sum test showed that the density distributions of the search radii

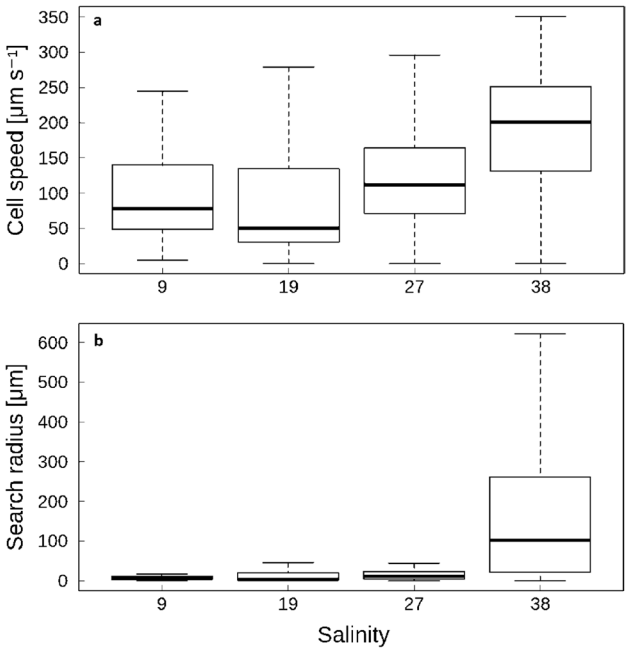

Fig. 2 Box plots of cell speed (**a**) and search radius (**b**) of *T. suecica* grown at salinities of 9, 19, 27, and 38 (control)

were significantly different from each other. The search radii of cells grown at salinities of 9 and 19 ($p = 0.027$) and cells grown at salinities of 9 and 27 ($p = 0.22$) were the narrowest. The group of significantly moving cells grown at salinities of 9, 19, 27, and 38 had an average search radius of 57 µm, 121 µm, 61 µm, and 174 µm, respectively. The linearity of moving cells with increasing salinity was 0.26, 0.58, 0.19, and 0.55, respectively, and reached the highest values at salinities of 19 and 38.

Electrochemical characterization of algal cells and released surface-active organic matter

The chronoamperometric curves for oxygen reduction recorded in the cell suspension of *D. tertiolecta* in seawater at potential of − 400 mV showed signals attributable to the adhesion of single cells to the charged interface (Fig. 3a).

The dependence of the signal frequency of *D. tertiolecta* grown at different salinities on the applied potentials is shown in Fig. 3b. The potential range of cell adhesion was defined with critical potentials of adhesion at the positively Ec^+ and negatively charged interface, Ec^-. The most negative and the most positive potentials, where at least one amperometric signal occurs per 10 consecutive *I-t* curves, correspond to the critical potentials (Žutić et al. 1993; Ivošević et al. 1994). The narrowest potential range of adhesion was recorded in the *D. tertiolecta* cell culture grown at salinity of 9, characterized by critical potentials of − 140 mV and − 990 mV in seawater, while the widest

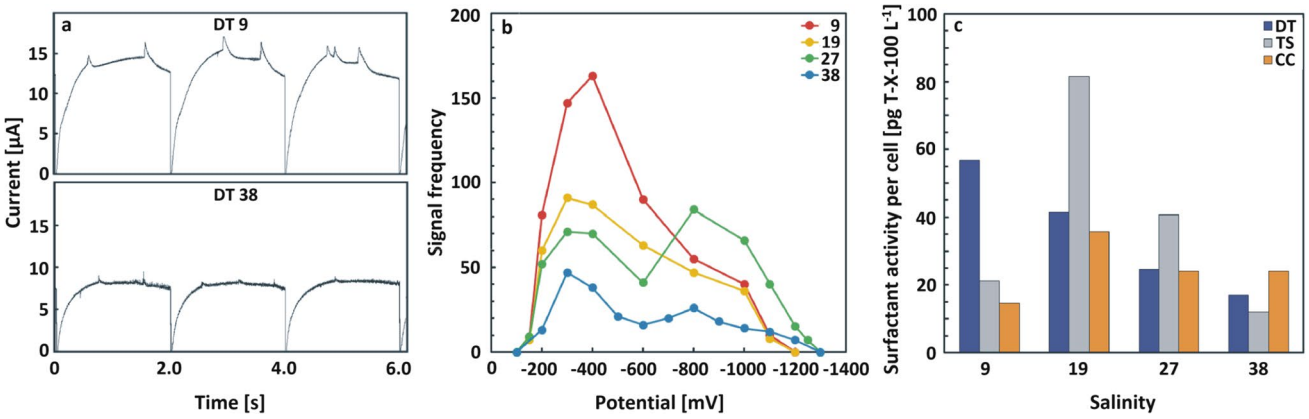

Fig. 3 Chronoamperometric curves for oxygen reduction at − 400 mV for three consecutive mercury drops recorded in *D. tertiolecta* cell suspension in seawater salinities of 9 and 38 (**a**); potential dependence of the signal frequency of *D. tertiolecta* cells grown at salinities of 9, 19, 27, and 38 (**b**); and surfactant activity for examined cell species at selected salinities (**c**)

potential range of cell adhesion was recorded in the cell suspension grown at 38 salinity, from − 110 to − 1240 mV, corresponding to favorable growth conditions. The frequency of amperometric signals increased with decreasing salinity due to the lower ionic strength of the medium, which was reflected in the increase in oxygen reduction current, thus enhancing the amperometric signals. The maximum number of amperometric signals occurred at potential of − 400 mV for all four salinities studied, as the interfacial tension is close to the maximum value (electrocapillary maximum). At potential of − 400 mV, the mercury electrode was positively charged and there was an electrostatic attraction between the positively charged interface and the negatively charged *D. tertiolecta* cells. By changing the potential in either direction, the interfacial tensions decreased and the number of amperometric signals from the cells decreased accordingly. At potential of − 800 mV, the mercury was negatively charged and the signal frequency decreased due to electrostatic repulsion with the negatively charged *D. tertiolecta* cells. Conversely, the chronoamperometric curves recorded in the suspensions of *T. suecica* and *C. closterium* were perfectly regular because there was no adhesion to the charged liquid interface due to cell rigidity (Novosel and Ivošević DeNardis 2021).

The electrochemical characterization of the released surface-active organic matter in the growth medium was determined by recording polarograms (current–potential curve) of Hg(II), which is proportional to the surfactant activity in the sample. The surfactant activity of the sample corresponded to a quantitative measure of the physiological activity of the cells in the growth medium. The data showed that the surfactant activity of the cells gradually decreased as follows: *T. suecica* (19) > *D. tertiolecta* (9) > *D. tertiolecta* (19) ~ *T. suecica* (27) (Fig. 3c).

Nanoscale imaging of algal cell and released extracellular biopolymers

Nanoscale imaging of single algal cells was performed at salinities of 9, 19, 27, and 38 (control). Regardless of salinity, all three species retained the same general cell shape. *Dunaliella tertiolecta* cells grown at all salinities tested had an ovoid shape with two flexible flagella. *Tetraselmis suecica* cells had an ellipsoidal shape at all salinities tested and the cell surface had granular structures corresponding to micropearls (Novosel et al. 2021). Most of the cells of *T. suecica* grown at salinity of 38 had flagella, and only half of the cells grown at salinity of 27 had flagella, whereas the cells grown at salinities of 9 and 19 had no flagella. The cells of *C. closterium* grown at all salinities tested had an elongated shape with flexible rostrae that could be clearly distinguished from the central part of the cell. Three morphologically distinct parts could be distinguished on the cell: the girdle band, the valve, and the raphe (Pletikapić et al. 2012; Novosel et al. 2021).

Based on AFM image analysis, the morphological parameters (length, width, height, and surface roughness) of cells grown at selected salinities are summarized in Table S4. The size of *D. tertiolecta* and *T. suecica* cells had the highest values at salinity of 38. The size of both, *D. tertiolecta* and *T. suecica*, grown at salinities of 9, 19, and 27 was similar and smaller than cells grown at 38. The roughness of *D. tertiolecta* cell surface was highest at salinity 38 and similar for salinities of 9, 19, and 27. The roughness of the cell surface of *T. suecica* was similar at all tested salinities. The length, width, and height range of *C. closterium* grown at salinities of 9, 19, and 27 were similar and greater compared with cells grown at salinity of 38.

The supramolecular organization of the released extracellular polymers (EPS) of *D. tertiolecta*, *T. suecica*, *and C. closterium* at selected salinities are shown in Fig. 4.

Around the cells of *D. tertiolecta* grown at salinities of 38 and 27, only globules and no fibrils or fibrillar networks were observed. Globules and some single fibrils were observed around the cells grown at salinity of 19. Around the cells grown at salinity of 9, a material consisting of globules, single fibrils and flat smooth structures was noted (Fig. 4a, b). The extracellular biopolymers around *T. suecica* grown at salinities of 9, 19, and 27 were in the form of a dense fibrillar networks and were located all around the cells, whereas no fibrillar material was observed at control salinity of 38 (Fig. 4c, d). The fibrils that formed the network ranged in height from 5 to 50 nm, with the highest network density found around the cells at salinity of 19 (Figure S7).

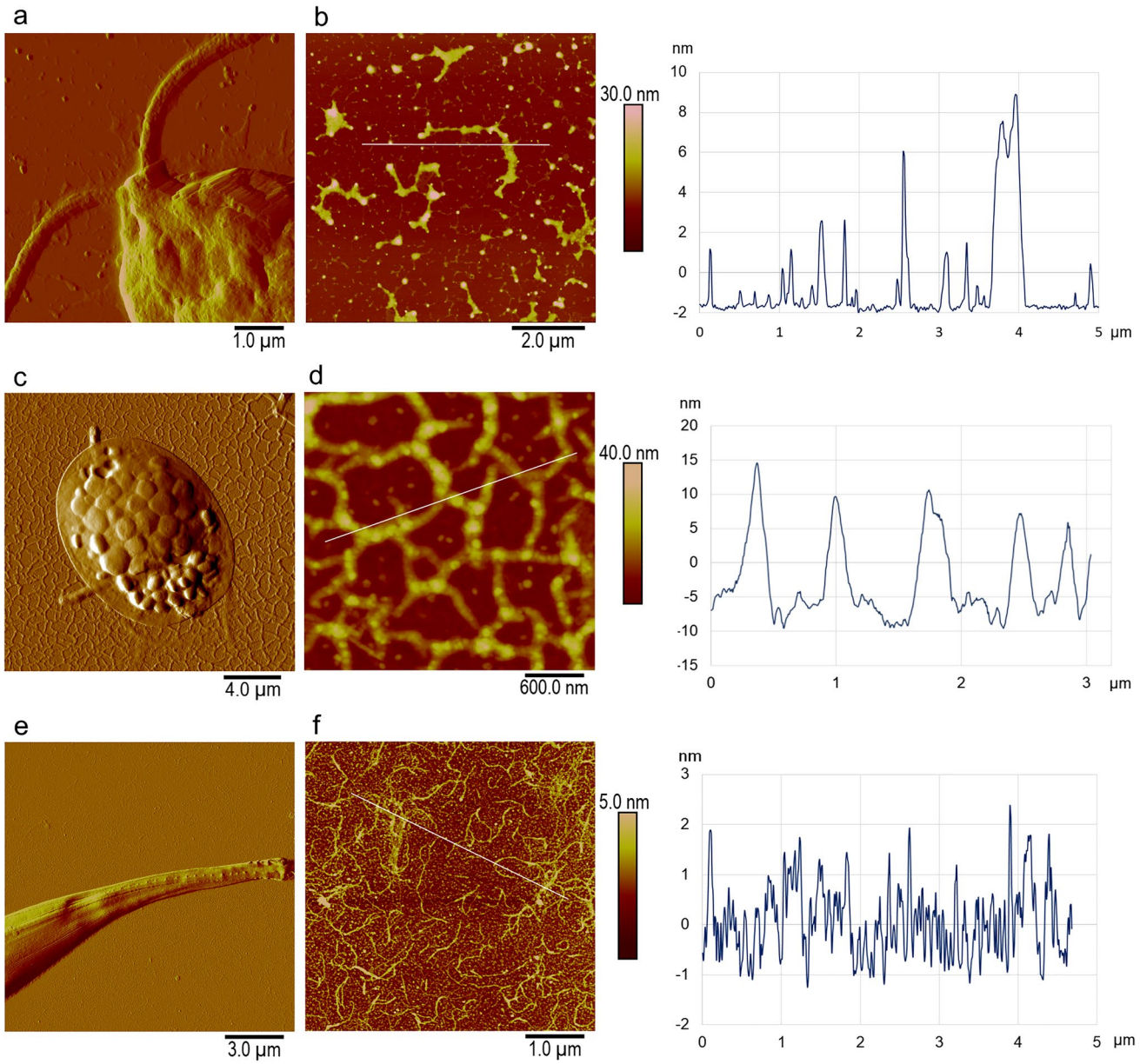

Fig. 4 AFM images of cells and extracellular polymers of *D. tertiolecta*, *T. suecica*, and *C. closterium* grown at selected salinities. Part of cell body with flagella of *D. tertiolecta* grown at salinity of 9 (**a**); EPS material around *D. tertiolecta* cell with vertical profile along indicated line (**b**); *T. suecica* cell grown at salinity of 19 (**c**); EPS network surrounding the *T. suecica* cell with vertical profile along indicated line (**d**); rostra of the *C. closterium* grown at salinity of 19 (**e**); EPS material around *C. closterium* with vertical profile along indicated line (**f**). Images are acquired using contact mode in air and presented as deflection (**a**, **c**, **e**) and height data with vertical profiles along indicated lines (**b**, **d**, **f**). Scan sizes: 6 µm×6 µm (**a**); 8 µm×8 µm, vertical scale 30 nm (**b**); 20 µm×20 µm (**c**); 3 µm×3 µm, vertical scale 40 nm (**d**); 15 µm×15 µm (**e**); 5 µm×5 µm, vertical scale 5 nm (**f**)

The extracellular biopolymers of *C. closterium* were in the form of single fibrils, locally cross-linked fibrils, and globules. For *C. closterium* grown at salinities of 9 and 19, a denser EPS material around the cells was noted and the fibrils exhibited a higher degree of cross-linking (Fig. 4e, f), whereas *C. closterium* grown at salinity of 27 had a lower degree of cross-linked fibrils near the cells, while single fibrils were mostly observed further from the cells.

Nanomechanical characterization of algal cells by AFM

The local elastic properties (*E*) of algal cells were quantified using the apparent Young's modulus calculated for the maximum indentation depth. At salinity of 38 (control), the cells of *D. tertiolecta* are characterized by the lowest *E* values. The cells of *T. suecica* are stiffer, while the local *E* values of *C. closterium* can be up to several MPa. The difference in mechanical response of these cells to compression could be due to differences in cell morphology. The cells of *T. suecica* are surrounded by close-fitting theca of fused organic scales. The cells of *C. closterium* contain stiff chloroplasts in the girdle band, and the cells of *D. tertiolecta* are covered only by the thick plasma membrane (Oliveira et al. 1980; Medlin and Kaczmarska 2004). Figure 5 shows the overlay of the box plots and Young's modulus distributions obtained for the algal cells of *D. tertiolecta*, *T. suecica*, and *C. closterium* cultured at salinities of 9, 19, 27, and 38, respectively.

Because the distributions of Young's moduli are broad and not symmetrical, we compared the median values of the cell populations studied. The median was accompanied by an interquartile range (IQR), which describes where the central 50% of the data lie (median (IQR). Statistical significance was determined using the Kruskal–Wallis ANOVA test ($p < 0.05$) to confirm differences between groups. Regardless of algal species, decreasing salinity increased the apparent Young's modulus (Fig. 5). The statistical significance for all groups was less than 0.0001 at the 0.05 level (Kruskal–Wallis ANOVA test) compared to the control group. Median (IQR) values obtained for *D. tertiolecta* cells increased from 3.5 kPa (3.2 kPa) at 38 to 8.6 kPa (7.6 kPa) at 27, 6.6 kPa (4.8 kPa) at 19, and 8.1 kPa (4.4 kPa) at 9, respectively. Statistical significance ($p < 0.05$) was also found for the measurements at salinities of 9 and 19, and at 19 and 27, whereas no statistically significant difference was found at salinities of 9 and 27. A similar trend of elastic modulus changes was observed in *T. suecica* cells. The cells were stiffer at low salinities, and $E(27) > E(9) > E(19)$. The corresponding medians were 138 kPa (190 kPa), 151 kPa (223 kPa), and 115 kPa (198 kPa), respectively. The value of *E* determined for *T. suecica* at salinity of 38 was 46 kPa (80 kPa). Weaker statistical significance was found between algal cells cultured at salinities of 9 and 27 ($p = 0.0011$), and

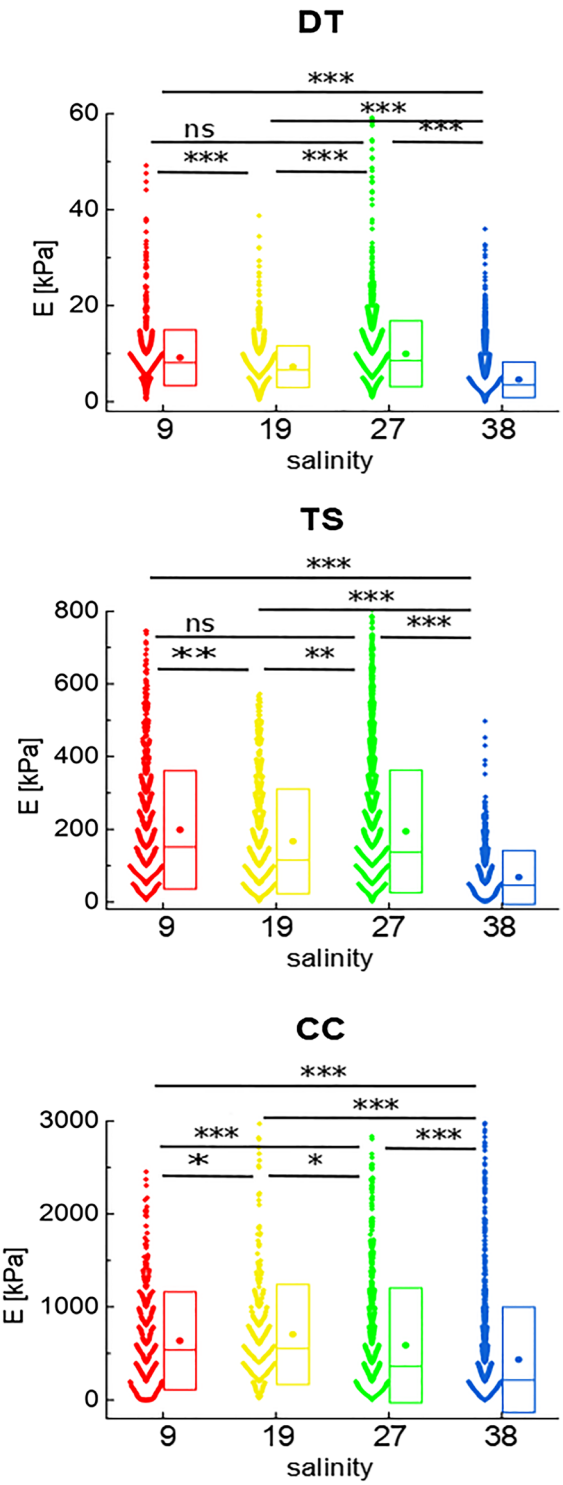

Fig. 5 Overlay of the box plots with Young's modulus distributions, obtained for *D. tertiolecta*, *T. suecica*, and *C. closterium* cells at salinities of 9, 19, 27, and 38. A box with whiskers represents a median ± interquartile range (Q3-Q1). Statistical significance was obtained from the Kruskal–Wallis ANOVA test at the level of 0.05 (*** $p < 0.001$, ns—not statistically significant)

19 and 27 ($p = 0.0019$). There was no statistical significance between cells of *T. suecica* cultured at salinities of 9 and 27. For *C. closterium*, the salinity stress increased the Young's modulus from 215 kPa (436 kPa) at normal conditions to 362 kPa (742 kPa) at salinity of 27. A further decrease in salinity to 19 and 9 was accompanied by an increase in the *E* to 553 kPa (532 kPa) and 537 kPa (759 kPa), respectively. The statistical significance for the 19 and 9 groups and 27 and 19 groups of *C. closterium* cells was less than 0.05, while the *p* value determined for the 9 and 27 groups was less than 0.001.

Adhesive and hydrophobic properties of algal cells

The adhesive properties, quantified by the maximum work of adhesion (W_{adh}), of algal cells grown at different salinities on chemically modified probes were studied. Cells were indented with hydrophilic (OTS −) and hydrophobic (OTS +) AFM probes. The change in hydrophobic properties (ΔW_{adh}) of the algal cell surface was determined by subtracting the work of adhesion determined for bare and OTS-coated cantilevers (Table S5): $\Delta W_{adh} = W_{adh(no\ OTS)} - W_{adh(OTS)}$. A positive value of ΔW_{adh} indicated that hydrophilic interactions dominate, while negative values indicated that hydrophobicity smothered the hydrophilicity. The mean values of the maximum work of adhesion (± standard error of the mean) obtained from measurements with bare and OTS-coated cantilevers are shown in Table S5.

We hypothesized that algal cells change their adhesion properties under salinity stress. Indeed, the hydrophobic properties of the cells changed depending on the salinity studied (Fig. 6), and these changes were species-dependent.

The resulting chemical properties of microalgae are shown in Figure S8. The data show that in the case of *D. tertiolecta*, the hydrophobic and hydrophilic properties were rather balanced, being characterized by low values of ΔW_{adh} (see Table S5). Only at salinities of 9 and 27 the cells became slightly more hydrophobic, as ΔW_{adh} is -0.018 ± 0.014 fJ and 0.047 ± 0.012 fJ, respectively. More pronounced salinity-dependent changes in surface properties were observed in *T. suecica* and *C. closterium*. At salinities of 38 and 27, ΔW_{adh} of *T. suecica* was close to zero. A further decrease in salinity resulted in high negative ΔW_{adh} values. In addition, we observed a significant decrease in the probability of adhesion to the bare AFM probe (P_{noOTS}), accompanied by an increase in P_{OTS} (see Figure S8 and Table S5). While the overall surface properties of *T. suecica* changed from balanced to hydrophobic with decreasing salinity, in the case of *C. closterium* we found that salinity can be a trigger between hydrophobic and hydrophilic surface properties. At salinity of 38, *C. closterium* cells had a hydrophilic surface ($\Delta W_{adh} = 0.0583 \pm 0.0072$ fJ). When the salinity decreased to 27, the ΔW_{adh} increased to 0.163 ± 0.085 fJ. Moreover, when

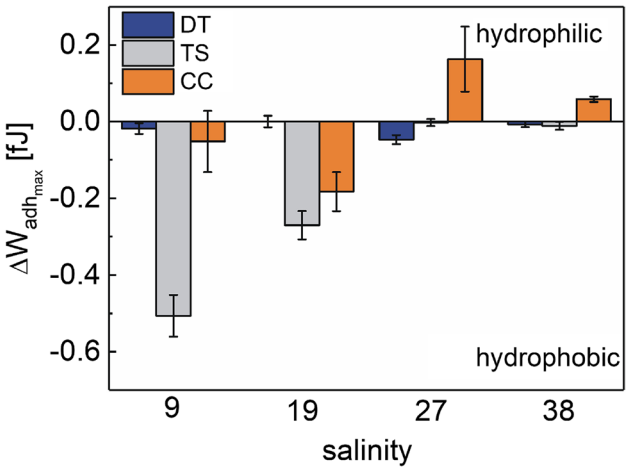

Fig. 6 The balance between hydrophilic and hydrophobic properties of algal cell surface plotted for salinities of 9, 19, 27, and 38. Data are presented as $\Delta W_{adh} \pm$ maximum error

the salinity decreased to 19, the relationship between the surface properties of the algal cells changed, and the cells of *C. closterium* became highly hydrophobic. At salinity of 9, the resulting work of adhesion was still negative. Moreover, the results of adhesion probability showed the affinity to hydrophilic materials depending on the structure and properties of the microalgal species (see Figure S8). *Dunaliella tertiolecta* showed a very low adhesion probability to the hydrophilic surfaces, in contrast to the cells of *C. closterium*, which preferentially adhered to the hydrophilic probe throughout the salinity studied. In the case of *T. suecica*, at salinities of 27 and 38, $P_{noOTS} > P_{OTS}$, while at salinities of 9 and 19, $P_{noOTS} << P_{OTS}$.

Lipid characterization of algal cells

The changes in cellular content of membrane lipids, ST, GL, and PL, caused by the decrease in salinity in the microalgal cell cultures of *D. tertiolecta*, *T. suecica*, and *C. closterium* are shown in Fig. 7.

In general, the least changes in total membrane lipids and classes with decreasing salinity were observed in *D. tertiolecta* (Fig. 7a, d, g, and j). In *T. suecica*, decreasing salinity resulted in a decrease in cellular content of total membrane lipids with a decrease of GL, followed by an increase of PL. In the microalga *C. closterium*, a decrease in total membrane lipid concentration, GL and PL was observed with a decrease in salinity from 38 to 9, but without a particular trend of change. Parallelly, a statistically significant ($p < 0.05$) increase in the cellular content of sterols was observed with the decrease in salinity in all three microalgae. At salinity of 9, the sterol content in diatom *C. closterium* was increased 3.8-fold compared to salinity of 38.

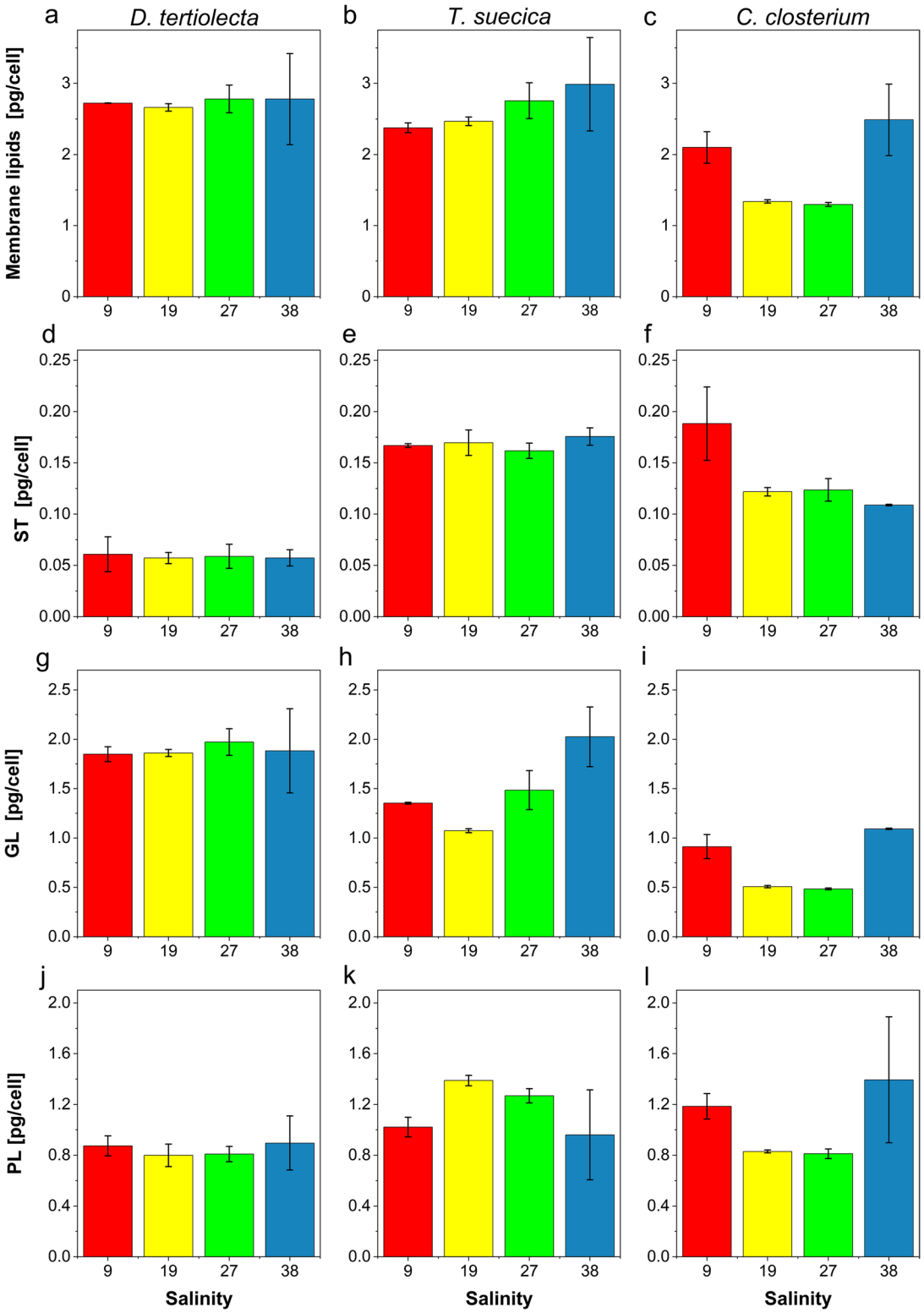

Fig. 7 Membrane lipid content of *D. tertiolecta* (**a**, **d**, **g**, and **j**), *T. suecica* (**b**, **e**, **h**, and **k**) and *C. closterium* (**c**, **f**, **i**, and **l**) at salinities of 9, 19, 27, and 38: total membrane lipids (**a**–**c**), sterols (ST) (**d**–**f**), glycolipids (GL) (**g**–**i**), and phospholipids (PL) (**j**–**l**). Data are shown as mean ± SD

However, the highest cellular sterol content was observed in *T. suecica* (Fig. 7e).

Discussion

We performed a comprehensive biophysical characterization at the level of a single algal cell to maintain structural integrity and clarify the poorly understood relationships between the chemical composition and mechanical properties of microalgae grown under selected salinity conditions. Three morphologically distinct marine microalgal species, *D. tertiolecta*, *T. suecica*, and *C. closterium*, were grown under four salinity conditions to mimic the broad salinity range in marine systems. We used a workflow that included chemical characterization (membrane lipids, hydrophobicity), nanomechanical characterization (stiffness), and behavioral characterization (physiological activity, motility, and adhesion to an interface) of microalgae in the stationary growth phase.

The responses of microalgae subjected to different salinity may also reflect cellular stress, resulting from the short-term salinity stress imposed on the cells which could trigger various morphological and biochemical changes (Borowitzka 2018b). Microalgae respond to abiotic stress through numerous mechanisms, including the adaptation of lipid composition and quantity to the new conditions. In response to various external stimuli, many microalgal species have evolved the ability to efficiently modify lipid metabolism by switching between nonpolar storage lipids (Thompson 1996; Guschina and Harwood 2006) and polar structural lipids. Storage lipids, composed mainly of polyunsaturated fatty acids are important for maintaining spontaneous curvature and flexural rigidity of membranes (De Carvalho and Caramujo 2018), while structural lipids are responsible for membrane fluidity, cell signaling pathways, and response to changes in the cellular environment (Aratboni et al. 2019; Rogowska and Szakiel 2020). Sterols are integral nonpolar components of eukaryotic membranes where, together with phospholipids, they regulate membrane permeability and fluidity and play an important role in sensing osmotic changes (Zelazny et al 1995). Notably, the cells of *T. suecica* were found to have the highest sterol production, in contrast to those of *D. tertiolecta*. In all three microalgae studied, total cellular concentrations of ST increased with decreasing salinity, indicating decreased membrane fluidity and increased cell hydrophobicity (Figs. 5 and 7). In contrast to the effects of decreasing salinity examined in our study, most studies of microalgal salinity accommodation examined the effects of higher than optimal salinity on lipid metabolism. Responses of *D. tertiolecta* and *Dunaliella salina* to growth in salinity concentrations above those of seawater resulted in a decrease in total sterol yield (Francavilla et al. 2010).

Profiling of microalgal membrane lipids is species- and abiotic stressor-specific (Ahmed et al. 2015; Novak et al. 2019). While changes in total PL and GL were observed in *T. suecica* and *C. closterium*, *D. tertiolecta* slightly altered cellular membrane lipid content. As observed in our concurrent study, the minimal but statistically significant changes in lipid remodeling in *D. tertiolecta* in response to low salinity (3) are attributed to the fact that *D. tertiolecta* is genetically adapted to large salinity fluctuations through polar lipid composition (Vrana et al. under revision). The fact that no linear response to salinity reduction was observed in *T. suecica* and *C. closterium* may indicate a change in nutrient and light availability for growth at different salinities. Similarly, no trend in total lipid content was observed in *T. suecica* growing in a salinity range of 15–90 g L^{-1} (Venckus et al. 2021).

As an euryhaline species, *D. tertiolecta* largely maintained membrane lipid content and hydrophobicity across the studied salinity range. When salinity decreased to 9, *Dunaliella* species became stiffer, which was accompanied by an increase in sterols, the formation of a thick actin layer, and pronounced physiological activity in the form of globular structures, which could indicate the transitioning of cells into palmella stage (Wei et al. 2017). Salinity-induced changes in cell stiffness would consequently affect cell adhesion behavior at the interface. The adhesion of *D. tertiolecta* cultured at salinity of 9 exhibited a narrow potential range, suggesting that the cells were stiffer and more hydrophobic than those cultured at salinity of 38 (Fig. 3b). These observations were consistent with the nanomechanical characterization of *Dunaliella* cells at selected salinities. Aging of *Dunaliella* cells also leads to changes affecting cell stiffness, hydrophobicity, and adhesion behavior, which may be related to molecular modification of the cell envelope (Pillet et al. 2019).

The second species, a calcite-encrusted thecate *T. suecica*, showed the most pronounced salinity-related changes which could indicate the formation of a cyst stage. At salinity of 9, cell exhibited the loss of flagella, the highest cell stiffness and hydrophobicity, accompanied by an increase in ST content and a decrease in GL content, which affected the distribution of surface charges and accordingly caused changes in the adhesive properties of the microalga (Figs. 6 and 7, Fig. S8). At salinity of 19, *T. suecica* showed the most pronounced physiological activity among all the species studied in the form of a dense EPS network (Figs. 3c and 4, Fig. S7), which was accompanied by a decrease in total membrane lipid content (Fig. 7b). A fundamental role in EPS production is played by variation in salinity, which exerts oxidative stress on cells and affects cellular ion balance (Guzman-Murillo and Ascencio 2001; Parra-Riofrío et al. 2020). At lower salinity, cellular ion concentrations increased and their ion ratios were constant, whereas at

salinity higher than 20, ion ratios became variable (Kirst 1990), affecting the amount of EPS production in *T. suecica* and its adaptation mechanisms to osmotic stress (Guzman-Murillo and Ascencio 2001).

Cylindrotheca closterium, a species enclosed within an organosilicate frustule, showed good adaptation to a wide range of salinity (Glaser and Karsten 2020). At lower salinities of 9 and 19, the cells of *C. closterium* showed hydrophobic behavior, whereas at higher salinities of 27 and 38, they showed a hydrophilic character accompanied with physiological activity (Figs. 3c and 6). This result could suggest that the observed salinity-induced transition of *C. closterium* cell properties from hydrophobic to hydrophilic might be related to the amount and ratio of sulfated (sPS) and carboxylated (cPS) polysaccharides, as has been reported for the adaptation of marine species to high salinity environments (Aquino et al. 2011; Arata et al. 2017). In this way, EPS composition mainly determined the adhesiveness of algal cells (Xiao and Zheng 2016). Whether a microalgal cell behaves hydrophobically or hydrophilically determines its ecological role in marine systems, whether they live in the benthos and/or form colonies or live as plankton (Griffiths and Harrison 2009; Ozkan and Berberoglu 2013; Novosel et al. 2021).

At the nanometer level, the morphology of microalgal cells did not show any specific changes, except for the change in cell size and the loss of flagella in the cells of *T. suecica*. The cells of *D. tertiolecta* and *T. suecica* grown at lower salinities were smaller than those grown at a salinity of 38. These results are consistent with the commonly known fact that phytoplankton cell size decreases not only with temperature (Atkinson et al. 2003) but also with decreasing salinity (Litchman et al. 2009). Fu et al. (2014) showed that the cell volume of *D. salina* fluctuated continuously for 10 days as a result of high salinity stress, eventually stabilizing at a slightly larger cell size compared to unstressed conditions. The loss of flagella in the cells of *T. suecica* grown at lower salinity could indicate development of cyst stage, as has been reported for other flagellated microalgae (Borowitzka and Siva 2007; Ma et al. 2012; Wei et al. 2017; Shetty et al. 2019; Hyung et al. 2021). On the other hand, the cells of *C. closterium* were larger compared to cells grown at salinity of 38, presumably not only related to salinity but also to its life cycle, in which the maximal cell size is attained by initial cells sprouting from the fully grown auxospores (Vanormelingen et al. 2013).

Reducing the salinity from 38 to 9 resulted in a much higher secretion of biopolymers in all species, which allowed the stressed cells to survive under unfavorable conditions. The extracellular biopolymers secreted by stressed *D. tertiolecta* cells changed their supramolecular structure with decreasing salinity, i.e., the spherical structure observed at salinity of 38 changed to a fibrillar structure at salinity of 9. Fibrillar structures were also present when cells were grown at a lower temperature (Novosel et al. 2021). The greatest difference in EPS organization was observed in *T. suecica* cells. Cells grown at salinities of 9, 19, and 27 released fibrillar networks, with the highest network density observed at salinity of 19 (Figure S7), which is similar to dense EPS network formation of *C. closterium* cells at 30 °C. In contrast, only spherical material was present around *T. suecica* cells exposed to temperature stress (Novosel et al. 2021).

At the population level, rapid and quantitative high-throughput analysis of several hundred cells allowed characterization of microalgal motility behavior (Novosel et al. 2020). Microalgal motility behavior depends on the complexity of the flagellar system. For example, biflagellated *Dunaliella* cells had about 3 times lower cell speed than tetraflagellated *T. suecica* (Figs. 1 and 2). Both cells showed that cell motility is dependent on salinity. At salinity of 9, the population of vibrating cells predominated, moving around the spot with minimal cell speed. When the salinity was increased to 38, the number of motile cells increased, and the cell speed and search radius increased accordingly. At salinity of 38, the search radius of both flagellar cells ranged from 6 to 13 body lengths per second and showed brisk movement. As cell motility can be influenced by cell physiological activity (Mayali et al. 2008), the pronounced cell physiological activity detected in *T. suecica* cell cultures at salinity of 19 could interfere with cell speed and search radius (Figs. 2, 3c, and 4c).

To place this study in a broader context, we compared the influence of individual abiotic stressors: temperature *vs.* salinity as the main environmental indicators of climate change on the adaptation response of selected microalgae in the stationary growth phase. A color wheel illustrating chemical, mechanical, and behavioral changes in terms of hydrophobicity, stiffness, EPS production, and motility of microalgae when exposed to a temperature maximum (Novosel et al. 2021) and salinity minimum is shown in Fig. 8.

Our results showed that the adaptive response of microalgae is species-specific and stressor-specific. Decrease in salinity triggered profound chemical, mechanical, and behavioral response in the studied microalgal cells. All three selected species became stiffer and behaved hydrophobically, while differing in physiological activity. Although cells of *T. suecica* are enclosed in a calcite-coated theca, they appeared to be sensitive to hyposaline conditions, as indicated by the highest hydrophobicity and physiological activity. In contrast, temperature did not elicit a major adaptive response in *T. suecica*, demonstrating a temperature tolerance. The green alga *Dunaliella*, which is surrounded by a glycocalyx layer, showed a profound chemical and mechanical response under both stressors, consistent with the extremophilic nature of *Dunaliella*. In contrast, the pennate diatom *C. closterium*,

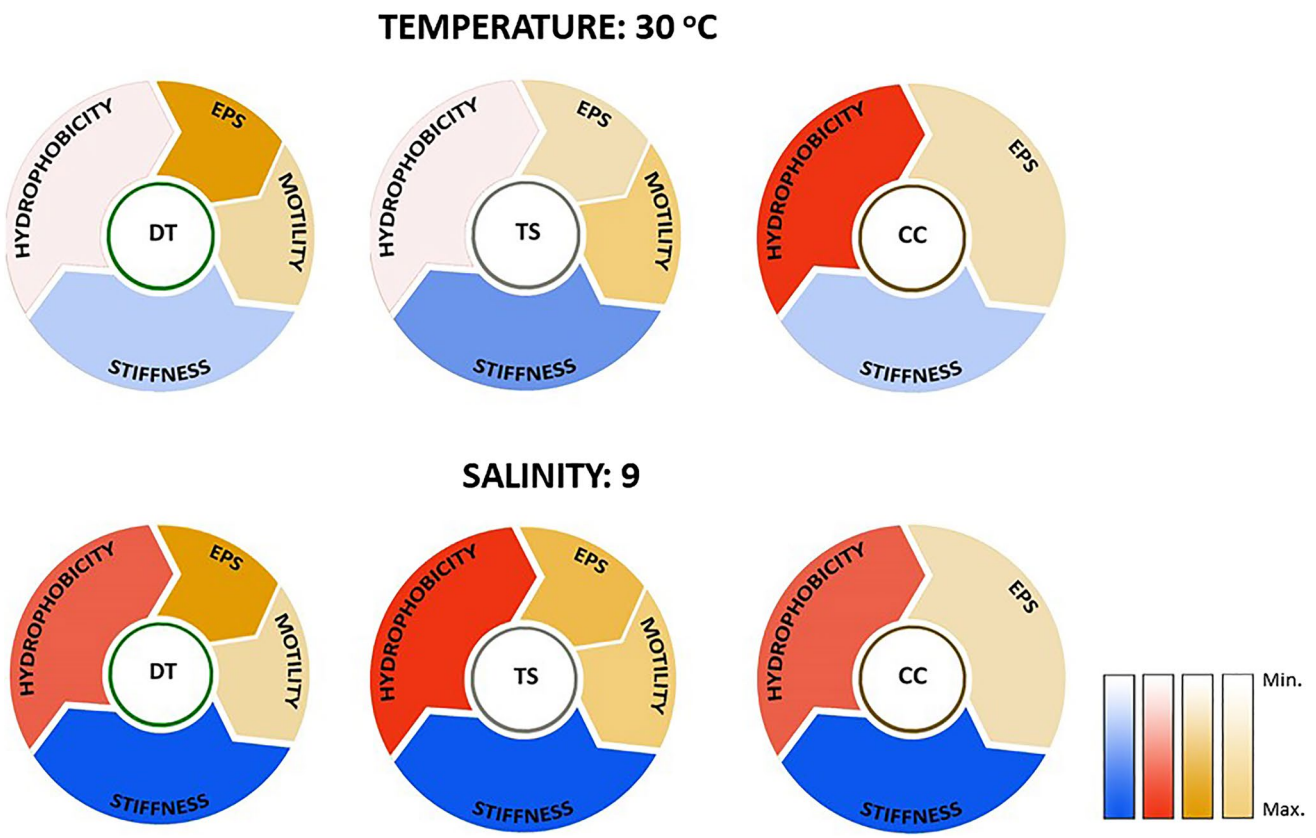

Fig. 8 Comparison of adaptive responses of microalgae triggered by individual stressors (temperature of 30 °C *vs*. salinity of 9). Temperature-induced adaptive responses of microalgae have been described in detail (Novosel et al. 2021). Color shading refers to the response of microalgae compared to control conditions (temperature of 18 °C and salinity of 38)

enclosed in an organosilicate frustule, maintained a nearly constant hydrophobicity and EPS production, regardless of the stressors studied. Such environmental adaptation of diatom cells derives from a long-lasting evolutionary advance in genetic, physiological, and morphological traits (Falkowski et al. 2004; Armbrust 2009).

Our results, based on a study conducted in the laboratory, showed that the adaptive response of algae to changes in abiotic stressors could be identified and quantified. In this way, the present fundamental study may help to understand how salinity controls the diversity, structure, and function of microbial communities in aquatic systems, with only those microorganisms that have successfully adapted to salinity being able to survive the ongoing and projected salinity fluctuations (Baek et al. 2011; Triadó-Margarit and Casamayor 2012; Bautista-Chamizo et al. 2018).

Conclusion

We investigated the salinity-induced adaptive response of two green microalgae and a diatom in the terms of chemical, mechanical, and behavioral changes. Our results showed that the adaptive response of microalgae is species- and salinity-specific. Although covered only with glycocalyx coat, the cells of *D. tertiolecta* adapt to a wide range of salinity levels without significant changes in membrane lipids and hydrophobicity, confirming their euryhaline nature. *Dunaliella tertiolecta* responded to a decrease in salinity to 9 with the formation of a thick actin layer, increase in cell stiffness, sterol content and physiological activity, and a decrease in motility, likely leading to the formation of a palmella stage. The cells of *T. suecica* proved to be sensitive to salinity fluctuations, despite being surrounded by a calcite-encrusted theca. In particular, a decrease in salinity to 19 in *T. suecica* resulted in growth reduction, loss of flagella, decrease in motility, increase in cell stiffness, hydrophobicity, sterol content, and the formation of a dense EPS network with a concomitant decrease in membrane lipids, which might indicate the progressing of cells into the cyst stage. *Cylindrotheca closterium*, enclosed in organosilicate frustule, proved to be tolerant to a decrease in salinity. At salinities of 9 and 19, *C. closterium* became stiffer and hydrophobic, whereas at salinities of 27 and 38, it behaved softer and hydrophilic, which might be related to a molecular change in the released biopolymers. This comprehensive study

provided a fundamental biophysical understanding of the adaptive mechanisms of individual algal species to changing salinity. Such understanding offers the basis for deciphering the complex interactions between abiotic stressors on microalgae in marine systems. The abovementioned changes in microalgal response showed that cell surface properties and behavior could be considered as markers of stress in marine communities and could be used to predict the effects of climate change on aquatic communities.

Supplementary Information The online version contains supplementary material available at https://doi.org/10.1007/s10811-022-02734-x.

Acknowledgements This work is supported by the Croatian Science Foundation Project "From algal cell surface properties to stress markers for aquatic ecosystems" (IP-2018-01-5840). The authors acknowledge networking in the COST action CA18238.

Data availability The datasets generated during the current study are available from the corresponding author.

References

Ahmed F, Zhou W, Schenk PM (2015) *Pavlova lutheri* is a high-level producer of phytosterols. Algal Res 10:210–217

Arata PX, Alberghina J, Confalonieri V, Errea MI, Estevez JM, Ciancia M (2017) Sulfated polysaccharides in the freshwater green macroalga *Cladophora surera* not linked to salinity adaptation. Front Plant Sci 8:1972–1982

Aratboni AH, Rafiei N, García-Granados R, Alemzadeh A, Morones-Ramirez J (2019) Biomass and lipid induction strategies in microalgae for biofuel production and other applications. Microb Cell Fact 18:178–195

Armbrust E (2009) The life of diatoms in the world's oceans. Nature 459:185–192

Atkinson D, Ciotti BJ, Montagnes DJS (2003) Protists decrease in size linearly with temperature: ca. 2.5% degrees C-1. Proc Roy Soc B 270:2605–2611

Aquino RS, Grativol C, Mourão PAS (2011) Rising from the sea: Correlations between sulfated polysaccharides and salinity in plants. PLoS One 6:e18862

Baek SH, Jung SW, Shin K (2011) Effects oftemperature and salinity on growth of *Thalassiosira pseudonana* (Bacillariophyceae) isolated from ballast water. J Freshwater Ecol 26:547–552

Bautista-Chamizo E, Sendra M, Cid Á, Seoane M, Romano de Orte M, Riba I (2018) Will temperature and salinity changes exacerbate the effects of seawater acidification on the marine microalga *Phaeodactylum tricornutum*? Sci Total Environ 634:87–94

Barati B, Gan S-Y, Lim P-E, Beardall J, Phang S-M (2019) Green algal molecular responses to temperature stress. Acta Physiol Plant 41:26–45

Benavente-Valdés JR, Aguilar C, Contreras-Esquivel JC, Méndez Zavala A, Montanez JC (2016) Strategies to enhance the production of photosynthetic pigments and lipids in chlorophycae species. Biotechnol Rep 10:117–125

Bligh EG, Dyer WJ (1959) A rapid method of total lipid extraction and purification. Can J Biochem Physiol 37:911–917

Borowitzka MA, Siva CJ (2007) The taxonomy of the genus *Dunaliella* (Chlorophyta, Dunaliellales) with emphasis on the marine and halophilic species. J Appl Phycol 19:567–590

Borowitzka MA (2018a) Biology of Microalgae. In: Levine IA, Fleurence J (eds) Microalgae in health and disease prevention. Academic Press, London, pp 23–72

Borowitzka MA (2018b) The "stress" concept in microalgal biology—homeostasis, acclimation and adaptation. J Appl Phycol 30:2815–2825

De Carvalho CCCR, Caramujo MJ (2018) The various roles of fatty acids. Molecules 23:2583–2619

Decho AW, Gutierrez T (2017) Microbial extracellular polymeric substances (EPSs) in ocean systems. Front Microbiol 8:922–950

El-Kassas HY, El-Sheekh MM (2016) Induction of the synthesis of bioactive compounds of the marine alga *Tetraselmis tetrathele* (West) Butcher grown under salinity stress. Egypt J Aquat Res 42:385–391

Falkowski P, Katz M, Knoll A, Quigg A, Raven J, Schofield O, Taylor F (2004) The evolution of modern eukaryotic phytoplankton. Science 305:354–360

Foflonker F, Mollegard D, Ong M, Su Yoon H, Bhattacharya D (2018) Genomic analysis of *Picochlorum* species reveals how microalgae may adapt to variable environments. Mol Biol Evol 35:2702–2711

Francavilla M, Trotta P, Luque R (2010) Phytosterols from *Dunaliella tertiolecta* and *Dunaliella salina*: a potentially novel industrial application. Bioresour Technol 101:4144–4150

Fu W, Paglia G, Magnúsdóttir M, Steinarsdóttir EA, Gudmundsson S, Palsson BØ, Brynjólfsson S (2014) Effects of abiotic stressors on lutein production in the green microalga *Dunaliella salina*. Microb Cell Fact 13:3

Gašparović B, Kazazić SP, Cvitešić A, Penezić A, Frka S (2015) Improved separation and analysis of glycolipids by Iatroscan thin-layer chromatography–flame ionization detection. J Chromatogr A 1409:259–267

Gašparović B, Kazazić SP, Cvitešić A, Penezić A, Frka S (2017) Corrigendum to "Improved separation and analysis of glycolipids by Iatroscan thin-layer chromatography–flame ionization detection" [J Chromatogr A 1409 (2015) 259–267]. J Chromatogr A 1521:168–169

Glaser K, Karsten U (2020) Salinity tolerance in biogeographically different strains of the marine benthic diatom *Cylindrotheca closterium* (Bacillariophyceae). J Appl Phycol 32:3809–3816

Griffiths MJ, Harrison STL (2009) Lipid productivity as a key characteristic for choosing algal species for biodiesel production. J Appl Phycol 21:493–507

Guillard RRL (1975) Culture of phytoplankton for feeding marine invertebrates. In: Smith WL, Chanley MH (eds) Culture of Marine Invertebrate Animals. Plenum Press, NY, pp 29–60

Guschina IA, Harwood JL (2006) Lipids and lipid metabolism in eukaryotic algae. Prog Lipid Res 45:160–186

Gustavs L, Eggert A, Michalik D, Karsten U (2010) Physiological and biochemical responses of green microalgae from different habitats to osmotic and matric stress. Protoplasma 243:3–14

Guzman-Murillo M, Ascencio F (2001) Enzyme-linked, biotin-streptavidin bacterial-adhesion assay for Helicobacter pylori lectin-like interactions with cultured cells. J Microbiol Biotechnol 11:35–39

Helm MM, Bourne N, Lovatelli A, Fisheries and Aquaculture Management Division, (2004) The hatchery culture of bivalves: a practical manual. FAO, Rome

Hunter KA, Liss PS (1981) Polarographic measurement of surface-active material in natural waters. Water Res 15:203–215

Hyung J-H, Kim E-J, Moon S-J, Kang NS, Park J (2021) *Tetraselmis jejuensis* sp. nov. (Chlorodendrophyceae), a euryhaline microalga found in supralittoral tide pools at Jeju Island, Korea. Plants 10:1289

Israelachvili JN (1992) Intermolecular forces & surface forces. Academic Press, New York

Ivošević N, Tomaić J, Žutić V (1994) Organic droplets at an electrified interface: critical potentials of wetting measured by polarography. Langmuir 7:2415–2418

Ivošević DeNardis N, Žutić V, Svetličić V, Frkanec R, Tomašić J (2007) In situ amperometric characterization of liposome suspensions with concomitant oxygen reduction. Electroanalysis 19:2444–2450

Ivošević DeNardis N, Ružić I, Pečar- Ilić J, El Shawish S, Ziherl P (2012) Reaction kinetics and mechanical models of liposome adhesion at charged interface. Bioelectrochemistry 88:48–56

Ivošević DeNardis N, Pečar Ilić J, Ružić I, Pletikapić G (2015) Cell adhesion and spreading at a charged interface: Insight into the mechanism using surface techniques and mathematical modelling. Electrochim Acta 176:743–754

Ivošević DeNardis N, Pečar Ilić J, Ružić I, Novosel N, Mišić Radić T, Weber A, Kasum D, Pavlinska P, Katalin Balogh R, Hajdu B, Marček Chorvátová A, Gyurcsik B (2019) Algal cell response to laboratory-induced cadmium stress: a multimethod approach. Eur Biophys J 48:231–248

Kefford B, Papas P, Crowther M, Nugegoda D (2002) Are salts toxicants? Australas J Ecotoxicol 8:63–68

Kim S-K (ed) (2015) Handbook of marine microalgae. Academic Press, London

Kirst GO (1990) Salinity tolerance of eukaryotic marine algae. Annu Rev Plant Physiol 41:21–53

Kovač S, Kraus R, Geček S, Žutić V (2000) Cell suspension as a model system for electrochemical analysis. Croat Chem Acta 73:279–291

Litchman E, Klausmeier CA, Yoshiyama K (2009) Contrasting size evolution in marine and freshwater diatoms. Proc Nat Acad Sci 106:2665–2670

Ma Z, Helbling EW, Li W, Villafañe VE, Gao K (2012) Motility and photosynthetic responses of the green microalga *Tetraselmis subcordiformis* to visible and UV light levels. J Appl Phycol 24:1613–1621

Mayali X, Franks PJS, Tanaka Y, Azam F (2008) Bacteria-induced motility reduction in *Lingulodinium polyedrum* (Dinophyceae). J Phycol 44:923–92836

Medlin L, Kaczmarska I (2004) Evolution of the diatoms: V. Morphological and cytological support for the major clades and a taxonomic revision. Phycologia 43:245–270

Minhas AK, Hodgson P, Barrow CJ, Adholeya A (2016) A review on the assessment of stress conditions for simultaneous production of microalgal lipids and carotenoids. Front Microbiol 7:1–19

Mišić Radić T, Čačković A, Penezić A, Dautović J, Lončar J, Omanović D, Juraić K, Ljubešić Z (2021) Physiological and morphological response of marine diatom *Cylindrotheca closterium* (Bacillariophyceae) exposed to cadmium. Eur J Phycol 56:24–36

Novak T, Godrijan J, Marić Pfannkuchen D, Djakovac T, Medić N, Ivančić I, Mlakar M, Gašparović B (2019) Global warming and oligotrophication lead to increased lipid production in marine phytoplankton. Sci Total Environ 668:171–183

Novosel N, Kasum D, Žutinić P, Legović T, Ivošević DeNardis N (2020) Short-term effect of cadmium on the motility of three flagellated algal species. J Appl Phycol 32:4057–4067

Novosel N, Mišić Radić T, Zemla J, Lekka M, Čačković A, Kasum D, Legović T, Žutinić P, Gligora Udovič M, Ivošević DeNardis N (2021) Temperature-induced response in algal cell surface properties and behaviour: an experimental approach. J Appl Phycol 33:1–17

Novosel N, Ivošević DeNardis N (2021) Structural features of the algal cell determine adhesion behavior at a charged interface. Electroanalysis 6:1436–1443

Oliveira L, Bisalputra T, Antia NJ (1980) Ultrastructural observation of the surface coat of *Dunaliella tertiolecta* from staining with cationic dyes and enzyme treatments. New Phytol 85:385–392

Ozkan A, Berberoglu H (2013) Physico-chemical surface properties of microalgae. Colloids Surf B 112:287–293

Parra-Riofrío G, García-Márquez J, Casas-Arrojo V, Uribe-Tapia E, Abdala-Díaz RT (2020) Antioxidant and cytotoxic effects on tumor cells of exopolysaccharides from *Tetraselmis suecica* (Kylin) Butcher grown under autotrophic and heterotrophic conditions. Mar Drugs 18:1–23

Pavlinska Z, Chorvat D, Mateasik A, Jerigova M, Velic D, Ivošević DeNardis N, Marcek Chorvatova A (2020) Fluorescence responsiveness of unicellular marine algae *Dunaliella* to stressors under laboratory conditions. J Biotechnol 324S:100018

Pillet F, Dague E, Pečar Ilić J, Ružić I, Rols M-P, Ivošević DeNardis N (2019) Changes in nanomechanical properties and adhesion dynamics of algal cells during their growth. Bioelectrochemistry 128:154–162

Pletikapić G, Berquand A, Mišić Radić T, Svetličić V (2012) Quantitative nanomechanical mapping of marine diatom in seawater using peak force tapping atomic force microscopy. J Phycol 48:174–185

Pletikapić G, Ivošević DeNardis N (2017) Application of surface analytical methods for hazardous situation in the Adriatic Sea: Monitoring of organic matter dynamics and oil pollution. Nat Hazards Earth Syst Sci 17:31–44

R Core Team (2020) R: A language and environment for statistical computing. R Foundation for Statistical Computing, Vienna, Austria.https://www.R-project.org/

Rogowska A, Szakiel A (2020) The role of sterols in plant response to abiotic stress. Phytochem Rev 19:1525–1538

Sader JE, Larson I, Mulvaney P, White LR (1995) Method for the calibration of atomic force microscope cantilevers. Rev Sci Instrum 66:3789–3798

Shetty P, Gitau MM, Maróti G (2019) Salinity stress responses and adaptation mechanisms in eukaryotic green microalgae. Cells 8:1657–1673

Sneddon IN (1965) The relation between load and penetration in the axisymmetric Boussinesq problem for a punch of arbitrary profile. Int J Eng Sci 3:47–57

Svetličić V, Ivošević N, Kovač S, Žutić V (2000) Charge displacement by adhesion and spreading of a cell: amperometric signals of living cells. Langmuir 16:8217–8220

Svetličić V, Balnois E, Žutić V, Chevalet J, Hozić Zimmermann A, Kovač S, Vdović N (2006) Electrochemical detection of gel microparticles in seawater. Croat Chem Acta 79:107–113

Thompson GA Jr (1996) Lipids and membrane function in green algae. Biochim Biophys Acta 1:17–45

Triadó-Margarit X, Casamayor E (2012) Genetic diversity of planktonic eukaryotes in high mountain lakes (Central Pyrenees, Spain). Environ Microbiol 14:2445–2456

Vanormelingen P, Vanelslander B, Sato S, Gillard J, Trobajo R, Sabbe K, Vyverman W (2013) Heterothallic sexual reproduction in the model diatom *Cylindrotheca*. Eur J Phycol 48:93–105

Venckus P, Cicchi B, Chini Zittelli G (2021) Effects of medium salinity on growth and biochemical composition of the green microalga *Tetraselmis suecica*. J Appl Phycol 33:1–9

Wei S, Bian Y, Zhao Q, Chen S, Mao J, Song C, Cheng K, Xiao Z, Zhang C, Ma W, Zou H, Ye M, Dai S (2017) Salinity-induced palmella formation mechanism in halotolerant algae *Dunaliella salina* revealed by quantitative proteomics and phosphoproteomics. Front Plant Sci 8:810

Xiao R, Zheng Y (2016) Overview of microalgal extracellular polymeric substances (EPS) and their applications. Biotechnol Adv 34:1225–1244

Zelazny AM, Shaish A, Pick U (1995) Plasma membrane sterols are essential for sensing osmotic changes in the halotolerant alga *Dunaliella*. Plant Physiol 109:1395–1403

Žutić V, Kovač S, Svetličić V (1993) Heterocoalescence between organic microdroplets and charged conductive interface. J Electroanal Chem 349:173–186

Žutić V, Ivošević N, Svetličić V, Long RA, Azam F (1999) Film formation by marine bacteria at a model fluid interface. Aquat Microb Ecol 17:231–238

Žutić V, Svetličić V, Ivošević N, Hozić A, Pečar O (2004) Northern Adriatic mesocosm experiment Rovinj 2003: dynamics of organic microparticles studied by the electrochemical technique. Period Biol 106:67–74

4. RASPRAVA

Istraživanja objedinjena u četiri znanstvena rada provedena su s tri monokulture mikroalga u stacionarnoj fazi rasta u laboratorijskim i djelomice prirodnim uvjetima. Odabrane vrste mikroalga *D. tertiolecta*, *T. suecica* i *C. closterium* odlikuju se specifičnim morfološkim značajkama stanične barijere (od glikokaliksa do čvrstih ljušturica) i flagelarnog sustava.

4.1. Utjecaj antropogenog stresora na ponašanje i površinska svojstva mikroalga u laboratorijskim uvjetima

Različiti antropogeni stresori kao što su teški metali, pesticidi, industrijske boje, deterdženti, naftni derivati, plastika ometaju primarne ekološke uloge mikroalga u vodenim ekosustavima (Häder i Gao, 2015). Rudarstvo, izgaranje fosilnih goriva i industrijski procesi imaju značajan utjecaj na biogeokemijske cikluse metala. Metali uneseni u prirodni okoliš tamo ostaju zauvijek, te kruže između granica faza: atmosfere, vode, sedimenta i organizama. Kako bismo razumjeli utjecaj metala na rast i produktivnosti mikroalga potrebno je poznavati koncentraciju metala i njegovu specijaciju koja određuje dostupnost metala algama (Hassler i sur., 2012). Biodostupan metal je metal u svom slobodnom ionskom obliku, kao i neki labilni kompleksi metala s anorganskim ili organskim ligandima.

Kadmij se javlja u okolišu u anorganskom obliku kao posljedica vulkanskih emisija i trošenja stijena, a njegovu prirodnu koncentraciju dodatno povećavaju antropogene aktivnosti, posebice poljoprivreda, rudarstvo, automobilska industrija (Das i sur., 1998), proizvodnja pigmenata za boje, industrija plastike, te proizvodnja Cd-Ni baterije (Madasamy i Babu, 2016). U vodenom okolišu kadmij se nalazi u stanju $Cd^{2+,}$ koje je ujedno i njegovo najstabilnije stanje (Hasan i sur., 2009), te maksimalna koncentracija u nezagađenim vodenim okolišima iznosi do 1 $\mu g\ L^{-1}$ (Friberg i sur., 1986).

Istraživanje utjecaja teških metala na stanice alga u vodenom okolišu nužno je za razumijevanje njihovih adaptacijskih mehanizama. Mikroalge izložene stresu teškim metalima razvijaju različite mehanizme koji uključuju alokaciju toka ugljika prema sintezi osmolita i molekula antioksidansa (npr. šećeri i β-karoten) (Einali i sur., 2017.), kao i promjene u fluorescenciji klorofila i ekspresiji proteina (Saha i sur., 2018.; Ivošević DeNardis i sur., 2019; Pavlinska i sur., 2020). Točan mehanizam interakcije kadmija i stanica mikroalga nije u potpunosti

jasan i vjerojatno se razlikuje od vrste do vrste. Smatra se da se ioni metala vežu na ligande na površini stanice, omogućujući transport unutar stanica u vakuole ili se pričvršćuju na membranu gdje izlučeni polimeri mogu igrati važnu ulogu (Morlon i sur., 2005, Scheidegger i sur., 2011.; Belghith i sur., 2016). Također, stanice mikroalga mogu isključivati metale (imajući manje reaktivne površine), unutarstanično sekvestrirati metale u bezopasne oblike ili ih ugrađivati dalje od vitalnih metaboličkih područja, te vezati metale stvarajući kompleks polipeptid-metal koji se izbacuje iz stanice (Fisher i sur., 1984, Tsuji i sur., 2002). Kadmij se može akumulirati u stanice, na način da se zamijeni cinkom na mjestu aktivnog enzima, što je popraćeno pojačanom respiracijom i smanjenjem fotosintetske aktivnosti (Stallwitz i Häder, 1994). Akumulacija kadmija u stanicama *D. tertiolecta* detektirana je sekundarnom ionskom masenom spektroskopijom što predstavlja dokaz ulaska kadmija u hranidbeni lanac u moru (Pavlinska i sur., 2020).

U našem nedavnom istraživanju, primjenom multimetodološkog pristupa dobiven je uvid u adaptacijski odgovor mikroalga *D. tertiolecta* pod utjecajem toksične koncentracije kadmija (Ivošević DeNardis i sur., 2019). Primjenom generaliziranog matematičkog modela za stvaranje kompleksa između jednog liganda i nekoliko metala u tragovima određena je koncentracija slobodnog biodostupnog Cd (II) koja je iznosila 600 µg/L. Stanice vrste *D. tertiolecta* uspješno su rasle i povećavale svoju abundanciju kroz 24 dana rasta, unatoč prisustvu kadmija u hranjivom mediju, tako stvarajući veću bioaktivnu površinu čime je smanjena toksičnost kadmija po stanici. Nadalje, stanice su se uspješno adaptirale na stres pri čemu je došlo do ekspresije proteina koji imaju ulogu u fotosintetskoj aktivnosti. U kulturama koje su uzgajane u prisustvu kadmija zabilježeno je povećanje u zelenoj fluorescenciji (najvjerojatnije povezano s vezikularnim transportom kadmija i/ili proizvodnjom beta-karotena), dok promjene u crvenoj endogenoj fluorescenciji (povezana s klorofilom) nisu zabilježene. Za održavanje iste stope emisije klorofila, adaptacijski odgovor stanica očitovao se kroz povećanu ekspresiju identificiranih proteina koji vežu klorofil, a koji su važni za fotosintezu. Budući da proizvodnja ovih proteina predstavlja stanične obrambene mehanizme, oni također mogu signalizirati prisutnost toksičnih metala u morskoj vodi. Uslijed stresa s teškim metalom kadmijem zabilježena i je povećana fiziološka aktivnost i statistički značajan porast čvrstoće stanica što se reflektiralo na 3 puta sporiju kinetiku adhezije stanica na modelnoj međupovršini u odnosu na kontrolne uvjete. Dodatno, u prisustvu kadmija čak se 91% stanica kretalo oko svog mjesta te je brzina kretanja stanica pala na minimalnu vrijednost.

Pokretljivost je važno autonomno svojstvo koje uključuje mnoge visoko usklađene stanične funkcije. Flagelatne stanice mikroalga koriste različite vanjske kemijske i fizikalne čimbenike za usmjeravanje prema hrani ili prikladnoj niši za preživljavanje i rast (Melkonian, 1992). Do sada je stanična pokretljivost praćena na manjem broju stanica, što je bilo nedostatno za statističku analizu, te u stručnoj literaturi nema dovoljno istraživanja stanične pokretljivosti koja daju uvid u fiziološko stanje populacije (Tanaka i sur., 2005; Liu i sur., 2011.). Metode za brz pregled fiziološkog stanja populacija alga s pouzdanim i netaksonomskim parametrima, kao što je pokretljivost, jednostavne su za korištenje i od velikog interesa za ekologiju i procjenu rizika za okoliš (Lavoie i sur., 2012; Pandey i sur., 2014; Coquillé i sur., 2015; Pandey i Bergey, 2016), no takvih istraživanja nema dovoljno i njihova primjena nije dovoljno istražena.

U znanstvenom radu I pod nazivom „Short-term effect of cadmium on the motility of three flagellated algal species“ razvijena je brza, pouzdana i ekonomski isplativa procedura za praćenje i istovremenu kvantitativnu analizu pokretljivosti nekoliko stotina stanica mikroalga primjenom programa otvorenog pristupa (ICY) te statističke analize. Istražen je utjecaj toksične koncentracije kadmija od 1 mg/L uz izlaganje od 1 h i 3 h na staničnu pokretljivost tri odabrane vrste mikroalga. Odabrane mikroalge *D. tertiolecta, T. suecica* i *R. maculata* sličnih su dimenzija, no različite složenosti flagelarnog sustava. Rezultati ukazuju da veća složenost flagelarnog sustava povećava brzinu kretanja stanica, a također utječe na oblik putanje kretanja. U kontrolnim uvjetima isokontne tetraflagelatne stanice vrste *T. suecica* pokazale su 2,6 puta veću brzinu pokretljivosti (190,10 ± 5,26 μm s^{-1}) od isokontnih biflagelatnih stanica vrste *D. tertiolecta* (71,83 ± 1,84 μm s^{-1}), te 3,5 puta veću brzinu pokretljivosti od heterkontnih biflagelatnih stanica vrste *R. maculata* (55,03 ± 1,53 μm s^{-1}). Nadalje, stanice vrsta *D. tertiolecta* i *T. suecica* pokazuju linearne, dok *R. maculata* pokazuje cik-cak tip putanje kao posljedicu flagelarne asimetrije. Rezultati su pokazali statistički značajnu razliku u staničnoj pokretljivosti kod svih vrsta nakon izlaganju kadmiju koja je ovisna o vremenu izlaganja. Nakon 1 h izlaganja toksičnoj koncentraciji kadmija, brzina svih istraživanih stanica pala je na minimalnu vrijednost; stanice *D.tertiolecta* gibale su se brzinom od 36,45 ± 1,77 μm s^{-1} , dok su se stanice *R. maculata* i *T. suecica* gibale brzinama od 29,97 ± 1,37 μm s^{-1}, odnosno 42,54 ± 4,63 μm s^{-1} (stanice su uglavnom vibrirale na svom mjestu). Nakon 3 h izlaganja kadmiju stanice *R. maculata,* čiju staničnu barijeru čini višeslojni periplast, pokazale su gotovo potpuni oporavak pokretljivosti u odnosnu na kontrolnu vrijednost. Nadalje, stanice vrsta

T. suecica, čiju barijeru čini tanka teka s ugrađenim biokalcitnim perlama i *D. tertiolecta,* čiju barijeru čini glikokaliks, doživjele oporavak brzine na 80%, odnosno 66% kontrolne vrijednosti.

Iz dobivenih rezultata, proizlazi da strukturne značajke flagelarnog sustava i stanične barijere mikroalga imaju važnu ulogu u pokretljivosti stanica i toleranciji na toksičnu koncentraciju teškog metala, tako pružajući dublje razumijevanje mehanizma adaptacije stanica. Parametri stanične pokretljivosti u smislu stanične brzine i radijusa pretraživanja daju kvantitativan uvid u adaptacijski odgovor na nivou populacije stanice. Znanstveni rad I potvrdio je hipoteze istraživanja; ponašanje alga u vidu njihove pokretljivosti može se smatrati pokazateljem stresa, te da su stanice alga sa složenijom staničnom barijerom otpornije su na prisustvo stresora u vodenom okolišu.

4.2. Uloga strukturnih značajki stanične barijere na adhezijsko ponašanje mikroalga

Razvojem elektrokemijske metode polarografije i kronoamperometrije na nabijenoj međupovršini živine elektrode omogućena je karakterizacija putem (i) adsorpcije površinski-aktivne organske tvari i submikronskih čestica, te (ii) adhezije organskih mikrometarskih čestica (Žutić i sur., 1993; Ivošević i Žutić 1998; Žutić i sur., 2004; Ivošević DeNardis i sur., 2007, 2015). S obzirom na to da je osnovni elektrokemijski oblik signala stanica sličan elektrokemijskom signalu organskih kapljica, proizlazi da osnovni mehanizam adhezije stanica uključuje brzo početno prianjanje, deformaciju praćenu pucanjem stanice oslobađanjem unutarstaničnog materijala širenjem i formiranjem kontaktne međupovršine (Svetličić i sur., 2001, Ivošević DeNardis i sur., 2015). Sličnost mehanizama adhezije stanica i organskih kapljica dokazuje da kolektivna svojstva staničnog omotača (hidrofobnost, fluidnost) upravljaju dinamikom prianjanja i širenja čestica po nabijenoj površini, pri čemu fluidnost igra glavnu ulogu (Žutić i sur., 2004, Ivošević DeNardis i sur., 2015, Pillet i sur., 2019).

Proces adhezije stanica na modelnoj međupovršini ovisi o površinskim svojstvima na tri granice faza koje su u kontaktu (stanica-medij, stanica-modelna međupovršina, medij-modelna međupovršina) (Israelachvili, 1992). Do sada je u literaturi istraženo kako se mijenjanjem površinskih svojstava modelne međupovršine može utjecati na proces adhezije stanica, dok su površinska svojstva stanica i strukturne značajke stanične barijere bile zanemarene.

S ciljem rasvjetljavanja uloga strukturnih značajki stanične barijere, na adheziju mikroalga na nabijenoj međupovršini, u znanstvenom radu II pod nazivom „Structural features of the algal

cell determine adhesion behavior at a charged interface“ razvijen je protokol za amperometrijsku karakterizaciju stanica mikroalga. Rezultati istraživanja pokazali su da se vrste mikroalga koje posjeduju organosilikatnu frustulu (*C. closterium*) i teku s ugrađenim biokalcitnim perlama (*T. suecica*) ponašaju kao krute, nedeformabilne i inertne na nabijenoj, fluidnoj međupovršini, bez generiranja amperometrijskih signala stanica. S druge strane, vrste stanica alga koje posjeduju glikokaliks (*D. tertiolecta*) i celuloznu amfijezmu (*P. micans*) ponašaju se kao mekane i deformabilne, te se njihovo prianjanje registrira kao amperometrijski signal stanica, u specifičnom području potencijala tipičnom za svaku vrstu. Kritična međupovršinska napetost kod koje dolazi do adhezije mikroalga može se koristiti kao parametar adhezijske diferencijacije mekih stanica mikroalga. Područje gustoće površinskog naboja na elektrodi potrebno za adheziju stanica mikroalga postaje šire s povećanjem složenosti strukture stanične barijere. S obzirom na to da je područje gustoće naboja na elektrodi različito za adheziju stanica mikroalga od drugih mekih čestica (npr. organskih kapljica različitog sastava, lipidnih vezikula, membranskih vezikula) (znanstveni rad II, slika 5), pokazuje da površinska svojstva materijala određuju adhezijsko ponašanje na modelnoj međupovršini. Dobivene razlike u adhezijskom ponašanju stanica mikroalga na modelnoj međupovršini posljedica su strukturnih značajki stanične barijere, što se reflektira na nanomehanička svojstva stanica mikroalga. Nanomehanička svojstva pokretnih stanica teško su dostupna. Pillet i suradnici su 2019. elektrostatskom imobilizacijom biflagelatnih stanica *D. tertiolecta* odredili su nanomehanička svojstva koja se mijenjaju sa starosti kulture. Rezultati su pokazali da su stanice statistički značajno hidrofobnije i čvršće u eksponencijalnoj (31 kPa) nego u stacionarnoj fazi rasta (19 kPa), vjerojatno zbog molekularne modifikacije stanične ovojnice. Veća čvrstoća stanica *D. tertiolecta* u eksponencijalnog fazi rasta odražava se na sporiju kinetiku adhezije stanica na nabijenoj međupovršini. Za razliku od vrlo mekane stanice *D. tertiolecta*, čvrstoća stanica slabo silicificirane morske dijatomeje *C. closterium* kreće se između 29,8 MPa za područje valva i 200 MPa za područje fibula (Pletikapić i sur., 2012). Navedeni rezultati znanstvenog rada II postavili su temelje za fundamentalno razumijevanje adhezijskog ponašanja mikroalga na modelnim međupovršinama koje ovisi o strukturnim značajkama stanične barijere, te o nanomehaničkim svojstvima stanica. Razumijevanje adhezijskog ponašanja stanica mikroalga na modelnih međupovršinama može doprinijeti razumijevanju adhezijskog ponašanja na prirodnim međupovršinama u vodenom okolišu u uvjetima stresa.

4.3. Utjecaj pojedinačnih abiotičkih stresora na ponašanje i površinska svojstva mikroalga u laboratorijskim uvjetima

Ključni indikatori klimatskih promjena u vodenim ekosustavima su temperatura i salinitet koji izravno utječu na razne fiziološke procese stanica mikroalga; stvaranje biomase, metaboličke reakcije, stanično disanje, fotosintezu, kao i na ekološke interakcije (Falkowski i Raven, 2007; Lewandowska i Sommer, 2010; Guinder i Molinero, 2013). Kao adaptacijski odgovor na promjene u vodenom okolišu, mikroalge mogu prilagoditi fluidnost membrane mijenjanjem sastava masnih kiselina, ekspresijom proteina, akumulacijom kompatibilnih otopljenih tvari za održavanje osmolarnosti stanica (Gustavs i sur., 2010; Shetty i sur., 2019), regulacijom fotosinteze kako bi uravnotežili proizvodnju i potrošnju energije (Barati i sur., 2019; Pavlinska i sur., 2020), te lučenjem izvanstaničnih polimernih tvari (Decho i Gutierrez, 2017). Navedeni adaptacijski mehanizmi mogu dovesti do promjena u površinskim svojstvima i ponašanju stanica mikroalga, no takva su istraživanja nedovoljno zastupljena u literaturi.

Stoga je u znanstvenim radovima III i IV istražen utjecaj pojedinih abiotičkih stresora temperature i saliniteta na ponašanje i površinska svojstva odabranih mikroalga u laboratorijski kontroliranim uvjetima. Utjecaj promjene temperature (pri konstantom salinitetu) na mikroalge istražen je u znanstvenom radu III pod nazivom „Temperature-induced response in algal cell surface properties and behavior". Istraživanja su provedena kod odabranih temperatura uzgoja koje bi odgovarale godišnjoj varijaciji temperature u vodenim okolišima. Rezultati pokazuju da su sve istraživane vrste alga, *D. tertiolecta, T. suecica* i *C. closterium* uspješno rasle pri temperaturama od 12 °C, 18 °C i 30 °C. Ponašanje mikroalga ispitano je u smislu pokretljivosti, adhezije na nabijenoj elektrodi i fiziološke aktivnost. Analiza pokretljivosti flageliranih vrsta pruža uvid u fiziološko stanje stanica mikroalga u kulturi. Stanice vrsta *D. tertiolecta* i *T. suecica* pokazale su izraženu pokretljivost u rasponu od 6 do 13 duljina stanica u sekundi u povoljnim temperaturnim uvjetima (18 °C). Brzina stanica ovisi o broju bičeva; dakle, tetraflagelatna vrsta *T. suecica* je tri puta brža od biflagelatne vrste *D. tertiolecta* kod 18 °C. Na nižoj temperaturi rasta (12 °C), pokretljivost stanica *D. tertiolecta* i *T. suecica* statistički je značajno smanjena, te su stanice vibrirale na mjestu. Na višoj temperature rasta (30 °C) *D. tertiolecta* i *T. suecica* nisu pokazale značajne promjene u brzini kretanja. Od tri istraživane vrste stanice, jedino su meke stanice *D. tertiolecta* okarakterizirane elektrokemijskom metodom polarografije i kronoamperometrije na nabijenoj kapajućoj živinoj elektrodi u svrhu analize utjecaja temperature na adhezijska svojstva

stanica. Najuže područje potencijala adhezije detektirano je kod stanica *D. tertiolecta* koje su uzgajane na 12 °C, što upućuje da su stanice čvršće i hidrofobnije, dok je najšire područje potencijala adhezije stanica zabilježeno kod stanica uzgajanih na 18 °C, što ukazuje da su stanice *D. tertiolecta* mekše i hidrofilnije. Navedeni rezultati elektrokemijske karakterizacije stanica pokazali su slaganje s nanomehaničkom karakterizacijom stanica primjenom metode AFM. Sve istraživane vrste stanica postale su statistički značajno čvršće na nižim temperaturama, što bi moglo ukazati na molekularne promjene stanične barijere. Porast temperature uzrokovao je neravnotežu stanične hidrofobnosti; zelene alge *D. tertiolecta* i *T. suecica* pokazale su izrazito hidrofilni karakter, dok je dijatomeja *C. closterium* pokazala najviši stupanj hidrofobnosti, što je od ekološke važnosti za razumijevanje mehanizma stvaranja biofilma, agregaciji i prianjanju stanica na površinama u vodenim ekosustavima (Donlan, 2002).

Nadalje, kvantitativno je određena količina izlučenih površinsko-aktivnih tvari (površinska aktivnost: mg (Triton X-100)/stanica), što predstavlja mjeru fiziološke aktivnosti stanica u kulturi. Najveća površinska aktivnost određena je elektrokemijski za *C. closterium* uzgajanoj na 12 °C, te za *D. tertiolecta* pri 30 °C, dok je najniža površinska aktivnost određena za *T. suecica* pri svim ispitivanim temperaturama. Količina izlučenih površinsko-aktivnih tvari po stanici mikroalge pokazala je slaganje s kvalitativnom strukturnom organizacijom izlučenih biopolimera, od globula do guste polimerne mreže, na nanometarskoj skali.

Utjecaj promjene saliniteta (pri stalnoj temperaturi) istražen u znanstvenom radu IV pod nazivom „Salinity induced chemical, mechanical and behavioral changes in marine microalgae". Istraživanja su provedena kod odabranih saliniteta hranjivih medija za uzgoj, koji bi odgovarali rasponu saliniteta u vodenim okolišima od euhalinog do mezohalinog. Rezultati su pokazali da su istraživane vrste alga, *D. tertiolecta* i *C. closterium* uspješno rasle pri ispitivanim salinitetima 9, 19, 27 i 38, dok je rast stanica vrste *T. suecica* bio usporen pri salinitetima 9 i 19. Adaptacijski odgovor mikroalga također je ispitan u smislu pokretljivosti, adhezije na nabijenoj elektrodi i fiziološke aktivnosti u kulturi. Stanična pokretljivost ovisi o salinitetu na kojem su stanice uzgajane. U kulturama stanica koje su rasle na salinitetu 9, prevladavala je populacija vibrirajućih stanica, koje su se kretale na mjestu, minimalnom brzinom od oko 20 $\mu m\ s^{-1}$. S porastom saliniteta na 38, povećao se i broj pokretnih stanica, a sukladno tome i brzina stanica i radijus pretraživanja. Nadalje, područje potencijala adhezije mekih stanica *D. tertiolecta* uzgajanih na salinitetu 9 bilo je uže što ukazuje da su stanice čvršće i hidrofobnije odnosu na više istraživane salinitete kada

postaju mekše i hidrofilnije. Ovi rezultati su u slaganju s nanomehaničkom karakterizacijom stanica, pri čemu sve stanice postaju statistički značajno čvršće s padom saliniteta, što je, također, u slaganju s povećanom koncentracijom sterola koje stanica sintetizira i na taj način doprinosi staničnoj hidrofobnosti. Sadržaj lipida u membrani i hidrofobnost stanice uglavnom su očuvani u širokom rasponu saliniteta, što potvrđuje eurihalinu prirodu vrste *D. tertiolecta*. Također kod vrste *D. tertiolecta* uzgajane na salinitetu 9 identificiran je debeli sloj aktina oko stanice, te najveća fiziološka aktivnost, što nepovoljno utječe na staničnu pokretljivost i ukazuje na moguće formiranje stadija palmele. Vrsta *T. suecica*, pokazala je najveću hidrofobnost od svih ispitivanih stanica na salinitetu 9. Pri salinitetu 19 stanice vrste *T. suecica* pokazale su najsporiji rast, gubitak bičeva, najmanju brzinu kretanja, najveću fiziološku aktivnost povezanu s gustom mrežom izvanstaničnih polimernih tvari i smanjenje lipida u membrani, što bi moglo ukazivati na razvoj stadija mirovanja tj. ciste, uzrokovanog nepovoljnim uvjetima rasta. Vrsta *C. closterium*, pokazala se najtolerantnijom na sniženje saliniteta. Stanice vrste *C. closterium* pokazale su se hidrofobnim na salinitetima 9 i 19, dok su pri salinitetima 27 i 38 postale hidrofilne, što može biti povezano s promjenom sastava oslobođenih biopolimerima.

Adaptacijski odgovor mikroalga rezultat je kompleksnog međudjelovanja koje uključuje kemijske promjene na molekularnom nivou, nanomehaničke promjene u površinskim svojstvima, te promjene u ponašanju stanica u smislu fiziološke aktivnosti i pokretljivosti shodno pojednostavljenom prikazu (slika 5).

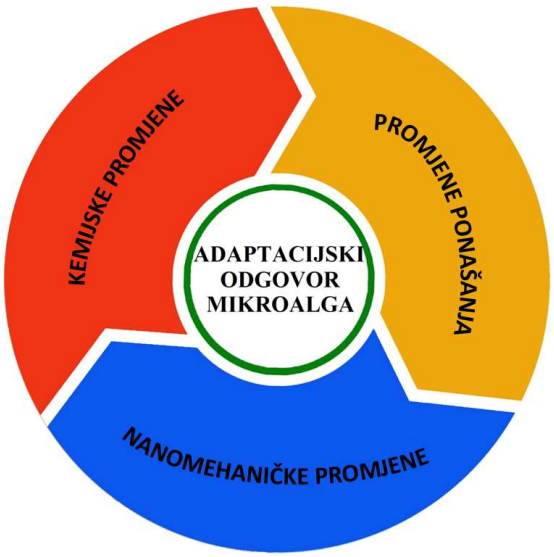

Slika 5. Adaptacijski odgovor mikroalga (prilagođeno iz Novosel i sur., 2022)

Vrsta koja se pokazala najosjetljivijom na temperaturne promjene je mikroalga bez čvrste stanične barijere *D. tertiolecta*, koja je doživjela najveće mehaničke i kemijske promjene. Vrsta s tekom u koju su uložene kalcitne bioperle, *T. suecica* pokazala se termostabilnom, ali i najosjetljivijom na promjene saliniteta. Vrsta s čvrstom organosilikatnom staničnom barijerom *C. closterium* pokazala se najmanje osjetljivom na variranje oba stresora. Adaptacijski odgovor stanica mikroalga je mjerljiv, te ovisi o (i) vrsti stanice i njenim strukturnim značajkama stanične barijere, te (ii) prirodi abiotičkog stresora.

Promjena saliniteta imala je puno veći utjecaj adaptacijski odgovor istraživanih vrsta u odnosu na promjene temperature, što je u slaganju s literaturom gdje se navodi da salinitet ima jači pojedinačni negativni učinak na svojstva mikroalga (Velasco i sur., 2019). Na temelju dobivenih rezultata prikazanih u znanstvenim radovima III i IV potvrđene su sve tri hipoteze istraživanja; ponašanje i površinska svojstva stanica mikroalga mogu se smatrati pokazateljima stresa; stanice u stresu mijenjaju površinska svojstva i fiziološku aktivnost i stanice mikroalga sa složenijom staničnom barijerom otpornije su na prisutnost stresora u vodenom okolišu.

4.4. Utjecaj pojedinačnog abiotičkog stresora na ponašanje i površinska svojstva mikroalga u djelomice prirodnim uvjetima

Ispitan je utjecaj okolišne temperature na adaptacijski odgovor *D. tertiolecta* i *C. closterium* pri salinitetima 38 i 9 u djelomice prirodnim uvjetima. Mikrokozmos eksperiment postavljen je u 10 L Nalgene bocama u duplikatima u vanjskom bazenu od 960 L, s konstantnim miješanjem 1-2 rpm (slika 6).

Slika 6. Postav mikrokozmos eksperimenta
(Institut Ruđer Bošković, Zagreb, 13. rujna 2021.)

Praćene su vrijednosti temperature zraka, vode u bazenu i u staničnim kulturama tijekom eksperimenta (tablica 1).

Tablica 1. Vrijednosti temperature zraka, vode u bazenu i u bocama sa staničnim kulturama tijekom mikrokozmos eksperimenta, mjereno svakodnevno u 10 h.

Dan rasta	t_{zrak} [° C]	$t_{voda\ u\ bazenu}$ [° C]	t_{DT} [° C]	t_{CC} [° C]	vrijeme
1.	25,0	26,2	26,0	25,9	sunčano
2.	24,0	28,7	29,4	28,9	sunčano
3.	24,6	30,6	30,9	30,8	sunčano
4.	26,5	31,7	31,4	31,7	sunčano
5.	19,0	29,4	28,8	28,7	sunčano uz naoblaku
6.	18,0	27,0	26,7	26,8	oblačno
7.	18,7	25,3	25,1	25,2	oblačno
8.	12,3	24,5	23,9	23,9	oblačno uz kišu
9.	12,5	26,0	25,7	25,9	sunčano
10.	13,2	23,8	22,9	23,0	oblačno

Rezultati ukazuju da su stanice mikroalga vrsta *D. tertiolecta* i *C. closterium* uspješno rasle u djelomice prirodnim uvjetima kod povišene okolišne temperature i stalnog saliniteta 38 (slike 7,8).

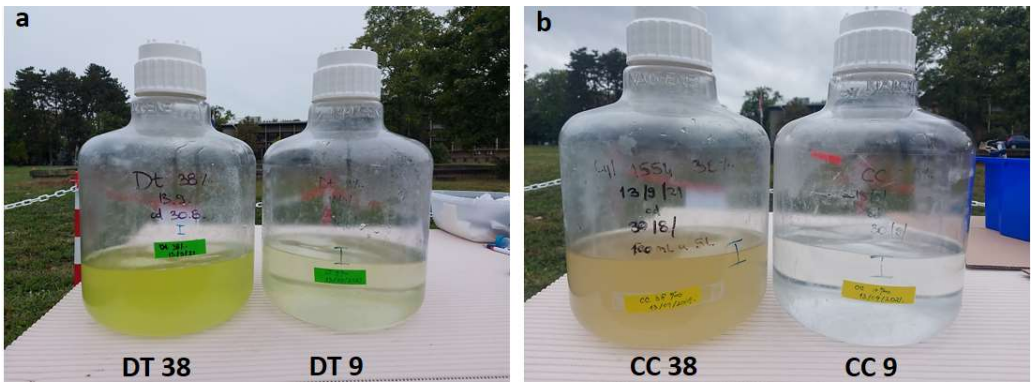

Slika 7. Kulture stanica uzgajane u djelomice prirodnim uvjetima, 10. dan rasta (lijevo: *D. tertiolecta* kod saliniteta 9 i 38, desno: *C. closterium* kod saliniteta 9 i 38).

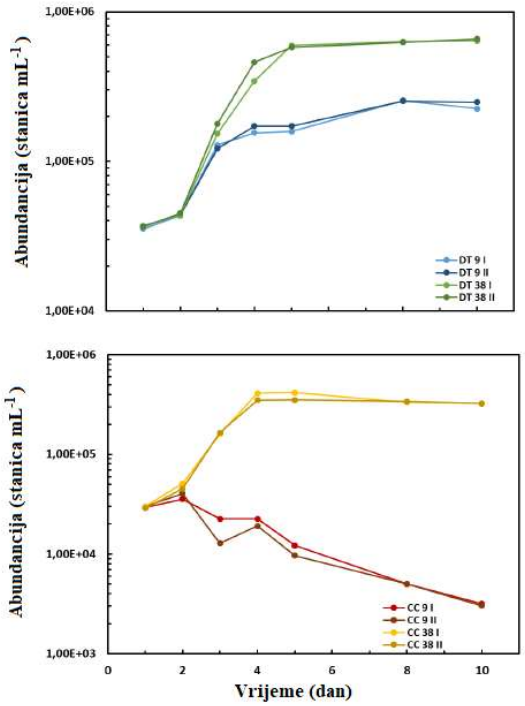

Slika 8. Krivulje rasta stanica *D. tertiolecta* kod saliniteta 38 i 9 (**a, b**) i *C. closterium* kod saliniteta 38 i 9 (**c, d**) u djelomice prirodnim uvjetima.

Konfokalne mikrografije prikazuju stanice *D. tertiolecta* i *C. closterium* nakon 10. dana rasta u djelomice prirodnim uvjetima (slika 9).

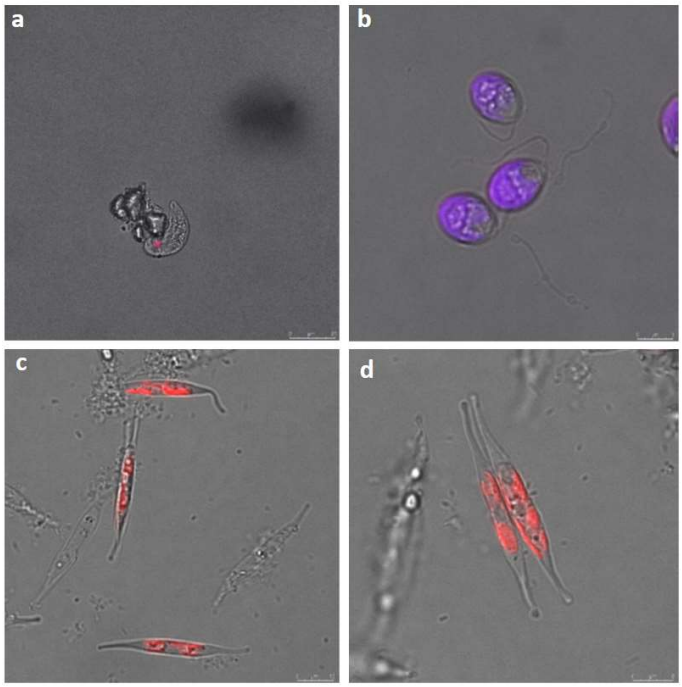

Slika 9. Konfokalne slike kultura stanica *D. tertiolecta* uzgajanih na salinitetima 9 i 38 (**a** i **b)**, te *C. closterium* uzgajanih na salinitetu 9 i 38 (**a** i **b**) u djelomice prirodnim uvjetima.

Usporedba rasta, ponašanja i površinskih svojstva *D. tertiolecta* i *C. closterium* kod saliniteta 38 kod djelomice prirodnih uvjeta i laboratorijskih uvjeta prikazana je u tablici 3. Rast stanica u djelomice prirodnim uvjetima kod povišene okolišne temperature bio je brži, nego u kontroliranim laboratorijskim uvjetima kod 30 ºC. Stanice su ušle u stacionarnu fazu rasta za 5 dana. Rast obje vrste stanica je bio nepovoljan kod saliniteta 9, (slike 7, 8). Usporedbom adaptacijskih odgovora stanica u djelomice prirodnim uvjetima s laboratorijskim uvjetima proizlazi da je brzina kretanja *D. tertiolecta* stanica, usporediva, dok je radijus pretraživanja manji što ukazuje da se veći dio stanica kretao na mjestu, što može biti posljedica veće fiziološke aktivnosti. Stanice *C. closterium* kod djelomice prirodnih uvjeta imale su veću fiziološku aktivnost u odnosu na laboratorijske uvjete. Elektrokemijskom karakterizacijom adhezije stanica *D. tertiolecta* u djelomice prirodnim uvjetima, dobiveno je da je područje potencijala adhezije nešto uže, što ukazuje da su stanice čvršće u odnosu na laboratorijske uvjete. Dobiveni rezultati

uspoređeni su s nanomehaničkim svojstvima stanica, čvrstoćom i hidrofobnošću. Stanice *D. tertiolecta* bile su hidrofilne, a stanice *C. closterium* hidrofobne u djelomice prirodnim uvjetima, što je u slaganju s laboratorijskim uvjetima. Na temelju navedenih rezultata koji su predmet pripreme znanstvenog rada, proizlazi da laboratorijska istraživanja staničnog stresa pod utjecajem temperature daju važan set podataka koji pokazuju slaganje s adaptacijskim odgovorima eksperimenata provedenih u djelomice prirodnim uvjetima, što predstavlja osnovu za bolje razumijevanje utjecaja abiotičkog čimbenika na mikroalge u kompleksnim vodenim ekosustavima.

Tablica 3. Adaptacijski odgovor stanica *D. tertiolecta* (DT) i *C. closterium* (CC) uzgajanih na salinitetu 38 u djelomice prirodnim uvjetima, i laboratorijskim uvjetima kod 30 °C.

Parametar	**Djelomice prirodni uvjeti**		**Laboratorijski uvjeti**	
	DT	**CC**	**DT**	**CC**
brzina rasta [d^{-1}]	2,61	2,41	0,25	0,35
vrijeme diobe [d]	0,27	0,29	2,76	1,99
stanična brzina [μm s^{-1}]	58	n.d.	62	n.d.
put [μm]	41	n.d.	80	n.d.
E_c^+, E_C^- adhezije [mV]	-130, -970	n.d.	-184, -1170	n.d.
PAT po stanici [pg T-X-100 L^{-1}]	42	82	35	2
Čvrstoća [kPa]	7.5	56 nN/μm*	1.5	152
Hidrofobnost	hidrofilne	hidrofobne	hidrofilne	hidrofobne

* konstanta opruge [nN/μm]

5. ZAKLJUČAK

Antropogeno uvjetovane globalne klimatske promjene utječu na brojne čimbenike okoliša, te posljedično mijenjaju svojstva, raznolikost i sastav zajednica mikroalga. Adaptacijski odgovori mikroalga na uvjete stresa se sve češće koriste u procjeni ekološkog stanja vodenih ekosustava, zbog čega su mikroalge u međunarodnim smjernicama preporučene kao modelni organizmi.

U ovom doktorskom radu povezan je stanični odgovor mikroalga u vidu ponašanja i površinskih svojstava u odnosu na antropogene i abiotičke stresore (teški metal, temperatura, salinitet) kako bi se bolje razumjele njihove strategije preživljavanja i prilagodbe u vodenim ekosustavima u uvjetima klimatskih promjena. Razvijena je metoda za analizu stanične pokretljivosti mikroalga. Također, razvijen je i protokol za amperometrijsku karakterizaciju stanica mikroalga različite kompleksnosti stanične barijere, što je pridonijelo boljem razumijevanju uloge strukturnih značajki stanične barijere na adheziju mikroalga na nabijenoj međupovršini.

Odgovor stanica mikroalga, u smislu površinskih svojstava i ponašanja, ovisi o istraživanoj vrsti i njenim strukturnim značajkama stanične barijere i flagelarnog aparata, te o prirodi i vrsti stresora. Stanice vrsta *T. suecica* i *R. maculata* koje posjeduju čvrste stanične barijere i morfološki odvedenije flagelarne aparate pokazale su brži i gotovo potpuni oporavak stanične pokretljivosti pod utjecajem toksične koncentracije teškog metala kadmija, u odnosu na vrstu *D. tertiolecta* čije su stanice „gole“ a flagelarni aparat jednostavne građe. Nadalje, vrsta *D. tertiolecta,* mikroalga bez čvrste stanične barijere, također se pokazala najosjetljivijom na promjene temperature uzgoja, uz najviše izraženi adaptacijski odgovor u vidu mehaničkih i kemijskih promjena. Vrsta s tekom u koju su uložene kalcitne bioperle, *T. suecica* pokazala se termostabilnom, ali i najosjetljivijom na promjene saliniteta. Vrsta s čvrstom organosilikatnom staničnom barijerom *C. closterium* pokazala se najmanje osjetljivom na variranje oba stresora. S obzirom na to da je fundamentalno istraživanje adaptacijskoga odgovora stanica mikroalga dalo mjerljivu razliku u odnosu na kontrolne uvjete, može biti od koristi za predviđanje ponašanja stanica u uvjetima stresa te razumijevanje njihove prilagodbe i sudbine u uvjetima klimatskih promjena u vodenim ekosustavima. Nadalje, primjenom elektrokemijske metode i analize stanične pokretljivosti korištenjem programa otvorenog koda, ICY, omogućena je direktna, brza i ekonomična karakterizaciju mikroalga u stresu, što može doprinijeti njihovoj budućoj implementaciji u ocjenjivanju stanja ekosustava, kao i u biotehnološkoj implementaciji u svrhu iskorištavanja vrijednog biopotencijala mikroalga.

6. POPIS LITERATURE

Abdel-Raouf, N., Al-Homaidan, A.A., Ibraheem, I.B.M., 2012. Microalgae and wastewater treatment. Saudi J. Biol. Sci. 19, 257–275.

Adenan, N.S., Yusoff, F.M., Shariff, M. 2013. Effect of Salinity and Temperature on the Growth of Diatoms and Green Algae. J. Fish. Aquat. Sci. 8,397–404.

Arrigo, K., 2005. Marine microorganisms and global nutrient cycles. Nature 437, 349–355.

Barati, B., Gan, S-Y., Lim, P-E., Beardall, J., Phang, S-M., 2019. Green algal molecular responses to temperature stress. Acta Physiol. Plant 41, 26–45.

Bariana, M., Aw, M.S., Losic, D., 2013. Tailoring morphological and interfacial properties of diatom silica microparticles for drug delivery applications. Adv. Powder Technol. 24, 757–763.

Belghith, T., Athmouni, K., Bellassoued, K., El Feki, A., Ayadi, H., 2016. Physiological and biochemical response of *Dunaliella salina* to cadmium pollution. J. Appl.Phycol. 28:991–999.

Ben-Amotz, A., 1996. Effect of low temperature on the stereoisomer composition of *β*- carotene in the halo-tolerant alga *Dunaliella bardawil* (Chlorophyta). J. Phycol. 32, 272–275.

Borowitzka, M., Siva, C.J., 2007. The taxonomy of the genus *Dunaliella* (Chlorophyta, Dunaliellales) with emphasis on the marine and halophilic species. J. Appl. Phycol. 19, 567–590.

Borowitzka, M., 2018. The 'stress' concept in microalgal biology—homeostasis, acclimation and adaptation. J. Appl. Phycol. 30, 2815–2825.

Boyce, D.G., Lewis, M.R., Worm, B., 2010. Global Phytoplankton Decline over the Past Century. Nature 466, 591–596.

Brennan, L., Owende, P., 2010. Biofuels from microalgae - A review of technologies for production, processing, and extractions of biofuels and co-products. J. Biosci. Bioeng. 14, 217–232.

Cavicchioli, R. Ripple, W.J., Timmis, K.N., Azam, F., Bakken, L.R., Baylis, M., Behrenfeld, M.J., Boetius, A., Boyd, P.W., Classen, A.T., Crowther, T.W., Danovaro, R., Foreman, C.M., Huisman, J., Hutchins, D.A., Jansson, J.K., Karl, D.M., Koskella, B., Moran, M.A., Orphan, V.J., Reay, D.S., Remais, J.V., Rich, V.I., Singh, B.K., Stein, L.Y., Stewart, F.J., Weaver, S.C., Webb, E.A., Webster N.S., 2019. Scientists' warning to humanity: microorganisms and climate change. Nat. Rev. Microbiol. 17, 569–586.

Converti, A., Casazza, A.A., Ortiz, E.Y., Perego, P., Del Borghi, M., 2009. Effect of Temperature and Nitrogen Concentration on the Growth and Lipid Content of *Nannochloropsis oculata* and *Chlorella vulgaris* for Biodiesel Production. Chem. Eng. Process.: Process Intensif. 48, 1146–1151.

Coquillé, N., Jan, G., Moreira, A., Morin, S., 2015. Use of diatom motility features as endpoints of metolachlor toxicity. Aquat. Toxicol. 158, 202–210.

Das, P., Samantaray, S., Rout, G.R., 1998. Studies on Cadmium toxicity in plants: A review. Environ. Pollut. 98, 29–36.

Decho, A.W., Gutierrez, T., 2017. Microbial extracellular polymeric substances (EPSs) in ocean systems. Front. Microbiol. 8, 922–950.

Demir, I., Blockx, J., Dague, E., Guiraud, P., Thielemans, W., Muylaert, K., Formosa-Dague, C., 2020. Nanoscale Evidence Unravels Microalgae Flocculation Mechanism Induced by Chitosan, Appl. Bio Mater. 3, 8446–8459.

Domozych, D.S., Ciancia, M., Fangel, J.U., Mikkelsen, M.D., Ulvskov, P., Willats, W.G.T., 2012. The cell walls of green algae: a journey through evolution and diversity. Front. Plant. Sci. 3, 1–7.

Donlan, R.M., 2002. Biofilms: microbial life on surfaces. Emerg. Infect. Dis. 8, 881–890.

Durack, P., Wijffels, S., 2010. Fifty-year trends in global ocean salinities and their relationship to broadscale warming. J climate. 23, 4342–4362.

Einali, A., Mazang-Ghasemi, S., Valizadeh, J., Noorozi, M., 2017. Metabolic responses and β-carotene production by the unicellular green alga *Dunaliella salina* exposed to leaf extracts. Acta Bot. Brasilica 31,180–190.

Falkowski, P.G., 1980. Light shade adaptation in microalgae, u: Falkowski, P.G., (ur), Primary Productivity in the Sea. Plenum Press, New York, str. 99–119.

Falkowski, P.G., Barber, R.T., Smetacek, V., 1998. Biogeochemical controls and feedbacks on ocean primary production. Science 281, 200–206.

Falkowski, P.G., Raven, J.A., 2007. Aquatic photosynthesis. Princeton University Press, New Jersey.

Feng, Y., Warner, M.E., Zhang, Y., Sun, J., Fu, F.-X., Rose, J.M., Hutchins, D.A., 2008. Interactive effects of increased pCO2, temperature and irradiance on the marine coccolithophore *Emiliania huxleyi* (Prymnesiophyceae). Eur. J. Phycol. 43, 87–98.

Fisher, N.S., Boh, M., Teyssi, J-L., 1984. Accumulation and toxicity of Cd, Zn, Ag, and Hg in four marine phytoplankters. Mar. Ecol. Prog. Ser. 18, 201–213.

Flöder, S., Jaschinski, S., Wells, G., Burns, C.W., 2010. Dominance and Compensatory Growth in Phytoplankton Communities under Salinity Stress. J. Exp. Mar. Biol. Ecol. 395, 223–231.

Friberg, L., Nordberg, G., Vouk, V., 1986. Handbook of the toxicology of metals, vol II. Amsterdam, Elsevier, str 130–184.

Formosa-Dague, C., Gernigon, V., Castelain, M., Daboussi, F., Guiraud, P., 2018. Towards a better understanding of the flocculation/flotation mechanism of the marine microalgae *Phaeodactylum tricornutum* under increased pH using atomic force microscopy. Algal Res. 33, 369– 378.

Gamal, A.E., 2010. Biological importance of marine algae. Saudi. Pharm. J. 18, 1–25.

Gebeshuber, I.C., Thompson, J.B., Amo, Y.D., Stachelberger, H., Kindt, J.H., 2002. In vivo nanoscale atomic force microscopy investigation of diatom adhesion properties. Mater. Sci. Technol. 18, 763–766.

Gonçalves, A., Ferreira, C., Loureiro, J., Pires, J., Simões, M. 2015. Surface physicochemical properties of selected single and mixed cultures of microalgae and cyanobacteria and their relationship with sedimentation kinetics. Bioresour Bioprocess. 2**,** 43–51.

Gonçalves, C., Figueredo, C., 2020. What we really know about the composition and function of microalgae cell coverings? - an overview. Acta Bot. Brasilica 34, 599–614.

Goñi, F.M., 2013. The basic structure and dynamics of cell membranes: An update of the Singer Nicolson model. Biochim. Biophys. Acta. 1838,1467–1476.

Guinder, V.A., Popovich, C.A., Molinero, J.C., Perillo, G.M.E., 2010. Long-Term Changes in Phytoplankton Phenology and Community Structure in the Bahía Blanca Estuary, Argentina. Mar. Biol. 157, 2703–2716.

Guinder, V.A., Molinero, J.C., 2013. Climate change effects on marine phytoplankton, u: Arias AH, Menéndez MC (eds) Marine ecology in a changing world. CRC Press-Taylor & Francis, Boca Raton, str. 68–90.

Gustavs, L., Eggert, A., Michalik, D., Karsten, U., 2010. Physiological and biochemical responses of green microalgae from different habitats to osmotic and matric stress. Protoplasma 243, 3–14.

Häder, D.-P., Gao, K., 2015. Interactions of anthropogenic stress factors on marine phytoplankton. Front. Environ. Sci. 3, 1–14.

Hadjoudja, S., Deluchat, V., Baudu, M., 2010. Cell surface characterisation of *Microcystis aeruginosa* and *Chlorella vulgaris*. J. Colloid. Interface. Sci. 342, 293–299.

Hansen, J., Sato, M., Ruedy, R., Lo, K., Lea, D.W., Medina-Elizade, M., 2006. Global temperature change. Proc. Natl. Acad. Sci. 103, 14288–14293.

Harun, R., Singh, M., Forde, G.M., Danquah, M.K., 2010. Bioprocess engineering of microalgae to produce a variety of consumer products. Renew. Sust. Energ. Rev. 14, 1037-1047.

Hasan, S.A., Fariduddin, Q., Ali, B., Hayat, S., Ahmad, A., 2009. Cadmium: Toxicity and Tolerance in plants. J. Environ. Biol. 30, 165–174.

Hassler, C.S., Sinoir, M., Clementson, L.A., Butler, E.C.V., 2012. Exploring the link between micronutrients and phytoplankton in the Southern Ocean during the 2007 austral summer. Front. Microbiol. 3, 202–228.

Higgins, M.J., Crawford, S.A., Mulvaney, P., Wetherbee, R., 2002. Characterization of the Adhesive Mucilages Secreted by Live Diatom Cells using Atomic Force Microscopy. Protist. 153, 25– 38.

Huertas, I.E., Rouco, M., López-Rodas, V., Costas, E., 2011. Warming Will Affect Phytoplankton Differently: Evidence through a Mechanistic Approach. Proc. R. Soc. B 278, 3534–3543.

Israelachvili, J.N., 2011. Intermolecular and Surface Forces (Third Edition). 3rd ed., Academic Press, New York.

Ivošević, N., Žutić, V., 1998. Spreading and detachment of organic droplets at an electrified interface. Langmuir 14, 231–234.

Ivošević DeNardis, N., Žutić, V., Svetličić, V., Urbani, R., 2007. In situ amperometric detection of vesicles and microgel phases in an aggregating system: Calcium alginate. Electroanalysis 4, 473–478.

Ivošević DeNardis, N., Pečar Ilić, J., Ružić, I., Pletikapić, G., 2015. Cell adhesion and spreading at a charged interface: Insight into the mechanism using surface techniques and mathematical modelling. Electrochim. Acta 176, 743–754.

Ivošević DeNardis, N., Pečar Ilić, J., Ružić, I., Novosel, N., Mišić Radić, T., Weber, A., Kasum, D., Pavlinska, Z., Katalin Balogh, R., Hajdu, B., Marček Chorvátová, A., Gyurcsik, B., 2019. Algal cell response to laboratory-induced cadmium stress: a multimethod approach. Eur. Biophys. J. 48, 231–248.

Ivošević DeNardis, N., Pletikapić, G., Frkanec, R., Horvat, L., Vernier, P.T., 2020. From algal cells to autofluorescent ghost plasma membrane vesicles. Bioelectrochemistry 134, 1–8.

Kotnik, T., Frey, W., Sack, M., Haberl Meglič, S., Peterka, M., Miklavcic, D., 2015. Electroporation-based applications in biotechnology. Trends Biotechnol. 33, 480–488.

Larson, C.A., Belovsky, G.E., 2013. Salinity and Nutrients Influence Species Richness and Evenness of Phytoplankton Communities in Microcosm Experiments from Great Salt Lake, Utah, USA. J. Plankton Res. 35, 1154–1166.

Lavoie, I., Lavoie, M., Fortin, C., 2012. A mine of information: Benthic algal communities as biomonitors of metal contamination from abandoned tailings. Sci. Total. Environ. 25, 231–241.

Lewandowska, A., Sommer, U., 2010. Climate change and the spring bloom: a mesocosm study on the influence of light and temperature on phytoplankton and mesozooplankton. Mar. Ecol. Prog. Ser. 405, 101–111.

Liu, G., Chai, X., Shao, Y., Hu, L., Xie, Q., Wu, H., 2011. Toxicity of copper, lead, and cadmium on the motility of two marine microalgae *Isochrysis galbana* and *Tetraselmis chui*. J. Environ. Sci. 2, 330–335.

Malerba, M.E., Palacios, M.M., Palacios Delgado, Y.M., Beardall, J. and Marshall, D.J., 2018. Cell size, photosynthesis and the package effect: an artificial selection approach. New Phytol. 219, 449–461.

Martignier, A., Filella, M., Pollok, K., Melkonian, M., Bensimon, M., Barja, F., Langenhorst, F., Jaquet, J.-M., Ariztegui, D., 2018. Marine and freshwater micropearls: Biomineralization producing strontium-rich amorphous calcium carbonate inclusions is widespread in the genus *Tetraselmis* (Chlorophyta). Biogeosci. Discuss. 15, 6591–6605.

McNeil, B.I., Matear, R.J., 2006. Projected Climate Change Impact on Oceanic Acidification. Carbon Balance Manag. 1, 2-11.

Melis, A., Happe, T., 2001. Hydrogen production. Green algae as a source of energy. Plant Physiol. 127, 740–748.

Melkonian, M., 1992. Algal cell motility. Springer, Berlin.

Miao, X., Wu, Q., Yang, C., 2004. Fast pyrolysis of microalgae to produce renewable fuels. J. Anal. Appl. Pyrolysis 71, 855–863.

Michel, G., Tonon, T., Scornet, D., Cock, J.M., Kloareg, B., 2010. The cell wall polysaccharide metabolism of the brown alga *Ectocarpus siliculosus*. Insights into the evolution of extracellular matrix polysaccharides in Eukaryotes. New. Phytol. 188, 82–97.

Mihanović, H., Vilibić, I., Šepić, J., Matić, F., Ljubešić, Z., Mauri, E., Gerin, R., Notarstefano, G., Poulain, P-M., 2021. Observation, preconditioning and recurrence of exceptionally high salinities in the Adriatic sea. Front. Mar. Sci. 8, 672210.

Minhas, A.K., Hodgson, P., Barrow, C.J. and Adholeya, A., 2016. A Review on the Assessment of Stress Conditions for Simultaneous Production of Microalgal Lipids and Carotenoids. Front Microbiol. 7, 546–557.

Mišić Radić, T., Čačković, A., Penezić, A., Dautović, J., Lončar, J., Omanović, D., Juraić, K., Ljubešić, Z., 2021. Physiological and morphological response of marine diatom *Cylindrotheca closterium* (Bacillariophyceae) exposed to Cadmium. Eur. J. Phycol. 56, 24–36.

Moreno García, L., Adjallé, K., Barnabé, S., Raghavan, V., 2017. Microalgae biomass production for a biorefinery system: Recent advances and the way towards sustainability. Renew. Sust. Energ. Rev. 76, 493–506.

Moullec, F., Asselot, R., Auch, D., 2021. Identifying and addressing the anthropogenic drivers of global change in the North Sea: a systematic map protocol. Environ. Evid. 10, 19-28.

Morlon, H., Fortin, C., Adam, C., Garnier-Laplace, J., 2005. Cellular quotas and induced toxicity of selenite in the unicellular green alga *Chlamydomonas reinhardtii*. Radioprotection 40, 101–106.

Mravec, J.J., Kračun, S.K., Rydahl, M.G., Westereng, B., Miart, F., Clausen, M.H., Fangel, J.U., Daugaard, M., Van Cutsem, P., De Fine Licht, H.H., Höfte, H., Malinovsky, F.G., Domozych, D.S., Willats, W.G.T., 2014. Tracking developmentally regulated post-synthetic processing of homogalacturonan and chitin using reciprocal oligosaccharide probes. Development 141, 4841–4850.

Niederwieser, T., Kociolek, P., Hoehn, A., Klaus, D., 2019. Effect of altered nitrogen partial pressure on Chlorellaceae for spaceflight applications. Algal Res.-Biomass Biofuels Bioprod. 41, 101543–101554.

Norici, A., Bazzoni, A.M., Pugnetti, A., Raven, J.A., Giordano, M., 2011. Impact of irradiance on the C allocation in the coastal marine diatom *Skeletonema marinoi* Sarno and Zingone. Plant Cell Environ. 34, 1666–1677.

Norton, T.A., Melkonian, M., Andersen, R.A., 1996. Algal biodiversity. Phycologia 35, 308–326.

Novoveská, L., Ross, M.E., Stanley, M.S., Pradelles, R., Wasiolek, V., Sassi, J.F., 2019. Microalgal Carotenoids: A Review of Production, Current Markets, Regulations, and Future Direction. Mar Drugs. 11, 640–658.

Olguín, E.J., 2012. Dual purpose microalgae-bacteria-based systems that treat wastewater and produce biodiesel and chemical products within a biorefinery. Biotechnol. Adv. 30, 1031–1046.
Oren A., 2005. A hundred years of *Dunaliella* research: 1905-2005. Saline Syst. 2, 14-28.

Ozkan, A., Berberoglu, H., 2013. Adhesion of algal cells to surfaces. Biofouling 29, 469–82.

Pandey, L.K., Kumar, D., Yadav, A, Rai, J, Gaur, J.P., 2014. Morphological abnormalities in periphytic diatoms as a tool for biomonitoring of heavy metal pollution in a river. Ecol. Indic. 36, 272–279.

Pandey, L.K., Bergey, E.A., 2016. Exploring the status of motility, lipid bodies, deformities and size reduction in periphytic diatom community from chronically metal (Cu, Zn) polluted waterbodies as a biomonitoring tool. Sci. Total. Environ. 550, 372–381.

Pavlinska, Z., Chorvat, D., Mateasik, A., Jerigova, M., Velic, D., Ivošević DeNardis, N., Marcek Chorvatova, A., 2020. Fluorescence responsiveness of unicellular marine algae *Dunaliella* to stressors under laboratory conditions. J. Biotechnol. 6,100018.

Pillet, F., Dague, E., Pečar Ilić, J., Ružić, I., Rols, M-P., Ivošević DeNardis, N., 2019. Changes in nanomechanical properties and adhesion dynamics of algal cells during their growth. Bioelectrochemistry 127, 154–162.

Pletikapić, G., Žutić, V., Vinković Vrček, I., Svetličić, V., 2012. Atomic force microscopy characterization of silver nanoparticles interactions with marine diatom cells and extracellular polymeric substance. J. Mol. Recognit. 25, 309–317.

Polle, J. E. W., Tran, D., Ben-Amotz, A., 2010. History, Distribution, and Habitats of Algae of the Genus *Dunaliella* Teodoresco, u: Oren, A. The Alga *Dunaliella*. Biodiversity, Physiology, Genomics and Biotechnology, str.1–5.

Raja, A., Vipin, C., Aiyappan, A., 2013. Biological importance of marine algaedan overview. Int. J. Curr. Microbiol. App. Sci. 2, 222–227.

Rotter, A., Barbier, M., Bertoni, F. i sur. (2021). The essentials of marine biotechnology. Front. Mar. Sci. 8, 2296–7745.

Rubio, F.C., Camacho, F.G., Sevilla, J.M.F., Chisti, Y., Grima, E.M. (2003). A mechanistic model of photosynthesis in microalgae. Biotechnol. Bioeng. 81, 459–473.

Saha, S.K., Kazipet, N., Murray, P., 2018. The carotenogenic *Dunaliella salina* CCAP 19/20 produces enhanced levels of carotenoid under specific nutrients limitation. BioMed. Res. Int. 18, 1–11.

Sarmiento, J.L., Slater, R., Barber, R., Bopp, L., Doney, S.C., Hirst, A.C., Kleypas, J., Matear, R., Mikolajewicz, U., Monfray, P., Soldatov, V., Spall, S.A. and Stouffer, R., 2004. Response of Ocean Ecosystems to Climate Warming. Global Biogeochem. Cy., 18, GB3003.

Scheidegger, C., Behra, R., Sigg, L., 2011. Phytochelatin formation kinetics and toxic effects in the freshwater alga *Chlamydomonas reinhardtii* upon short- and long-term exposure to lead (II). Aquat. Toxicol. 101, 423–429.

Shetty, P., Gitau, M.M., Maróti, G., 2019. Salinity stress responses and adaptation mechanisms in eukaryotic green microalgae. Cells 8, 1657–1673.

Simoons, F.J., 1990. Food in China: A Cultural and Historical Inquiry. CRC Press.

Sørensen, I., Pettolino, F.A., Bacic, A., Ralph, J., Lu, F., O'Neill, M.A., Fei, Z., Rose, J.K.C., Domozych, D.S., Willats, W.G.T., 2011. The charophycean green algae provide insights into the early origins of plant cell walls. Plant. J. 68, 201–211.

Spolaore, P., Joannis-Cassan, C., Duran, E., Isambert, A., 2006. Commercial applications of microalgae. J. Biosci. Bioeng. 101, 87–96.

Stallwitz, E., Häder, D.-P., 1994. Effects of heavy metals on motility and gravitactic orientation of the flagellate, *Euglena gracilis*. Eur. J. Protistol. 30, 18–24.

Svetličić, V., Ivošević, N., Kovač, S., Žutić, V., 2001. Charge displacement by adhesion and spreading of a cell. Bioelectrochemistry 53, 79–86.

Takagi, M., Karseno, B., Yoshida, T., 2006. Effect of Salt Concentration on Intracellular Accumulation of Lipids and Triacylglyceride in Marine Microalgae Dunaliella Cells. J. Biosci. Bioeng. 101, 223–226.

Tanaka, H., Nishimura, O., Nakamura, S., Sudo, R., 2005. Effect of alkylphenols on motility of *Chlamydomonas reinhardtii* and crustacea *Daphnia magna*. J. Jpn. Soc. Water. Environ. 28, 333–338.

Tesson, B., Hildebrand, M., 2013. Characterization and Localization of Insoluble Organic Matrices Associated with Diatom Cell Walls: Insight into Their Roles during Cell Wall Formation. PLOS ONE, 8, e61675.

Tsuji, N., Hirayanagi, N., Okada, M., Miyasaka, H., Hirata, K., Zenk, M.H., Miyamotoa, K., 2002. Enhancement of tolerance to heavy metals and oxidative stress in *Dunaliella tertiolecta* by Zn-induced phytochelatin synthesis. Biochem. Biophys. Res. Commun. 293, 653–659.

Van Vooren, G., Le Grand, F., Legrand, J., Cuiné, S., Peltier, G., Pruvost, J., 2012. Investigation of fatty acids accumulation in *Nannochloropsis oculata* for biodiesel application. Bioresour. Technol. 124, 421–432.

Velasco, J., Gutiérrez-Cánovas, T., Botella-Cruz, M., Sánchez-Fernández, D., Arribas, P., Carbonell, J., Millán, A., Pallarés, S., 2019. Effects of salinity changes on aquatic organisms in a multiple stressor context. Philos. Trans. R. Soc. Lond., B, Biol. Sci. 374.

Vignesh, G., Barik, D., 2019. Chapter 6 - Toxic Waste From Biodiesel Production Industries and Its Utilization, u: Editor(s): Debabrata Barik, Woodhead Publishing Series in Energy, Energy from Toxic Organic Waste for Heat and Power Generation, Woodhead Publishing, str. 69–82.

West, M., Zubeck, M., 2012. Evaluation of microalgae for use as nutraceuticals and nutritional supplements. J. Nutr. Food Sci. 2, 147–158.

Wetz, M.S., Hutchinson, E.A., Lunetta, R.S., Paerl, H.W., Christopher Taylor, J., 2011. Severe Droughts Reduce Estuarine Primary Productivity with Cascading Effects on Higher Trophic Levels. Limnol. Oceanogr. 56, 627–638.

Wiessner, W., Schnepf, E., Starr, R.C., 1995. Algae, Environment and Human Affairs. Biopress Ltd., Bristol.

Xu, X.-Q., Beardall, J., 1997. Effect of Salinity on Fatty Acid Composition of a Green Microalga from an Antarctic Hypersaline Lake. Phytochemistry 45, 655–658.

Yodsuwan, N., Sawayama, S., Sirisansaneeyakul, S., 2017. Effect of nitrogen concentration on growth, lipid production and fatty acid profiles of the marine diatom *Phaeodactylum tricornutum*. Agric. Nat. Resour 51, 190–197.

Yong YYR, Lee YK (1991) Do carotenoids play a photoprotective role in the cytoplasm of Haematococcus lacustris (Chlorophyta). Phycologia 30:257–261

Zeno, W. F., Day, K. J., Gordon, V. D., Stachowiak, J. C., 2020. Principles and Applications of Biological Membrane Organization. Annu. Rev. Biophys. 49, 19–39.

Žutić, V., Kovač, S., Tomaić, J., Svetličić, V., 1993. Heterocoalescence between dispersed organic microdroplets and a charged conductive interface. J. Electroanal. Chem. 349, 173–186.

Žutić, V., Svetličić, V., Ivošević, N., Hozić, A., Pečar, O., 2004. Northern Adriatic mesocosm experiment Rovinj 2003: dynamics of organic microparticles studied by the electrochemical technique. Period. Biolog. 106, 67–74.

7. ŽIVOTOPIS

Ime i prezime	***Nives Novosel***
Datum i mjesto rođenja	14. srpnja 1994., Zagreb, Hrvatska
Obrazovanje	2019.– **Prirodoslovno-matematički fakultet, Sveučilište u Zagrebu** **Interdisciplinarni doktorski studij oceanologije** 2016.–2018. **Prirodoslovno-matematički fakultet, Sveučilište u Zagrebu** **Magistra struke znanosti o okolišu, mag. oecol.** 2013.–2016. **Prirodoslovno-matematički fakultet, Sveučilište u Zagrebu** **Sveučilišna prvostupnica struke znanosti o okolišu, univ. bacc. oecol.** 2009.–2013. **XV. gimnazija, Zagreb**
Radno iskustvo	2019.– **Institut Ruđer Bošković, Zagreb, *asistent*** Zavod za istraživanje mora i okoliša Laboratorij za biogeokemiju mora i atmosfere
Suradnik na projektima	2021.–2022. **hrvatsko-francuski Program Cogito** Evaluation of the biophysical and physiological effects of salinity stress on algal cells and its consequences for cell aggregation (N.Ivošević DeNardis, C.Formosa-Dague) 2018.–2022. **Hrvatska zaklada za znanost** Od površinskih svojstava stanica alga do pokazatelja stresa u vodenim ekosustavima (N.Ivošević DeNardis) 2017.–2018. **International Visegrad Fund, Bratislava, Slovačka** Algal cell biophysical properties as markers for environmental stress in aquatic systems (N.Ivošević DeNardis) 2017. Istraživačko-edukacijski projekt Dugi otok, Udruga studenata biologije

Rad u međunarodnim društvima	2019.–2023. **COST ACTION CA18238, European transdisciplinary networking platform for marine biotechnology**, zamjenski član upravnog odbora
Članstva	2019.– International Society of Electrochemistry
Organizacijske vještine	2022. 11th ISE Satellite Student Regional Symposium on Electrochemistry 2019. 11th Symposium for European Freshwater Science, Zagreb 2019. 7th European Phycology Congres, Zagreb *2019. STEM radionica, Morski mikrosvijet, Dani otvorenih vrata IRB*
Nagrade	2021. Godišnja nagrada Instituta Ruđer Bošković za znanstveni rad 2021. 10th ISE Satellite Student Regional Symposium, *najbolje usmeno priopćenje* 2020. Simpozij studenata doktorskih studija PMF-a, *najbolje postersko priopćenje*
Znanstvene aktivnosti	6 znanstvenih radova, 24 kongresna priopćenja

Popis znanstvenih aktivnosti

Radovi u časopisima

1. Vrana, I., Bakija Alempijević, S., Novosel, N., Ivošević DeNardis, N., Zigon, D., Ogrinc, N., Gašparović, B., 2022. Hyposalinity induces significant polar lipid remodeling in the marine microalga *Dunaliella tertiolecta* (Chlorophyceae). Journal of applied phycology 34, 1457–1470. https://doi.org/10.1007/s10811-022-02745-8

2. Novosel, N., Mišić Radić, T., Levak Zorinc, M., Zemla, J., Lekka, M., Vrana, I., Gašparović, B., Horvat, L., Kasum, D., Legović, T., Žutinić, P., Gligora Udovič, M., Ivošević DeNardis, N., 2022. Salinity induced chemical, mechanical and behavioral changes in marine microalgae. Journal of applied phycology 34, 1293–1309. https://doi.org/10.1007/s10811-022-02734-x

3. Novosel, N., Mišić Radić, T., Zemla, J., Lekka, M., Čačković, A., Kasum, D., Legović, T., Žutinić, P., Gligora Udovič, M., Ivošević DeNardis, N., 2022. Temperature-induced response in algal cell surface properties and behavior. Journal of applied phycology 34, 243–259. https://doi.org/10.1007/s10811-021-02591-0

4. Novosel, N., Ivošević DeNardis, N., 2021. Structural Features of the Algal Cell Determine Adhesion Behavior at a Charged Interface. Electroanalysis 33, 1436–1443. https://doi.org/10.1002/elan.202060580

5. Novosel, N., Kasum, D., Žutinić, P., Legović, T., Ivošević DeNardis, N., 2020. Short-term effect of cadmium on the motility of three flagellated algal species. Journal of applied phycology 32, 4057–4067. https://doi.org/10.1007/s10811-020-02283-1

6. Ivošević DeNardis, N., Pečar Ilić, J., Ružić, I., Novosel, N., Mišić Radić, T., Weber, A., Kasum, D., Pavlinska, Z., Balogh Katalin, R., Hajdu, B., Marček Chorvátová, A., Gyurcsik, B., 2019. Algal cell response to laboratory-induced cadmium stress: a multimethod approach. European biophysics journal, 48, 124–142. https://doi.org/10.1007/s00249-019-01347-6.

Sažeci u zbornicima skupova

Usmena priopćenja na međunarodnim i domaćim znanstvenim skupovima

1. Novosel, N., Ivošević DeNardis. Algal cell surface properties and behaviour as stress markers for aquatic ecosystems. 6th Faculty of Science PhD Student Symposium Book Of Abstracts, Zagreb, Hrvatska 2022. str 82.
2. Mišić Radić, T., Levak Zorinc, M., Novosel, N., Ivošević DeNardis, N. Marine microalgae under temperature and salinity stress – insight from AFM study. 4th Croatian Microscopy Congress with international participation, Poreč, Hrvatska, 2022. str. 24.
3. Novosel, N**.,** Levak, M., Ivošević DeNardis, N. Surface method approach in characterization of plasma membrane vesicles derived from algal cells. 10th ISE Satellite Student Regional Symposium on Electrochemistry - Book of Abstracts, Zagreb, Hrvatska 2021. str. 21.
4. Novosel, N., Mišić Radić, T., Zemla, J., Lekka, M., Čačkovic, A., Kasum, D., Legović, T., Žutinić, P., Gligora Udovič, M., Ivošević DeNardis, N. Temperature alterations cause change in algal cell surface properties and behaviour. ASLO 2021 Aquatic Sciences Meeting, Palma de Mallorca, Španjolska (Virtual), 2021. str. 1.
5. Mišić Radić, T., Čačković, A., Novosel, N., Ivošević DeNardis, N. Impact of environmental stress on marine diatoms: insight from AFM study. ASLO 2021 Aquatic Sciences Meeting, Palma de Mallorca, Španjolska (Virtual), 2021. str. 2.
6. Novosel, N., Ivošević DeNardis, N. Electrochemical adhesion based differentiation of algal cell species. Elecnano9 - book of abstract, Pariz, Francuska, 2020. str. 112-112.
7. Novosel, N., Kasum, D., Žutinić, P., Legović, T., Ivošević DeNardis, N. Application of ICY software to motility analysis in cadmium polluted algal cell cultures. Ocean4Biotech CA18238-European transdisciplinary networking platform for marine biotechnology Book of Abstracts, Piran, Slovenija, 2020. str. 25.
8. Ivošević DeNardis, N., Pečar Ilić, J., Ružić, I., Novosel, N.**,** Mišić Radić, T., Weber, A., Kasum, D., Pavlinska, Z., Balogh Katalin, R., Hajdu, B. From ARBRE-MOBIEU networking to regional research cooperation: Multimethod study of algal cell response to laboratory-induced cadmium stress. The 3rd COST-sponsored ARBRE-MOBIEU plenary meeting Book of abstracts Zagreb: Croatian Biophysical Society, ARBRE-MOBIEU COST Action CA15126, 2019. str. 3.

Posterska priopćenja na međunarodnim i domaćim znanstvenim skupovima

1. Novosel, N., Ivošević DeNardis, N. Electrochemical adhesion-based differentiation of algal cells. XXVII International symposium on Bioelectrochemistry and Bioenergetics - Book of abstracts, Antwerpen, Belgija, 2022. str. 88.
2. Novosel, N., Mišić Radić, T., Zemla, J., Lekka, M., Čačković, A., Žutinić, P., Gligora Udovič, M., Ivošević DeNardis, N. Does temperature induce response in algal cell surface properties and behaviour? 35th Congress of the International Society of Limnology - Book of abstracts Gwangju, Korea, 2021. str. 1.
3. Novosel, N., Kasum, D., Žutinić, P., Legović, T., Ivošević DeNardis, N. Algal motility as an indicator of environmental stress. 27th Croatian Meeting of Chemists and Chemical Engineers (HSKIKI) - book of abstracts, Mali Lošinj, Hrvatska 2021. str. 206.
4. Novosel, N., Ivošević DeNardis, N. How to Utilize Structural Features of the Algal Cells for Electrochemical Differentiation at the Liquid-Liquid Interfaces? 72nd Annual Meeting of the International Society of Electrochemistry, Jeju Island, Korea (Hybrid), 2021, str. 208.

5. Novosel, N., Ivošević DeNardis, N. The role of structural features of algal cells on adhesion behavior at the interface. 7th Conference on International Society of Applied Phycology, Virtual platform, Tsukuba, Japan, 2021. str. 113.
6. Novosel, N., Kasum, D., Žutinić, P., Legović, T., Ivošević DeNardis, N. Utjecaj morfoloških karakteristika stanica zelenih alga na međupovršinski proces adhezije i pokretljivost. Simpozij studenata doktorskih studija PMF-a, Knjiga sažetaka. Zagreb, Hrvatska, 2020. str. 78.
7. Novosel, N., Kasum, D., Žutinić, P., Legović, T., Ivošević DeNardis, N. Application of electrochemical approach and motility analysis in algal cells characterization. 71st Annual International Society of Electrochemistry Meeting Belgrade Online, Beograd, Srbija, 2020. str. 221.
8. Novosel, N., Ivošević DeNardis, N. Adhesion behavior of algal cells under stress in laboratory conditions: electrochemical approach. 11th Symposium for European Freshwater Sciences (SEFS 11) - Abstract book, Zagreb, Hrvatska, 2019. str. 381.
9. Novosel, N., Žutinić, P., Kasum, D., Legović, T., Ivošević DeNardis, N. Motility as an indicator of algal cell stress in modified batch cultures. 11th Symposium for European Freshwater Sciences (SEFS 11) - Abstract book, Zagreb, Hrvatska, 2019. str. 384.
10. Novosel, N., Žutinić, P., Kasum, D., Legović, T., Ivošević DeNardis, N. Changes in motility and adhesion behavior of *Dunaliella tertiolecta* Butcher under presence of heavy metal cadmium. Seventh European Phycological Congress. Programme and Book of Abstracts, Zagreb, Hrvatska, 2019. str. 165.

Usmena priopćenja na radionicama/sastancima

1. Novosel, N. Effect of salinity on cell growth dynamics, motility, cell adhesion and released organic matter. Croatian Science Foundation Project: From algal cell surface properties to stress markers for aquatic ecosystems 4rd Work Group Meeting, 2022., Zagreb, Hrvatska.
2. Novosel, N., Kasum, D., Žutinić, P., Legović, T., Ivošević DeNardis, N., Algal cell motility under stress. hrvatsko-francuski Program „Cogito“ Partnerstvo Hubert Curien Evaluation of the biophysical and physiological effects of salinity stress on algal cells and its consequences for cell aggregation, 2021., Toulouse, Francuska.
3. Novosel, N., Mišić Radić, T., Zemla, J., Lekka, M., Čačković, A., Kasum, D., Legović, T., Žutinić, P., Gligora Udovič, M., Ivošević DeNardis, N. Algal cell adaptation responses under influence of single stressor. hrvatsko-francuski Program „Cogito“ Partnerstvo Hubert Curien Evaluation of the biophysical and physiological effects of salinity stress on algal cells and its consequences for cell aggregation, 2021., Toulouse, Francuska, koautor.
4. Novosel, N. Cell culturing & Motility analysis & electrochemical characterization of algal cell response induced by temperature. Croatian Science Foundation Project: From algal cell surface properties to stress markers for aquatic ecosystems 3rd Work Group Meeting, 2021., Zagreb, Hrvatska.
5. Novosel, N. Cell growth dynamics and motility analysis; Electrochemical characterization of algal cells under favorable conditions. Croatian Science Foundation Project: From algal cell surface properties to stress markers for aquatic ecosystems 2nd Work Group Meeting, 2020., Zagreb, Hrvatska.
6. Novosel, N. Genus *Dunaliella*. Visegrad Fund Project: Algal cell biopysical properties as markers for environmental stress in aquatic systems Final Workshop, 2018., Zagreb, Hrvatska.

Sudjelovanje na radionici i školi

1. Precambrian Paleocanography, Prof. Alexey Kamyshy, 2.-6.3.2020., Zagreb, Hrvatska.
2. AFM BioMed Summer School 2020, 20.-22.7.2020., online

8. PRILOZI

8.1. Dodatni materijali objavljenih znanstvenih radova III i IV

Supplementary material

Temperature-induced response in algal cell surface properties and behaviour: an experimental approach

N. Novosel[1], T. Mišić Radić[1], J. Zemla[2], M. Lekka[2], A. Čačković[1], D. Kasum[1], T. Legović[1,3,4], P. Žutinić[5], M. Gligora Udovič[5], N. Ivošević DeNardis[1*]

[1]Ruđer Bošković Institute, Zagreb, Croatia, [2]Institute of Nuclear Physics Polish Academy of Sciences, Kraków, Poland, [3]Libertas International University, Zagreb, Croatia, [4]OIKON-Institute for Applied Ecology, Zagreb, Croatia, [5]Department of Biology, Faculty of Science, University of Zagreb, Zagreb, Croatia

Corresponding author:
N. Ivošević DeNardis
Tel: +385 1 4561-128
E-mail address: ivosevic@irb.hr

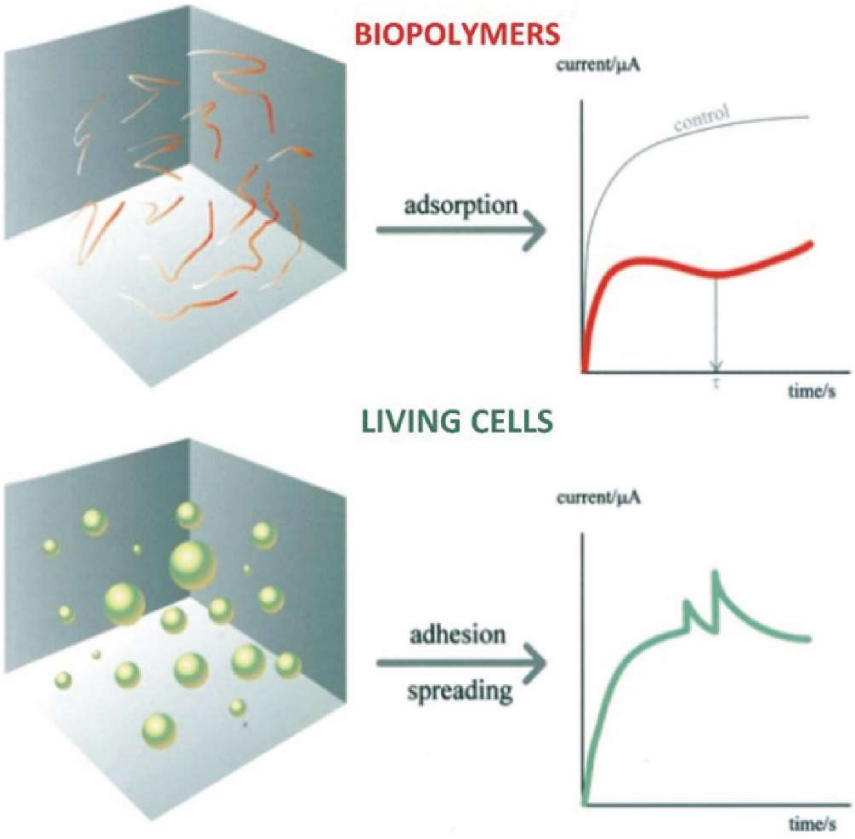

Figure S1. Illustration of organic constituents in seawater (biopolymers and living cells) and their electrochemical signals at the electrode [adapted 26].

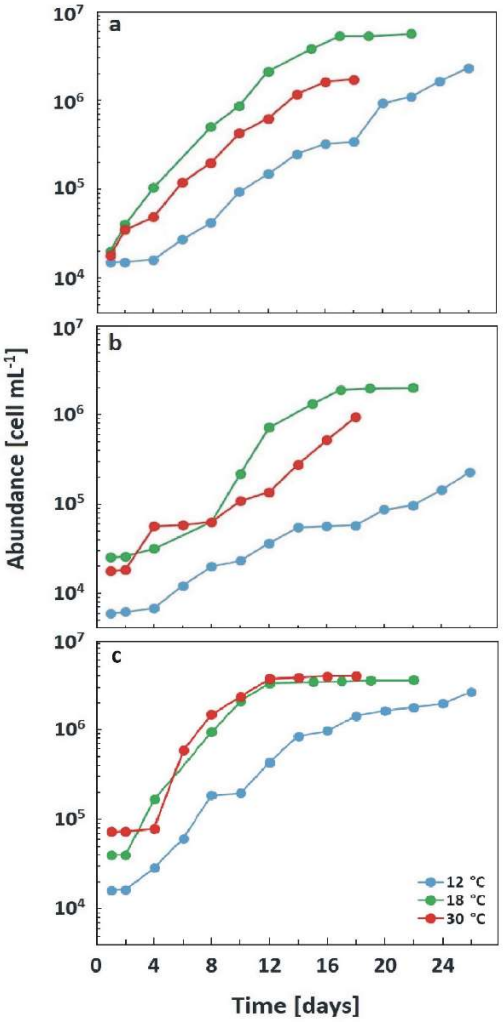

Figure S2. Growth curves of *D. tertiolecta* (a), *T. suecica* (b), and *C. closterium* (c) at temperatures of 12 °C, 18 °C and 30 °C. The data are not accompanied by the experimental error so ± s.d. is not specified.

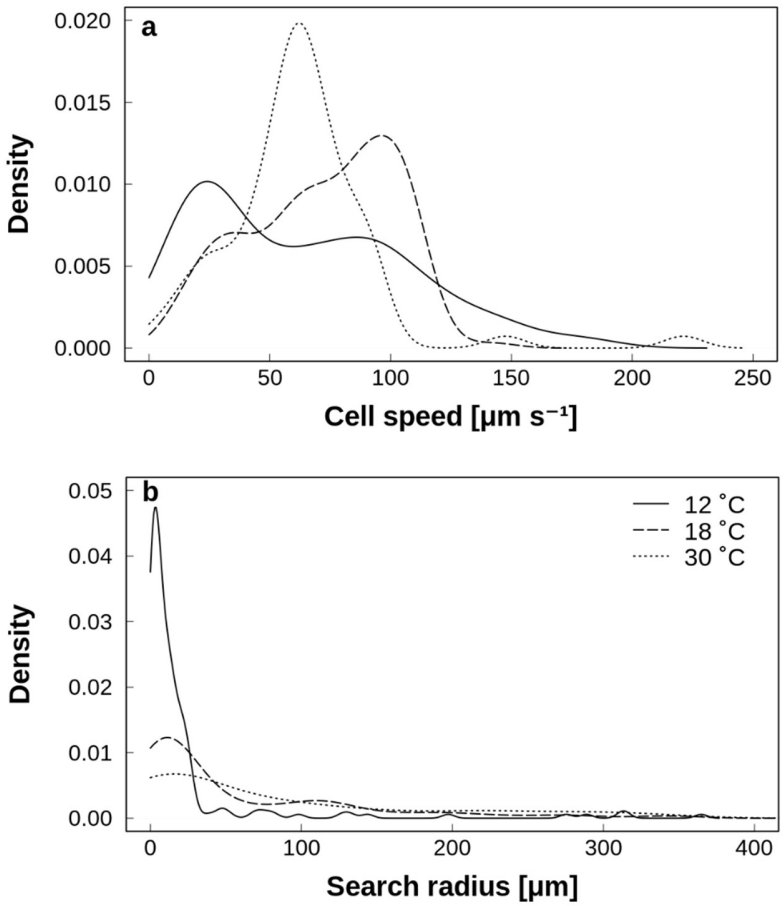

Figure S3. Probability density distributions of cell speed (a) and search radius (b) for *D. tertiolecta* cells grown at temperatures of 12 °C ($2.3x10^6$ cell mL^{-1}), 18 °C ($5.3x10^6$ cell mL^{-1}) and 30 °C ($1.7x10^6$ cell mL^{-1}).

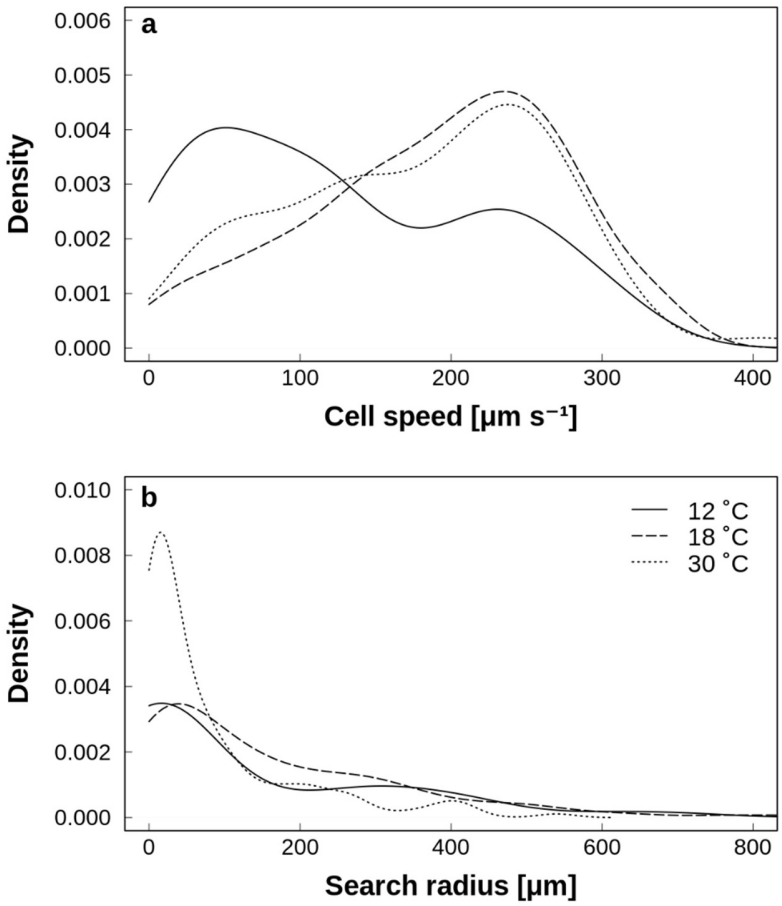

Figure S4. Probability density distributions of cell speed (a) and search radius (b) for *T. suecica* cells grown at temperatures of 12 °C (2.3x10^5 cell mL^{-1}), 18 °C (1.9 x10^6 cell mL^{-1}) and 30 °C (9.4x10^5 cell mL^{-1}).

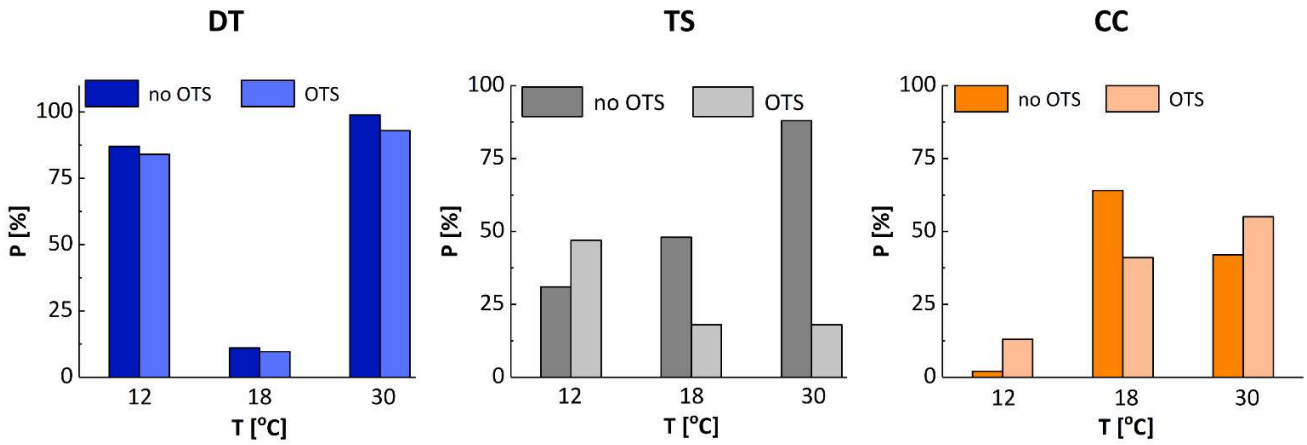

Figure S5. Probability of adhesion between *D. tertiolecta* (a), *T. suecica* (b), and *C. closterium* (c) cells, cultured at 12 °C, 18 °C and 30 °C, at the bare silicon nitride (no OTS) and CH_3 – modified OTS cantilevers.

Table S1. Calculated growth rate (μ) and doubling time (T) of algal species in the exponential phase determined at three temperatures.

T [°C]	*D. tertiolecta*		*T. suecica*		*C. closterium*	
	μ [d^{-1}]	**T [d]**	**μ [d^{-1}]**	**T [d]**	**μ [d^{-1}]**	**T [d]**
12	0.24	2.83	0.21	3.23	0.20	3.46
18	0.30	2.33	0.36	1.92	0.12	5.58
30	0.25	2.76	0.23	2.93	0.35	1.99

Table S2. Selected temperatures, sample size, no. of vibrating cells, average speed and average search radius, no. of moving cells, average speed, standard error of the mean speed, average search radius, and standard error of the mean search radius for *D. tertiolecta*. Avg. – average, SEM – standard error of the mean.

T [°C]	Sample size	No. vibrating	Avg. speed [$\mu m s^{-1}$]	Avg. search radius [µm]	No. moving	Avg. speed [$\mu m\ s^{-1}$]	SEM speed [$\mu m\ s^{-1}$]	Avg. search radius [µm]	SEM search radius
12	170	69	29	2	101	87	3	40	4
18	264	56	38	2	208	81	2	72	5
30	68	15	28	3	53	71	4	102	12

Table S3. Selected temperatures, sample size, cells speed (a) and search path (b) data of *D. tertiolecta* obtained by the analysis of 502 individual cells. Q1 – the first quartile; Q3 – the third quartile, SD – standard deviation, SEM – standard error of the mean.

a

T [°C]	Size	Min	Q1	Median	Mean	Q3	Max	SD	SEM
12	170	0	24	60	63	96	189	44	3
18	264	7.8	50	75	72	97	146	30	2
30	68	0	47	62	62	75	221	31	4

b

T [°C]	Size	Min	Q1	Median	Mean	Q3	Max	SD	SEM
12	170	0	2	8	24	19	385	57	4
18	264	0.6	6	18	57	90	359	77	5
30	68	0	9	37	80	122	340	97	12

Table S4. Selected temperatures, sample size, cells speed (a) and search path (b) data of *T. suecica* obtained by the analysis of 452 individual cells. Q1 – the first quartile; Q3 – the third quartile, SD – standard deviation, SEM – standard error of the mean.

a

T [°C]	Size	Min	Q1	Median	Mean	Q3	Max	SD	SEM
12	48	6	43	113	128	209	309	94	14
18	257	0	132	201	190	251	351	84	5
30	147	0	116	194	179	247	413	88	7

b

T [°C]	Size	Min	Q1	Median	Mean	Q3	Max	SD	SEM
12	48	0.5	5	16	127	261	699	180	26
18	257	0	21	102	163	262	878	173	11
30	147	0	10	32	80	110	540	108	9

Table S5. Cell dimensions (l – length, w – width, h – height) and surface roughness (R_a) *of D. tertiolecta, T. suecica* and *C. closterium* cells grown at 12 °C, 18 °C and 30 °C based on AFM images analysis.

T [°C]	*D. tertiolecta*				*T. suecica*				*C. closterium*			
	l [µm]	**w [µm]**	**h [µm]**	**R_a [nm]***	**l [µm]**	**w [µm]**	**h [µm]**	**R_a [nm] ****	**l [µm]**	**w [µm]**	**h [µm]**	**R_a [nm]***
12	10.5-12.1	6.0-6.8	2.4-2.5	4-12	17.9-20.1	13.1-14.7	1.3-2.0	35-63	56.4-60.2	6.6-8	1.0-1.2	1-3 (v) 2-4 (g)
18	11.7-12.8	7.6-8.5	1.0-1.6	5-6	16.8-19.0	12.6-13.1	1.9-2.2	30-54	38.3-42.0	5.0-6.0	0.9-1.5	2-3 (v) 3-5 (g)
30	7.5-9.5	4.5-6.5	2.2-3.0	5-17	14.0-16.5	8.5-9.9	1.7-2.0	34-48	30.5-50.1	2.8-4	0.6-0.8	4-8 (v) 4-9 (g)

v – valve; g – girdle bands

* roughness analysis performed on area 500 x 500 nm

**roughness analysis performed on area 2 x 2 µm

Table S6. Maximum work of adhesion calculated from measurements with a bare and OTS – coated probe. Data presented as mean ± SEM. ΔW_{adh} and adhesion probability if probing with bare ($P_{no\ OTS}$) and functionalised (P_{OTS}) tip.

Cells	T [°C]	$W_{adh\ (no\ OTS)}$ [fJ]	$W_{adh\ (OTS)}$ [fJ]	ΔW_{adh} [fJ]	$P_{no\ OTS}$ [%]	P_{OTS} [%]
	12	0.21 ± 0.01	0.069 ± 0.003	0.14 ± 0.02	87	84
DT	18	0.030 ± 0.004	0.037 ± 0.003	- 0.0074 ± 0.0073	11	9.6
	30	0.55 ± 0.02	0.35 ± 0.03	0.20 ± 0.05	99	93
	12	0.17 ± 0.02	0.066 ± 0.007	0.11 ± 0.03	31	47
TS	18	0.027 ± 0.003	0.037 ± 0.008	- 0.011 ± 0.011	48	18
	30	0.25 ± 0.02	0.061 ± 0.014	0.19 ± 0.04	88	18
	12	0.00025 ± 0.00001	0.030 ± 0.003	- 0.030 ± 0.003	2	13
CC	18	0.067 ± 0.006	0.0085 ± 0.0011	0.058 ± 0.007	64	41
	30	0.15 ± 0.03	0.69 ± 0.05	- 0.53 ± 0.07	42	55

Salinity-induced chemical, mechanical and behavioral changes in marine microalgae

N. Novosel[1], T. Mišić Radić[1], M. Levak Zorinc[1], J. Zemla[2], M. Lekka[2], I. Vrana[1], B. Gašparović[1], L. Horvat[1], D. Kasum[1], T. Legović[1,3,4], P. Žutinić[5], M. Gligora Udovič[5], N. Ivošević DeNardis[1*]

[1]Ruđer Bošković Institute, Zagreb, Croatia, [2]Institute of Nuclear Physics Polish Academy of Sciences, Kraków, Poland, [3]Libertas International University, Zagreb, Croatia, [4]OIKON-Institute for Applied Ecology, Zagreb, Croatia, [5]Department of Biology, Faculty of Science, University of Zagreb, Zagreb, Croatia

Corresponding author:
N. Ivošević DeNardis
Tel: +385 1 4561-128
E-mail address: ivosevic@irb.hr

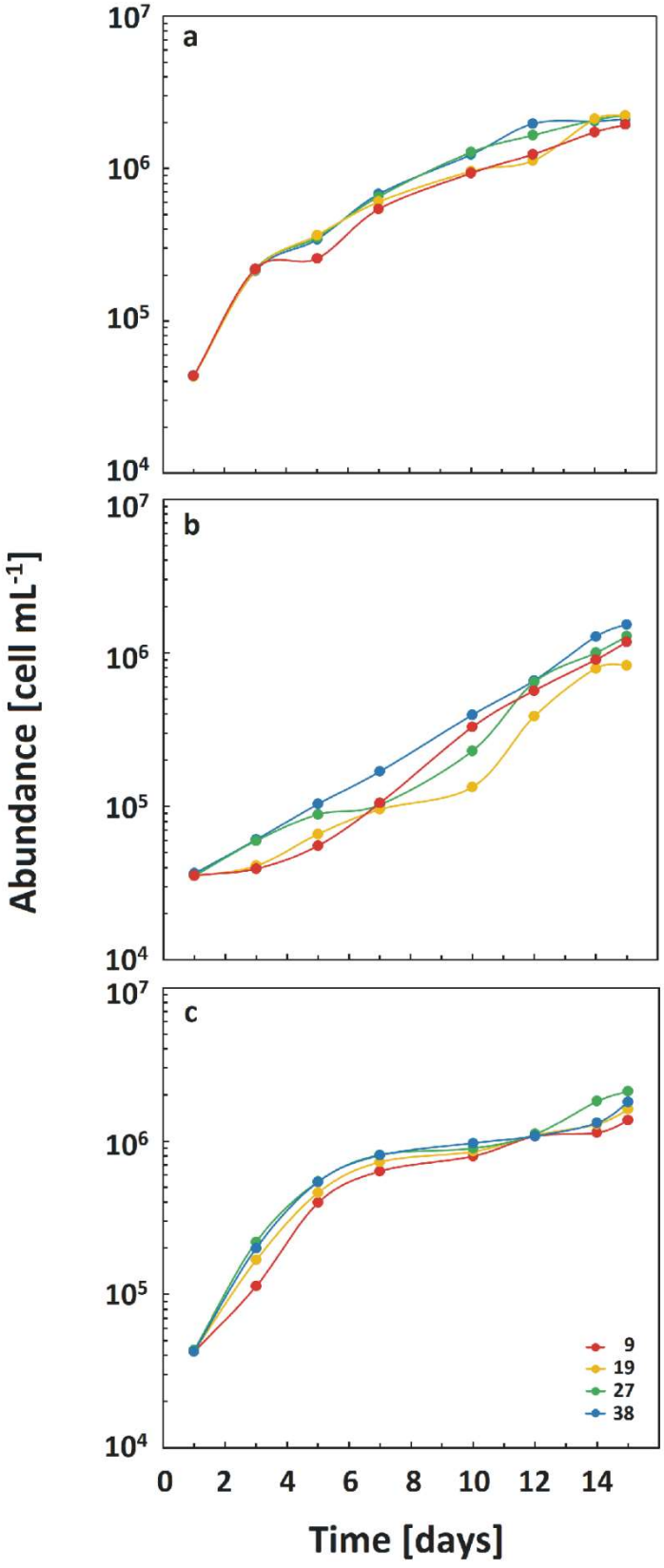

Figure S1. Growth curves of *D. tertiolecta* (a), *T. suecica* (b), and *C. closterium* (c) at salinities of 9, 19, 27, and 38. The data are not accompanied by the experimental error, so ± s.d. is not specified.

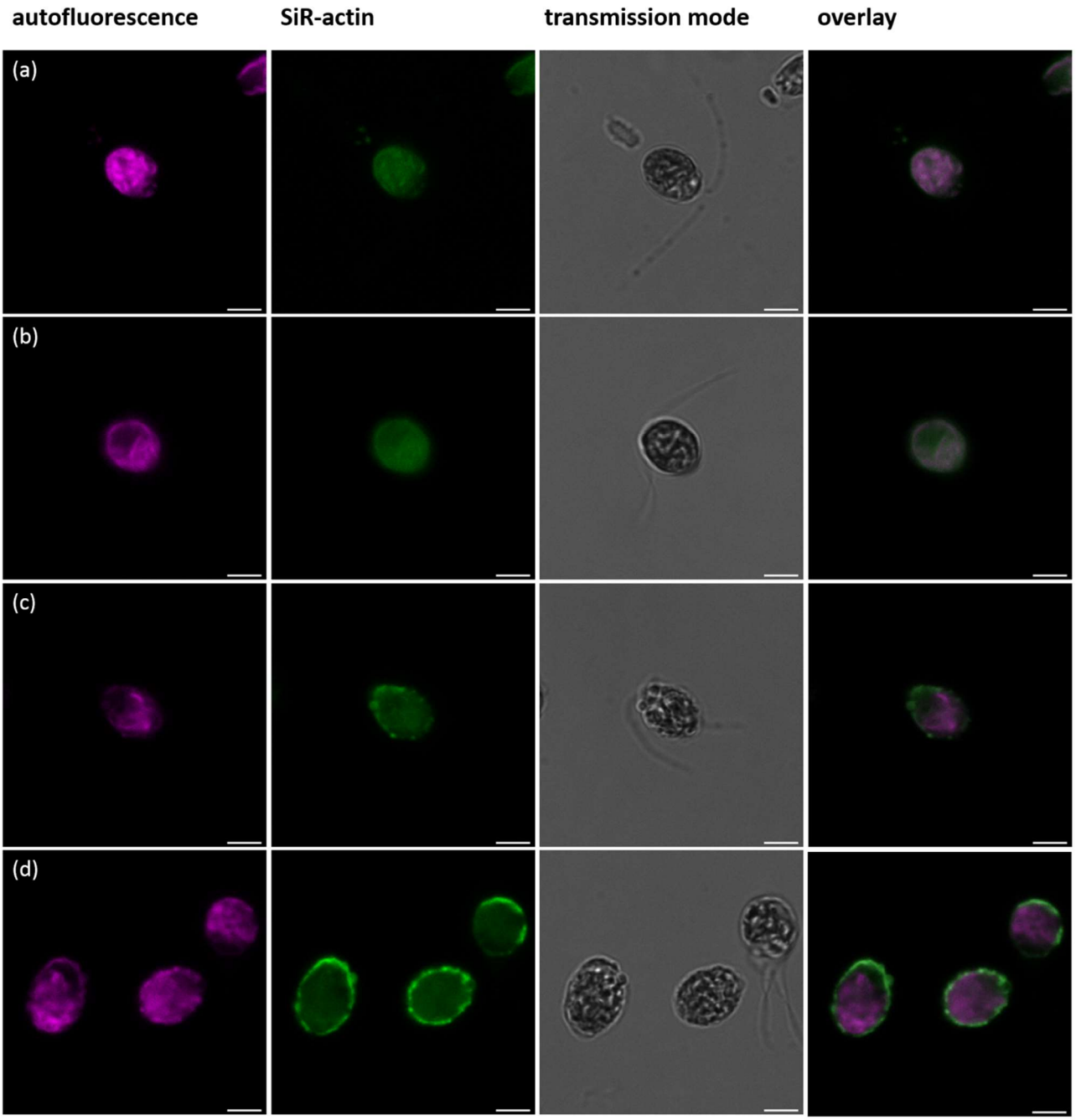

Figure S2. Confocal images of *D. tertiolecta* grown at salinities of 38 (a), 27 (b), 19 (c), and 9 (d). Bar corresponds to 5 µm.

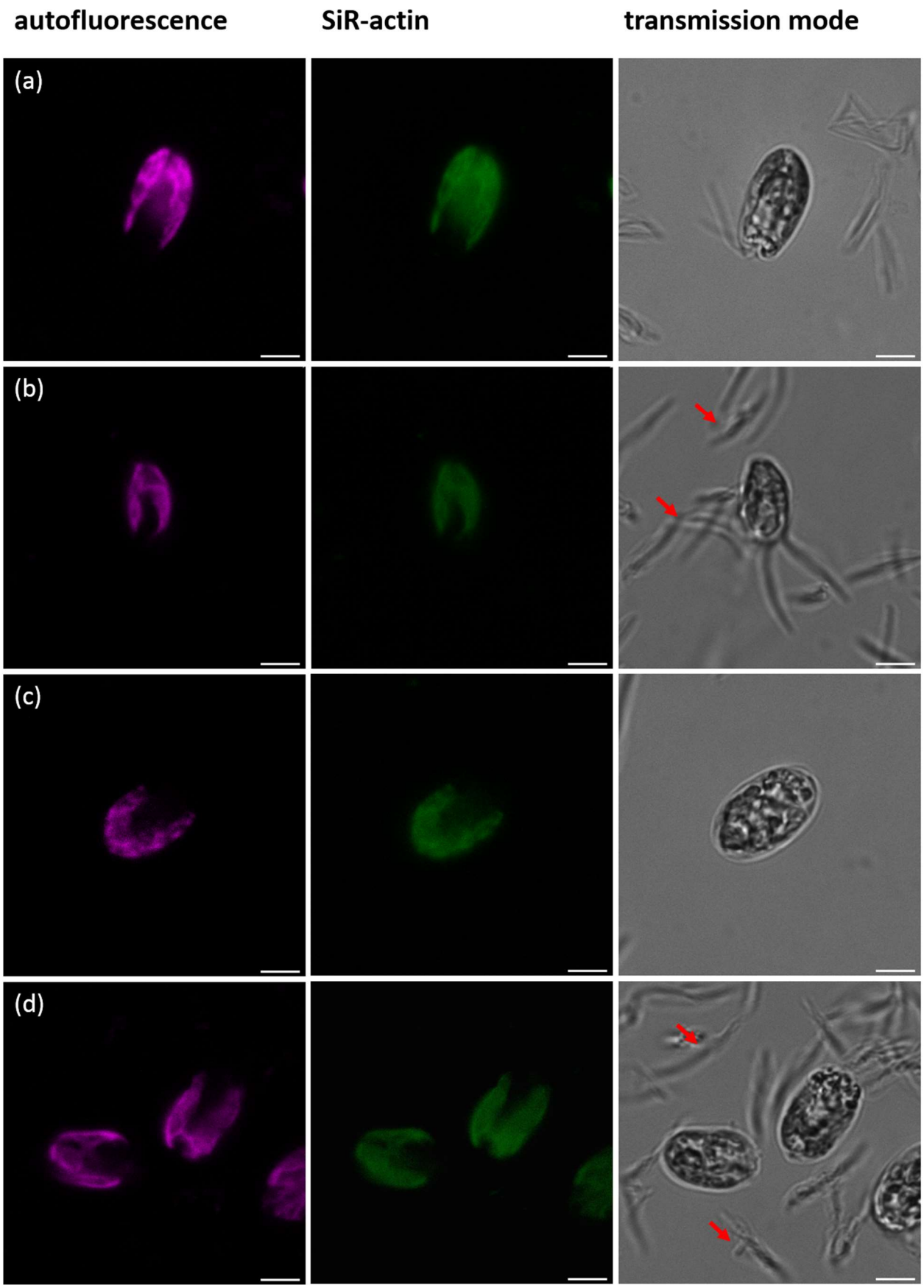

Figure S3. Confocal images of *T. suecica* grown at salinities of 38 (a), 27 (b), 19 (c), and 9 (d). Arrows indicate detached flagella. Bar corresponds to 5 µm.

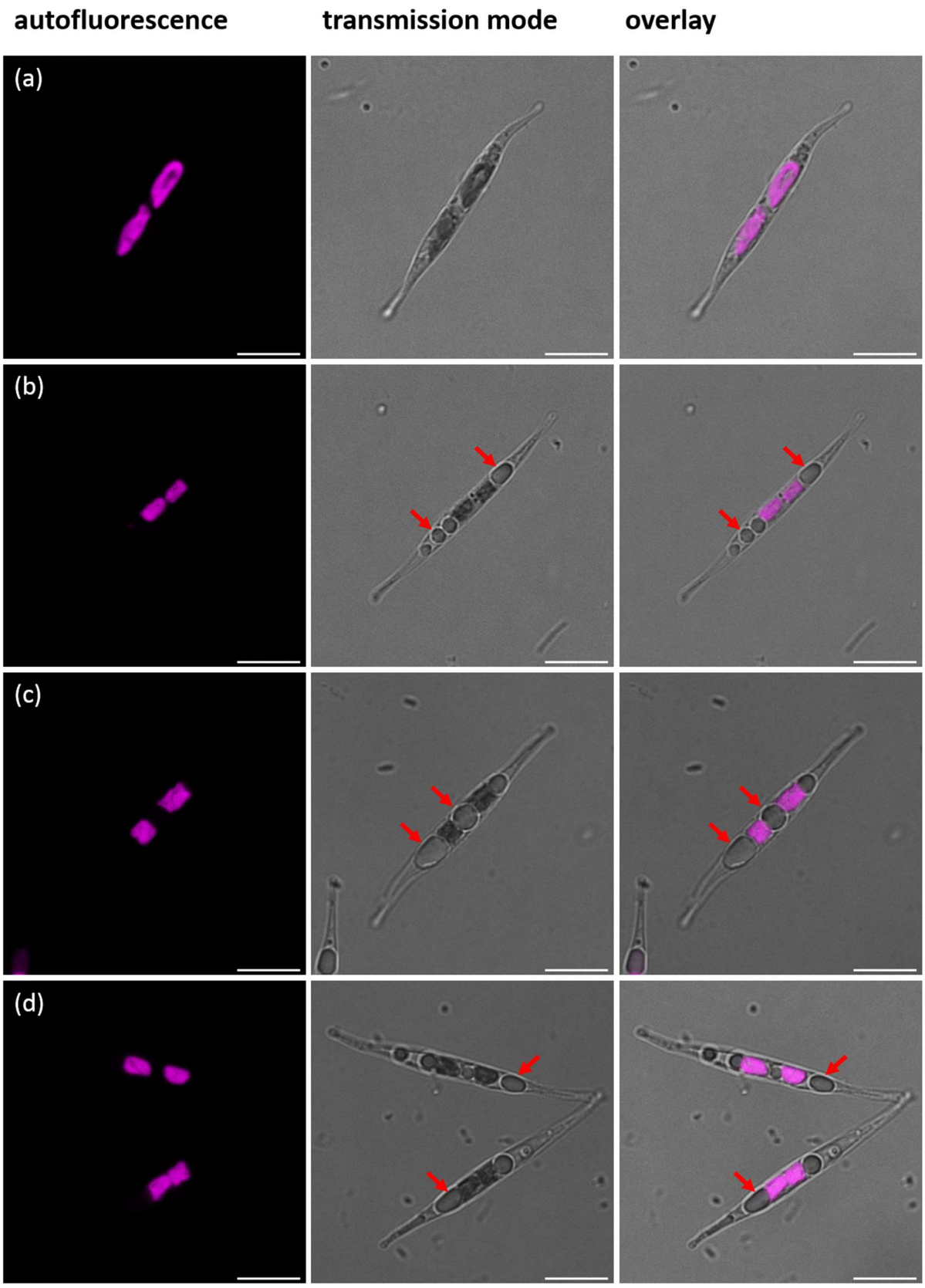

Figure S4. Confocal images of *C. closterium* grown at salinities of 38 (a), 27 (b), 19 (c), and 9 (d). Arrows indicate intracellular droplets. Bar corresponds to 5 µm.

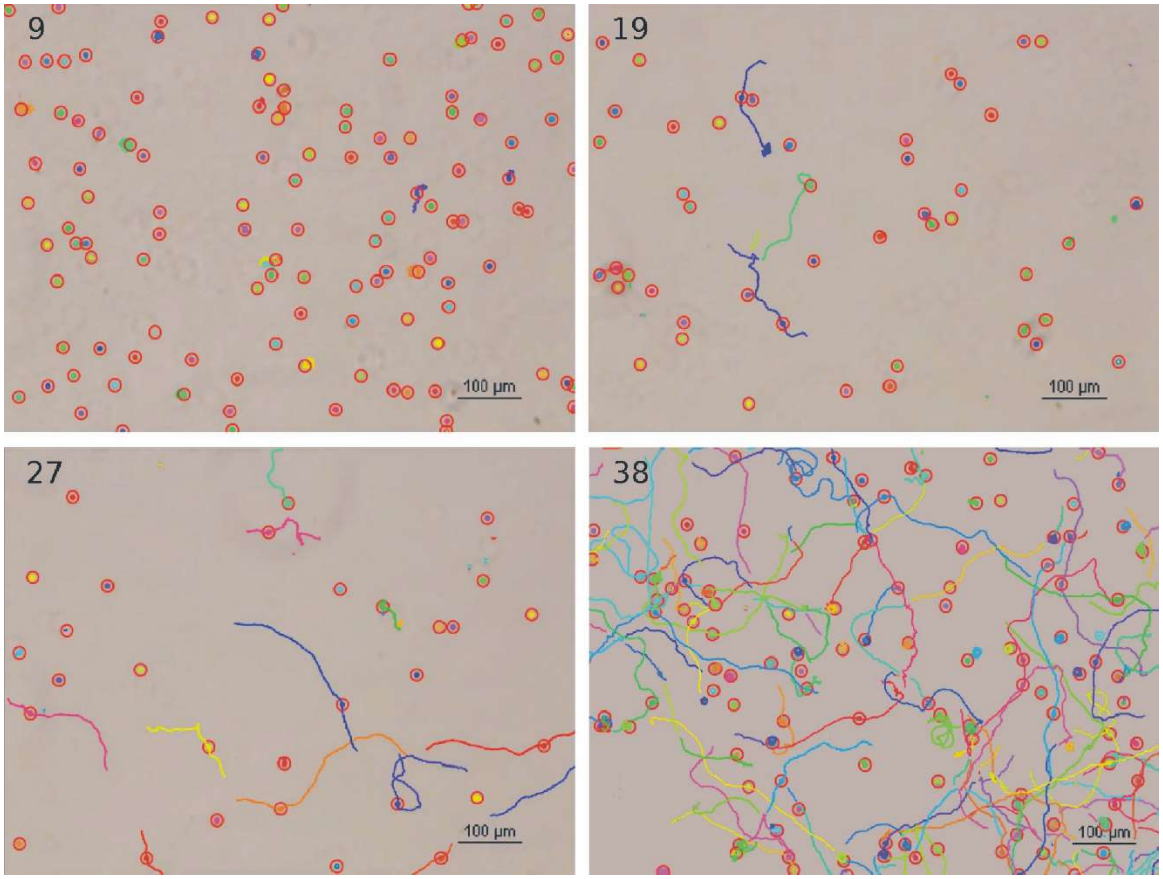

Figure S5. Reconstructed ICY images of *D. tertiolecta* grown at salinities of (a) 9 ($1.94x10^6$ cells mL^{-1}), (b) 19 ($2.23x10^6$ cells mL^{-1}), and (c) 27 ($2.23x10^6$ cells mL^{-1}) and (d) 38 ($2.13 x10^6$ cells mL^{-1}). The cells are indicated by colored circles, while a line represents their trajectory.

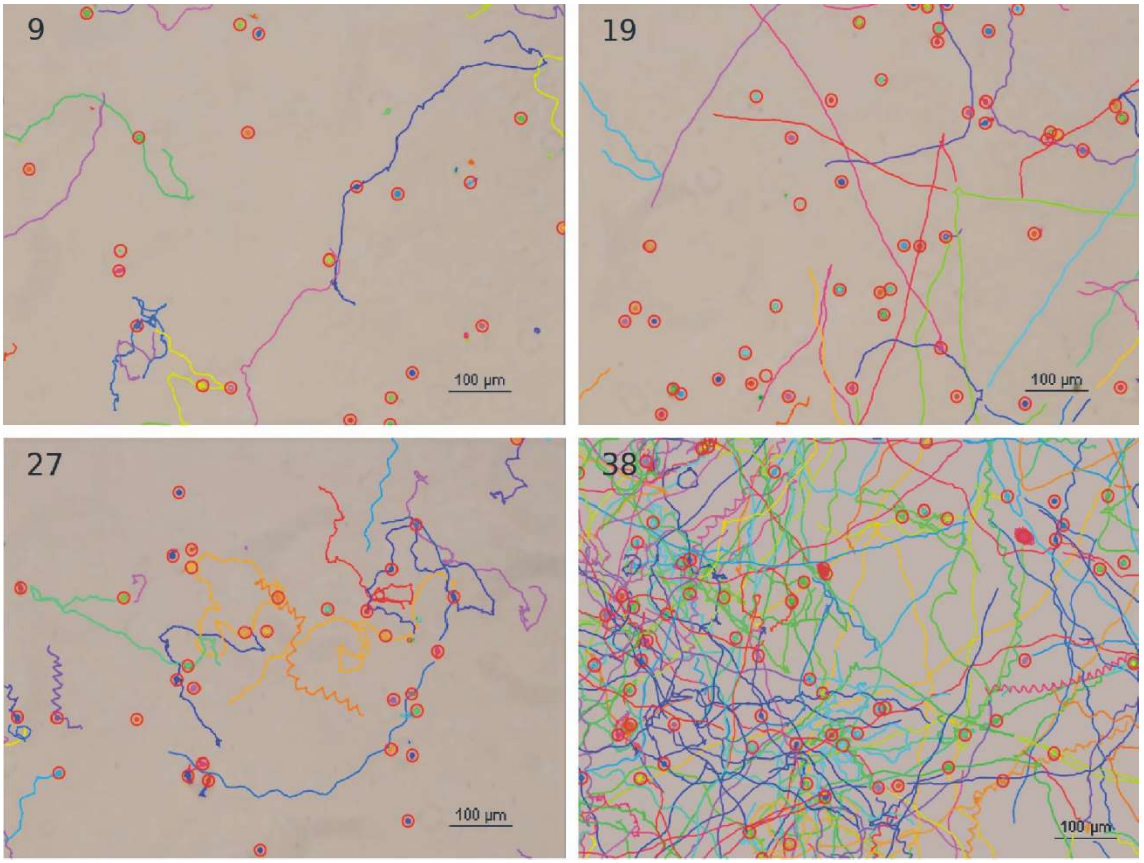

Figure S6. Reconstructed ICY images of *T. suecica* grown at salinities of (a) 9 ($1.18x10^6$ cells mL^{-1}), (b) 19 ($8.28x10^6$ cells mL^{-1}), and (c) 27 ($1.28x10^6$ cells mL^{-1}) and (d) 38 ($1,53x10^6$ cells mL^{-1}). The cells are indicated by coloured circles, while a line represents their trajectory.

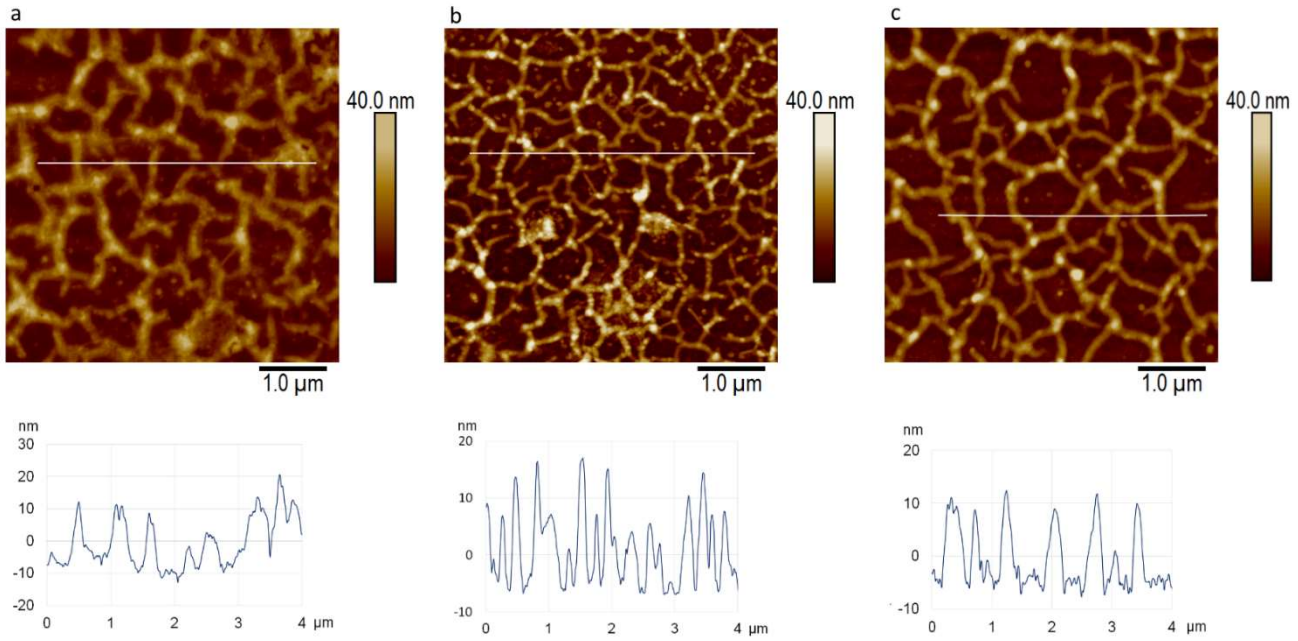

Figure S7. AFM images of a network of extracellular polymers of *T. suecica* grown at a salinity of 9 (a); 19 (b) and 27 (c). Images were acquired in contact mode in air and presented as height data, scan size 5 µm x 5 µm, vertical scale 40 nm, with vertical profiles along the indicated lines.

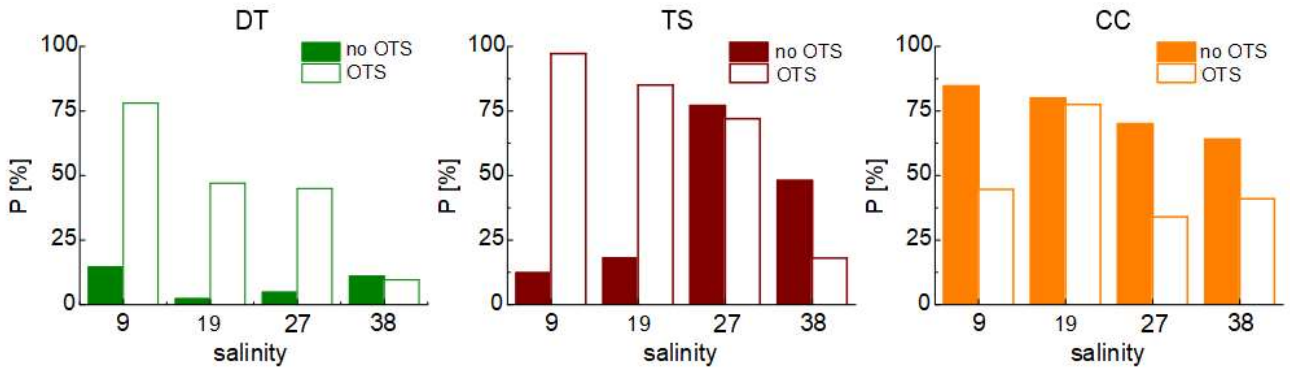

Figure S8. Probability, P[%], of cell adhesion to hydrophilic (no OTS) and hydrophobic (OTS) probe, filled and empty bars, respectively. Probability is calculated as the ratio between the number of retraction curves with $W_{adh} > 0$ and the total number of force curves collected.

Table S1. Calculated growth rate (μ) and doubling time (T) of microalgal species in exponential growth phase under selected salinity conditions.

S	*D. tertiolecta*		*T. suecica*		*C. closterium*	
	μ [d^{-1}]	**T [d]**	**μ [d^{-1}]**	**T [d]**	**μ [d^{-1}]**	**T [d]**
9	0.37	1.86	0.32	2.17	0.24	2.93
19	0.25	2.74	0.18	3.75	0.23	3.02
27	0.31	2.25	0.07	9.59	0.20	3.45
38	0.34	2.02	0.24	2.85	0.20	3.49

Table S2.1. Selected salinities, sample size, no. of vibrating cells, average speed and average search radius and no. of moving cells, average speed, standard error of the mean speed, average search radius, and standard error of the mean search radius for *D. tertiolecta*.

S	Sample size	No. vibrating	Avg. speed [µms^{-1}]	Avg. search radius [µm]	No. moving	Avg. speed [µm s^{-1}]	SEM speed [µm s^{-1}]	Avg. search radius [µm]	SEM search radius [µm]
9	164	109	25	2	55	74	4	12	1
19	68	39	35	3	29	103	13	27	9
27	65	41	43	3	24	77	7	79	18
38	264	56	38	2	208	81	2	72	6

Table S2.2. Selected salinities, sample size, cells speed [µm s^{-1}] (a) and search path [µm] (b) data of *D. tertiolecta* obtained by the analysis of 561 individual cells. Q1 – the first quartile; Q3 – the third quartile, SD – standard deviation, SEM – standard error of the mean.

(a) Speed

S	Size	Min	Q1	Median	Mean	Q3	Max	SD	SEM
9	164	0	16	29	42	59	152	34	3
19	68	7.5	25	50	64	78	351	57	7
27	65	7.9	34	50	56	77	183	32	4
38	264	7.8	50	75	72	97	146	30	2

(b) Search radius

S	Size	Min	Q1	Median	Mean	Q3	Max	SD	SEM
9	164	0	1	2	5	7	45	6	0.5
19	68	1	2	4	13	8	186	33	4
27	65	1	2	3	31	8	275	65	8
38	264	1	6	18	57	90	359	77	5

Table S3.1. Selected salinities, sample size, no. of vibrating cells, average speed and average search radius, no. of moving cells, average speed, standard error of the mean speed, average search radius, and standard error of the mean search radius for *T. suecica*.

S	Sample size	No. vibrating	Avg. speed [μms^{-1}]	Avg. search radius [μm]	No. moving	Avg. speed [μm s^{-1}]	SEM speed [μm s^{-1}]	Avg. search radius [μm]	SEM search radius
9	81	35	63	3	46	124	10	57	15
19	124	73	38	2	51	155	11	121	21
27	95	26	51	3	69	137	7	61	12
38	257	16	31	2	241	201	5	174	11

Table S3.2. Selected salinities, sample size, cells speed [μm s^{-1}] (a) and search radius [μm] (b) data of *T. suecica* obtained by the analysis of 557 individual cells. Q1 – the first quartile; Q3 – the third quartile, SD – standard deviation, SEM – standard error of the mean.

(a) Speed

S	Size	Min	Q1	Median	Mean	Q3	Max	SD	SEM
9	81	5	49	78	98	140	315	67	7
19	124	0	31	50	86	134	368	78	7
27	95	0	71	112	113	164	296	65	7
38	257	0	132	201	190	251	351	84	5

(b) Search radius

S	Size	Min	Q1	Median	Mean	Q3	Max	SD	SEM
9	81	1	4	6	34	12	494	81	9
19	124	0	2	4	51	20	615	114	10
27	95	0	5	12	45	24	444	89	9
38	257	0	21	102	163	262	878	173	11

Table S4. Cell dimensions (l-length, w-width, h-height) and surface roughness (R_a) *of D. tertiolecta, T. suecica* and *C. closterium* cells grown at salinities of 9, 19, 27 and 38 based on analysis of AFM images.

S	*D. tertiolecta*				*T. suecica*				*C. closterium*			
	l [µm]	**w [µm]**	**h [µm]**	**R_a [nm]***	**l [µm]**	**w [µm]**	**h [µm]**	**R_a [nm] ****	**l [µm]**	**w [µm]**	**h [µm]**	**R_a [nm]***
9	9.4 ± 0.8	5.6 ± 0.4	2.4 ± 0.3	13.5 ± 4.6	15.0 ± 0.8	10.8 ± 0.7	2.3 ± 0.8	46.6 ± 19,4	45.0 ± 1.6	4.5 ± 0.5	0.8 ± 0.1	4.4 ± 2.0 (v) 4.9 ± 1.2 (g)
19	10.0 ± 0.8	6.8 ± 0.6	2.0 ± 0.4	11.7 ± 2.0	15.8 ± 1.0	12.1 ± 0.9	1.8± 0.3	37.4 ± 7.5	45.9 ± 1.8	4.7 ± 0.7	1.0 ± 0.6	4.6 ± 1.5 (v) 4.0 ± 1.5 (g)
27	8.8 ± 0.6	5.6 ± 0.8	2.3 ± 0.3	12.4 ± 2.0	15.3 ± 1.0	10.7 ± 1.0	1.6± 0.4	30.8 ± 15.2	44.3 ± 1.2	4.3 ± 0.8	0.9 ± 0.2	4.5 ± 1.5 (v) 4.4 ± 0.8 (g)
38	12.3 ± 0.7	8.1 ± 0.6	1.3 ± 0.4	5.5 ± 3.3	17.9 ± 0.9	12.9 ± 0.9	2.1 ± 0.6	42.0 ± 11.0	40.2 ± 1.6	5.5 ± 0.6	1.2 ± 0.4	2.5 ± 1.8 (v) 4.5 ± 1.2 (g)

v – valve; g- girdle bands

* roughness analysis performed on area 500 x 500 nm

**roughness analysis performed on area 2 x 2 µm

Table S5. Maximum work of adhesion obtained for *D. tertiolecta*, *T. suecica*, and *C. closteri*um cells probed with hydrophilic (no OTS) and hydrophobic (OTS) AFM tips. Data are shown as mean ± SEM. Hydrophobic properties (ΔW_{adh}) of algal cells. Data are shown as mean ± maximum error. Probability, P[%], of cell adhesion to hydrophilic (no OTS) and hydrophobic (OTS) probes. Probability is calculated as the ratio of the number of retraction curves with $W_{adh} > 0$, and the total number of collected force curves.

Cells	S	$W_{adh(no\ OTS)}$ [fJ]	$W_{adh(OTS)}$ [fJ]	ΔW_{adh} [fJ]	P_{noOTS} [%]	P_{OTS} [%]
DT	9	0.070±0.008	0.088±0.006	-0.018±0.014	15	78
	19	0.030±0.013	0.030±0.002	0±0.015	2.3	47
	27	0.0211±0.0051	0.0683±0.0052	-0.047±0.012	4.8	45
	38	0.0299±0.0043	0.037±0.003	-0.0074±0.0073	11	9.6
TS	9	0.039±0.006	0.55±0.05	-0.506±0.054	12	97
	19	0.0327±0.0033	0.303±0.034	-0.270±0.037	18	85
	27	0.0551±0.0029	0.0575±0.0058	-0.0024±0.009	77	72
	38	0.0266±0.0025	0.0374±0.0078	-0.011±0.010	48	18
CC	9	0.274±0.034	0.326±0.046	-0.0517±0.0801	85	45
	19	0.096±0.011	0.279±0.041	-0.183±0.051	80	77
	27	0.209±0.023	0.177±0.032	0.032±0.055	70	34
	38	0.0668±0.0062	0.0085±0.0011	0.0583±0.0072	64	41